THE INFLUENCE OF ENVIRONMENTAL AND BIOTIC FILTERS ON INVERTEBRATE COMMUNITY DYNAMICS AND SPATIAL SYNCHRONY

Jacob D. Buchanan

A Dissertation

Submitted to the Graduate College of Bowling Green
State University in partial fulfillment of the
requirements for the degree of

DOCTOR OF PHILOSOPHY

April 2024

Committee:

Kevin McCluney, Committee Chair

Abby Braden,
Graduate Faculty Representative

Helen Michaels

Jeffrey Miner

Chris Patrick

This content is unable to be made fully accessible because it would result in a fundamental alteration of the document.

ABSTRACT

Kevin McCluney, Committee Chair

Each chapter of this dissertation is intended to address a piece of the central hypothesis that complex, interacting biotic and abiotic filters drive community dynamics, including temporal synchrony between communities arising from distant propagule sources. In Chapter I, I examine the influence of three different synchrony metrics on measures of similarity between real and simulated time series, comparing methods for identifying clusters of more synchronous populations or communities, and revealing environmental drivers of those clusters. My results for this study indicate that wavelet analysis works best if the data have high frequency effects or high levels of noise. Empirical orthogonal functions work well if there are large differences in between-site magnitudes. If there are phase-lagged effects of interest, cross-correlation or empirical orthogonal function work well. For all other cases, each of these three metrics performed similarly. Therefore, these metrics may provide complimentary information if each

are used to analyze the same dataset. Chapter II quantifies the filtering effects of temperature, egg bank composition, and disturbance on wetland invertebrate community dynamics and Chapter III quantifies the filtering effects of temperature, egg bank composition, and predation on wetland invertebrate community dynamics. Both chapters employ in-field mesocosm experiments in 100-gallon cattle tanks that were seeded with invertebrate propagules from either local ecosystems or from 5 different states. My results for these studies indicate that prairie pothole wetland communities are largely resistant to fluctuations in water levels though a few taxa (cladocerans, clam shrimp, fairy shrimp, damselfly larvae) saw decreased abundances in certain cases. Small changes in temperature (+1.1 °C) had little effect on the community except

for intensifying the impact of the drawdown on clam shrimp and fairy shrimp. A greater change in temperature (+2.0 °C) led to more abundant clam shrimp and green algae, and larger-sized fairy shrimp, clam shrimp, and dytiscid larvae Predation by diving beetles led to decreased abundances of clam shrimp under warmer conditions or decreased abundances of copepods where alternative prey were scarce. In total, this work is a step toward improved understanding of the temporal dynamics of distant ecological communities.

To my friends and family

ACKNOWLEDGMENTS

Thank you to all the people listed below and everyone else who helped me along the way. I'd like to thank my advisor, Kevin McCluney, and my committee members: Helen Michaels, Jeffrey Miner, Chris Patrick, and Abby Braden. I was fortunate enough to have wonderful undergraduate researchers: Taylor Arens, Ashlia Toles, Daniel Clarke, and Jordan Gessner. Thanks to the PIs on NSF grant that my work is associated with: James H. Thorp, Chris J. Patrick, J. Derek Hogan, Kevin E. McCluney, Wiebke Boeing. Thanks to those who collected sediment that I used: Mica Rumbach, Jackob Lutchen, John Tran, Wiebke Boeing, J. Derek Hogan, Christopher Frazier, and Sherridan Torres. Thanks to everyone at the US FWS Chase Lake WMD, especially Jennifer Jewett, Scott Baker, Jeff Dion, and Jacob Hourt. Thanks to the folks at NEON and the USGS in the Jamestown, ND area. Thanks to everyone at CAP-LTER. A special thanks to my fellow graduate students, especially Margaret Duffy, Rachel Paull, Alessia Saul, MJ Lashbrook, Jonathan Brokaw, Toby Shaya, Mica Rumbach, Caroline Barth, Bridget Harter. Thanks again to my friends and family. One final thank you to NSF for funding grant 1926555.

TABLE OF CONTENTS

Page

CHAPTER I: COMPARING METRICS USED IN CLUSTERING SYNCHRONOUS ECOLOGICAL COMMUNITIES

Abstract

In ecological processes, spatial synchrony is a phenomenon wherein populations or communities of organisms fluctuate in phase through time. Several methods have been used to quantify synchrony, including the cross-correlation function (CCF), wavelet, and empirical orthogonal function (EOF) analyses. This study compares how these metrics of synchrony influence interpretations regarding the similarities between time series using both simulated and a real dataset—ground beetle pitfall trap data from Phoenix, AZ. Using simulated data, I compared the ability of each metric to appropriately categorize time series into one or two groups when those groups differed in frequency, magnitude, or phase lag. I found that wavelet analysis works best if the data have high frequency effects or high levels of noise. Empirical orthogonal functions work well if there are large differences in between-site magnitudes. If there are phase-lagged effects of interest, cross-correlation or empirical orthogonal function work well. For all other cases, each of these three metrics performed similarly. Therefore, these metrics may provide complimentary information if each are used to analyze the same dataset. When applied to the real dataset, each metric yielded different clusters though some sites were identified as synchronous with one another regardless of the metric used, suggesting that some sites are highly synchronous with one another while others are not. Likewise, the environmental drivers implicated for these different clusters varied by the method used and the number of clusters. Overall, these results suggest that different synchrony metrics result in slightly dissimilar clusters due to differences in their sensitivities to different magnitudes, frequencies, time lags, and noise.

Therefore, these metrics are complementary, revealing different information about the synchrony of the data sets.

Introduction

Spatial synchrony is defined as, “coincident changes in the abundance or other timevarying characteristics of geographically disjunct populations” (Liebhold et al., 2004). The broader study of synchronous processes occurs in fields as diverse as mathematics, physics, climatology, engineering, computer science, neuroscience, psychology, and ecology (Strogatz & Stewart, 1993; Fries et al., 2001; Li et al., 2003). Patterns of synchronization may occur not just through time, but across space, or simultaneously in both time and space (Bjørnstad et al., 1999). In the context of ecology, spatial synchrony typically refers to a phenomenon wherein populations or communities of organisms in different locations fluctuate in phase through time. This includes patterns of abundance (Sutcliffe et al., 1996), biomass (Batchelder et al., 2012), nutrients (Fontaine et al., 2023), or measures like species richness (Özkan et al., 2016). Studies have focused on a variety of taxa including birds (Koenig & Liebhold, 2016), mountain pine beetles (Aukema et al., 2006), common voles (Gouveia et al., 2016), salmon (Moore et al., 2010), marine zooplankton (Batchelder et al., 2012), and terrestrial vegetation (Defriez & Reuman, 2017).

Three recognized driving forces of synchrony in ecological systems are dispersal, trophic interactions, and environmental forcing factors collectively called Moran effects (Liebhold et al., 2004). Moran effects include, but are not limited to, weather variables like temperature and precipitation and landscape or land use variables (Koenig, 2002). Because these variables are often assumed to be more similar the closer two locations are to one another, distance between sites is thought to be an important consideration when examining spatial synchrony (Walter et al., 2017).

Measurement and quantification of synchrony can be performed using several different methods (Buonaccorsi et al., 2001). Since synchrony is already a well-studied concept in other fields, the techniques used are adequately developed for widespread general use. The cross-correlation function has been extensively used in ecological studies (Bjørnstad & Bascompte, 2001; Ranta et al., 1999). Spectral techniques like the Fourier transform (Bush et al., 2017), a special case of the broader wavelet transform (Cazelles, Chavez, Berteaux, Ménard, et al., 2008), are also common approaches used to measure synchrony in time series data. Eigenvalue-based approaches like principal components analysis (PCA), of which empirical orthogonal functions (EOFs) are a specialized case, are less common in synchrony analyses, especially in ecology, but still appear in the literature as an option for time series analysis (Andersen et al., 2009) and have been used in fields ranging from climatology (Dawson, 2016; Hannachi, n.d.) to ecology (Bergamino et al., 2007; Thorson et al., 2020; Patrick et al., 2021). R packages like 'codyn' (Hallett et al., 2016) and 'wsyn' (Sheppard et al., n.d.) also include functions to quantify spatial synchrony.

In this study, I compared the performance of three commonly used synchrony metrics to cluster multiple populations or communities. First, I compared the ability of these metrics to correctly cluster two groups of simulated time series that differed in either frequency, magnitude, lag, or noise. Second, I compared the clustering of sites using each metric within a real dataset (which inherently contains varying degrees of the selected parameters in the simulated data) to determine how within- and between-cluster similarity varied for the three metrics. Additionally, environmental drivers of these clusters were determined and differences between the drivers determined by each method were examined.

Methods

Overview

I compared three commonly used metrics of synchrony: cross-correlation function (CCF), wavelet, and empirical orthogonal function (EOF) using both simulated and real data. For the simulated dataset, two base time series were generated: one where a single parameter was varied over a range (a "treatment" base time series) and one where fixed values of all parameters were used (a "control" base time series). 10 white noise replicates of each base time series were generated for each test and one test was conducted for each parameter (frequency, magnitude, phase lag, or noise), wherein only that one parameter was varied over a range while the others were held constant. The ability of each synchrony metric to correctly separate the "treatment" group of time series from the "control" group of time series was examined (Table S1). For the real dataset, clusters of real sites were generated using each metric. These clusters from each metric and their identified environmental drivers were compared.

Cross Correlation

Cross correlation is a mathematical technique used to measure the similarity between two signals through time. This technique has been used extensively in signal analysis but can be applied to many types of time series data. In cross correlation analysis, one signal is fixed in place while the dot product is calculated with a second signal as it is translated through time in relation to the first. The result of this operation is information revealing the positive and negative correlations between the two signals for a set of time lags, the number of which depends upon the length of the time series.

The cross correlation of two continuous functions f(t) and g(t) is defined by EQ 1:

$$(f*g)(\tau)=\int_{-\infty}^{\infty}\overline{f(t)}g(t+\tau)dt \quad \text{EQ. 1}$$

Where τ is a displacement or lag in time t and $f(t)$ is the complex conjugate of f(t).

Cross correlation analyses have been applied to ecological systems at multiple scales (Gouhier & Guichard, 2014). Some examples include showing synchrony of sub-populations of multiple fish, bird (Ranta, Lindstrom, et al., 1995), and mammal species in Finland (Ranta, Kaitala, et al., 1995). They have been used to examine the influence of weather on populations of mosquitoes (Chuang et al., 2012) and lepidopterans (Raimondo et al., 2004). Spatial crosscorrelation functions have given insight into host-parasitoid dynamics (Bjørnstad & Bascompte, 2001). Spearman correlation is an alternative analytical technique to cross correlation which is used to characterize monotonic relationships (Jassby & Powell, 1990), but was not considered in this study.

In this study, cross-correlations were computed pairwise for every possible pair of sites. The value of the cross-correlation function at time = 0 (i.e., time lags were not considered) was taken to be the primary measure of synchrony for this method. The cross-correlation computation was performed using the 'ccf' function in the 'stats' package in R. Using the same function, cross correlograms were generated for each pair. The cross-correlation value for each pair was then entered into a correlation matrix before the clustering step outlined below.

Wavelet Transform

The wavelet transform is another powerful tool in signal analysis which has seen applications in many other fields. Wavelet analysis is performed first by selecting a short wave packet known as a wavelet. The wavelet is scaled, translated along the time series to be analyzed, multiplied with that time series at each point. Then, the frequency of the wavelet is increased incrementally, and the process is repeated. The resultant set of waveforms represents a decomposition of the original signal into its component frequencies.

The continuous wavelet transform of a function x(t) is defined by EQ. 2:

$$W_x(a,b)=\frac{1}{|a|^{1/2}}\int_{-\infty}^{\infty} x(t)\,\psi^{\frac{t-b}{a}}\,dt \quad \text{..... EQ. 2}$$

Where a is a scale factor, b is a displacement in time t, and $\psi(t)$ is the complex conjugate of the mother wavelet $\psi(t)$.

Two primary wavelet-based techniques exist for comparing time series data. These are the wavelet cross spectrum and wavelet coherence analyses (Grinsted et al., 2004). Wavelet cross spectra compares the distribution of power of the two signals, revealing any possible time or frequency where they may fall in sync with one another. Meanwhile, wavelet coherence, also called wavelet squared coherence, is a measure of correlation between the two signals. In this study, coherency will be the measure of synchrony for the wavelet-based method, which is similar to the approach used in the 'wsyn' R package (Sheppard et al., n.d.; Pak et al., 2023). One prominent study detailed the wavelet coherence method for time series data while examining a correlation between the winter Arctic Oscillation and the extent of ice in the Baltic Sea (Grinsted et al., 2004). Although wavelet-based techniques are not new, their usage in biological systems has been relatively recent compared to the physical sciences. That said, wavelet analyses are well understood and suitable for ecological time series (Cazelles, Chavez, Berteaux, Ménard, et al., 2008). They have also seen use in linking climatic variables to populations of aphids (Sheppard et al., 2016), lepidopterans (Walter et al., 2020), and gypsy moths (D. M. Johnson et al., 2005). If, instead of wavelet coherence, wavelet cross power were used as the metric, there would be bias toward lower frequencies which would require correction (Ng & Chan, 2012).

The wavelet squared coherence between two wavelet transforms $C_x(a,b)$ and $C_y(a,b)$ is defined by EQ. 3:

$$C(a,b)=\frac{S(W^{x}(a,b)W^{y}(a,b))^{2}}{S(|W_{x}(a,b)|^{2})(W_{y}(a,b)_{2})} \quad \text{EQ. 3}$$

Where S(a,b) is a smoothing operator and $W_x(a,b)$ is the complex conjugate of $W_x(a,b)$.

In this study, the measure of synchrony for this method is the value of pairwise wavelet coherency between two sites for all possible site pairs. The wavelet transform was computed using the 'analyze.coherency' function in the 'WaveletComp' package in R. The wavelet selected in this function was the Morlet wavelet because it can be used to detect signals whose frequency is not constant over time. Wavelet scalograms were generated using the 'wc.image' function in the 'WaveletComp' package. Contours were drawn upon the scalograms showing areas of significant ($p \leq 0.05$) coherency. The p-values for these contours were generated using 1,000 white noise simulations of the data. The cone of influence (COI) present in each of the scalograms denotes the region beyond which boundary effects influence the coherency and therefore become untrustworthy (Cazelles, Chavez, Berteaux, Ménard, et al., 2008). A single coherency value was computed for each pair by taking the mean of all coherency values within that pair's scalogram. The mean coherency value for each pair of time series was then entered into correlation matrix before the clustering step outlined below.

Empirical Orthogonal Function

The empirical orthogonal function (EOF) is used to quantify spatial synchrony through an empirical approach that relies on generating results which are based on underlying structures in the data. EOF analysis first creates a covariance matrix from the original N x M data matrix with N observations (measurements over time) of M variables (locations in space). It then calculates the eigenvectors of that matrix and generates either N or M basis functions depending

upon whether a spatial or temporal EOF is used. The output of an EOF can either be the eigenvectors themselves or a set of principal components called EOF modes.

At its core, EOF analysis is a principal component analysis (PCA) for time series data that additionally accounts for spatial distributions. As is the case with PCA, EOF aims to reduce the dimensionality of the data, allowing one to analyze multivariate processes (Jassby & Powell, 1990). PCA methods for spatial analysis are well-developed (Horel, 1984; Demšar et al., 2013) and have already been used to compare time series data (Yang & Shahabi, 2004).

EOF analysis has seen use in climatology, particularly at global scales (Dai & Wigley, 2000), (Shakun & Carlson, 2010). The influence of these large-scale events on biological systems is a more recent development. One study linked the modes of climate dipoles like the El Niño–Southern Oscillation (ENSO) with a host of ecological response variables in populations and communities at both regional and continental scales (Zuckerberg et al., 2020). It has also been applied in estimating prey density for Pacific fishes (Ueno et al., 2016). Another study using EOF analysis examined synchrony and stability of submerged aquatic vegetation and fishes in the Chesapeake Bay watershed and ground beetles in Phoenix, AZ (Patrick et al., 2021). In this study, all 24 time series were input simultaneously as an N x M matrix in a single temporal EOF operation. Due to the nature of the EOF calculation, pairwise analyses of each site need not be computed. Data were standardized as differences in the relative magnitudes of measurement scales can influence the results (Abdi & Williams, 2010). Principal component values for the combined set of time series were computed using the ‘eof’ function after converting the data into the class STFDF using the ‘STFDF’ function, both from the ‘spacetime’ package in R. The first two principal components were used to generate a plot of each of the 24 sites. The eigenvectors were represented on the same plot by arrows and each one corresponded

to a year in the data set. It is worth noting here that shorter distance in PC space does not necessarily imply stronger synchrony between sites (Elmore & Richman, 2001). This plot was generated using the 'autoplot' function in the 'ggplot2' package in R. The cross-correlation value for each pair was then entered into correlation matrix before the clustering step outlined below.

Hierarchical Clustering and Similarity Index

The correlation matrix from each synchrony metric above was then processed using a clustering algorithm. Hierarchical clustering using Ward's minimum variance method was implemented in R using the 'eclust' function from the 'clusters' package. The output of each was a list of the unique ID or name of each site and which cluster it was found to belong to. For all analyses, the maximum number of optimal clusters was the total number of sites divided by two (10 for simulated data, or 12 for the real data) to force the generation of meaningful clusters (avoiding many small clusters with little interpretation of their meaning), especially for the real data. The list of clusters for a given dataset was then loaded into another script that was used to compute a coefficient of similarity between the cluster lists using Jaccard's index. This index was then used to quantitatively compare, pairwise, which proportion of sites are placed within the same cluster using each synchrony metric.

Data

Simulated Dataset

Two groups of simulated time series were created, a baseline group of 10 time series that had default values for frequency, magnitude, and time lag, plus noise and a treatment group of 10 time series that had a different value of either frequency, magnitude, lag, or noise. Simulated time series were created through the linear summation of two components: a sine wave,

representing the underlying ecological pattern, and high frequency Gaussian noise, representing natural random variations in collected data.

The idealized shape of the simulated data is defined by EQ. 4:

$$Y(t)=A*\sin(t*f*2\pi+L)+M \quad \text{EQ. 4}$$

Where Y(t) is the generated waveform, A is its magnitude, t is time, f is the frequency, L is additional phase lag, and M is a scaling factor to make the generated output values more like positive-valued abundances.

The Gaussian noise component is given by EQ. 5:

$$N(t)=\frac{B*R(t)}{2*Y(t)_{max}-Y(t)_{min}} \quad \text{EQ. 5}$$

Where N(t) is the generated noise component, B is the magnitude of the noise, R(t) is a random number generated by the 'rnorm' function in the 'stats' package in R (mean = 0, sd = 1), and $Y(t)_{max}$ and $Y(t)_{min}$ are the maximum and minimum of Y(t).

The simulated data is then a linear summation of the idealized waveform and the noise component, given by EQ. 6:

$$Z(t)=Y(t)+N(t) \quad \text{EQ. 6}$$

Two base time series were generated using this method where one, the control base time series (also referred to as TS1), had constant parameters (A = 1, f = 1/3, L = 0) and the other, the treatment base time series (also referred to as TS2), had one of these parameters varied over a range (Figure S26). Replicates of both base time series were created through the rerandomization of the Gaussian noise component, for a total of 10 replicates of the "control" time series and 10 replicates of the "treatment" time series. Therefore, the simulated data consisted of two base time series replicated 10 times each for a total of 20 time series per analysis (Figure S27). This was done to characterize the performance of each synchrony metric simultaneously as one

parameter changes across a range of values. Magnitude was varied from A = 1 to A = 9 in increments of 1 and from A = 10 to A = 90 in increments of 10. I expected that differences in magnitude alone could cause groups to differ but ideally there should be only one cluster because any differences in magnitude are still in phase and additive. Frequency was varied from f = 1 to f = 1/9 by varying the period from 1/f = 1 to 1/f = 9 in increments of 1. I expected that differences in frequency alone would cause the control and treatment (TS1, TS2, and their replicates) to diverge into two clusters as each cluster would have its own distinct frequency mode. Phase lag was varied from L = 0 to L = 2π is increments of π/4. I expected that differences in phase lag alone would cause the control and treatment (TS1, TS2, and their replicates) to diverge into two clusters as each cluster would have its own distinct phase (they become less synchronous). The magnitude of the noise varied from B = 0 to B = 5 in increments of 0.5 I expected that differences in the magnitude of noise alone could cause groups to differ but ideally there should be only one cluster because any differences due to random variations in magnitude are still in phase and additive (at least within the selected range of noise values). As one parameter was changed, 10 of the 20 time series, the treatment time series, TS2, and its white noise replicates, were affected while the remaining 10, the control time series, TS1, and its white noise replicates, were not. Thus, perfectly performing synchrony metrics would always result in two clusters of time series. However, I expected that as the changing parameter of TS2 approaches a value equal to that of TS1, the number of clusters will tend toward one. Likewise, as the value for TS2 diverges from that of TS1, the number of clusters will increase to two (or more if the metrics do not perform perfectly). The number of time points for each waveform was fixed at 20, a realistic number of time points for an ecological dataset For all waveforms, M=3 was held constant.

As described previously, the simulated time series were then loaded into an R script that clusters sites based on each one of the three selected metrics of synchrony: CCF, wavelet, or EOF. Hierarchical clustering using Ward's minimum variance was used for clustering, using the 'eclust' function from the 'clusters' package in R. The output of each of these three analytical methods is a list of the unique ID or name of each time series alongside the cluster to which it belonged. The number of clusters generated can either be specified beforehand or be optimized by the algorithm, the latter yielding an optimal number of clusters that best fits the data. A custom script was then used to compute a coefficient of similarity between the cluster lists from the three techniques using an approach based on Jaccard's similarity index. The similarity index and optimal number of clusters were retained for each metric during each iteration.

Phoenix CAP-LTER Pitfall Dataset

I compared clustering from the three synchrony metrics on a real ecological dataset, using a 9-year time series (2006 to 2014) of mean annual abundances of ground beetles at each of 24 sites across Phoenix, Arizona, USA (Figure S25), collected by the Central Arizona Phoenix Long-term Ecological Research site. The Phoenix-Mesa-Chandler metropolitan area covers over 37,000 sq. km and is home to over 4.8 million people (2020 census). It is in the northern part of the Sonoran Desert, characterized by an arid subtropical climate with warm winters and little rainfall. Mean annual temperatures in the Phoenix range from 19.9°C to 25.2°C and mean annual precipitation is around 183 mm. The Phoenix area has a mosaic of habitats including lowland desert, mountainous wooded uplands, residential areas with desert xeriscaping or irrigated lawns, (primarily irrigated) farmland, seasonal rivers, and impervious infrastructure like roads, sidewalks, parking lots, and buildings.

Although beetles were typically collected four times per year, we produced annual estimates of abundance by averaging over the course of each year, yielding mean annual abundance per trap, per sampling, correcting for potential bias in cases where an unequal number of traps were collected. The same three synchrony metrics were used to analyze these data: CCF, wavelet, and EOF. Regardless of the method used, the output was a set of clusters of the time series from each site. Sites with similar time series were clustered together and, therefore, were interpreted to be more synchronous with one another than with sites found in the other clusters. The optimal number of clusters as determined by the algorithm and various predetermined numbers of clusters were examined to explore differences between them. Also, the predetermined number of clusters varied from one to 23, one short of the total number of sites in the dataset, and the resulting cluster similarity index was recorded over that range.

After the site clusters were generated, an attempt was made to justify these clusters using a set of environmental variables collected at each site. The list of variables consisted of mean annual Normalized Difference Vegetation Index (NDVI), mean annual precipitation, mean annual maximum temperature, mean annual minimum temperature, percent impervious surface, elevation, and displacement from the city center. This testing was implemented through an Akaike's Information Criterion (AIC) based approach. First, various linear models were created using the 'lm' function from the 'stats' package in R. The output variable was selected to be the optimal set of clusters from one of the three synchrony metrics while the set of environmental variables listed above were the predictor variables. The AIC value for each model was computed using the 'AIC' function from the 'stats' package in R. The simplest model with the lowest AIC value was used to explain the clusters for each metric.

Results

Simulated Data

For nearly all parameters tested, the clustering behavior of each metric varied, with noticeable differences according to the specific parameter. At equal magnitudes, all three metrics yielded one cluster; there was no difference between the treatment and control time series (Figure 2). As the magnitude of TS2 increased, the optimal number of clusters quickly rose to 10 (differences between time series were identified, but not due to the parameter change alone) for CCF and wavelet or two (closer to the correct number) for EOF (Figure 2). Cluster similarity between CCF and wavelet remained high (0.9) at greater magnitudes while the similarity of EOF with either method was low (0.25; Figure 3).

As expected, when the frequency of TS1 and TS2 were equal (1/3), the three metrics yielded one cluster (no difference between control and treatment, Figure 4). Below this value, CCF and EOF yielded 10 clusters (differences between time series were identified, likely related to the noise component and not due to the parameter change) while wavelet yielded two (the correct number; Figure 4). These clusters were more similar between CCF and EOF (0.85) than either one was with wavelet (0.25; Figure 5). As the frequency of TS2 increased above 1/3, the clusters from all three methods converged to two that were identical (Figure 4; Figure 5). As expected, when the phase lag between TS2 and TS1 was zero, and at the identical phase $+2\pi$, the three metrics yielded one cluster (no difference between control and treatment; Figure 6). With any degree of phase lag between zero and $+2\pi$, both CCF and EOF yielded two clusters with the techniques producing the same cluster composition (the correct number; Figure 6; Figure 7). This behavior differed for wavelet only at $+5\pi/4$ phase lag, where the automated optimal number of clusters became nine (differences between time series were identified, but not due to the

parameter change alone), and was otherwise identical to CCF and EOF (Figure 6). When the noise component for TS2 had zero magnitude, but TS1 had non-zero magnitude, all three metrics yielded 10 clusters (differences between time series were unrelated to the parameter change, but instead seemed related to the differences in time series caused by noise; CCF and wavelet had identical clusters while those of EOF were about 85% similar to CCF and wavelet; (Figure 8; Figure 9). As the noise for TS2 reached unity with TS1, all three metrics yielded one cluster (the expected number, no difference between treatment and control; Figure 8). As the noise for TS2 increased further, the number of clusters from CCF and EOF tended to increase, as did their similarity (differences between time series were identified, but not due to the parameter change alone; Figure 8; Figure 9). Wavelet held constant with one cluster over the entire range (the expected number, no difference between treatment and control; Figure 8).

CAP-LTER Pitfall Data

Visual inspection of time series shows varying patterns over time, suggesting that not all sites are synchronous with each other (Figure S28 and Figure S29). Each synchrony metric yielded different numbers of optimal clusters with notably similar structure at the finer levels of the dendrograms (Figure 10; Figure 11; Figure 12; Spatial maps of these clusters are also provided Figure 14, Figure 15, Figure 16). CCF yielded two clusters while wavelet and EOF yielded one, meaning the optimal clustering of the latter two was unable to split the 24 sites into meaningful groups. Pairwise Jaccard indices of the clusters generated by each method were 0.35 for CCF and wavelet, 0.53 for CCF and EOF, and 0.35 for wavelet and EOF. Closer inspection of the dendrograms reveals sites that are clustered together regardless of the method used (Figure 10; Figure 11; Figure 12). These core groupings become more apparent when manually splitting the sites into greater numbers of predetermined clusters.

Looking at the structure of the dendrograms reveals important site groupings. When a predetermined number of clusters was selected, these core groupings emerge, though their sizes were reduced as the number of clusters increased (i.e., fewer sites were considered highly synchronous with one another). Grouping the sites into a pre-specified two clusters, one can discern consistent (across metrics) sub-groups within the dendrograms (1) AC-16, AD-10, AF12, NDV-C, DREAMY, L-7 and Q-7 (2) AB-19 and AC-20 (3) ADODAM, NDV-X, T-11, U12, and V-14, (4) NDV-O and Y-19, and (5) DBG, I-17, NDV-M, NDV-N, P-18, W-15, and W6, the remaining site, M-16, was inconsistently placed among these core groupings. Grouping the sites into a pre-specified four clusters revealed similar but different sub-groups within the dendrograms: (1) AC-16, AD-10, and AF-12, (2) DREAMY, L-7, and Q-7, (3) NDV-X and V14, (4) T-11 and U-12, (5) DBG and W-15, and (6) I-17 and NDV-N with sites AB-19, NDV-C, AC-20, M-16, Y-19, ADODAM, NDV-O, P-18, NDV-M, and W-6 remaining. Grouping the sites into a pre-specified eight clusters, showed fewer consistent sub-groupings containing fewer sites per grouping: (1) AC-16 and AD-10 (2) DREAMY and Q-7, (3) NDV-X and V-14, (4) I-17 and NDV-N, with sixteen sites remaining. Visual similarities in these pairs can be confirmed by viewing the unprocessed time series data (Figure S28, Figure S29). Combined, these observations suggest that there were actually 4-6 small groups of more highly synchronous sites, but the optimal clustering algorithm missed these.

Cluster similarity between the different metrics was intermediate to low (0.25-0.55) and highly variable for lower number of clusters (two to six), with a maximum at 0.55 between CCF and EOF for three clusters and a minimum at 0.25 between wavelet and EOF at six clusters (Figure 17). There is, however, a near-convergence in similarity of these metrics (0.35) at four clusters (Figure 17). Cluster similarity between all three metrics was far less variable (increasing

from around 0.4 to 0.5) in the range of seven to 12 clusters, with wavelet and EOF performing the most similarly, though marginally so (Figure 17). For high numbers of clusters (13 to 23), cluster similarity increased somewhat linearly from 0.5 to 1.0, with CCF and wavelet performing the most similarly and wavelet and EOF performing the least similarly, especially between 13 and 19 clusters (Figure 17).

The optimal clusters determined by CCF were best explained by the product of mean annual minimum temperature, elevation, and displacement from the city center ($t = 3.081$, $p = 0.0024$; Table S2; model: $F = 10.14$, $df = 15, 200$, adjusted $R2 = 0.3894$). The optimal clusters determined through wavelet and EOF could not be explained using the environmental variables because the optimal number of clusters was one. Two-cluster models, equal in number to the optimal two clusters for CCF, were tested for wavelet and EOF. The two clusters determined by wavelet were not explained well by any of the variables in the leading model. For EOF, the two clusters were best explained by the product of percent impervious surface, elevation, displacement from the city center, and mean annual precipitation ($t = 3.618$, $p = 0.0004$; Table S3; model: $F = 18.6$, $df = 15, 200$, adjusted $R2 = 0.5511$). Synchronous groupings appeared unrelated to distances between sites.

Discussion

Overview

For simulated data, CCF was most capable of differentiating between groups of time series split by a difference in frequency or phase lag but did not perform well when there were large differences in magnitude, high frequency signals, or high noise. Wavelet was most capable of differentiating between groups of time series split by a difference in frequency, a small difference in magnitude, or low to intermediate phase lag, and it was the most tolerant of noise,

but it did not perform well when there were large differences in magnitude or maximal phase lag. EOF was most capable of differentiating between groups of time series split by a difference in phase lag, greater magnitudes, or higher frequencies but did not perform well when there were high frequency signals or high noise. For the real dataset, similar groups of highly synchronous sites were identified using all three metrics, but these groups were not correctly separated by the automated optimal cluster algorithm for any synchrony metric. The environmental drivers that explained each cluster varied, with elevation and displacement from the city center identified as key drivers. Further, our results implicate environmental conditions more than dispersal as drivers of synchrony within this metacommunity.

Simulated Dataset

The characterization of each metric using the simulated data reveals the differential sensitivities of each metric to individual parameters. CCF worked well for differences in frequency or phase lag, but not for large differences in magnitude, high frequency signals, or high noise. At greater magnitudes, CCF incorrectly yielded a large number of clusters, . Similar behavior was observed at high frequencies. At low frequencies or with any non-zero phase lag, the number of clusters using CCF was reduced to just two, correctly separating the two base time series by the two values of those individual parameters. Noise with a magnitude of 0.5 to 1.5 times that of the base time series, that itself had a noise magnitude of 1, made any clusters unrecognizable (control and treatment time series were identical) while noise with a magnitude beyond that upper bound led to a large number of clusters (until each site is its own cluster) on average. At this point, clustering would be increasingly driven by variations due to noise. High noise and high frequency signals are both difficult for this metric to handle, perhaps owing to their similar frequency scales which affect every time point. Taken together, CCF performed

incorrectly for large differences in magnitude, high frequencies, and intermediate to high noise but did correctly differentiate between groups of time series split by a difference in frequency or phase lag.

Wavelet worked well for differences in frequency, low to intermediate phase lag, and all levels of noise, but it not for large differences in magnitude or maximal phase lag. At a smaller difference in magnitude (TS2 being twice TS1), wavelet yielded a low number of clusters (but two rather than the expected single cluster). At all frequencies or with most phase lags, the number of clusters using wavelet was reduced to just two, correctly separating the two base time series by the two values of those individual parameters. There was, however, a spike near the maximal phase lag (at $+5\pi/4$) where the number of clusters incorrectly rose to nine even though the cluster structure was correct and identical to both CCF and EOF—given the cluster structure was correct, this is likely a failing of the algorithm used to generate an optimal number of clusters. Noise did not influence wavelet-based clustering, with noise magnitudes between 0.5 and 5 considered no different from the base time series where the magnitude of noise was 1. Taken together, wavelet performed incorrectly for large differences in magnitude and high phase lag (if using the optimal cluster algorithm) but is insensitive to noise, the latter likely due to the white noise simulations built into the wavelet coherence function. Wavelet was also able to correctly differentiate between groups of time series split by a difference in frequency, a small difference in magnitude, or low to intermediate phase lag.

EOF worked well for differences in phase lag, magnitude, or higher frequencies but not for high frequency signals or high noise. At greater magnitudes, low frequencies, or with any non-zero phase lag, EOF yielded two clusters, correctly separating the two base time series by the two values of those individual parameters. At high frequencies, EOF incorrectly yielded

many clusters. EOF was largely unresponsive to stronger noise, with noise magnitudes between 0.5 and 1 and between 2 and 3 considered no different from the base time series where the magnitude of noise was 1. This is excluding the spike in the number of clusters when the noise magnitude was 1.5. When the noise magnitude exceeded 3, the number of clusters incorrectly rose. At this point, clustering would be increasingly driven by variations due to noise. High noise and high frequency signals are both difficult for this metric to handle, perhaps owing to their similar frequency scales which affect every time point. Taken together, EOF was incorrect for low frequencies and high noise. EOF was able to correctly differentiate between groups of time series split by a difference in phase lag, greater magnitudes, or higher frequencies.

Pairwise similarities between the three metrics can be observed from the cluster similarity indices. CCF and EOF performed identically at differences in higher frequencies and at all phase lags and they are increasingly similar at greater magnitudes of noise. They were dissimilar when magnitude differences were greater and at intermediate levels of noise. CCF and wavelet performed identically at differences in low frequencies and low to intermediate phase lags. They performed similarly at greater differences in magnitude and low noise. They performed dissimilarly at higher frequencies, with high phase lag, and with greater noise. Wavelet and EOF performed identically with smaller differences in magnitude, high frequencies, low to intermediate phase lag, and with low to intermediate noise. They performed dissimilarly at greater differences in magnitude, differences in higher frequencies, at high phase lag, and with greater noise. Pairwise, CCF and EOF seemed to perform more similarly with one another than either one did with wavelet for the simulated data, though all three behaved similarly with minor differences.

CAP-LTER Dataset

The pairwise similarity indices for the CAP-LTER clusters suggest that wavelet and EOF performed more identically (1.0) while either one individually had intermediate similarity with CCF (0.53). However, regardless of which metric was used, the optimal cluster algorithm yielded sites placed into several core sub-groupings, highly synchronous site pairs, mentioned above. These highly synchronous sub-groups were recognized by CCF, wavelet, and EOF, but the number of clusters considered optimal varied by method (CCF = 2, wavelet = 1, EOF = 1), and none of the optimal clusters identified the common highly synchronous groups as separate clusters. When one metric clusters all sites together (clusters = 1), and another splits the sites into two equal clusters, then only one half of the sites can belong to the same cluster when examined pairwise. Therefore, the approximate maximum similarity indices for each pair given these cluster numbers are: CCF-EOF = 0.5, CCF-wavelet = 0.5, and wavelet-EOF = 1.0, though these values would be marginally increased if the clusters are of unequal size. Constrained by the optimal number of clusters, the CCF-EOF and CCF-wavelet pairs could not be more similar than they already were.

Though the limiting factor for the similarity indices appears to be differences in cluster size, forcing a cluster size did not necessarily lead to a greater similarity index value (Figure 17). This becomes apparent when viewing the dendrograms (Figure 10, Figure 11, Figure 12) as the clustering technique separated the clusters from the top-down. Though these highly synchronous pairs were divided into groups, there are small differences between them, including overlap, and noticeable differences in their heights along the dendrograms. These highly synchronous site pairs were reduced by an increasing number of forced clusters that varied by the method used. The near convergence in cluster similarity between the three metrics at four clusters may

represent the ideal number of clusters for this dataset in determining the groupings of highly synchronous sites. This may represent an alternative method for determining the optimal number of clusters.

Several spatial patterns can be identified from these highly synchronous site clusters. From the two-cluster pairs, (1) sites AC-16, AD-10, AF-12, and NDV-C are all located on the eastern edge of the city or into the surrounding mountains (Figure 14, Figure 15, Figure 16). L-7 and Q-7 are far from the others but are close to one another and also outside of the city. DREAMY is located more centrally and quite distant from the other sites, which stands out from the others. (2) AB-19 and AC-20 are next to one another near the southeast edge of the city. (3) ADODAM, T-11, U-12, and V-14 are close together near the northern edge of the city, but far from NDV-X. Still, NDV-X is at the southwest edge of the city. (4) NDV-O and Y-19 don't appear especially similar geographically. Lastly, (5) the pairs NDV-M and NDV-N and DBG and W-15 are close together. P-18 and I-17 are at the southwestern edge or outside of the of the city, respectively, while W-6 is outside of the city to the north. The eight-cluster highly synchronous pairs are also of interest, as only (1) AC-16 and AD-10 seem reasonably close to one another while (2) DREAMY and Q-7 and (4) I-17 and NDV-N are halfway across the map as one another and (3) NDV-X and V-14 are on opposite sides of the city. These latter clusters suggest that distance between sites may not be a strong driver of cluster synchrony in this system.

High rates of dispersal can theoretically increase synchrony among locations (Kendall et al., 2000; Leibold et al., 2004). However, the cluster of sites in the southwest (NDV-N, -X, -C, O, and -M), were never clustered together despite the short distances between them. In this system, dissimilarities between many of the sites that are close to one another, suggests that dispersal is unlikely to be driving synchrony. Perhaps this is not surprising given that ground

beetles are unlikely to disperse further than 500 m in their lifetime (Baars, 1979) and are often thought to be sensitive to local environmental conditions (Rainio & Niemelä, 2003). Moreover, cities are heterogeneous places where proximity in space does not necessarily mean similarity in environmental conditions for these species (McIntyre et al., 2001; Magura & Lövei, 2021). It therefore appears more likely that similarity in local environmental conditions within the urban and natural areas are driving these patterns of synchrony more than dispersal between sites near one another.

The optimal site clusters from CCF were best explained by the product of mean annual minimum temperature, elevation, and displacement from the city center ($t = 3.081$, $p = 0.002$). These three factors may be interrelated due to the urban heat island effect, as minimum temperatures in Phoenix in the summer (Balling & Brazel, 1987) and winter (Hsu, 1984) are lower outside of the city proper. Minimum temperatures are known to decrease at higher elevations as well. As the city of Phoenix is within the Salt River Valley, increasing displacement from the city center would involve increasing elevation up into the surrounding mountains. The two site clusters from EOF were best explained by the product of percent impervious surface, elevation, displacement from the city center, and mean annual precipitation ($t = 3.618$, $p = 0.0004$). These variables are also likely interrelated, as precipitation in the Salt Valley is greater in the surrounding mountains, which are further from the city, higher in elevation, and have less impervious surface. Also, percent impervious surface tends to be greater toward the city center than at the margins or outside the city. Site groupings obtained via wavelet might implicate similar driving variables, but the optimal and two-cluster scenarios did not support such a conclusion. Either way, both CCF and EOF identified elevation and displacement from the city center as important variables in forming their clusters. This lends further support to

the idea that similarity in certain environmental conditions is driving these patterns of synchrony.

Strengths, Weaknesses, and Complementarity

Addressing the differences between the results of the three analytical methods is also a matter of examining the strengths of each method. The CCF reveals synchrony throughout the entire time series at zero lag. It can also reveal time lagged effects of other factors on population dynamics. For example, trophic interactions can appear as time-lagged events with similar patterns (Liebhold et al., 2004). Time lagged dynamics have also been observed in populations of moths in relation to outbreak events (Tenow et al., 2007) but also are associated with dispersal events (Martin et al., 2017). We are unaware of studies of dispersal of other non-carabid ground beetles (e.g. tenebrionids, which were abundant in our data set), but their dispersal across significant distances seems less likely, especially within cities with both natural and artificial barriers to dispersal. Drivers of synchrony, as in the effects of weather and climate, often have time lagged components and, if the appropriate time scale is captured by the data, could be observed in the study populations (Orell et al., 2007; Tenow et al., 2007).

Unlike the other two methods, wavelet analysis can assess correlations within a piece of the time series rather than only the entire sequence (Cazelles, Chavez, Berteaux, Menard, et al., 2008; Carey et al., 2013). It also examines different frequencies within those sections, revealing frequency modes within the data that the other techniques are less able to do, like those correlated with periodic climate oscillations. For example, populations of aphids are synchronous at a similar timescale due to winter climate shifts driven by the North Atlantic Oscillation

(Sheppard et al., 2016). Synchrony in dengue fever outbreaks (caused by mosquitos) driven by ENSO in Thailand has a period of 2-3 years (Cazelles et al., 2005). Identification of such frequency modes are important in determining the drivers of synchrony in populations or communities and how that frequency may change in time (Walter et al., 2017).

The EOF method offers an empirical approach to clustering sites according to their synchrony. In addition, EOF could cluster sites based on nonlinear relationships that the two other techniques are not well-equipped to detect (Andersen et al., 2009). Optimal cluster size limited the interpretive power of these results in our study more than the actual cluster structure. All things considered, the grouping of similar time series together by this PCA-based method is a quick and simple process that offers complementary information to other methods, similar to data exploration via ordination (Haynes et al., 2013).

Though use of an optimal cluster algorithm is convenient and objective, it seems to have obscured ecologically interesting patterns within our CAP-LTER dataset and led to non-sensical results for particular scenarios within the simulated data. Though each synchrony metric generated a different hierarchical clustering dendrogram, closer inspection of those dendrograms allowed us to identify groups of highly synchronous sites common to all three metrics. These same groups were not revealed by the optimal clusters alone. Additionally, the automatically generated optimal number of clusters can yield counterintuitive results, as was the case with wavelet at high phase lag. Thus, we present an alternative to optimal clustering algorithms which relies instead on comparing fine-scale structure of clusters across multiple metrics of synchrony. In theory, a longer time series would strengthen the power of all three methods. For instance, some studies suggest that the criteria for spectral analysis of time series having at least 25 points and detecting periods less than one third of that length (Murdoch et al., 2002). This is a

drawback of the wavelet analysis as the Fourier period is limited to the range of two to three years. Also, the first and last two years of the time series fall entirely outside of the cone of influence (COI) in the scalograms and are therefore subject to boundary effects. Low frequency modes became increasingly harder to verify as the COI narrows toward these frequencies. The result is a greater focus on patterns of synchrony at higher frequencies that happen to fall in the middle years of the time series. Any strong correlations that may be present near the ends of the time series then become clouded with uncertainty. This is likely a problem for both CCF and EOF as well, but the degree to which this issue impacts each method requires additional study. The risk of results tainted by edge effects using one method could be diminished by the complementary results of the others. The groups of highly synchronous sites that all three methods agreed upon are likely to be robust, even for short time series. We also note that our use of annual means could be hiding important interannual patterns of synchrony in this system or patterns at lower frequencies (longer time spans) that are not captured by the data. Taking wavelet analysis as an example again, Fourier periods shorter than two years were unable to be represented in the scalograms.

Finally, the measured quantity being examined for synchrony is also an important consideration. Here, we examined total abundance of a particular functional group from a particular order of arthropods. Other studies have examined the synchrony of abundance of particular species (Raimondo et al., 2004; Loreau & de Mazancourt, 2008; Vendrametto Granzotti et al., 2022), of species or community-level biomass (Batchelder et al., 2012) or species richness (Özkan et al., 2016). Such quantities may have different patterns, frequency modes, or drivers.

Conclusions

Characterization of the three synchrony metrics, cross-correlation function, wavelet coherency, and empirical orthogonal functions, revealed small differences in response to changes in single parameters. These metrics were differentially sensitive to the magnitude, frequency, phase lag, and white noise components of simulated time series data. When applied to a real dataset, the clusters from each method helped identify groups of highly synchronous sites, but the environmental drivers of those clusters were dependent upon the structure of those clusters, leading to different interpretations of which variables are most important. Therefore, we recommend the use of multiple synchrony metrics for cross-validation that builds a more informed result with greater insight into the underlying patterns and their respective drivers.

CHAPTER II. COMMUNITY ASSEMBLY AND DYNAMICS OF TEMPORARY WETLAND MACROINVERTEBRATES DRIVEN MORE BY REGIONAL SPATIAL VARIATION IN EGG BANKS THAN BY HEATING IN THE NORTH AMERICAN GREAT PLAINS

Abstract

Communities assemble and change over time due to the complex interactions of environmental conditions, historical trajectory, and species interactions. This array of factors acting upon a potential species pool ultimately determines community dynamics. Temporal variation is also rather high within temporary wetlands, leading to rapidly shifting conditions and frequent disturbance over short and long timescales. Temperature, for example, is known to have an important effect on the hatching success of dormant invertebrate eggs and yet it varies considerably in space and time within seasonal wetlands. Although these sorts of variables are known to influence one another, the subsequent effects on entire wetland communities not well known. In this study, assembly and dynamics were investigated for impermanent wetland invertebrate communities in mesocosms containing dry wetland sediments collected from across

the North American Great Plains. Three factors were manipulated in combination: the source sediment, a small temperature differential, and water drawdown (disturbance) halfway through the experiment. The results indicate that the sediment source had a strong effect on populations of egg bank forming crustaceans and, therefore, community assembly, with additional differences in community structure arising over the course of the experiment. The strong effect of sediment source may indicate dispersal limitation of these invertebrates across the Great Plains, although more work is needed to confirm this. The drawdown had a negative effect on cladocerans and damselfly larvae, but a positive effect on tadpole shrimp. Heating had a positive effect on clam shrimp abundances, but only in the absence of a drawdown. These results indicate that spatial variation in ephemeral wetland egg banks across the Great Plains is high and that small changes in temperature and disturbance can influence community assembly and dynamics in impermanent wetlands, but responses vary by taxon, complicating the predictions regarding the impacts of climate change on these systems.

Introduction

Community structure continuously changes over time while under the influence of an interrelated set of factors in a process termed community dynamics. A framework of the initial stages of community dynamics, often termed community assembly, is a common approach to understanding the processes through which an ecological community arises. These processes include dispersal, species interactions, environmental conditions, and regional context (E. S. Lindström & Langenheder, 2012) which themselves act upon the local and regional species pools (Weiher et al., 2011; Kraft et al., 2015). Historical development (Chase, 2003), or trajectory, plays an important role in subsequent community dynamics as do stochastic demographic processes (Auger et al., 2008). Similar sets of conditions may lead to convergence in traits (Matthews et al., 2009; Frazier & Schriever, 2022) or community structure or alternatively may produce multiple stable states (Drake, 1991; Chase, 2003). Though many factors affecting community dynamics have been identified, their relative strengths and interactions are likely context-dependent (Batzer, 2013).

Impermanent wetlands are ideal systems in which to study community assembly and dynamics (*e.g.* Kneitel, 2014). These wetlands feature standing water lasting for days to weeks to months and completely dry out during a typical year. This creates a high degree of temporal variability in habitat conditions within a wetland basin (Beeri & Phillips, 2007; de Almeida et al., 2015). Obligate aquatic organisms will only survive during the brief period of standing water while facultative and more mobile organisms may relocate when conditions deteriorate. The resident fauna seasonal wetlands are typically high mobility organisms, moving between wetlands by themselves or using other mobile organisms as a vector (Sim et al., 2013).

Obligately aquatic invertebrate populations may only persist across years in a wetland basin if they can withstand the frequent dry periods through dormancy (*sensu* Chesson, 1983) or relocate to more permanent bodies of water. One such adaptation which allows for long term, localized persistence in the face of uncertain environmental conditions is the formation of dormant reproductive propagules like seeds or resting eggs (*e.g.* De Stasio & Hairston, 1992; Levine & Rees, 2004) like the cysts of Branchiopod crustaceans. These cysts are drought tolerant, can withstand extreme temperatures, and may remain viable after decades of dormancy (Brendonck, 1996; Fryer, 1996). Once deposited into the wetland, they remain in a state of quiescence, only to be broken by external cues that signal favorable environmental conditions (Brendonck, 1996). Localized accumulation of these propagules leads, in turn, to the formation of an egg bank within the basin (Brendonck & De Meester, 2003; Waterkeyn et al., 2009). Temporary wetlands often contain propagule banks of crustaceans, including organisms of the orders Branchiopoda, Copepoda, and Ostracoda (termed egg bank forming crustaceans). Although some egg bank forming crustaceans are cosmopolitan in their distributions, it is unclear how often the reproductive propagules of these organisms are moved and across what distances.

Upon deposition, the hatching dynamics of dormant reproductive propagules are greatly influenced by environmental conditions and the timing of those conditions. Water temperature can influence both how quickly (hatching rate) and what proportion (hatching percentage) of these propagules become active (Atashbar et al., 2014; Radzikowski et al., 2018). Additional cues are provided by other factors like light (Vanhaecke et al., 1981), dissolved oxygen (Brendonck, 1996), salinity (Atashbar et al., 2014), and pH (Schönbrunner & Eder, 2006). Differences in these conditions can lead to vastly different communities, even when the propagule egg bank is the same (Kneitel, 2014; Mushet et al., 2019). Thus, understanding

variation in these environmental conditions is important. Soranno et al., (2019) found that spatial variation in wetland parameters between wetlands in a Northeast US macrosystem was greater than temporal variation within those wetlands. Great spatial variation then leads to greater divergence among the communities in those systems as the organisms in those communities adapt to the local conditions. For example, *Daphnia* ephippia collected from permanent waters hatch at lower percentages, slower rates, and with peaks of hatching at lower temperatures than those collected from temporary waters (Radzikowski et al., 2018). Interannual variation in conditions must still be considered, as egg bank forming invertebrates in temporary wetlands complete their entire life cycle within a period of days to weeks, whenever that period might happen to occur. In theory, a wetland's egg bank that has developed over decades would contain a resilient, highly diverse assemblage which could respond to a range of environmental conditions (*e.g.* Hairston Jr., 1996; Mushet et al., 2019). Thus, hatching dynamics, environmental conditions, and community assembly processes all interact with one another in a highly complex way, making it unclear how a given system will behave as it assembles.

Variability in environmental conditions also play a major role in these systems. Global and regional climate change pose a potential threat to the conservation of impermanent wetlands, though the likely impacts are currently unclear. Changes in temperature and precipitation are expected to alter the number, surface area, and hydroperiods of these wetlands globally (W. C. Johnson et al., 2005; Junk et al., 2013; W. C. Johnson & Poiani, 2016; Lefebvre et al., 2019). Shorter hydroperiods place a constraint on aquatic invertebrates by reducing the amount of time they have to hatch, develop, and reproduce before the pool dries. Changes in the timing rather than the magnitude of precipitation events can be just as impactful (Schalau et al., 2008). Kneitel (2014) found that the timing of inundation had a greater impact on wetland community assembly

than the length of the hydroperiod. In some cases, greater environmental variability may benefit some functional or taxonomic groups and harm others (Levine & Rees, 2004; Domisch et al., 2011).

Changes in temperature may also have direct effects on temporary wetland macroinvertebrates. Pinceel et al., (2018) found that survival rates of propagules of fairy shrimp (*Branchipodopsis wolfi*) declined and hatching percentages increased with elevated temperatures.

However, entire communities, with variable responses to temperatures, might be expected to be resistant to these temperature shifts, given the range of conditions they may encounter during wet periods in any given year. The combination of changes in historical environmental conditions, greater variability in those conditions, and the differential responses of organisms to those conditions make it difficult to predict the impacts of climate change on even a single wetland community. Additional studies are key in better understanding these dynamic processes and systems.

In this study, we describe a test of the relative importance of several primary drivers of seasonal wetland macroinvertebrate community assembly using a common garden, in-field mesocosm experiment wherein temperature, sediment source, and disturbance (via drawdown) are manipulated. We predict that due to dispersal limitation and local filtering, the divergent compositions of egg banks collected from various sites (i.e., sediment source) will yield differing communities, with additional changes in trajectory compounding due to differential heating and added disturbance. In particular, we predict that (1) wetland sediments collected from a wider range of sites will contain a more diverse assemblage of organisms than the locally-collected sediment resulting from the larger range of climatic and geographic diversity; and that both (2)

additional heating and (3) drawdown will differentially impact the taxa present due to differences in life history, nutritional requirements, and behavior.

Methods

Mesocosm Study Site

Extending from Mexico through Canada, the North American Great Plains contains a multitude of wetlands of varying permanence. These wetlands are connected via several potential dispersal vectors of macroinvertebrate propagules in the form of migratory waterbirds (Figuerola & Green, 2002; Brochet et al., 2010; van Leeuwen et al., 2012; Costea et al., 2016), large mammals (Vanschoenwinkel, Gielen, Vandewaerde, et al., 2008), strong winds (Graham & Wirth, 2008; Vanschoenwinkel, Gielen, Seaman, et al., 2008), and human activity (Waterkeyn et al., 2010). Coinciding with this region is the North American Central Flyway, a major migration route for several million waterfowl and shorebirds each year (Olson, 2021). The northern terminus of this route is the massive wetland complex known as the Prairie Pothole Region (PPR) of the United States and Canada. The region covers over 770,000 km^2 in south-central North America and includes some 3.44 million wetlands covering an estimated 3.68 million ha, around a quarter of which is temporary or seasonal wetlands (Doherty et al., 2018). The PPR is geologically young, only existing in its current state since the end of the Pleistocene glaciation (Doherty et al., 2018). Since then, numerous species of aquatic macroinvertebrates have established populations in the PPR.

Sediment Collection and Preparation

In each of five states, North Dakota, Colorado, Kansas, New Mexico, and Texas, five dry wetlands were selected for sediment collection with two criteria as constraints: (1) the wetlands are temporarily or seasonally flooded, with standing water lasting for weeks or up to several

months and drying completely in a typical year and (2) the wetlands are expected to or have prior evidence of the presence of branchiopod crustaceans. For wetlands which were not entirely dry, we collected from the parts of those wetlands without standing water. Sediments were collected in late summer to early fall of 2020 when most seasonal wetlands throughout the range were expected to be dry. At each wetland, the top 2 cm of sediment were collected at various locations within the wetland basin, ensuring that the center, edges, and the regions in between would be represented within the sample.

Following collection, the sediments collected in North Dakota were transported back to Bowling Green State University and thoroughly mixed. Half of the collected sediment was shipped to a centralized location at the University of Kansas for further mixing and redistribution. The sediments from all locations were mixed at the University of Kansas in a cold storage building in December of 2020 using the cone and quarter method (Campos-M & Campos-C, 2017) to create a homogeneous, 5-state mixture which, for the purposes of this study, will be called “mixed sediment”. Likewise, an equal amount of unmixed sediment collected from the North Dakota sites was shipped directly to the field site in North Dakota (hereafter called “local sediment”). Upon arrival at the field site in January 2021, all buckets remained sealed and were placed in a shaded spot outdoors for winterization.

Experimental Design

An in-field mesocosm experiment was conducted in the spring of 2021, beginning on May 19th and ending on June 30th (42 days). A field location was selected in the US Fish and Wildlife’s Chase Lake Wetland Management District Headquarters near Woodworth, ND (approximate GPS coordinates: +47.134253, -99.243489) which also doubles as a NEON site. In this experiment, forty 100-gallon HDPE stock tanks were arranged in a five-by-eight

randomized array. To each mesocosm, commercially available topsoil was added to a depth of 2.5 cm which was then covered by commercially available play sand to a depth of 2.5 cm. The mesocosms were then filled with water to a depth of 30.5 cm which was maintained over the six-week duration of the experiment. During filling, tap water conditioner (API Tap Water Conditioner) was added to remove chlorine compounds. After filling, each mesocosm was seeded with 800 grams of either the local or mixed sediments. Two stems of an aquatic macrophyte,

Ceratophyllum demersum, were added to each mesocosm for two main reasons: (1) to maintain water chemistry, notably to reduce soluble reactive phosphorus (Zhang et al., 2021) and excessive algal growth (Romo et al., 2004) and increase dissolved oxygen, and (2) to provide habitat structure for both predators and prey. A fiberglass window screen was used to cover each mesocosm to reduce the influx of colonizing insects, as the focus of this study was on sediment egg bank forming crustaceans.

Three factors were manipulated in combination for a total of eight treatment groups consisting of five mesocosms each. The first factor was sediment origin, with sediments collected from either five dry wetlands in the ND PPR (local sediment) or an equal mixture of sediment from five wetlands in each of five states along the Central Flyway (mixed sediment). The second factor was the presence or absence of a two-day drawdown to a depth of 5 cm of water as a disturbance event. For the mesocosms which this was applied, the drawdown occurred at the end of week three of the experiment. At the start of the drawdown period, water in the mesocosm was filtered through a sampling net and removed using a 74.6 W transfer pump. At the end of the drawdown period, water was added to the mesocosms by hose until the water depth was brought back up to 30.5 cm. The third factor was a heat treatment applied to the entire

mesocosm. An open-top greenhouse with a rectangular wooden frame and walls of polyethylene sheeting was constructed around the individual mesocosms. The ceiling was omitted in this greenhouse design in order to avoid unwanted changes in the intensity and spectral composition of the incoming sunlight. Continuous temperature loggers (HOBO Pendant, Onset) were submerged within 19 of the 40 mesocosms to record the water temperature at one-hour intervals. Diagrams and photographs of the experimental setup can be found in Figure S37 through Figure S41 the Supporting Information.

Sample Collection

Over the course of the experiment, non-destructive samples of the aquatic macroinvertebrates were collected every three days by dip net for a total of 14 samples. Each sample was composed of six standard net sweeps using a 15.2 x 20.3 cm aquarium net with a mesh size of 0.8 mm. Each mesocosm had its own net to reduce cross-contamination. One sweep was taken just below the water's surface along the longer dimension of the mesocosm, another was taken in the same location but halfway down the water column. A third and fourth sweep were taken at the bottom of the water column just above the substrate along the short dimension of the mesocosm. The fifth and sixth sweeps were taken vertically upward along the walls of the mesocosm. The contents of each sweep were rinsed into a white plastic dish bin. For these samples, organisms were counted, identified in the field to order, and then returned to the mesocosms alive. If a population within the sample was too large to be practically counted, a subsample of a countable number of organisms was taken. The volume of the sample and the subsample were recorded and used to scale up the population in the subsample to the size of the sample. Alongside each non-destructive sample, specific conductivity, pH, percent dissolved

oxygen, and turbidity were measured using a sonde (YSI, ProDSS). Diagrams and photographs of the sampling procedure can be found in Figure S42 through Figure S46 in the Supporting Information.

Statistical Analysis

To examine how the relative abundance of each taxa responded to each treatment individually, over time, I employed multivariate generalized linear regression according to Szöcs et al. (2015), henceforth referred to as multivariate generalized linear model (MVGLM). MVGLM fits a separate GLM to each taxon using a negative binomial distribution which was found to offer a better fit than a Poisson distribution for the current dataset. Then, it combines those GLMs using a sum-of-likelihood-ratios statistic. In this method, p-values are generated through permutation. I selected 50 permutations of the data to generate these p-values and limited permutations by specifying each individual mesocosm as a stratum. The univariate response of each taxon can be viewed, relative to others, since each one is initially fitted to a separate GLM and the contribution of each is given by a deviance value. These deviance values were then plotted over time for visualization.

Because the MVGLM can only examine the influence of one factor at a time, we explored interactions of multiple factors on each taxon's abundance through repeated measures ANOVA using the 'ezANOVA' function from the 'ez' package in R. For taxa violating the normality and/or equal variance assumption(s), a square root transform was applied. The taxonomic response variables not corrected by this transform were not analyzed on their own, as these abundances tend to have few and inconsistent observations.

To determine the response of the water temperature to the heat treatment, hourly temperature values for each calendar day were summarized into mean daily water temperature.

These mean daily temperature values were then analyzed using a repeated measures ANOVA using the ‘ezANOVA’ function from the ‘ez’ package in R.

Population growth rates between treatments were compared using breakpoint regression. First, the logarithm of the total abundances grouped by each single treatment were calculated. To avoid undefined values from taking the logarithm of zero, a single count was added to every total abundance value. These values were then converted to a linear function using the ‘segmented’ function from the ‘segmented’ package in R. In practice, this is equivalent to fitting the total abundance over time to two separate exponential functions, wherein the first segment corresponds to unlimited growth and the second segment corresponds to some lower rate, be it limited growth, decline, or stagnation. The point of transition between the two segments is the breakpoint. A graphical representation of this curve is shown in Figure S47 in the supplementary materials. Three model parameters were taken from these curves: the breakpoint, the slope before the breakpoint, and the y-intercept. Changes in these model parameters between experimental treatments were determined through ANOVA using the ‘ezANOVA’ function from the ‘ez’ package in R.

Synchrony Analysis

Synchrony between mesocosms was assessed using the CCF clustering algorithm from Chapter I. Time series of total abundance and order-level richness for each mesocosm were used as input. The resulting output is a dendrogram and a list containing the clusters to which each mesocosm best belongs. Cluster listings for 2-, 4-, and 8-cluster scenarios were generated, each of which can be verified on the corresponding dendrograms. These cluster numbers reflect the scenarios where one factor (2-cluster), two factors (4-cluster), or three factors (8-cluster) measurably influenced these community-level metrics, separating them by each of the two levels of those factors. Any influence of these factors as drivers of the clusters were determined by

visual assessment of cluster structure within the dendrograms and calculation of percentage of replicates of each treatment within each cluster.

Results

Organisms

The organisms present included six Orders of egg bank-forming crustaceans: Anostraca (fairy shrimp), Spinicaudata (clam shrimp), Notostraca (tadpole shrimp), Cladocera (water fleas), Ostracoda (seed shrimp), and Copepoda (copepods). Also present were aquatic insects and their larvae: Coleoptera (beetles), Culicidae (mosquitoes), Chironomidae (midges), Zygoptera
(damselflies), Corixidae (water boatmen), and the related Acari (mites).

Heat Treatment

The difference in the long-term average temperature due to the heat treatment was approximately +1.1 °C. The heat treatment generated a significant difference in temperature between the two groups of mesocosms ($F = 47.09$, $df = 1, 16$, $p = 3.82e\text{-}6$; Table S4, Figure S49). We did not detect an interaction of this heat treatment with time, suggesting a relatively constant effect throughout the experiment. The average water temperature of the mesocosms without heating over the entire experiment was 18.7 ± 0.055 °C (mean ± SE) while the same measurement for those with heating was 19.8 ± 0.055 °C (mean ± SE).

Community Responses (Multivariate Generalized Linear Models)

The MVGLM was conducted for each of the three manipulated factors to examine how abundance-level effects of each order varied through time. The factor with the greatest impact on the community was sediment source (res. $df = 531$, deviance = 1264, $p = 0.001$; Table S5), with greater abundances in the mixed sediment than the local for the egg bank forming crustaceans

Anostaca (fairy shrimp; deviance = 640.457, p = 0.001; Table S6, Figure S48), Spinicaudata (clam shrimp; deviance = 262.657, p = 0.001; Table S6, Figure S48), Cladocera (water fleas; deviance = 63.688, p = 0.001; Table S6, Figure S48), Copepoda (copepods; deviance = 29.048, p = 0.040; Table S6, Figure S48), Ostracoda (seed shrimp; deviance = 32.87, p = 0.015; Table S6, Figure S48) as well as Amphipoda (scuds; deviance = 0.015, p = 0.015; Table S6, Figure S48). Chironomidae (midge larvae) showed the inverse relationship, with greater abundances in the local sediment than the mixed (deviance = 33.329, p = 0.014; Table S6, Figure S48). Only one of the six egg bank-forming crustaceans present, Notostraca (tadpole shrimp), did not show a detectable effect due to the sediment. The effect of the sediment on populations of Anostraca (fairy shrimp), Copepoda (copepods), Ostracoda (seed shrimp), Amphipoda (scuds), and Chironomidae (midge larvae) were shown to be time invariant, with a relatively constant effect over the course of the experiment, while the effect on Spinicaudata (clam shrimp; deviance = 684.026, p = 0.001; Table S7, Figure S50) and Cladocera (water fleas; deviance = 32.164, p = 0.015; Table S7, Figure S50) varied through time. Spinicaudata (clam shrimp) populations arising from the mixed sediment began to grow around day 15-18, peaked around day 27, and declined until the end of the experiment, while those arising from local sediments remained near zero but started to grow on the final day of the experiment. Cladocera (water flea) populations arising from the mixed sediment began to grow around day 15-18, peaked around day 24, and declined until the end of the experiment, while those arising from local sediments began to grow around the same time, never reached a defined peak, and continued to grow throughout the entire experiment (see Supplementary Information). The drawdown reduced the abundances of only Zygoptera (damselfly nymphs) (deviance = 35.516, p = 0.008; Table S8, Figure S51). We did not

detect a change in community composition or any Order's abundance due to the heat treatment alone.

Total Abundance, Diversity, and Individual Taxonomic Responses (Repeated Measures ANOVA)

Community-level total abundance ($F = 4.467$, $df = 1, 32$, $p = 0.0.042$; Table S15, Figure S52) and abundance of Cladocera ($F = 17.099$, $df = 1, 32$, $p = 0.030$; Table S10, Figure S52) were greater in the mixed sediment mesocosms than the local, with a relatively constant difference over the experiment. Similarly, there was a positive effect of the mixed sediment on community richness ($F = 115.653$, $df = 1, 32$, $p = 3.716e\text{-}12$; Table S16) and Shannon diversity ($F = 5.746$, $df = 1, 32$, $p = 0.022$; Table S17), the egg bank forming crustaceans Spinicaudata (clam shrimp; $F = 11.124$, $df = 1, 32$, $p = 0.002$; Table S9), Copepoda (copepods; $F = 14.378$, $df = 1, 32$, $p = 6.262e\text{-}04$; Table S11), and Ostracoda (seed shrimp; $F = 35.920$, $df = 1, 32$, $p = 1.107e\text{-}06$; Table S19, Figure S53), but with a greater increase in the latter half of the experiment for the mixed sediment than the local. The opposite relationship was measured for Chironomidae (midge larvae; $F = 5.473$, $df = 1, 32$, $p = 0.026$; Table S12), with greater abundances in the mesocosms with local sediment than mixed (Figure 19).

The drawdown led to a greater reduction in total abundance ($F = 21.508$, $df = 1, 32$, $p = 5.680e\text{-}05$; Table S15) and abundance of Cladocera (water fleas; $F = 17.099$, $df = 1, 32$, $p = 2.393e\text{-}04$; Table S10) in the mixed sediment mesocosms than it did in the local sediment mescosms (Figure S54). The heat treatment increased Spinicaudata (clam shrimp) in the mesocosms without a drawdown, while those mesocosms with a drawdown saw comparable abundances between the two heating conditions ($F = 4.302$, $df = 1, 32$, $p = 0.046$; Table S9, Figure 20). There was a complex interaction between sediment, heating, and disturbance for

Anostracans (fairy shrimp; F = 5.100, df = 1, 32, p = 0.031; Table S18) and Zygoptera (damselfly nymphs; F = 4.215, df = 1, 32, p = 0.048; Table S20). For Anostracans, the drawdown increased their abundance in the mixed sediment treatment without heating, but decreased abundance with heating. For the Anostracans arising from the local sediment, the greatest abundances were found in the mesocosms without heating or a drawdown (Figure S55). Abundances of Zygoptera in the local sediment communities were greatest in the mesocosms without a drawdown, regardless of heating, while those in the mixed sediment communities were greatest in the mesocosms without a drawdown but only concurrent with additional heating (Figure S56).

Breakpoint Regression

Of the three factors examined, only one, sediment source, yielded a measurable change in a model parameter: an increase in the slope before the breakpoint (F = 12.276, df = 1, 32, p = 0.0014; Table S21, Figure S58). This parameter corresponds to the rate of increase in total abundance during the initial period of unlimited exponential growth. We did not detect a change in model parameters with heating or drawdown disturbance.

Synchrony Analysis

Treatment-driven clusters are evident for both total abundance (Table S22; Figure S61) and order-level richness (Table S23; Figure S62) using the CCF algorithm. The synchrony clusters reveal a strong effect of sediment on community-level metrics. By checking the percent composition of each level of each factor for all clusters, several trends are present. Under a 2cluster scenario for total abundance, the clusters are organized by (Cluster 1) local sediment (83%) and drawdown (64%) and (Cluster 2) mixed sediment (77%). Under a 4-cluster scenario for total abundance, the clusters are organized by (Cluster 1) mixed sediment (83%), (Cluster 2)

local sediment (89%), (Cluster 3) mixed sediment (66%) and drawdown (66%), and (Cluster 4) local sediment (100%). Thus, for total abundance, sediment source was the strongest driver of synchrony, followed by the drawdown. Heating did not noticeably influence synchrony clusters.

Under a 2-cluster scenario for order-level richness, the clusters are organized by (Cluster 1) mixed sediment (76%) and (Cluster 2) local sediment (79%). Under a 4-cluster scenario for total abundance, the clusters are organized by (1) mixed sediment (80%), (Cluster 2) local sediment (62%) and no drawdown (62%), (Cluster 3) heating (83%), mixed sediment (66%), no drawdown (66%), and (Cluster 4) local sediment (91%). Thus, for order-level richness, sediment source is the strongest driver of synchrony, followed by the drawdown and heating treatments.

Discussion

Overall, there was a strong effect of sediment source on community composition, with mixed sediment having greater abundances of five of the six egg bank forming crustaceans: Anostraca, Spinicaudata, Cladocera, Ostracoda, and Copepoda. Additionally, total abundance, richness, Shannon diversity, and the community abundance growth rate were greater in the mixed sediment throughout the experiment. These results indicate that the mixed sediment contained a more diverse assemblage of dormant reproductive propagules than the local sediment, possibly due to dispersal limitations on the macrosystem scale. Although effects of the drawdown (disturbance) were more limited, it did reduce community level total abundance and the abundances of Cladocera. In the case of Cladocera, I suggest that the mechanism is likely the imposition of resource limitation resulting from the reduced volume of water rather than direct mortality, because the breakpoint regression indicates that the slope of the growth in total abundance (which is dominated by Cladocera populations) was unchanged and that peak abundance occurred earlier, about the same day as the drawdown. After the drawdown

concluded, the undisturbed communities exhibited a similar plateau in population size. The heat treatment also had limited effects. This may be due to the variable nature of temporary wetlands to which these macroinvertebrates are adapted to, which may experience large variability in temperatures. However, heating did increase the rate of growth of total abundance, the abundance of Spinicaudata where the drawdown was absent, and either increased or decreased abundances of Anostraca and Zygoptera, depending upon the drawdown and sediment source.

Overall, these three results appear to be the product of three factors: heating bringing these organisms closer to or further from the conditions to which they are adapted, the imposition of resource limitation (and increased competition) via the drawdown, and, in the case of Zygoptera, increased rates of emergence or mortality.

Sediment Source

Five of the six egg bank forming taxa were found in greater abundance in the mixed sediment communities: Anostraca, Spinicaudata, Cladocera, Ostracoda, and Copepoda. The lack of an effect detected for the sixth, Notostraca, is likely due to the low representation of this taxa in the samples due to their comparatively small populations in the mesocosms. However, 20 out of 21 observations of Notostraca were in the mesocosms seeded with mixed sediment. Populations of Anostraca and Spinicuadata were most strongly affected by sediment source, with greater populations of both in the mixed sediment than the local. These results imply that either reproductive propagules were more abundant in the mixed sediment than in the local sediment or that the conditions for hatching were more favorable for the eggs in the mixed sediment than for those in the local sediment. The latter, although possible, is unlikely given that the climatic

conditions and timing of inundation are similar to the natural conditions to which the local sediment egg banks are subject in North Dakota. Therefore, we can assume that the propagule banks indeed had differing compositions and densities which suggests that dispersal of these propagules between wetlands on a macrosystem scale is relatively weak or that other locations have wetlands that achieve higher densities and diversities of propagules than those in North Dakota, for unknown reasons, or likely some combination of these explanations.

The segmented regression indicated that the local sediment community developed slower than the mixed sediment community under the set of environmental conditions they were subjected to. Similarly, the time series for total abundance in the mixed sediment shows a dramatic increase, a plateau, and then decline while the local sediment community steadily increases over the entire experiment. One explanation for this is that the variety of cyst forming crustaceans in the mixed sediment included those adapted to wetlands with shorter hydroperiods present in the southernmost states of Texas and New Mexico, which should lead to more rapid growth. This idea is supported by Radzikowski et al. (2018), in which Daphnia cysts collected from temporary waters hatched quicker and in greater proportions than those collected from lakes, with the comparatively longer-lasting North Dakota wetlands acting more like the lakecollected cysts. Additionally, this idea is also supported by the plot of Shannon diversity over time, with Shannon diversity in the mesocosms containing mixed sediment peaking around 12 days after filling while the local sediment communities peaked around 18 days after filling and at a lesser magnitude. During the first week or two of the experiment, reproduction was minimal, meaning the mixed sediment must have initially contained a more diverse assemblage of propagules. Shannon diversity for the two sediment sources began to converge as populations

of Cladocera far outgrew those of any other organisms, a pattern that held until near the end of the experiment when Cladocera populations began to decline in the mixed sediment.

The results lend strong support to the idea that the two source egg banks are different in terms of the species present, their relative abundances, their genetic diversity and traits, or a combination of these factors. This is a somewhat expected result given the extensive geographic range of sediment sources and the current and historical differences in climate between the sediment collection sites, but importantly it suggests that dispersal limitation likely plays some role in driving differences in macroinvertebrate communities across the North American Great Plains. Perfect homogeneity between these sediment sources would likely only occur in the case of extremely high intermixing of organisms or propagules by wind or migratory birds or mammals. However, we note that local sediment was derived from 5 wetlands whereas mixed sediment was derived from 25 wetlands. Thus, differences in diversity might simply be the result of sampling more wetlands and had 25 local North Dakota wetlands been sampled, diversity may have been more similar. However, that would not explain differences in density unless some wetlands have much larger densities of propagules than others and we randomly did not sample any of these wetlands for the local North Dakota sediment. While it remains important to investigate wetland to wetland variation in the density and diversity of propagules in each state, overall this study still suggests dispersal across the Great Plains is likely relatively low, although more work is needed to confirm the degree of connectivity.

Drawdown

The drawdown reduced total abundance and the abundance of Cladocera (by repeated measures ANOVA) and perhaps Zygoptera (by MVGLM). In theory, a decline in the total amount of phytoplankton and algae (resource limitation) following the drawdown may have

reduced the carrying capacity of the system. Notably, population growth rates of Daphnia are positively correlated with greater food resources (Heugens et al., 2006). Although we did not detect a significant effect of drawdown on Cladocera population growth via breakpoint regression, trends were in congruence with this idea.

Heating, Drawdown, and Sediment Interactions

Populations of Spinicaudata were increased by the heat treatment, but only in the mesocosms which did not receive a drawdown. Given the low abundances of clam shrimp in the mesocosms with local sediment, it logically follows that the majority of eggs for this taxon were sourced from wetlands outside of North Dakota and are, therefore, not abundant in the local sediment. Combined with the fact that North Dakota is the coldest and most northern state from which sediment was collected, the additional heating may have given rise to more favorable (i.e., warmer) conditions for those displaced organisms. This may have also played a role in the dynamics of the other egg bank forming taxa, just to a lesser degree which was not detectable during this study. This interaction between sediment source and heat suggests some role for filtering of taxa due to local environmental conditions. Moreover, it suggests that clam shrimp could become more prevalent in North Dakota wetlands with climate change.

Higher rates of population growth at higher temperatures was an expected result (Gillooly et al., 2001; Heugens et al., 2006; Huang & Chou, 2017). The long-term average difference in temperature between treatments was 1.1 °C, which, as previous studies indicate, could lead to significant differences in assembly (Radzikowski et al., 2018) and community dynamics (Heugens et al., 2006; Jocque et al., 2010; Amarasekare et al., 2014). One possible explanation for why stronger effects of temperature were not observed is that impermanent wetlands are subject to greater variation in their parameters, including temperature, than more

permanent bodies of water. A difference of 1.1 °C in average temperature might be trivial compared to the daily and weekly variations these systems experience.

The four-way interaction between heating, drawdown, sediment, and time observed for Anostraca and Zygoptera is interesting for other reasons. Given the drastic reduction in Zygoptera nymphs during all cases where a drawdown occurred, it would seem that the drawdown either directly killed these organisms or greatly promoted earlier emergence of their adult forms (Block & Stoks, 2005). There is anecdotal evidence for the latter as adult Zygoptera were occasionally observed within mesocosms (personal observation). Populations of larval Zygoptera were greater in the mixed sediment, but only for the mesocosms with additional heating and no drawdown. Their greater total abundance in the mixed sediment may have sustained greater populations of adult damselflies, while the adults themselves may have been attracted to the artificially heated mesocosms, either due to the increased temperature (Deacon & Samways, 2017) or the visual appearance of the greenhouse plastic to water (Wildermuth, 1998). Although window screen was used to prevent entrance of non-sediment derived taxa, some degree of oviposition may still have occurred.

Heating and drawdown appeared to have been detrimental to Anostracans in the local sediment populations, though the total number of observations was low. One possible explanation is that these locally-sourced organisms are better adapted to the temperatures of the un-heated mesocosms (Brendonck, 1996; Radzikowski et al., 2018). This is logical given these organisms tend to hatch during the spring thaw in North Dakota (Krapu, 1974). In the mixed sediment, the drawdown decreased populations of Anostraca when concurrent with heating but may have actually increased these populations in the absence of heating. This could potentially be explained by competition between Anostraca and Spinicaudata, as they are both consumers of

detritus and phytoplankton and given the Spinicaudatans saw the inverse heat-drawdown relationship. A study by Thiéry (1991) found that multispecies coexistence of branchiopods was a result of differences in growth rates and life spans, implying that branchiopods compete with one another, but this competition is eased by life history differences.

Conclusions

Taken together, these results indicate that there is great spatial heterogeneity between wetland egg banks within the Great Plains wetland macrosystem. This is likely driven by historical development under different environmental conditions combined with dispersal limitations. Given the variable nature of impermanent wetlands, there does appear to be a degree of built in resistance to smaller changes in temperature and to mild disturbance. Still, some taxa are more sensitive than others to these changes. More research is needed to quantify the impacts of climatic variation on the long-term, interannual dynamics of such a macrosystem.

CHAPTER III: TOP-DOWN EFFECTS OF PREDACEOUS DIVING BEETLES (DYTISCIDAE) ON TEMPORARY WETLAND MACROINVERTEBRATE COMMUNITIES AS A FUNCTION OF WARMING AND PROPAGULE SOURCE

Abstract

Local species assemblages are thought to be a product of filtering of regional species pools, local climatic conditions, and modification by species interactions. However, much is still unknown about how these processes interact to shape communities, despite the importance for understanding the effects of climate change. Here, we examined the influence of a common predator and experimental warming on seasonal wetland communities that developed from both locally and distantly sourced propagules using field mesocosms. We hypothesized that temporary wetland community composition is influenced by (H1) warming, that alters the physiology, behavior, and interactions of predators and prey, and (H2) local species pool, that limits the choice of prey available to predators. We found that an average warming of 2.0 °C yielded greater numbers of clam shrimp and predatory dytiscids greatly depleted their abundance only under the warmer condition. There was little evidence of prey selection by dytiscids based on species pool (sediment source) alone. These results have implications for how temporary wetland communities might respond to rising temperatures.

Introduction

The impacts of predators on community structure and dynamics are wide-ranging and well documented (e.g. Thrush, 1999; DeWitt & Langerhans, 2003; Baum & Worm, 2009; Start & Gilbert, 2017). For example, some predators, like dystiscids living in temporary wetlands, will preferentially target certain species of prey over others (Kehl & Dettner, 2003; L. Culler et al., 2014). When offered a choice, larval *Agabus* (Coleoptera: Dytiscidae) consumed copepods,

ostracods, and mosquito larvae but strongly preferred mosquito larvae, likely because the latter were easier to capture (Culler & Lamp, 2009).

Selective predation may lead to a reduction in the abundance of the target prey while non-target species, that might directly or indirectly compete with the target species, could become more abundant (i.e., apparent competition; Holt, 1977). In Laske et al. (2017), the introduction of Ninespine Stickleback (*Pungitius pungitius*) to fishless ponds led to the extirpation of Daphniidae and Copepod nauplii while Chironomidae, Harpacticoida, and Ostracoda populations increased substantially. However, this is not the only possible result of top-down control regimes since the presence of predators will not always lead to a reduction in the abundance of their prey. In Batzer et al. (2000), the abundance of midges (Chironomidae) was lower in a marsh where fish were excluded even though those fish were primarily consuming midges elsewhere.

Body size is another important factor in prey selection. Predaceous diving beetles (family Dytiscidae) and giant water bugs in the genus *Belostoma* preferentially target smaller prey but this doesn't always significantly alter the body size structure of the prey (Jara, 2016). To better understand the community dynamics of temporary wetland systems, more studies are needed to reveal the preferences of the predators within these systems, including the relatively understudied invertebrate predators. Further, it is difficult to predict how these predators might alter a community through their selective predation.

Environmental and climatic conditions are another key factor in shaping community dynamics (e.g. Mutshinda et al., 2009; Batzer, 2013), but effects of changes may not be easily predictable in temporary wetlands. One relatively straightforward prediction is that increasing average temperatures could increase evaporation of surface waters, shortening hydroperiods and

reducing the time window for hatching, growth, and reproduction (Pinceel et al., 2018). Changes in precipitation could have similar effects. Sim et al. (2013) found that having a mosaic of wetlands of varying hydroperiods helped mitigate the threats imposed by changes in precipitation and evaporation.

Some organisms have developed adaptations that allow for localized persistence under highly variable environmental conditions, as is the case in impermanent wetlands. The formation of dormant reproductive propagules, like the eggs of branchiopod crustaceans, is one such adaptation (*e.g.* De Stasio & Hairston, 1992; Levine & Rees, 2004). As these eggs accumulate over generations in a wetland basin, they form a resilient egg bank from which the community will assemble when favorable conditions arise (Fryer, 1996; Brendonck & De Meester, 2003; Waterkeyn et al., 2009). Environmental conditions, like water temperature, can influence both the hatching success and rate of these propagules (Atashbar et al., 2014; Radzikowski et al., 2018) and variation in environmental conditions leads to the assembly of different communities of organisms from the same egg bank (Kneitel, 2014; Mushet et al., 2019).

Temperature can also alter the life history parameters of wetland invertebrates. For some egg-forming species, hatching success may benefit from the rising temperatures if those temperatures are closer to their optimal range (Brendonck, 1996; Radzikowski et al., 2018). Differences in life history may help predict taxa-specific responses to warming. Huang & Chou (2017) compared the life history (hatch rate, maturation time, sex ratio, growth, survival, clutch size, reproductive rate, generation time, and intrinsic rate of increase) of two species of ephemeral wetland fairy shrimp in response to temperature. They found different optimal temperatures for the rates of growth, survival, and reproduction, with *Eulimnadia braueriana*

responding positively to increased temperatures while *Branchinella kugenumaensis* either did not respond or responded negatively to the same temperature differentials. Additionally, *E. braueriana* increasingly relied on reproduction by less developed, hermaphoditic individuals at higher temperatures, leading to a greater overall reproductive rate. This suggests that ability to switch to this reproductive strategy could allow prediction of responses to warming. Likewise, another study by Inoda et al. (2007) found that the diving beetle *Dytiscus sharpi* (family Dytiscidae) requires temperatures below 20 °C for mating and spermatogenesis and that exposure to winter temperatures below 8 °C are required for egg maturation and spring spawning. But other species may show different requirements. As temperatures shift away from their historical ranges, some species may proliferate while others may decline. But predicting the responses of individual taxa are complicated because they exist in a complex food web.

Environmental conditions can also alter interactions between species. Top-down effects of mosquito larvae on protozoa within pitcher plants increased at higher temperatures, while bottom-up effects showed no consistent trend with temperature (Hoekman, 2010). The suggested mechanisms for this shift were an increase in the predators' metabolic rates and behavioral changes (specifically activity and foraging). Shurin et al. (2012) found that pond community dynamics are structured by both bottom-up (through phytoplankton) and top-down effects, with increased warming causing a shift toward stronger top-down control. Together, these results provide further evidence that top-down effects could become stronger in a warming world. However, Mutshinda et al. (2009) found that environmental fluctuations are often stronger drivers of community dynamics than the effects of species interactions. While previous studies have documented the effects of warming on trophic interactions in other aquatic systems, it

remains unclear how warming might alter predator-prey relationships in temporary wetlands and what implications this shift would have for these communities.

The combination of widely varying conditions and the interactive effects between them complicates our ability to synthesize a general framework of community dynamics in temporary wetland invertebrate communities. A review of wetland invertebrate studies by Batzer (2013) found that hydrology, plant factors, disturbance by humans, and predation were the most important control factors, but that generalizations about invertebrate responses to these factors were complex and difficult to predict. Moreover, this work did not investigate how the species pool and warming influenced responses of these communities. This supports the idea that these kinds of factors and their interactions produce community- and taxon-specific changes, complicating our understanding of the behavior of these systems. More studies examining the influence of these factors at all levels within these systems are necessary in better understanding and formulating theories of wetland community dynamics.

We describe a test of the relative importance of temperature, sediment source (egg bank composition), and predator density in seasonal wetland macroinvertebrate communities using a field mesocosm experiment. We predict that the predators will selectively consume different prey depending on which organisms are present and abundant, and how easily those prey are captured. Specifically, we predicted that community composition will vary depending upon (1) the composition of the egg banks used to seed the mesocosms (i.e. sediment source), (2) experimental warming, that influences invertebrate hatching success, growth, behavior, and trophic interactions, (3) top-down effect of predators through selective consumption of preferred prey, and (4) shifts in predator behavior resulting from interactions with the first two factors (sediment source and temperature). These predictions are summarized into two hypotheses

which were tested: that (H1) the strength of top-down control by a predator on seasonal wetland invertebrate communities varies with water temperature that induces physiological changes (e.g. swimming speed, metabolism, activity) in both predators and prey and (H2) the effect of topdown control by a predator on seasonal wetland invertebrate communities varies according to the differences in presence and relative abundance of species in the local species pool and their relative ease of capture by that predator.

Methods

Mesocosm Study Site

Extending from Mexico through Canada, the North American Great Plains contains a multitude of wetlands of varying permanence. There are several potential dispersal vectors of macroinvertebrate propagules in the form of migratory waterbirds (Figuerola & Green, 2002; Brochet et al., 2010; van Leeuwen et al., 2012; Costea et al., 2016), large mammals (Vanschoenwinkel, Gielen, Vandewaerde, et al., 2008), strong winds (Graham & Wirth, 2008; Vanschoenwinkel, Gielen, Seaman, et al., 2008), and human activity (Waterkeyn et al., 2010). The North American Central Flyway, a major migration route for millions of waterfowl each year, extends across this region (Olson, 2021). The northern terminus of this route is the massive wetland complex known as the Prairie Pothole Region (PPR) of the United States and Canada. The PPR covers over 770,000 km^2 in south-central North America and includes some 3.4 million wetlands covering an estimated 3.7 million ha, approximately a quarter of which are temporary or seasonal wetlands (Doherty et al., 2018). It is worth noting that the PPR is geologically young, only existing in its current state since the end of the Pleistocene glaciation (Doherty et al., 2018). Many invertebrates present in the region, and therefore, any egg banks within the soil, have established between that time and the present.

Sediment Collection and Preparation

In each of five states, North Dakota, Colorado, Kansas, New Mexico, and Texas, five dry wetlands were selected for sediment collection with two criteria as constraints: (1) the wetlands were temporarily or seasonally flooded, with standing water lasting for weeks or up to several months and drying completely in a typical year, and (2) the wetlands were expected to or had prior evidence of the presence of branchiopod crustaceans. For wetlands that were not entirely dry, we collected from the parts of those wetlands without standing water. Sediments were collected in late summer to early fall of 2020 when most seasonal wetlands throughout the range were expected to be dry. At each wetland, the top 2 cm of sediment were collected at various locations within the wetland basin, ensuring that the center, edges, and the regions in between would be represented within the sample.

Following collection, the sediments collected in North Dakota were transported back to Bowling Green State University and thoroughly mixed. Half of the sediment was shipped to a centralized location at the University of Kansas for further mixing and redistribution. These sediments were mixed at the University of Kansas in a cold storage building in December of 2020 using the cone and quarter method (Campos-M & Campos-C, 2017) to create a homogeneous mixture which, for the purposes of this study, will be called “mixed sediment”. Likewise, an equal amount of unmixed sediment collected from the North Dakota sites was shipped directly to the field site in North Dakota. This sediment will be called “local sediment”. Upon arrival at the field site in January 2021, all buckets remained sealed and were placed in a shaded location outdoors to undergo winterization. Approximately 10 gallons of these sediments were used in a mesocosm experiment in spring 2021 (see Chapter II of this dissertation) and approximately 10 more gallons, much of the remainder, was used in this study.

Experimental Design

A field mesocosm experiment was conducted in the spring of 2022, beginning on May 20th and ending on June 23rd. A field location was selected in the US Fish and Wildlife's Chase Lake Wetland Management District Headquarters near Woodworth, ND (approximate GPS coordinates: +47.134253, -99.243489) that also doubles as a National Ecological Observatory Network (NEON) site. In this experiment, sixteen 100-gallon HDPE stock tanks were arranged in pairs of two within a two-by-four grid of pairs. Pairs received warming or acted as ambient temperature controls, while one mesocosm of each pair had predatory diving beetles added, with the other acting as a predator-free control. These 16 mesocosms were later seeded with the mixed sediment, while eight more mesocosms, also arranged in pairs, were later seeded with local sediment, bring the total to 24 mesocosms. To each of these mesocosms, commercially available topsoil (Timberline brand) was added to a depth of 0.25 cm which was then covered by sand to a depth of 1 cm. The mesocosms were then filled with tap water delivered through a garden hose to a depth of 30.5 cm which was maintained over the five-week duration of the experiment. Once filled, tap water conditioner was added (API Tap Water Conditioner) at the directed rate of 1 mL per 75 liters of water to remove chlorine compounds. The water was allowed to acclimate overnight to equalize temperatures and dissolved oxygen levels across mesocosms. To each of the twenty-four mesocosms, two stems of an aquatic macrophyte, *Ceratophyllum demersum*, were added to each mesocosm for two main reasons: (1) to maintain water chemistry, notably to reduce soluble reactive phosphorus (Zhang et al., 2021) and excessive algal growth (Romo et al., 2004) and increase dissolved oxygen, and (2) provide habitat structure for both predators and prey. A fiberglass window screen was used to cover each mesocosm to reduce the influx of colonizing insects, as the focus of this study was on sediment

egg bank forming crustaceans. The following day, each mesocosm was seeded with 800 grams of the sediments detailed in the previous paragraph.

Three factors (sediment source, experimental warming, predator addition) were manipulated in combination in an unbalanced (unequal replication per treatment combination), paired design for a total of six treatment combinations. The first factor was sediment origin, with sediments collected from either five dry wetlands in the ND PPR (local sediment) or an equal mixture of sediment from five wetlands in each of five states along the Central Flyway (mixed sediment). As mentioned above, sixteen mesocosms in eight pairs were seeded with the mixed sediment while the other eight mesocosms in four pairs were seeded with the local sediment. No mesocosms seeded with local sediment were given a heat treatment. This was done for two reasons: (1) there was a shortage of local sediment collected in 2020 and a new collection would have a different composition of invertebrate eggs, and (2) there were not enough mesocosms to have a full, balanced design at the current level of replication.

A heating treatment, applied to pairs of mesocosms, was provided by an open-top greenhouse constructed around these pairs of mesocosms consisting of a rectangular wooden frame and walls of polyethylene sheeting (opaque, 6 mil thickness; Figure S64). The ceiling was omitted in this greenhouse design to avoid unwanted changes in the intensity and spectral composition of the incoming sunlight. Two wooden boards were placed beneath each mesocosm to minimize heat loss via ground contact (Figure S65). Continuous temperature loggers (HOBO Pendant, Onset) were submerged within 19 of the 24 mesocosms, with at least one logger per mesocosm pair, to record the water temperature at one-hour intervals.

Predaceous diving beetle (family *Dytiscidae*) presence was manipulated by adding four of these beetles at the start of the experiment. One of each pair of mesocosms had additions of

these predators while the other did not. The beetles used were captured from prairie pothole wetlands on the same plot of land using a D-net and consisted of three genera of undetermined species: *Graphoderus*, *Hydaticus*, and *Acilius*. Every three days, the number of beetles in a mesocosm was visually counted and adjusted to the appropriate density of either zero or four beetles per mesocosm. To increase visibility during these counts, a 5000 lumen LED light was shined into the mesocosm. Of the four dytiscids in a mesocosm, I attempted to maintain a ratio of two *Graphoderus* to two of the smaller genera, of which an estimated 90% were *Hydaticus* and the remaining 10% were *Acilius*. A stock of these beetles was kept in a clear, 19-liter HPDE box with a rigid, locking lid and air holes. Habitat structure was provided in the form of leftover *Ceratophyllum demersum* plants, rocks, and *Typha spp.* stem pieces and the container was kept outdoors but out of direct sunlight. This stock was fed every two to three days with a mixture of invertebrates also collected from nearby wetlands and included fairy shrimp (Anostraca), clam shrimp (Spinicaudata), copepods (Copepoda), midge larvae (Chironomidae), seed shrimp (Ostracoda), and water fleas (Cladocera).

Sample Collection

Over the course of the experiment, non-destructive samples of the aquatic macroinvertebrates were collected every three days by dip net for a total of 12 samples. Each sample was composed of six standard net sweeps using a 15.2 x 20.3 cm aquarium net with a mesh size of 0.8 mm. Each mesocosm had its own net to reduce cross-contamination. One sweep was taken just below the water's surface along the longer dimension of the mesocosm, another was taken in the same location but halfway down the water column. A third and fourth sweep were taken at the bottom of the water column just above the substrate along the short dimension of the mesocosm. The fifth and sixth sweeps were taken vertically upward along the walls of the

mesocosm. The contents of each sweep were rinsed into a white plastic dish bin using tap water delivered through a garden hose. These organisms were counted, identified in the field to order, and then returned to the mesocosms alive.

For fairy shrimp, clam shrimp, dytiscid larvae, and tadpole shrimp, the length of the organisms was recorded as a metric of body size. For ease and quickness of measurement, size classes were used rather than exact length. Since these organisms are of comparable size, the classes were assigned as follows: “small” organisms are less than 0.5 cm in length, “medium” organisms are greater than 0.5 cm and less than 1.0 cm in length, and “large” organisms are greater than 1.0 cm in length.

If a population within the sample was too large to be practically counted, a subsample of a lesser number of those organisms was taken. The volume of the sample and the subsample were recorded and used to scale up the population in the subsample to the size of the sample. Only cladocerans were abundant enough to necessitate this subsampling protocol. Alongside each non-destructive sample, specific conductivity, pH, and dissolved oxygen were measured using a sonde (YSI, ProDSS) and turbidity was measured using a 120 cm turbidity tube (Carolina). Diagrams and photographs of the experimental setup and sampling procedure can be found in the Supporting Information (Figure S66, Figure S67, Figure S42, Figure S43, Figure S44, Figure S45, Figure S46).

Beetle surfacing behavior was quantified on four days during the middle of the experiment on June 4th, June 7th, June 10th, and June 13th, because an increase in the rate of surfacing in diving beetles at higher temperatures could be indicative of an increase in respiration and, thus, their metabolic rate (Calosi et al., 2007); more broadly, this itself is a change in behavior. On each of these days, I spent 15 consecutive minutes counting the number of times that a Dytiscid beetle returned to the surface of the water. Prior to the 15-minute

window of observation, water temperature was recorded and the density of beetles per mesocosm (four) was verified and, if necessary, adjusted. The observation dates and times were intentionally staggered to span a range of temperatures, times of day, and ambient light levels.

To examine treatment effects on suspended algal biomass and community composition, I collected one 50 mL water sample from each mesocosm on June 7th, approximately halfway through the experiment, in a plastic 50 mL Falcon tube. These samples were packed into a cooler with ice, shipped overnight back to Bowling Green State University in Bowling Green, Ohio, and analyzed on June 8th by fluorescence excitation spectrometry (FluoroProbe) (Catherine et al., 2012) to determine algal abundances. As outputs, this technique yielded concentrations of green algae, bluegreen algae, diatoms, cryptophyta, chromophoric dissolved organic matter (CDOM, also known as yellow substance) and percent optical transmission.

Statistical Analysis

Responses of the invertebrate and algal community were assessed first through NonMetric Multidimensional Scaling (NMDS) using the 'metaMDS' function from the 'vegan' package in R. The responses of the invertebrate community to each treatment were determined through Permutational Analysis of Variance (PERMANOVA) using the 'adonis2' function from the 'vegan' package in R, which produces a Type II ANOVA table that is better for unbalanced designs. Two PERMANOVAs were executed using the invertebrate community data to test the two separate hypotheses. The first was executed using only the mesocosms containing mixed sediment to determine the effect of predator additions and heating on community dynamics (H1). This was implemented using the linear equation $Y \sim A * B * C$, where Y is a distance matrix derived from all invertebrate samples collected during the experiment, A and B are binomial factors (heating and predator presence), and C is time. For all PERMANOVA operations, the

permutations were limited by the specification of each individual mesocosm nested within each mesocosm pair as a stratum, meaning the temporal samples within each mesocosm are permuted but not any samples between two different mesocosms or two different pairs. P-values were generated from 999 permutations of the data. Dytiscids and their larvae were excluded from the PERMANOVA calculations since their influence on community composition was explicitly examined as a causal factor. It is also important to note that the 'adonis2' function does not correctly model temporal autocorrelation, which could lead to a bias in resulting p-values. But multivariate techniques that correctly deal with temporal autocorrelation, especially for multifactor unbalanced designs, are not readily available.

The second PERMANOVA was executed using only the mesocosms without heating to determine the effect of predator additions and sediment source on community dynamics (H2). This was implemented using the linear equation Y ~ A * B * C, where Y is a distance matrix derived from all invertebrate samples collected during the experiment, A and B are binomial factors (sediment source and predator presence), and C is time. Following either of these PERMANOVA operations, post-hoc, univariate repeated measures ANOVAs were executed for each taxon that appeared to influence the NMDS plot to determine which of them responded to the treatments. These were implemented using the 'aov_4' function from the 'afex' package in R.

PERMANOVAs were also implemented to determine the effect of heating, predator presence, and time on the body sizes of the prey taxa fairy shrimp and clam shrimp. This was executed using only the mixed sediment seeded mesocosms using the linear equation Y ~ A * B * C, where Y is a distance matrix derived including the three size categories for one of the two prey taxa, A and B are binomial factors (heating and predator presence), and C is time. Again, post-hoc, univariate repeated measures ANOVAs were executed for each size class of each taxon

to determine which ones responded to the treatments. These were implemented using the ‘aov_4’ function from the ‘afex’ package in R.

To quantify the response of the water temperature to the heat treatment, hourly temperature values for each calendar day were summarized into mean daily water temperature. These mean daily temperature values were then analyzed using a repeated measures ANOVA using the ‘ezANOVA’ function from the ‘ez’ package in R.

The relationship between the number of diving beetle surfacing events and temperature was determined through linear regression using the ‘lm’ function from the ‘stats’ package in R. This linear regression used the formula Y ~ X where Y is the beetle surfacing counts and X is water temperature.

The response of each algal taxon to the treatments was assessed through ANOVA using the ‘aov’ function from the ‘stats’ package in R. The equation Y ~ B * H * S + P was used where the response, Y, is the algal taxon (green algae, bluegreen algae, diatoms, or cryptophyta) or related variable (concentration of CDOM or percent transmission), B is the predator treatment, H is the heating treatment, and S is the sediment treatment, while P is the unique mesocosm pair as a blocking factor.

Synchrony Analysis

Synchrony between mesocosms was assessed using the CCF clustering algorithm from Chapter I. Time series of total abundance and order-level richness for each mesocosm were used as input. The resulting output is a dendrogram and a list containing the clusters to which each mesocosm best belongs. Cluster listings for 2- and 4-cluster scenarios were generated for both H1 and H2, each of which can be verified on the corresponding dendrograms. These cluster numbers reflect the scenarios where one factor (2-cluster) or two factors (4-cluster) measurably

influenced these community-level metrics, separating them by each of the two levels of those factors. Any influence of these factors as drivers of the clusters were determined by visual assessment of cluster structure within the dendrograms and calculation of percentage of replicates of each treatment within each cluster.

Results

Organisms

The organisms present included six Orders of egg bank forming crustaceans: Anostraca (fairy shrimp), Spinicaudata (clam shrimp), Notostraca (tadpole shrimp), Cladocera (water fleas), Ostracoda (seed shrimp), and Copepoda (copepods). Also present were aquatic insects and their larvae: Dytiscidae (predaceous diving beetles) and their larvae, other non-dytiscid Coleoptera (beetles), Chironomidae (midges), Zygoptera (damselfly nymphs), Odonata (dragonfly nymphs),

Corixidae (water boatmen), and non-insectoid Acari (mites).

Heat Treatment

The heat treatment generated significantly greater water temperature over the entire experiment in the heated mesocosms ($F = 402.15$, $df = 1, 14$, $p = 1.04e\text{-}11$, $ges = 0.97$; Table S28, Figure S73). We did not detect an interaction of this heat treatment with time, suggesting a relatively constant effect throughout the experiment. The average water temperature of the mesocosms without heating over the entire experiment was 17.0 ± 0.06 °C (mean ± SE) while the same measurement for those with heating was 19.0 ± 0.08 °C (mean ± SE). Therefore, the increase in the long-term average temperature due to the heat treatment was approximately +2.0 °C. This temperature differential was noticeably larger than the one in Chapter II, resulting from modifications to the greenhouses that (1) reduced ground-contact heat loss and (2) made a tighter seal around the mesocosm itself using the plastic sheeting.

Mixed Sediment-Derived Communities

I found that the community shifted due to a significant interaction between heating and predator presence in the mesocosms seeded with the mixed sediment ($F = 0.27$, $df = 1, 184$, $p = <0.001$; Table S24, Figure 21). Since there was no detectable interaction between predator presence and time or heating and time, the effects of the predators and heating on the communities were constant throughout the experiment. The post-hoc repeated measures ANOVAs revealed that clam shrimp were more abundant with heating, but only where dytiscids were absent ($F = 8.67$, $df = 1, 12$, $p = 0.012$; Table S29; Figure 21). Experimental heating caused Shannon diversity to peak earlier at a greater magnitude and remain higher later in the experiment (Table S31; Figure S80) and yielded greater richness throughout the experiment (Table S30). Experimental heating did not have a measurable effect on the abundance of dytiscid larvae (Table S48) but did increase the abundance of medium sized dytiscid larvae ($F = 5.6$, $df = 1, 14$, $p = 0.033$; Table S49; Figure S84).

Sediment Source and Predators in Communities Without Heating

I found that the community shifted due to a significant interaction between sediment source and predator presence in the mesocosms without experimental heating ($F = 1.06$, $df = 1, 184$, $p = 0.001$; Table S25; Figure 22). Since there was no detectable interaction between predator presence and time, the interactive effect of the predators and sediment source was constant throughout the experiment. The post-hoc repeated measures ANOVAs revealed that the abundance of copepods was increased in the mixed sediment over days 21-24 but only when dytiscids were present ($F = 2.03$, $df = 1, 132$, $p = 0.03$; Figure 22; Figure S82). This coincided with an increase in Order-level richness when dytiscids were present over the same period ($F = 2.2$, $df = 1, 132$, $p = 0.018$; Table S37; Figure S79).

Fairy Shrimp Size Structure

I found a significant interaction between predator presence and heating on the size structure of fairy shrimp (F = 0.34, df = 1, 184, p = 0.001; Table S26) and between heating and time (F = 3.2240, df = 1, 184, p = 0.029; Table S26). The post-hoc repeated measures ANOVAs indicated that the abundance of the large size class fairy shrimp increased due to the heating treatment between days 21 and 30 compared to the control (F = 2.81, df = 1, 132, p = 0.003; Table S39; Figure 23). Overall, predator presence did not significantly alter the body size structure of the fairy shrimp.

Clam Shrimp Size Structure

I found a significant interaction between predator presence, heating, and time on clam shrimp size structure (F = 4.9184, df = 1, 184, p = <0.001; Table S27). The post-hoc repeated measures ANOVAs revealed that the abundance of small-sized clam shrimp increased with heating (F = 2.81, df = 11, 132, p = 0.003; Table S40; Figure 24) while the abundance of medium (F = 4.76, df = 11, 132, p = <0.001; Table S41; Figure 24) and large (F = 3.89, df = 11, 132, p = <0.001; Table S42; Figure 24) sized clam shrimp increased with heating but was reduced where dytiscids co-occurred.

Beetle Surfacing vs Temperature

The linear regression returned a significant effect of water temperature (F = 14.82, df = 1, 30, adjusted R^2 = 0.31, p = 0.0006; Table S43, Figure S75) on the number of beetle surfacing events during the observation windows.

Algal Abundance

Heating increased the concentration of green algae (F = 10.563, df = 1, 17, p = 0.047; Table S44; Figure S76) and the total concentration of algae (F = 9.38, df = 1, 17, p = 0.0071;

Table S46; Figure S76) and decreased the optical transmission of the water ($F = 10.61$, $df = 1, 17$, $p = 0.0046$; Table S47; Figure S76). Mesocosms seeded with mixed sediment contained higher concentrations of CDOM than those seeded with local sediment ($F = 8.10$, $df = 1, 17$, $p = 0.011$; Table S45; Figure S77). No effect of the heating or sediment source was detected for concentrations of bluegreen algae, diatoms, or cryptophyta. Predator presence had no detectable effect on algal concentrations.

Synchrony Analysis

Treatment-driven clusters are evident for both total abundance (Table S50; Figure S85) and order-level richness (Table S51; Figure S86) using the CCF algorithm. The synchrony clusters indicate an effect of predators and heating on community-level metrics. Under a 2cluster scenario for total abundance, the clusters are organized by (Cluster 1) no predators (70%) and no heating (60%) and (Cluster 2) with predators (83%) and heating (66%). Under a 4-cluster scenario for total abundance, the clusters are organized by (Cluster 1) no predators (75%) and no heating (62%), (Cluster 2) with predators (80%) and heating (60%), (Cluster 3) consistent of two mesocosms with opposite conditions, and (Cluster 4) consisted of a single mesocosm. Thus, overall, for total abundance, the presence or absence of both heating and predators appeared to induce synchrony in dynamics.

Under a 2-cluster scenario for order-level richness, the clusters are organized by (Cluster 1) no heating (62%) and (Cluster 2) with heating (100%) and predators (66%). Under a 4-cluster scenario for order-level richness, the clusters are organized by (1) with heating (80%) and predators (83%), (Cluster 2) no heating (88%) or predators (62%), (Cluster 3) with heating (100%) and predators (100%), and (Cluster 4) consisted of a single mesocosm. Thus, for

orderlevel richness, the presence or absence of both heating and predators appeared to induce synchrony.

The synchrony clusters also indicate an effect of predators and heating on communitylevel metrics. By checking the percent composition of each level of each factor for all clusters, several trends are present. Under a 2-cluster scenario for total abundance, the clusters are organized by (Cluster 1) no predators (62%) and (Cluster 2) with predators (100%) and mixed sediment (66%). Under a 4-cluster scenario for total abundance, the clusters are organized by (Cluster 1) local sediment (100%) and no predators (66%), (Cluster 2) with predators (66%), (Cluster 3) no predators (100%) and mixed sediment (75%), and (Cluster 4) with predators (100%) and mixed sediment (66%). For total abundance, the sediment source and the presence or absence of predators appeared to induce synchrony.

Under a 2-cluster scenario for order-level richness, the clusters are organized by (Cluster 1) mixed sediment (70%) and no predators (70%) and (Cluster 2) local sediment (83%) with predators (83%). Under a 4-cluster scenario for total abundance, the clusters are organized by (1) local sediment (100%) without predators (100%), (Cluster 2) local sediment (100%), (Cluster 3) with predators (100%) and local sediment (75%), and (Cluster 4) mixed sediment (100%). For order-level richness, the sediment source and the presence or absence of predators appeared to induce synchrony.

Discussion

Each of the three treatments (sediment source, heating, and predator presence) induced measurable changes in macroinvertebrate community composition and all except predator presence induced measurable changes in algal abundance. I found support for the hypothesis that heating would increase top-down control, specifically for dytiscids and clam shrimp but not for

any other predator-prey pairings. Heating increased the abundance of clam shrimp, richness, Shannon diversity, and green algae and reduced optical transmission of the water in the mesocosms seeded with mixed sediment. However, clam shrimp populations in heated mesocosms were greatly reduced if dytiscids were present, notably so for medium to large sized clam shrimp. It is likely that a physiological response on the part of dytiscids (e.g., increased consumption or movement) or clam shrimp (e.g., increased activity, leading to greater encounter rates) produced this result, given the lack of an effect of dytiscids on clam shrimp in the absence of heating. I did not find strong support for the hypothesis that sediment source influences prey selection. The local sediment yielded greater numbers of cladocerans and copepods while the mixed sediment yielded greater numbers of fairy shrimp, clam shrimp, and CDOM (in the absence of experimental heating). No invertebrate taxon's abundance was measurably reduced by the presence of dytiscids in these un-heated mesocosms. However, dytiscid presence increased the abundance of copepods in the mixed sediment mesocosms, potentially resulting from decreased competition with other macroinvertebrates in that system, possibly due to behavioral changes of competitors rather than direct predation since there were no declines in abundance with predators in these mesocosms.

Experimental Heating

Passive heating, which yielded a mean 2 °C increase in temperature over the duration of the experiment, induced changes in both macroinvertebrate and algal community composition. Warming led to an increase in the abundance of clam shrimp only where dytiscids were absent. When dytiscids were present, populations of clam shrimp were low. We also found that abundance of medium and large-sized clam shrimp decreased when predators were present, but not small sized ones. This indicates that warming increased the abundance (hatching percentage)

of clam shrimp, of which the dytiscids were consuming the larger individuals. On the other hand, fairy shrimp were not found to be especially targeted by the dytiscids. Neither their abundance nor size class structure were measurably altered by predator presence.

Multiple explanations are possible for temperature dependence of the predator-prey relationship between dytiscids and clam shrimp. Some studies have found that dytiscids will preferentially consume prey that are easier for them to capture (Pajunen, 1983; Velasco & Millan, 1998; L. E. Culler & Lamp, 2009). Ease of capture is influenced by the swimming speed of the prey, a factor which, in crustaceans, is affected by temperature (M. Lindström & Fortelius, 2001) and size (Dierckens et al., 1995), rendering those smaller bodied organisms more vulnerable to predation, especially at lower temperatures. However, the opposite trend was observed: larger-bodied clam shrimp were consumed at greater rates under warmer conditions. Alternatively, an increase in movement speed resulting from increased body size, temperature, or both may have led to greater rates of detection by dytiscids, which is another important factor in prey selection for these predators (Johansson & Nilsson, 1992). There is little published on the behavior of clam shrimp, but it is apparent that they are primarily bottom dwelling, spend much of the time partially buried while filter feeding (Emberton, n.d.), and, aside from swimming in water, are capable of dragging themselves across the substrate (Tasch, 1964). If the proportion of time spent engaging in active swimming, as opposed to being buried in the substrate, increases with water temperature, then this could explain the observed predator-prey response.

The linear regression of dytiscid surfacing rate versus temperature indicates that, under warmer conditions, these predatory beetles were resurfacing more frequently. This increase in the rate of resurfacing suggests that these beetles are moving vertically through the water column more often, perhaps encountering more organisms close to the surface. Clam shrimp are capable

of swimming through the water column, but tend to prefer benthic habitat (Pérez-Bote, 2006). In the water column, clam shrimp, fairy shrimp, and larval dytiscids swim smoothly and at far slower speeds than adult dytiscids, though fairy shrimp are capable of quick, jerky bursts of movement over small distances (personal observations). An increase in the rate of predation on the clam shrimp within the water column could be part of this explanation if fairy shrimp are better able to avoid dytsicids in that zone.

Though the abundance of larval dytiscids was not influenced by temperature, there is some indication that their size was. Additional warming increased the abundance of medium sized dysticid larvae. The box plots for other size classes of larval dytiscids suggest a similar trend, but the difference was not found to be significant for those other sizes. This would suggest that some of the effect of the interaction between predators and heating was, in part, due to consumption by larval dytiscids. Clam shrimp have a hinged, shell-like carapace reminiscent of a bivalve, but thinner and softer. This shell may act as a deterrent to predation though some larval dytiscids, like *Hyphydrus japonicus*, have specialized mouthparts for handling and consuming seed shrimp (Hayashi & Ohba, 2018). Interestingly, during this experiment, both adult and larval dytiscids were observed on several occasions with fairy shrimp in their jaws, while neither was observed having captured clam shrimp (personal observation).

Prey Selection and Dytiscids

The dytiscids deployed within each mesocosm consisted of two *Graphoderus spp.* and two more individuals of either *Hydaticus spp*. or *Acilius spp.*, an estimated 90% of the latter pair being *Hydaticus spp*. Klecka & Boukal (2012) found that adult *Hydaticus seminiger* preferentially consumed larval *Chironomus sp.* (Chironomidae), adult *Acilius canaliculatus*

preferentially consumed larval *Chironomus sp.* and larval *Culex sp.* (Diptera), and larval *A. canaliculatus* preferentially consumed larval *Culex sp.* and larval *Cloeon dipterum* (Ephemeroptera) out of a selection of seven prey orders. These prey were not commonly available in the mesocosms in this study, but because adult *H. seminiger* and *A. canaliculatus* were found to have 94% overlap in diet in Klecka and Boukal (2012), the *Hydaticus spp.* and *Acilius spp.* used in the current study likely had similar diets and, therefore, similar impacts on the community. The same study by Klecka & Boukal (2012) also found that adult *H. seminiger* and *A. canaliculatus* forage along the bottom while larval *A. canaliculatus* forage through the water column. As clam shrimp are primarily bottom dwelling, these organisms would have likely come into contact with adult dytiscids of these two genera in their preferred foraging location. Moreover, D. Schneider & Frost (1996) provide evidence that adult *Acilius spp*. consumed *Eubranchipus spp*. (fairy shrimp), *Lynceus spp.,* (clam shrimp), and *Daphnia spp*., while larval *Acilius spp*. consumed *Diaptomus spp*. (calanoid copepods) in temporary ponds. Thus, it is reasonable to believe that the *Acilius spp*. in the experimental mesocosms were consuming clam shrimp at the sediment surface and other taxa or life stages may have done similarly, either along the bottom, or in the water column.

A study on *Graphoderus spp*., Jackson, (2005) bears some similarity to those of the current study. They found that the presence of larval *Graphoderus liberus* reduced the concentration of *Daphnia spp.*, increased the length of those *Daphnia spp.,* and increased the concentration of calanoid copepod nauplii. Similarly, here I also found that copepod populations increased within the mixed sediment mesocosms but only when dytiscids were present and a

trend of reduced abundance of cladocera with predator presence in the local sediment mesocosms was observed, though the latter was not determined to be significant.

Algal Community Composition

Experimental heating increased the concentration of green algae while percent optical transmission of the water decreased. The growth rates of various green algae species (Singh & Singh, 2015) are known to be strongly dependent upon temperature, so a minor increase in the cool spring temperatures in North Dakota may have increased algal growth. The increase in algal abundance in spite of the simultaneous increase in grazer abundance (clam shrimp) or size (fairy shrimp) suggests a primarily bottom-up control paradigm for these systems at least during the first 2.5 weeks of the experiment. However, shifts in the strength of top-down and bottom-up control are possible. For instance, Velthuis et al. (2017) found that +4 °C warming allowed zooplankton grazer populations to grow more rapidly, increasing top-down control of phytoplankton, and therefore reducing phytoplankton biomass. In the present study, I did not detect an effect of predators on algal concentrations. This may have been due to a combination of the low statistical power from the single time point measurement of algal abundances (unlike other tests) and the low relative abundances of the few grazer taxa that showed a strong response to warming. Additional work may reveal stronger top-down control, especially since we did observe strong effects of predators on certain prey taxa.

Sediment Source

Selection of sediment source, and therefore egg bank composition, was an important determinant of community composition; a result echoed by the experiment during the year prior (see Chapter II of this dissertation). In the current study, cladocerans and copepods were more abundant in the mesocosms seeded with local sediment than those seeded with mixed sediment

while fairy shrimp and clam shrimp were more abundant in the mesocosms seeded with mixed sediment. Peak order-level Shannon diversity was also greater in the mixed sediment. The additions of dytiscids altered the abundances of only copepods, which became more abundant in the mesocosms seeded with mixed sediment. It is possible that copepods or their propagules were inadvertently introduced into the mesocosms when new dysticids were added, because copepods, among other invertebrate taxa, were present in the separate container housing spare dytiscids. However, it is also possible that dytiscids released copepods from competition, possibly through behavioral changes in prey, induced by the presence of the predators (e.g., Jackson, 2005). If this is the underlying mechanism, it could represent behaviorally induced apparent competition (Holt & Bonsall, 2017).

The lack of a top-down, consumption-driven decline in certain prey without warming was unexpected, as there is a strong basis in the literature. In fact, several species of dytiscid have even been suggested as biological control agents against mosquitoes (Chandra et al., 2008; L. E.

Culler & Lamp, 2009). In the study D. Schneider & Frost (1996), adult *Acilius spp*. preferentially consumed *Aedes spp.* (mosquito larvae), *Eubranchipus spp*. (fairy shrimp), and *Daphnia spp*. when given a choice but preferentially consumed *Lynceus spp.,* (clam shrimp) or *Daphnia spp*. in the absence of other non-copepod prey. It seems likely that choice prey (whether it be fairy shrimp, clam shrimp, or cladocerans) for our dyticids were present in the mesocosms, but perhaps other conspecific or congeneric prey (which may not have been present) are preferred. Likewise, larger densities of predators might have yielded stronger effects like those observed in the heated mesocosms (see above).

There was a trend for reduced abundance of Cladocera with dytiscid presence in some local sediment mesocosms (Figure S83) but this effect was not significant. The suggestion that dytiscids were consuming cladocerans in these communities is reasonable as cladocerans are one of the preferred prey of both *Graphoderus spp*. (Jackson, 2005) and *Acilius spp*. (D. Schneider & Frost, 1996). It is also notable that Cladocerans and copepods of similar size can directly compete with one another for food of similar particle size (Dodson, 1974). Therefore, it is possible that predation of cladocera by the dytiscids lessened the effect of competition on copepods, increasing copepod populations. As mentioned above, it is also possible that predators induced a behavioral change in cladocerans, releasing copepods from competition.

The results of our study suggest a relatively weak top-down effect of dytiscids on temporary wetland community structure but stronger effects on particular taxa. This is supported by Schneider, (1999) which suggests that dytiscids are unable to establish in short-duration ponds due to their long life cycles and that predation is a minor process in the community structure of temporary wetlands. Results of the present study support that conclusion, but only at present temperatures. In the future, as the Prairie Pothole Region continues to warm, predators may begin to play a larger role in structuring temporary wetland communities.

Peak macroinvertebrate diversity in mixed sediment communities was similar regardless of heating but peaked three days earlier with +2 °C warming. Without heated local sediment, potential explanations are limited. But in a prior experiment (Chapter II of this dissertation), heated local sediment did not show peaks earlier, whereas heated mixed sediments did, as with this experiment. Thus, the result from this experiment is consistent with the idea that organisms in the mixed sediment, sourced from more southerly states, are better adapted to warmer conditions, approaching their optimal temperature for hatching and growth under the +2 °C

warming condition. Because the effect of warming was small in both experiments, the critical temperature which many macroinvertebrates in these systems are sensitive to may be greater than + 2.0 °C above present temperatures.

Conclusions

In this study, the composition of resting egg banks (the underlying species pool), warming, and predatory dytiscids each contribute to structuring temporary wetland macroinvertebrate communities, with interactions between these factors. Warming equivalent to +2 °C above present increased the abundance of fairy shrimp and clam shrimp, the body size of fairy shrimp, and induced changes in predator-prey interactions between dytiscids and larger sized clam shrimp. In the presence of experiment warming, clam shrimp were substantially reduced by dytiscids. However, when clam and fairy shrimp were absent, dytiscids may have consumed cladocerans and copepods. This study indicates that predatory diving beetles exert a strong top-down influence on certain taxa (notably clam shrimp) in prairie pothole wetland communities with warming. These findings offer insights into how these wetland communities might respond to climate change.

REFERENCES

Abdi, H., & Williams, L. J. (2010). *Principal Component Analysis*.

Amarasekare, P., Coutinho, R. M., Kearney, A. E. M., & Day, E. T. (2014). Effects of Temperature on Intraspecific Competition in Ectotherms. *The American Naturalist*, *184*(3), E50–E65. https://doi.org/10.1086/677386

Andersen, T., Carstensen, J., Hernandez-Garcia, E., & Duarte, C. M. (2009). Ecological thresholds and regime shifts: Approaches to identification. *Trends in Ecology & Evolution*, *24*(1), 49–57.

Atashbar, B., Agh, N., Stappen, G., Mertens, J., & Beladjal, L. (2014). Combined effect of temperature and salinity on hatching characteristics of three fairy shrimp species (Crustacea: Anostraca). *Journal of Limnology*, *73*(3). https://doi.org/10.4081/jlimnol.2014.954

Auger, P., de la Parra, R. B., Poggiale, J. C., Sánchez, E., & Sanz, L. (2008). Aggregation methods in dynamical systems and applications in population and community dynamics. *Physics of Life Reviews*, *5*(2), 79–105. https://doi.org/10.1016/j.plrev.2008.02.001

Aukema, B. H., Carroll, A. L., Zhu, J., Raffa, K. F., Sickley, T. A., & Taylor, S. W. (2006). Landscape level analysis of mountain pine beetle in British Columbia, Canada: Spatiotemporal development and spatial synchrony within the present outbreak. *Ecography*, *29*(3), 427–441. https://doi.org/10.1111/j.2006.0906-7590.04445.x Baars,

M. A. (1979). Patterns of Movement of Radioactive Carabid Beetles. *Oecologia*, *44*(1), 125–140.

Balling, R. C., & Brazel, S. W. (1987). Time and Space Characteristics of the Phoenix Urban Heat Island. *Journal of the Arizona-Nevada Academy of Science*, *21*(2), 75–81.

Batchelder, H. P., Mackas, D. L., & O'Brien, T. D. (2012). Spatial–temporal scales of synchrony in marine zooplankton biomass and abundance patterns: A world-wide comparison. *Progress in Oceanography*, *97–100*, 15–30. https://doi.org/10.1016/j.pocean.2011.11.010

Batzer, D. P. (2013). The Seemingly Intractable Ecological Responses of Invertebrates in North American Wetlands: A Review. *Wetlands*, *33*(1), 1–15. https://doi.org/10.1007/s13157-012-0360-2

Batzer, D. P., Pusateri, C. R., & Vetter, R. (2000). Impacts of fish predation on marsh invertebrates: Direct and indirect effects. *Wetlands*, *20*(2), 307–312. https://doi.org/10.1672/0277-5212(2000)020[0307:IOFPOM]2.0.CO;2

Baum, J. K., & Worm, B. (2009). Cascading top-down effects of changing oceanic predator abundances. *Journal of Animal Ecology*, *78*(4), 699–714. https://doi.org/10.1111/j.1365-2656.2009.01531.x

Beeri, O., & Phillips, R. L. (2007). Tracking palustrine water seasonal and annual variability in agricultural wetland landscapes using Landsat from 1997 to 2005. *Global Change Biology*, *13*(4), 897–912. https://doi.org/10.1111/j.1365-2486.2006.01306.x

Bergamino, N., Loiselle, S. A., Cózar, A., Dattilo, A. M., Bracchini, L., & Rossi, C. (2007). Examining the dynamics of phytoplankton biomass in Lake Tanganyika using Empirical Orthogonal Functions. *Ecological Modelling*, *204*(1), 156–162. https://doi.org/10.1016/j.ecolmodel.2006.12.031

Bjørnstad, O. N., & Bascompte, J. (2001). Synchrony and second-order spatial correlation in host–parasitoid systems. *Journal of Animal Ecology*, *70*(6), 924–933. https://doi.org/10.1046/j.0021-8790.2001.00560.x

Bjørnstad, O. N., Ims, R. A., & Lambin, X. (1999). Spatial population dynamics: Analyzing patterns and processes of population synchrony. *Trends in Ecology & Evolution*, *14*(11), 427–432. https://doi.org/10.1016/S0169-5347(99)01677-8

Block, M. D., & Stoks, R. (2005). Pond drying and hatching date shape the tradeoff between age and size at emergence in a damselfly. *Oikos*, *108*(3), 485–494. https://doi.org/10.1111/j.0030-1299.2005.13471.x

Brendonck, L. (1996). Diapause, quiescence, hatching requirements: What we can learn from large freshwater branchiopods (Crustacea: Branchiopoda: Anostraca, Notostraca, Conchostraca). *Hydrobiologia*, *320*(1), 85–97. https://doi.org/10.1007/BF00016809

Brendonck, L., & De Meester, L. (2003). Egg banks in freshwater zooplankton: Evolutionary and ecological archives in the sediment. *Hydrobiologia*, *491*(1–3), 65–84. https://doi.org/10.1023/A:1024454905119

Brochet, A. L., Gauthier-Clerc, M., Guillemain, M., Fritz, H., Waterkeyn, A., Baltanás, Á., & Green, A. J. (2010). Field evidence of dispersal of branchiopods, ostracods and bryozoans by teal (Anas crecca) in the Camargue (southern France). *Hydrobiologia*, *637*(1), 255–261. https://doi.org/10.1007/s10750-009-9975-6

Buonaccorsi, J. P., Elkinton, J. S., Evans, S. R., & Liebhold, A. M. (2001). *MEASURING AND TESTING FOR SPATIAL SYNCHRONY*. *82*(6), 12.

Bush, E. R., Abernethy, K. A., Jeffery, K., Tutin, C., White, L., Dimoto, E., Dikangadissi, J.-T., Jump, A. S., & Bunnefeld, N. (2017). Fourier analysis to detect phenological cycles using long-term tropical field data and simulations. *Methods in Ecology and Evolution*, *8*(5), 530–540. https://doi.org/10.1111/2041-210X.12704

Calosi, P., Bilton, D. T., & Spicer, J. I. (2007). The diving response of a diving beetle: Effects of temperature and acidification*. *Journal of Zoology*, *273*(3), 289–297. https://doi.org/10.1111/j.1469-7998.2007.00326.x

Campos-M, M., & Campos-C, R. (2017). Applications of quartering method in soils and foods. *International Journal of Engineering Research and Applications*, *7*(1), 35–39. https://doi.org/10.9790/9622-0701023539

Carey, S. K., Tetzlaff, D., Buttle, J., Laudon, H., McDonnell, J., McGuire, K., Seibert, J., Soulsby, C., & Shanley, J. (2013). Use of color maps and wavelet coherence to discern seasonal and interannual climate influences on streamflow variability in northern catchments. *Water Resources Research*, *49*(10), 6194–6207. https://doi.org/10.1002/wrcr.20469

Catherine, A., Escoffier, N., Belhocine, A., Nasri, A. B., Hamlaoui, S., Yéprémian, C., Bernard, C., & Troussellier, M. (2012). On the use of the FluoroProbe®, a phytoplankton quantification method based on fluorescence excitation spectra for large-scale surveys of lakes and reservoirs. *Water Research*, *46*(6), 1771–1784. https://doi.org/10.1016/j.watres.2011.12.056

Cazelles, B., Chavez, M., Berteaux, D., Ménard, F., Vik, J. O., Jenouvrier, S., & Stenseth, N. C. (2008). Wavelet analysis of ecological time series. *Oecologia*, *156*(2), 287–304. https://doi.org/10.1007/s00442-008-0993-2

Cazelles, B., Chavez, M., Berteaux, D., Menard, F., Vik, J. O., Jenouvrier, S., & Stenseth, N. C. (2008). *Wavelet analysis of ecological time series*. 18.

Cazelles, B., Chavez, M., McMichael, A. J., & Hales, S. (2005). Nonstationary Influence of El Niño on the Synchronous Dengue Epidemics in Thailand. *PLOS Medicine*, *2*(4), e106. https://doi.org/10.1371/journal.pmed.0020106

Chandra, G., Mandal, S. K., Ghosh, A. K., Das, D., Banerjee, S. S., & Chakraborty, S. (2008). Biocontrol of larval mosquitoes by Acilius sulcatus (Coleoptera: Dytiscidae). *BMC Infectious Diseases*, *8*(1), 138. https://doi.org/10.1186/1471-2334-8-138

Chase, J. M. (2003). Community assembly: When should history matter? *Oecologia*, *136*(4),

489–498. https://doi.org/10.1007/s00442-003-1311-7

Chesson, P. L. (1983). Coexistence of Competitors in a Stochastic Environment: The Storage Effect. In H. I. Freedman & C. Strobeck (Eds.), *Population Biology* (pp. 188–198). Springer. https://doi.org/10.1007/978-3-642-87893-0_25

Chuang, T.-W., Ionides, E. L., Knepper, R. G., Stanuszek, W. W., Walker, E. D., & Wilson, M. L. (2012). Cross-Correlation Map Analyses Show Weather Variation Influences on Mosquito Abundance Patterns in Saginaw County, Michigan, 1989–2005. *Journal of Medical Entomology*, *49*(4), 851–858. https://doi.org/10.1603/ME11150

Costea, M., Stefanović, S., García, M. A., De La Cruz, S., Casazza, M. L., & Green, A. J. (2016). Waterfowl endozoochory: An overlooked long-distance dispersal mode for Cuscuta (dodder). *American Journal of Botany*, *103*(5), 957–962. https://doi.org/10.3732/ajb.1500507

Culler, L. E., & Lamp, W. O. (2009). Selective predation by larval *Agabus* (Coleoptera: Dytiscidae) on mosquitoes: support for conservation-based mosquito suppression in constructed wetlands. *Freshwater Biology*, *54*(9), 2003–2014. https://doi.org/10.1111/j.1365-2427.2009.02230.x

Culler, L., Ohba, S., & Crumrine, P. (2014). *Predator-Prey Interactions of Dytiscids* (pp. 363–386). https://doi.org/10.1007/978-94-017-9109-0_8

Dai, A., & Wigley, T. M. L. (2000). Global patterns of ENSO-induced precipitation. *Geophysical Research Letters*, *27*(9), 1283–1286. https://doi.org/10.1029/1999GL011140

Dawson, A. (2016). *eofs: A Library for EOF Analysis of Meteorological, Oceanographic, and Climate Data* (1). *4*(1), Article 1. https://doi.org/10.5334/jors.122 de Almeida, T. I. R., Penatti, N. C., Ferreira, L. G., Arantes, A. E., & do Amaral, C. H. (2015). Principal component

analysis applied to a time series of MODIS images: The spatiotemporal variability of the Pantanal wetland, Brazil. *Wetlands Ecology and Management*, *23*(4), 737–748. https://doi.org/10.1007/s11273-015-9416-4

De Stasio, B. T., & Hairston, N. G. (1992). Environmental variability and the persistence of multiple emergence strategies. *Bulletin of Mathematical Biology*, *54*(2), 313–334. https://doi.org/10.1007/BF02464836

Deacon, C., & Samways, M. J. (2017). Conservation planning for the extraordinary and Endangered Spesbona damselfly. *Journal of Insect Conservation*, *21*(1), 121–128. https://doi.org/10.1007/s10841-017-9960-8

Defriez, E. J., & Reuman, D. C. (2017). A global geography of synchrony for terrestrial vegetation. *Global Ecology and Biogeography*, *26*(8), 878–888. https://doi.org/10.1111/geb.12595

Demšar, U., Harris, P., Brunsdon, C., Fotheringham, A. S., & McLoone, S. (2013). Principal Component Analysis on Spatial Data: An Overview. *Annals of the Association of American Geographers*, *103*(1), 106–128.

DeWitt, T. J., & Langerhans, R. B. (2003). Multiple prey traits, multiple predators: Keys to understanding complex community dynamics. *Journal of Sea Research*, *49*(2), 143–155. https://doi.org/10.1016/S1385-1101(02)00220-4

Dierckens, K. R., Sarma, S. S. S., Mertens, J., & Dumont, H. J. (1995). Feeding the fairy shrimp Streptocephalus (Anostraca—Crustacea) with the rotifer Anuraeopsis. *Hydrobiologia*, *308*(1), 29–33. https://doi.org/10.1007/BF00037784

Dodson, S. I. (1974). Zooplankton Competition and Predation: An Experimental Test of the Size-Efficiency Hypothesis. *Ecology*, *55*(3), 605–613. https://doi.org/10.2307/1935150

Doherty, K., Howerter, D., Devries, J., & Walker, J. (2018). *Prairie Pothole Region of North America* (pp. 679–688). https://doi.org/10.1007/978-94-007-4001-3_15

Domisch, S., Jahnig, S. C., & Haase, P. (2011). Climate-change winners and losers: Stream macroinvertebrates of a submontane region in Central Europe. *Freshwater Biology*, *56*(10).

Drake, J. A. (1991). Community-Assembly Mechanics and the Structure of an Experimental Species Ensemble. *The American Naturalist*, *137*(1), 1–26. https://doi.org/10.1086/285143

Elmore, K., & Richman, M. (2001). Euclidean Distance as a Similarity Metric for Principal Component Analysis. *Monthly Weather Review - MON WEATHER REV*, *129*. https://doi.org/10.1175/1520-0493(2001)129<0540:EDAASM>2.0.CO;2

Emberton, K. C. (n.d.). Brief Note: Ecology of a Fall Population of the Clam Shrimp Caenestheriella Gynecia Mattox (Crustacea: Conchostraca). *Ohio J. Sci.*, *80*.

Figuerola, J., & Green, A. J. (2002). Dispersal of aquatic organisms by waterbirds: A review of past research and priorities for future studies. *Freshwater Biology*, *47*(3), 483–494. https://doi.org/10.1046/j.1365-2427.2002.00829.x

Fontaine, S., Abbadie, L., Aubert, M., Barot, S., Bloor, J., Derrien, D., Duchene, O., Gross, N., Henneron, L., Roux, X. L., Loeuille, N., Michel, J., Recous, S., Wipf, D., & Alvarez, G. (2023). *Plant-soil synchrony in nutrient cycles: Learning from natural ecosystems to design sustainable agrosystems* (p. 1). https://hal.science/hal-04056769

Frazier, C. F., & Schriever, T. A. (2022). Patterns of Invertebrate Community Composition and Functional Structure Across a Dune Succession Gradient. *Wetlands*, *42*(7), 75. https://doi.org/10.1007/s13157-022-01596-w

Fries, P., Neuenschwander, S., Engel, A., Goebel, R., & Singer, W. (2001). Rapid feature selective neuronal synchronization through correlated latency shifting. *Nature Neuroscience*, *4*, 194–200. https://doi.org/10.1038/84032

Fryer, G. (1996). Diapause, a potent force in the evolution of freshwater crustaceans. *Hydrobiologia*, *320*(1), 1–14. https://doi.org/10.1007/BF00016800

Gillooly, J. F., Brown, J. H., West, G. B., Savage, V. M., & Charnov, E. L. (2001). Effects of Size and Temperature on Metabolic Rate. *Science*, *293*(5538), 2248–2251. https://doi.org/10.1126/science.1061967

Gouhier, T. C., & Guichard, F. (2014). Synchrony: Quantifying variability in space and time. *Methods Ecol. Evol. 5: 524*, 533.

Gouveia, A. R., Bjørnstad, O. N., & Tkadlec, E. (2016). Dissecting geographic variation in population synchrony using the common vole in central Europe as a test bed. *Ecology and Evolution*, *6*(1), 212–218. https://doi.org/10.1002/ece3.1863

Graham, T. B., & Wirth, D. (2008). Dispersal of large branchiopod cysts: Potential movement by wind from potholes on the Colorado Plateau. *Hydrobiologia*, *600*(1), 17–27. https://doi.org/10.1007/s10750-007-9171-5

Grinsted, A., Moore, J. C., & Jevrejeva, S. (2004). Application of the cross wavelet transform and wavelet coherence to geophysical time series. *Nonlinear Processes in Geophysics*, *11*(5/6), 561–566.

Hairston Jr., N. G. (1996). Zooplankton egg banks as biotic reservoirs in changing environments. *Limnology and Oceanography*, *41*(5), 1087–1092. https://doi.org/10.4319/lo.1996.41.5.1087

Hallett, L. M., Jones, S. K., MacDonald, A. A. M., Jones, M. B., Flynn, D. F. B., Ripplinger, J., Slaughter, P., Gries, C., & Collins, S. L. (2016). codyn: An r package of community dynamics metrics. *Methods in Ecology and Evolution*, *7*(10), 1146–1151. https://doi.org/10.1111/2041-210X.12569

Hannachi, A. (n.d.). *A Primer for EOF Analysis of Climate Data*.

Hayashi, M., & Ohba, S.-Y. (2018). Mouth morphology of the diving beetle Hyphydrus japonicus (Dytiscidae: Hydroporinae) is specialized for predation on seed shrimps. *Biological Journal of the Linnean Society*, *125*(2), 315–320. https://doi.org/10.1093/biolinnean/bly113

Haynes, K. J., Bjørnstad, O. N., Allstadt, A. J., & Liebhold, A. M. (2013). Geographical variation in the spatial synchrony of a forest-defoliating insect: Isolation of environmental and spatial drivers. *Proceedings of the Royal Society B: Biological Sciences*, *280*(1753), 20122373. https://doi.org/10.1098/rspb.2012.2373

Heugens, E. H. W., Tokkie, L. T. B., Kraak, M. H. S., Hendriks, A. J., van Straalen, N. M., & Admiraal, W. (2006). Population growth of Daphnia magna under multiple stress conditions: Joint effects of temperature, food, and cadmium. *Environmental Toxicology and Chemistry*, *25*(5), 1399–1407. https://doi.org/10.1897/05-294R.1

Hoekman, D. (2010). Turning up the heat: Temperature influences the relative importance of top-down and bottom-up effects. *Ecology*, *91*(10), 2819–2825. https://doi.org/10.1890/10-0260.1

Holt, R. D. (1977). Predation, apparent competition, and the structure of prey communities. *Theoretical Population Biology*, *12*(2), 197–229. https://doi.org/10.1016/0040-5809(77)90042-9

Holt, R. D., & Bonsall, M. B. (2017). Apparent Competition. *Annual Review of Ecology, Evolution, and Systematics*, *48*(1), 447–471. https://doi.org/10.1146/annurev-ecolsys-110316-022628

Horel, J. D. (1984). Complex Principal Component Analysis: Theory and Examples. *Journal of Climate and Applied Meteorology*, *23*(12), 1660–1673.

Hsu, S.-I. (1984). Variation of an Urban Heat Island in Phoenix. *The Professional Geographer*, *36*(2), 196–200. https://doi.org/10.1111/j.0033-0124.1984.00196.x

Huang, W.-P., & Chou, L.-S. (2017). Temperature effects on life history traits of two sympatric branchiopods from an ephemeral wetland. *PLOS ONE*, *12*(6), e0179449. https://doi.org/10.1371/journal.pone.0179449

Inoda, T., Tajima, F., Taniguchi, H., Saeki, M., Numakura, K., Hasegawa, M., & Kamimura, S. (2007). Temperature-Dependent Regulation of Reproduction in the Diving Beetle Dytiscus sharpi (Coleoptera: Dytiscidae). *Zoological Science*, *24*(11), 1115–1121. https://doi.org/10.2108/zsj.24.1115

Jackson, A. (2005). *The importance of predation by the macroinvertebrate Graphoderus liberus (Coleoptera: Dytiscidae), on crustacean zooplankton.* [Library and Archives Canada = Bibliothèque et Archives Canada]. https://central.baclac.gc.ca/.item?id=mq99909&op=pdf&app=Library

Jara, F. G. (2016). Predator-prey body size relationship in temporary wetlands: Effect of predatory insects on prey size spectra and survival. *Annales de Limnologie - International Journal of Limnology*, *52*, 205–216. https://doi.org/10.1051/limn/2016011

Jassby, A. D., & Powell, T. M. (1990). Detecting Changes in Ecological Time Series. *Ecology*, *71*(6), 2044–2052. https://doi.org/10.2307/1938618

Jocque, M., Vanschoenwinkel, B., & Brendonck, L. (2010). Anostracan monopolisation of early successional phases in temporary waters? *Fundamental and Applied Limnology*, *176*(2), 127–132. https://doi.org/10.1127/1863-9135/2010/0176-0127

Johansson, A., & Nilsson, A. N. (1992). Dytiscus latissimus and D. circumcinctus (Coleoptera, Dytiscidae) larvae as predators on three case-making caddis larvae. *Hydrobiologia*, *248*(3), 201–213. https://doi.org/10.1007/BF00006148

Johnson, D. M., Liebhold, A. M., Bjornstad, O. N., & Mcmanus, M. L. (2005). Circumpolar variation in periodicity and synchrony among gypsy moth populations. *Journal of Animal Ecology*, *74*(5), 882–892. https://doi.org/10.1111/j.1365-2656.2005.00980.x

Johnson, W. C., Millett, B. V., Gilmanov, T., Voldseth, R. A., Guntenspergen, G. R., & Naugle, D. E. (2005). Vulnerability of Northern Prairie Wetlands to Climate Change. *BioScience*, *55*(10), 863–872. https://doi.org/10.1641/0006-3568(2005)055[0863:VONPWT]2.0.CO;2 Johnson, W. C., & Poiani, K. A. (2016). Climate Change Effects on Prairie Pothole Wetlands: Findings from a Twenty-five Year Numerical Modeling Project. *Wetlands*, *36*(S2), 273–285. https://doi.org/10.1007/s13157-016-0790-3

Junk, W. J., An, S., Finlayson, C. M., Gopal, B., Květ, J., Mitchell, S. A., Mitsch, W. J., & Robarts, R. D. (2013). Current state of knowledge regarding the world's wetlands and their future under global climate change: A synthesis. *Aquatic Sciences*, *75*(1), 151–167. https://doi.org/10.1007/s00027-012-0278-z

Kehl, S., & Dettner, K. (2003). Predation by pioneer water beetles (Coleoptera, Dytiscidae) from sandpit ponds, based on crop-content analysis and laboratory experiments. *Archiv Für Hydrobiologie*, *158*, 109–126. https://doi.org/10.1127/0003-9136/2003/0158-0109

Kendall, B. E., Bjørnstad, O. N., Bascompte, J., Keitt, T. H., & Fagan, W. F. (2000). Dispersal, Environmental Correlation, and Spatial Synchrony in Population Dynamics. *The American Naturalist*, *155*(5), 628–636. https://doi.org/10.1086/303350

Klecka, J., & Boukal, D. S. (2012). Who Eats Whom in a Pool? A Comparative Study of Prey Selectivity by Predatory Aquatic Insects. *PLOS ONE*, *7*(6), e37741. https://doi.org/10.1371/journal.pone.0037741

Kneitel, J. (2014). Inundation timing, more than duration, affects the community structure of California vernal pool mesocosms. *Hydrobiologia*, *732*. https://doi.org/10.1007/s10750-014-1845-1

Koenig, W. D. (2002). Global patterns of environmental synchrony and the Moran effect. *Ecography*, *25*(3), 283–288. https://doi.org/10.1034/j.1600-0587.2002.250304.x

Koenig, W. D., & Liebhold, A. M. (2016). Temporally increasing spatial synchrony of North American temperature and bird populations. *Nature Climate Change*, *6*(6), 614–617. https://doi.org/10.1038/nclimate2933

Kraft, N. J. B., Adler, P. B., Godoy, O., James, E. C., Fuller, S., & Levine, J. M. (2015).

Community assembly, coexistence and the environmental filtering metaphor. *Functional Ecology*, *29*(5), 592–599. https://doi.org/10.1111/1365-2435.12345

Krapu, G. L. (1974). Foods of Breeding Pintails in North Dakota. *The Journal of Wildlife Management*, *38*(3), 408–417. https://doi.org/10.2307/3800870

Laske, S. M., Rosenberger, A. E., Kane, W. J., Wipfli, M. S., & Zimmerman, C. E. (2017). Topdown control of invertebrates by Ninespine Stickleback in Arctic ponds. *Freshwater Science*, *36*(1), 124–137. https://doi.org/10.1086/690675

Lefebvre, G., Redmond, L., Germain, C., Palazzi, E., Terzago, S., Willm, L., & Poulin, B. (2019). Predicting the vulnerability of seasonally-flooded wetlands to climate change across the Mediterranean Basin. *Science of The Total Environment*, *692*, 546–555. https://doi.org/10.1016/j.scitotenv.2019.07.263

Leibold, M. A., Holyoak, M., Mouquet, N., Amarasekare, P., Chase, J. M., Hoopes, M. F., Holt, R. D., Shurin, J. B., Law, R., Tilman, D., Loreau, M., & Gonzalez, A. (2004). The metacommunity concept: A framework for multi-scale community ecology: The metacommunity concept. *Ecology Letters*, *7*(7), 601–613. https://doi.org/10.1111/j.1461-0248.2004.00608.x

Levine, J. M., & Rees, M. (2004). Effects of Temporal Variability on Rare Plant Persistence in Annual Systems. *The American Naturalist*, *164*(3), 350–363. https://doi.org/10.1086/422859

Li, K., Soh, Y. C., & Li, Z. G. (2003). Chaotic cryptosystem with high sensitivity to parameter mismatch. *IEEE Transactions on Circuits and Systems I: Fundamental Theory and Applications*, *50*(4), 579–583. https://doi.org/10.1109/TCSI.2003.809808

Liebhold, A., Koenig, W. D., & Bjørnstad, O. N. (2004). Spatial Synchrony in Population Dynamics. *Annual Review of Ecology, Evolution, and Systematics*, *35*(1), 467–490. https://doi.org/10.1146/annurev.ecolsys.34.011802.132516

Lindström, E. S., & Langenheder, S. (2012). Local and regional factors influencing bacterial community assembly. *Environmental Microbiology Reports*, *4*(1), 1–9. https://doi.org/10.1111/j.1758-2229.2011.00257.x

Lindström, M., & Fortelius, W. (2001). Swimming behaviour in Monoporeia affinis (Crustacea: Amphipoda) — dependence on temperature and population density. *Journal of Experimental Marine Biology and Ecology*, *256*(1), 73–83. https://doi.org/10.1016/S0022-0981(00)00309-9

Loreau, M., & de Mazancourt, C. (2008). Species Synchrony and Its Drivers: Neutral and Nonneutral Community Dynamics in Fluctuating Environments. *The American Naturalist*, *172*(2), E48–E66. https://doi.org/10.1086/589746

Magura, T., & Lövei, G. L. (2021). Consequences of Urban Living: Urbanization and Ground Beetles. *Current Landscape Ecology Reports*, *6*(1), 9–21. https://doi.org/10.1007/s40823-020-00060-x

Martin, A. E., Pearce-Higgins, J. W., & Fahrig, L. (2017). The spatial scale of time-lagged population synchrony increases with species dispersal distance. *Global Ecology and Biogeography*, *26*(10), 1201–1210. https://doi.org/10.1111/geb.12630

Matthews, J. W., Peralta, A. L., Flanagan, D. N., Baldwin, P. M., Soni, A., Kent, A. D., & Endress, A. G. (2009). Relative influence of landscape vs. Local factors on plant community assembly in restored wetlands. *Ecological Applications*, *19*(8), 2108–2123. https://doi.org/10.1890/08-1836.1

McIntyre, N. E., Rango, J., Fagan, W. F., & Faeth, S. H. (2001). Ground arthropod community structure in a heterogeneous urban environment. *Landscape and Urban Planning*, *52*(4), 257–274. https://doi.org/10.1016/S0169-2046(00)00122-5

Moore, J. W., McClure, M., Rogers, L. A., & Schindler, D. E. (2010). Synchronization and portfolio performance of threatened salmon: Synchronization of salmon populations. *Conservation Letters*, *3*(5), 340–348. https://doi.org/10.1111/j.1755-263X.2010.00119.x

Murdoch, W., Kendall, B., Nisbet, R., Briggs, C., McCauley, E., & Bolser, R. (2002). Singlespecies models for many-species food webs. *Nature*, *417*, 541–543. https://doi.org/10.1038/417541a

Mushet, D. M., Solensky, M. J., & Erickson, S. F. (2019). Temporal gamma-diversity meets spatial alpha-diversity in dynamically varying ecosystems. *Biodiversity and Conservation*, *28*(7), 1783–1797. https://doi.org/10.1007/s10531-019-01756-1

Mutshinda, C. M., O'Hara, R. B., & Woiwod, I. P. (2009). What drives community dynamics? *Proceedings of the Royal Society B: Biological Sciences*, *276*(1669), 2923–2929. https://doi.org/10.1098/rspb.2009.0523

Ng, E., & Chan, J. (2012). Geophysical Applications of Partial Wavelet Coherence and Multiple Wavelet Coherence. *Journal of Atmospheric and Oceanic Technology*, *29*, 1845–1853. https://doi.org/10.1175/JTECH-D-12-00056.1

Olson, D. (2021). *2021 Mid-Winter Waterfowl Survey Central Flyway*. 39.

Orell, P., Erkinaro, J., Svenning, M. A., Davidsen, J. G., & Niemelä, E. (2007). Synchrony in the downstream migration of smolts and upstream migration of adult Atlantic salmon in the subarctic River Utsjoki. *Journal of Fish Biology*, *71*(6), 1735–1750.

https://doi.org/10.1111/j.1095-8649.2007.01641.x

Özkan, K., Jeppesen, E., Davidson, T. A., Bjerring, R., Johansson, L. S., Søndergaard, M., Lauridsen, T. L., & Svenning, J.-C. (2016). Long-Term Trends and Temporal Synchrony in Plankton Richness, Diversity and Biomass Driven by Re-Oligotrophication and Climate across 17 Danish Lakes. *Water*, *8*(10), Article 10. https://doi.org/10.3390/w8100427

Pajunen, V. I. (1983). Prey selection by larvae of Potamonectes griseostriatus (Degeer) (Coleoptera, Dytiscidae). *Annales Zoologici Fennici*, *20*(1), 31–35.

Pak, N., Colombano, D. D., Greiner, T., Hobbs, J. A., Carlson, S. M., & Ruhi, A. (2023). Disentangling abiotic and biotic controls of age-0 Pacific herring population stability across the San Francisco Estuary. *Ecosphere*, *14*(5), e4440. https://doi.org/10.1002/ecs2.4440

Patrick, C. J., McCluney, K. E., Ruhi, A., Gregory, A., Sabo, J., & Thorp, J. H. (2021). Multiscale biodiversity drives temporal variability in macrosystems. *Frontiers in Ecology and the Environment*, *19*(1), 47–56. https://doi.org/10.1002/fee.2297

Pérez-Bote, J. L. (2006). Swimming Behaviour of Cyzicus grubei (Simon, 1866) (Branchiopoda, Spinicaudata). *Crustaceana*, *79*(5), 601–605.

Pinceel, T., Buschke, F., Weckx, M., Brendonck, L., & Vanschoenwinkel, B. (2018). Climate change jeopardizes the persistence of freshwater zooplankton by reducing both habitat suitability and demographic resilience. *BMC Ecology*, *18*(1), 2. https://doi.org/10.1186/s12898-018-0158-z

Radzikowski, J., Krupińska, K., & Ślusarczyk, M. (2018). Different thermal stimuli initiate hatching of Daphnia diapausing eggs originating from lakes and temporary waters. *Limnology*, *19*(1), 81–88. https://doi.org/10.1007/s10201-017-0520-4

Raimondo, S., Liebhold, A. M., Strazanac, J. S., & Butler, L. (2004). Population synchrony within and among Lepidoptera species in relation to weather, phylogeny, and larval phenology. *Ecological Entomology*, *29*(1), 96–105. https://doi.org/10.1111/j.0307-6946.2004.00579.x

Rainio, J., & Niemelä, J. (2003). Ground beetles (Coleoptera: Carabidae) as bioindicators. *Biodiversity & Conservation*, *12*(3), 487–506. https://doi.org/10.1023/A:1022412617568

Ranta, E., Kaitala, V., Lindström, J., & Lindén, H. (1995). Synchrony in population dynamics. *Proceedings of the Royal Society of London. Series B: Biological Sciences*, *262*(1364), 113–118. https://doi.org/10.1098/rspb.1995.0184

Ranta, E., Kaitala, V., & m, J. L. (1999). Spatially autocorrelated disturbances and patterns in population synchrony. *Proceedings of the Royal Society B: Biological Sciences*, *266*(1431), 1851. https://doi.org/10.1098/rspb.1999.0856

Ranta, E., Lindstrom, J., & Linden, H. (1995). Synchrony in Tetraonid Population Dynamics. *Journal of Animal Ecology*, *64*(6), 767–776. https://doi.org/10.2307/5855

Romo, S., Miracle, M. R., Villena, M.-J., Rueda, J., Ferriol, C., & Vicente, E. (2004). Mesocosm experiments on nutrient and fish effects on shallow lake food webs in a Mediterranean climate. *Freshwater Biology*, *49*(12), 1593–1607. https://doi.org/10.1111/j.1365-2427.2004.01305.x

Schalau, K., Rinke, K., Straile, D., & Peeters, F. (2008). Temperature is the key factor explaining interannual variability of Daphnia development in spring: A modelling study. *Oecologia*,

157(3), 531–543. https://doi.org/10.1007/s00442-008-1081-3

Schneider, D., & Frost, T. (1996). Habitat Duration and Community Structure in Temporary Ponds. *Journal of the North American Benthological Society*, *15*, 64–86. https://doi.org/10.2307/1467433

Schneider, D. W. (1999). Snowmelt ponds in Wisconsin. Influence of hydroperiod on invertebrate community structure. *Invertebrates in Freshwater Wetlands of North America: Ecology and Management.*, 299–318.

Schönbrunner, I. M., & Eder, E. (2006). pH-related Hatching Success of Triops cancriformis (Crustacea: Branchiopoda: Notostraca). *Hydrobiologia*, *563*(1), 515–520. https://doi.org/10.1007/s10750-006-0018-2

Shakun, J. D., & Carlson, A. E. (2010). A global perspective on Last Glacial Maximum to Holocene climate change. *Quaternary Science Reviews*, *29*(15–16), 1801–1816. https://doi.org/10.1016/j.quascirev.2010.03.016

Sheppard, L., Bell, J. R., Harrington, R., & Reuman, D. C. (2016). Changes in large-scale climate alter spatial synchrony of aphid pests. *Nature Climate Change*, *6*(6), 610. https://doi.org/10.1038/NCLIMATE2881

Sheppard, L., Walter, J., Anderson, T., Zhao, L., & Reuman, D. (n.d.). *Wavelet approaches to synchrony (wsyn) package vignette*.

Shurin, J. B., Clasen, J. L., Greig, H. S., Kratina, P., & Thompson, P. L. (2012). Warming shifts top-down and bottom-up control of pond food web structure and function. *Philosophical Transactions of the Royal Society B: Biological Sciences*, *367*(1605), 3008–3017. https://doi.org/10.1098/rstb.2012.0243

Sim, L. L., Davis, J. A., Strehlow, K., McGuire, M., Trayler, K. M., Wild, S., Papas, P. J., & O'Connor, J. (2013). The influence of changing hydroregime on the invertebrate communities of temporary seasonal wetlands. *Freshwater Science*, *32*(1), 327–342. https://doi.org/10.1899/12-024.1

Singh, S. P., & Singh, P. (2015). Effect of temperature and light on the growth of algae species: A review. *Renewable and Sustainable Energy Reviews*, *50*, 431–444. https://doi.org/10.1016/j.rser.2015.05.024

Soranno, P. A., Wagner, T., Collins, S. M., Lapierre, J., Lottig, N. R., & Oliver, S. K. (2019). Spatial and temporal variation of ecosystem properties at macroscales. *Ecology Letters*, *22*(10), 1587–1598. https://doi.org/10.1111/ele.13346

Start, D., & Gilbert, B. (2017). Predator personality structures prey communities and trophic cascades. *Ecology Letters*, *20*(3), 366–374. https://doi.org/10.1111/ele.12735

Strogatz, S. H., & Stewart, I. (1993). Coupled Oscillators and Biological Synchronization. *Scientific American*, *269*(6), 102–109. https://doi.org/10.1038/scientificamerican1293-102

Sutcliffe, O. L., Thomas, C. D., & Moss, D. (1996). Spatial Synchrony and Asynchrony in Butterfly Population Dynamics. *Journal of Animal Ecology*, *65*(1), 85–95. https://doi.org/10.2307/5702

Szöcs, E., Van den Brink, P. J., Lagadic, L., Caquet, T., Roucaute, M., Auber, A., Bayona, Y., Liess, M., Ebke, P., Ippolito, A., ter Braak, C. J. F., Brock, T. C. M., & Schäfer, R. B. (2015). Analysing chemical-induced changes in macroinvertebrate communities in aquatic mesocosm experiments: A comparison of methods. *Ecotoxicology*, *24*(4), 760–769. https://doi.org/10.1007/s10646-015-1421-0

Tasch, P. (1964). Conchostracan Trails in Bottom Clay Muds and on Turbid Water Surfaces. *Transactions of the Kansas Academy of Science (1903-)*, *67*(1), 126–128. https://doi.org/10.2307/3626685

Tenow, O., Nilssen, A., Bylund, H., & Hogstad, O. (2007). Waves and synchrony in Epirrita autumnata/Operophtera brumata outbreaks. I. Lagged synchrony: Regionally, locally and among species. *The Journal of Animal Ecology*, *76*, 258–268. https://doi.org/10.1111/j.1365-2656.2006.01204.x

Thiéry, A. (1991). Multispecies coexistence of branchiopods (Anostraca, Notostraca & Spinicaudata) in temporary ponds of Chaouia plain (western Morocco): Sympatry or syntopy between usually allopatric species. In D. Belk, H. J. Dumont, & N. Munuswamy (Eds.), *Studies on Large Branchiopod Biology and Aquaculture* (pp. 117–136). Springer Netherlands. https://doi.org/10.1007/978-94-011-3366-1_15

Thorson, J. T., Cheng, W., Hermann, A. J., Ianelli, J. N., Litzow, M. A., O'Leary, C. A., & Thompson, G. G. (2020). Empirical orthogonal function regression: Linking population biology to spatial varying environmental conditions using climate projections. *Global Change Biology*, *26*(8), 4638–4649. https://doi.org/10.1111/gcb.15149

Thrush, S. F. (1999). Complex role of predators in structuring soft-sediment macrobenthic communities: Implications of changes in spatial scale for experimental studies. *Australian Journal of Ecology*, *24*(4), 344–354. https://doi.org/10.1046/j.1442-9993.1999.00981.x

Ueno, H., Kaeriyama, M., Otani, M., Oe, M., Qin, Y., Aita, M., Yoon, S., & Kishi, M. (2016). Temporal and Spatial Variation in Growth Condition of Pacific Salmon. *North Pacific Anadromous Fish Commission Bulletin*, *6*(1), 181–187.

https://doi.org/10.23849/npafcb6/181.187 van Leeuwen, C., Van der Velde, G., van Groenendael, J., & Klaassen, M. (2012). Gut travellers: Internal dispersal of aquatic organisms by waterfowl. *Journal of Biogeography*, *39*, 2031–2040. https://doi.org/10.1111/jbi.12004

Vanhaecke, P., Cooreman, A., & Sorgeloos, P. (1981). International Study on Artemia*. XV. Effect of Light Intensity on Hatching Rate of Artemia Cysts from Different Geographical Origin. *Mar. Ecol. Prog. Ser.*, 4.

Vanschoenwinkel, B., Gielen, S., Seaman, M., & Brendonck, L. (2008). Any way the wind blows—Frequent wind dispersal drives species sorting in ephemeral aquatic communities. *Oikos*, *117*(1), 125–134. https://doi.org/10.1111/j.2007.0030-1299.16349.x

Vanschoenwinkel, B., Gielen, S., Vandewaerde, H., Seaman, M., & Brendonck, L. (2008). Relative importance of different dispersal vectors for small aquatic invertebrates in a rock pool metacommunity. *Ecography*, *31*(5), 567–577. https://doi.org/10.1111/j.0906-7590.2008.05442.x

Velasco, J., & Millan, V. H. (1998). Feeding Habits of Two Large Insects from a Desert Stream: Abedus herberti (Hemiptera: Belostomatidae) and Thermonectus marmoratus (Coleoptera: Dytiscidae). *Aquatic Insects*, *20*(2), 85–96. https://doi.org/10.1076/aqin.20.2.85.4500

Velthuis, M., de Senerpont Domis, L. N., Frenken, T., Stephan, S., Kazanjian, G., Aben, R., Hilt, S., Kosten, S., van Donk, E., & Van de Waal, D. B. (2017). Warming advances top-down control and reduces producer biomass in a freshwater plankton community. *Ecosphere*, *8*(1), e01651. https://doi.org/10.1002/ecs2.1651

Vendrametto Granzotti, R., Agostinho, A. A., & Bini, L. M. (2022). Drivers and spatial patterns of population synchrony of fish species in a floodplain. *Freshwater Biology*, *67*(5), 857–872. https://doi.org/10.1111/fwb.13886

Walter, J. A., Sheppard, L. W., Anderson, T. L., Kastens, J. H., Bjørnstad, O. N., Liebhold, A. M., & Reuman, D. C. (2017). The geography of spatial synchrony. *Ecology Letters*, *20*(7), 801–814. https://doi.org/10.1111/ele.12782

Walter, J. A., Sheppard, L. W., Venugopal, P. D., Reuman, D. C., Dively, G., Tooker, J. F., & Johnson, D. M. (2020). Weather and regional crop composition variation drive spatial synchrony of lepidopteran agricultural pests. *Ecological Entomology*, *45*(3), 573–582. https://doi.org/10.1111/een.12830

Waterkeyn, A., Grillas, P., De Roeck, E. R. M., Boven, L., & Brendonck, L. (2009). Assemblage structure and dynamics of large branchiopods in Mediterranean temporary wetlands: Patterns and processes. *Freshwater Biology*, *54*(6), 1256–1270. https://doi.org/10.1111/j.1365-2427.2009.02174.x

Waterkeyn, A., Vanschoenwinkel, B., Elsen, S., Anton-Pardo, M., Grillas, P., & Brendonck, L. (2010). Unintentional dispersal of aquatic invertebrates via footwear and motor vehicles in a Mediterranean wetland area. *Aquatic Conservation: Marine and Freshwater Ecosystems*, *20*(5), 580–587. https://doi.org/10.1002/aqc.1122

Weiher, E., Freund, D., Bunton, T., Stefanski, A., Lee, T., & Bentivenga, S. (2011). Advances, challenges and a developing synthesis of ecological community assembly theory. *Philosophical Transactions of the Royal Society B: Biological Sciences*, *366*(1576), 2403–2413. https://doi.org/10.1098/rstb.2011.0056

Wildermuth, H. (1998). Dragonflies Recognize the Water of Rendezvous and Oviposition Sites by Horizontally Polarized Light: A Behavioural Field Test. *Naturwissenschaften*, *85*(6), 297–302. https://doi.org/10.1007/s001140050504

Yang, K., & Shahabi, C. (2004). A PCA-based similarity measure for multivariate time series. In *Proceedings of The 2nd ACM International Workshop on Multimedia Databases (MMDB)* (p. 74). https://doi.org/10.1145/1032604.1032616

Zhang, X., Zhen, W., Jensen, H. S., Reitzel, K., Jeppesen, E., & Liu, Z. (2021). The combined effects of macrophytes (Vallisneria denseserrulata) and a lanthanum-modified bentonite on water quality of shallow eutrophic lakes: A mesocosm study. *Environmental Pollution*, *277*, 116720. https://doi.org/10.1016/j.envpol.2021.116720

Zuckerberg, B., Strong, C., LaMontagne, J. M., St. George, S., Betancourt, J. L., & Koenig, W. D. (2020). Climate Dipoles as Continental Drivers of Plant and Animal Populations. *Trends in Ecology & Evolution*, *35*(5), 440–453. https://doi.org/10.1016/j.tree.2020.01.010

APPENDIX A. FIGURES

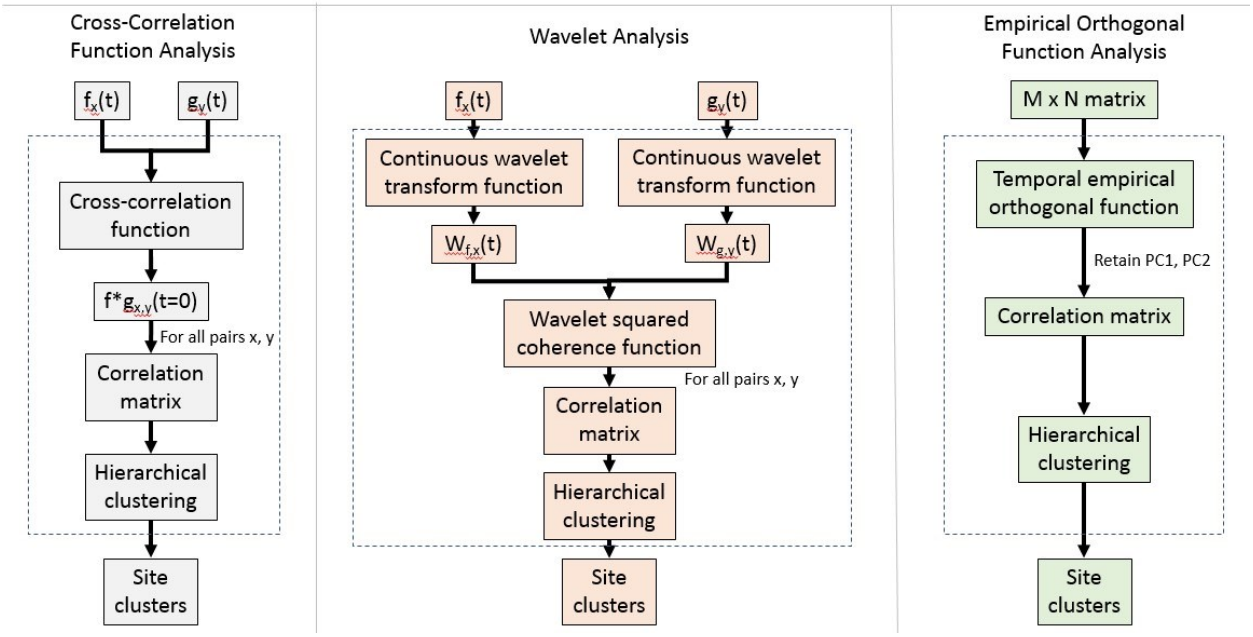

Figure 1: A flowchart showing the implementation of the three synchrony metrics in this study. Above each dashed box are the inputs to each process and below are the outputs. Note that for the cross-correlation and wavelet techniques, the input is a pair of individual time series each corresponding to a single site. These processes must therefore be repeated for all possible pairs of sites. The empirical orthogonal function approach instead uses an M x N matrix (sites x observations) as an input, meaning that all sites can be compared simultaneously.

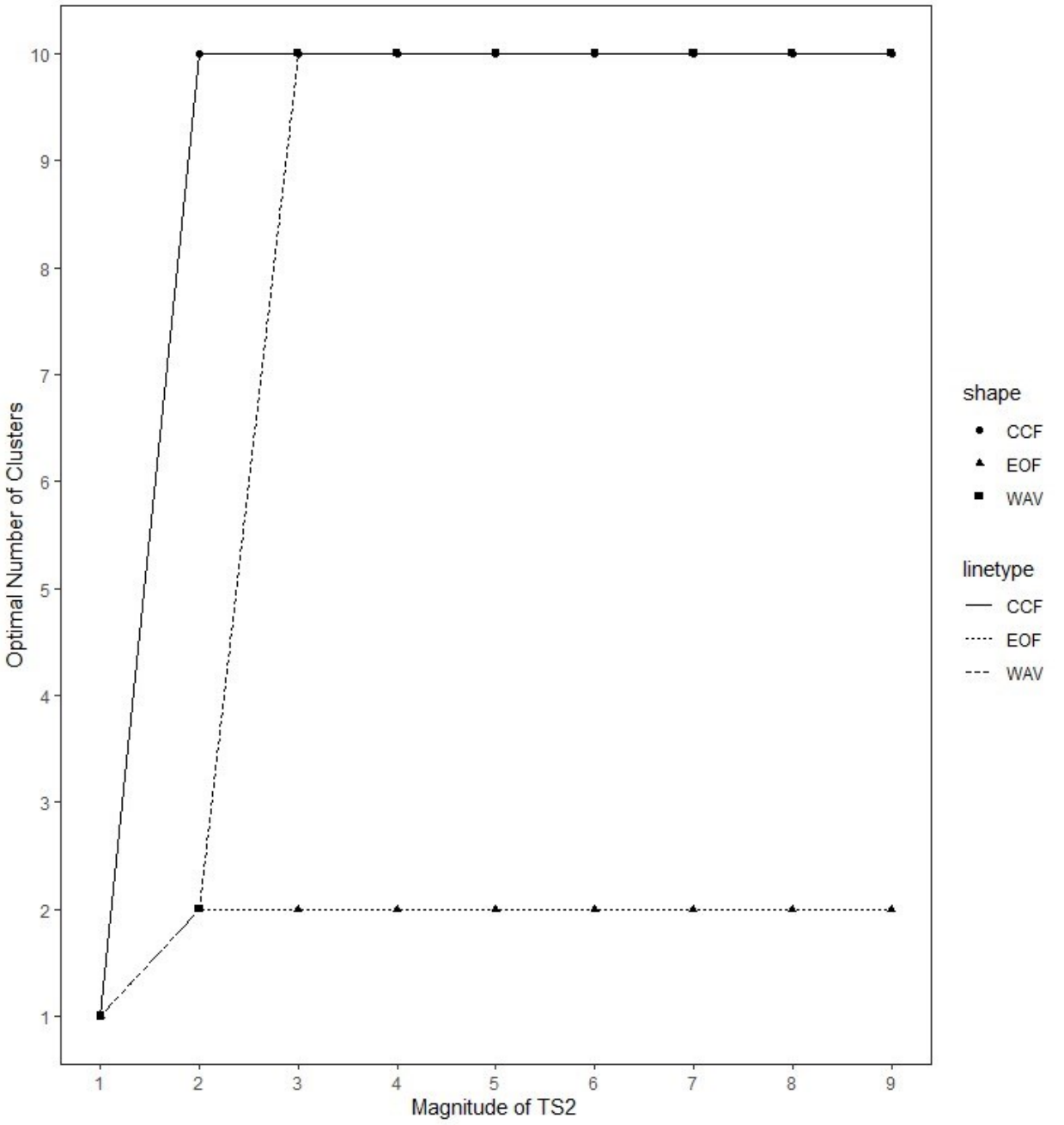

Figure 2: Plot showing the optimal number of clusters obtained through each of the three synchrony metrics against the idealized sine wave's magnitude for the simulated data.

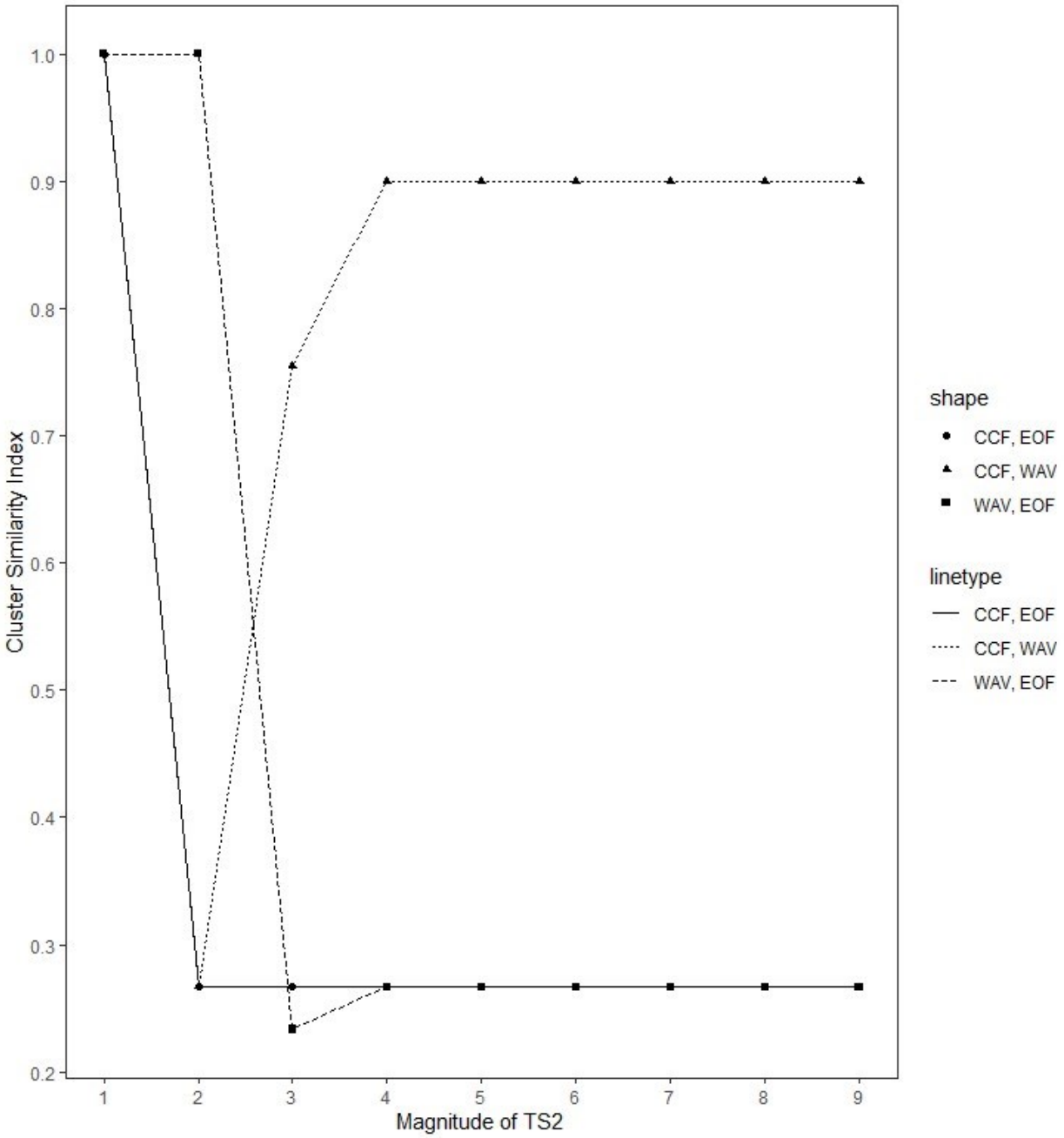

Figure 3: Plot showing the similarity of clusters obtained through each of the three synchrony metrics against the idealized sine wave's magnitude for the simulated data.

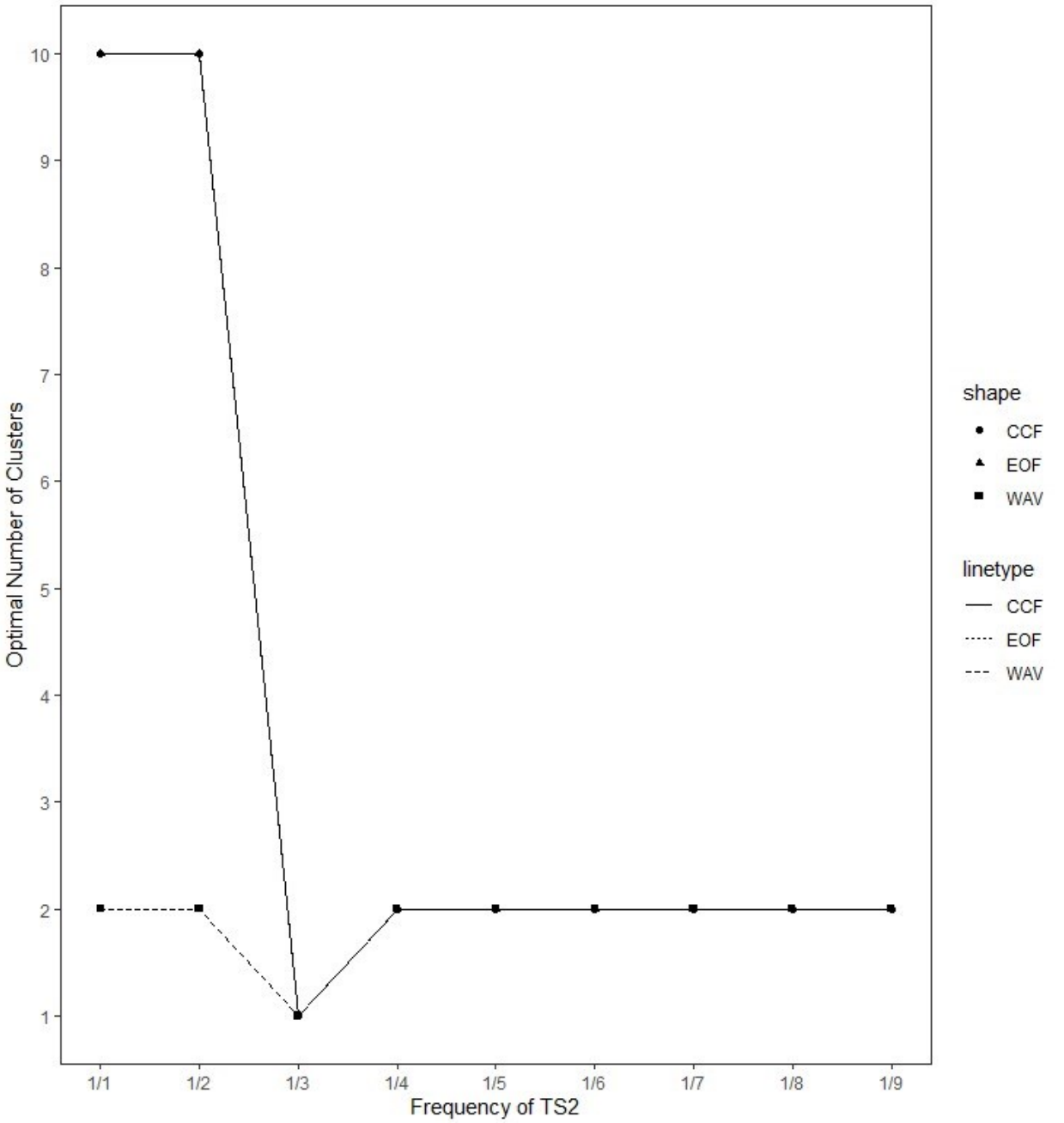

Figure 4: Plot showing the optimal number of clusters obtained through each of the three synchrony metrics against the idealized sine wave's frequency for the simulated data.

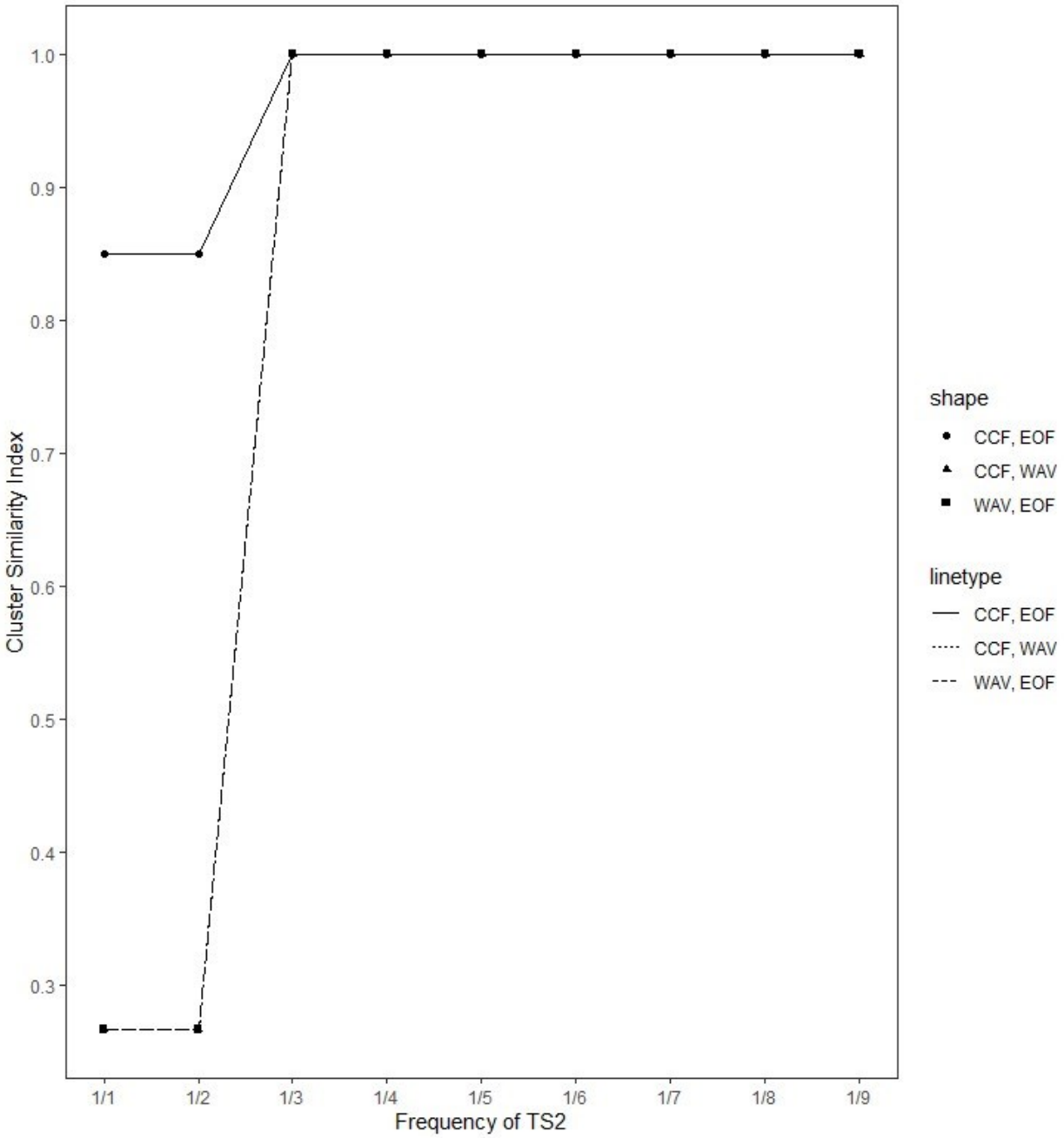

Figure 5: Plot showing the similarity of clusters obtained through each of the three synchrony metrics against the idealized sine wave's frequency for the simulated data.

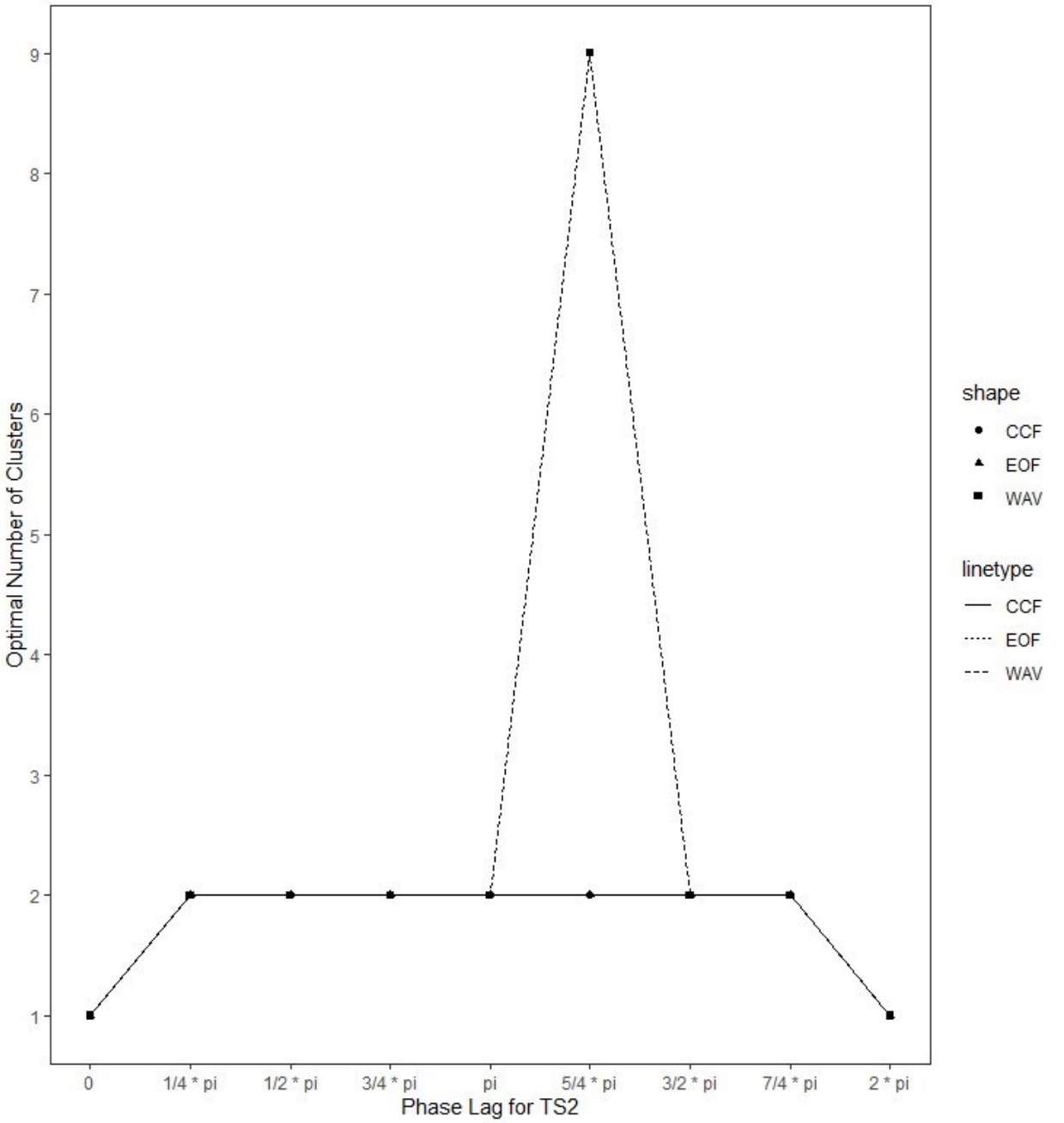

Figure 6: Plot showing the optimal number of clusters obtained through each of the three synchrony metrics against the idealized sine wave's phase lag for the simulated data.

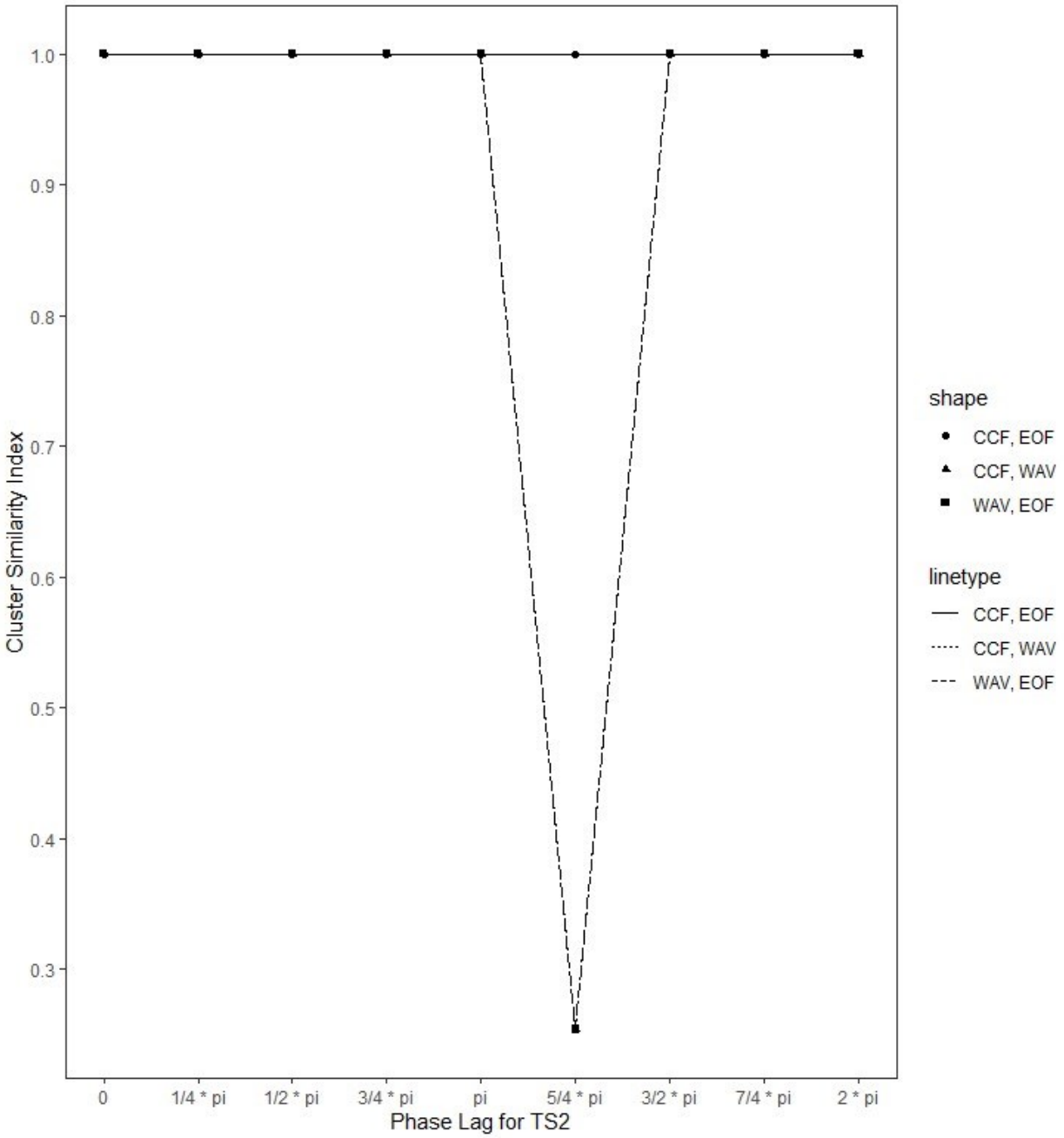

Figure 7: Plot showing the similarity of clusters obtained through each of the three synchrony metrics against the idealized sine wave's phase lag for the simulated data.

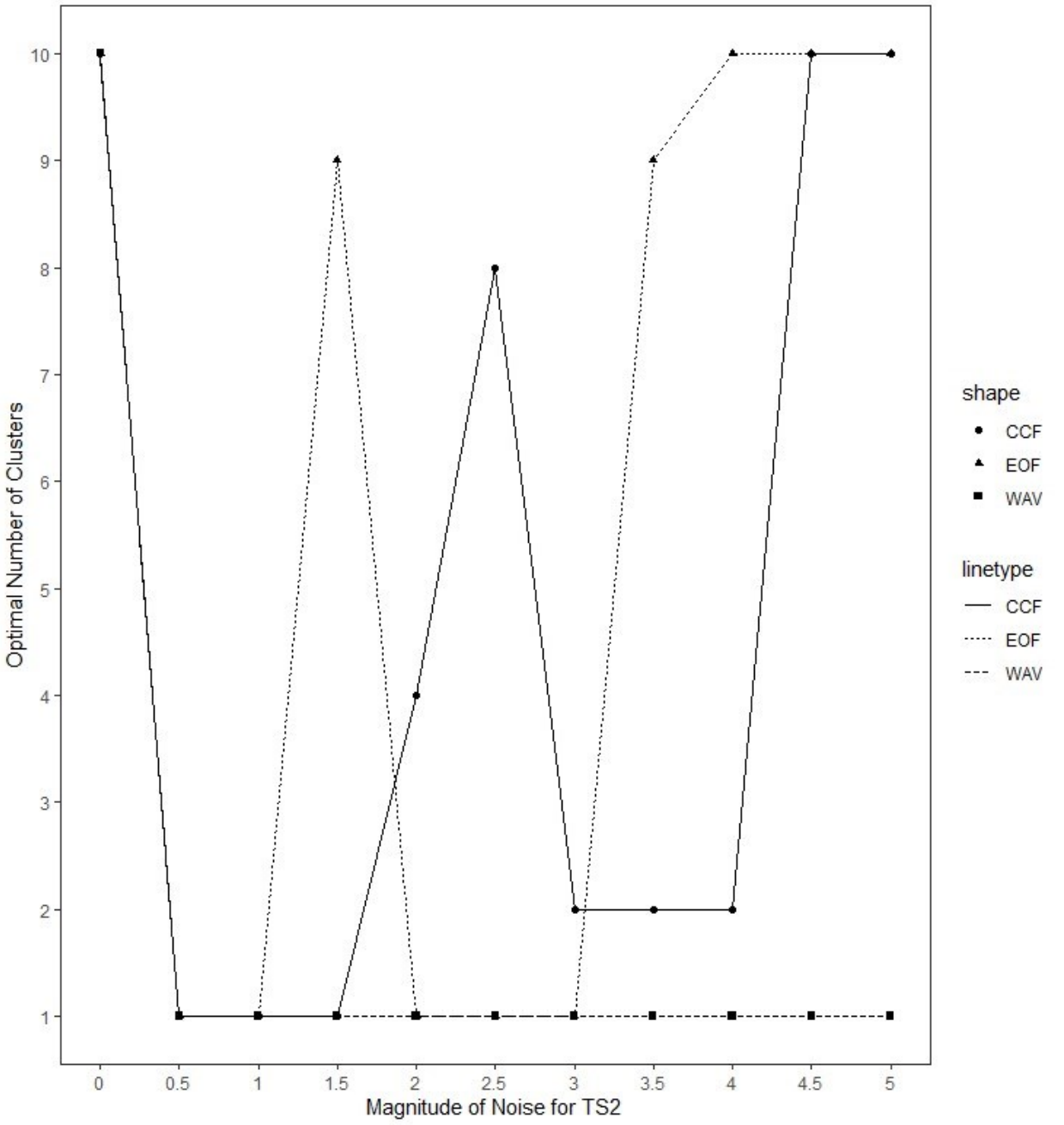

Figure 8: Plot showing the optimal number of clusters obtained through each of the three synchrony metrics against the magnitude of the noise for the simulated data.

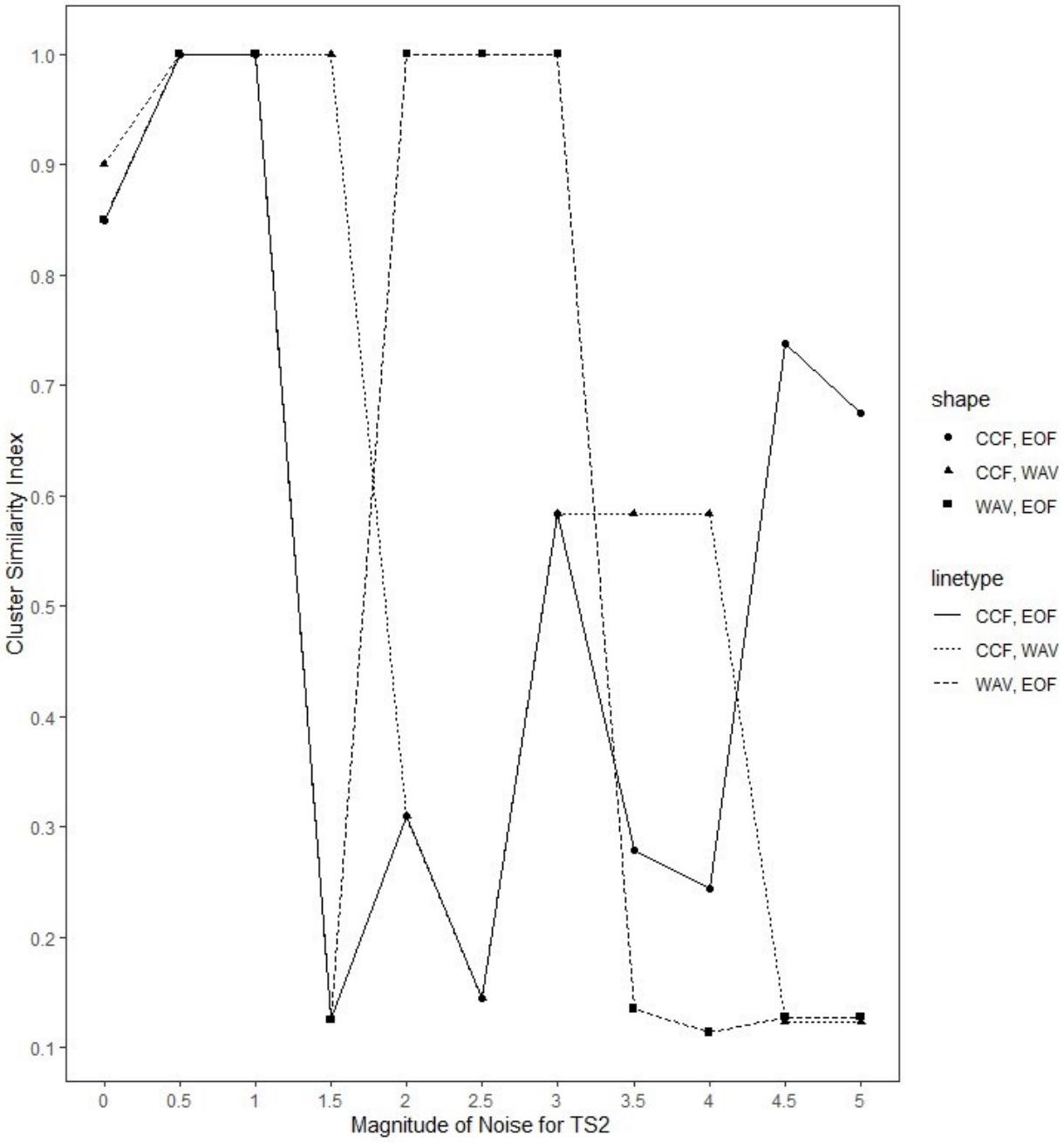

Figure 9: Plot showing the similarity of clusters obtained through each of the three synchrony metrics against the magnitude of the noise for the simulated data.

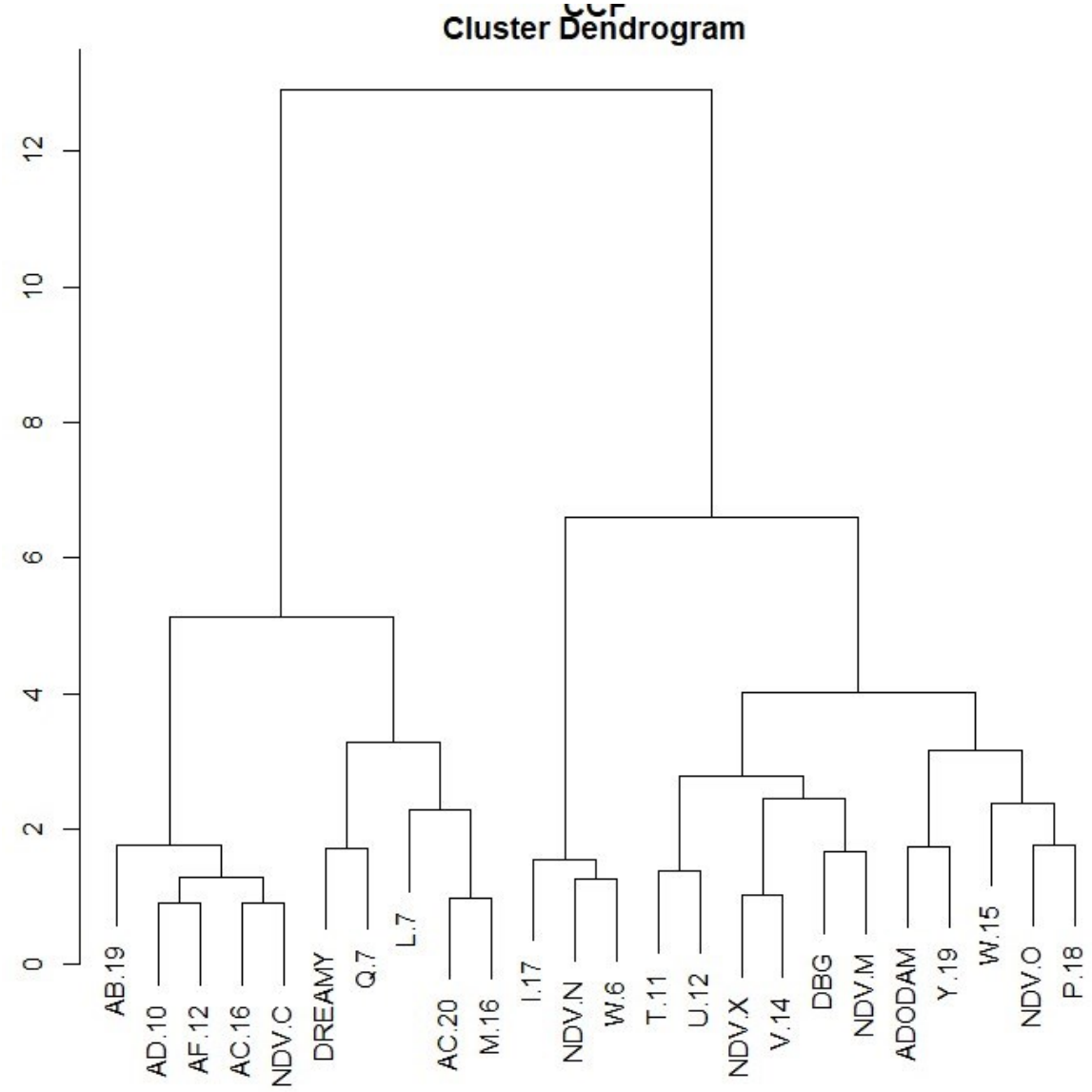

Figure 10: A dendrogram showing the optimal clusters generated by the CCF method and hierarchical clustering algorithm. The optimal number of clusters is two.

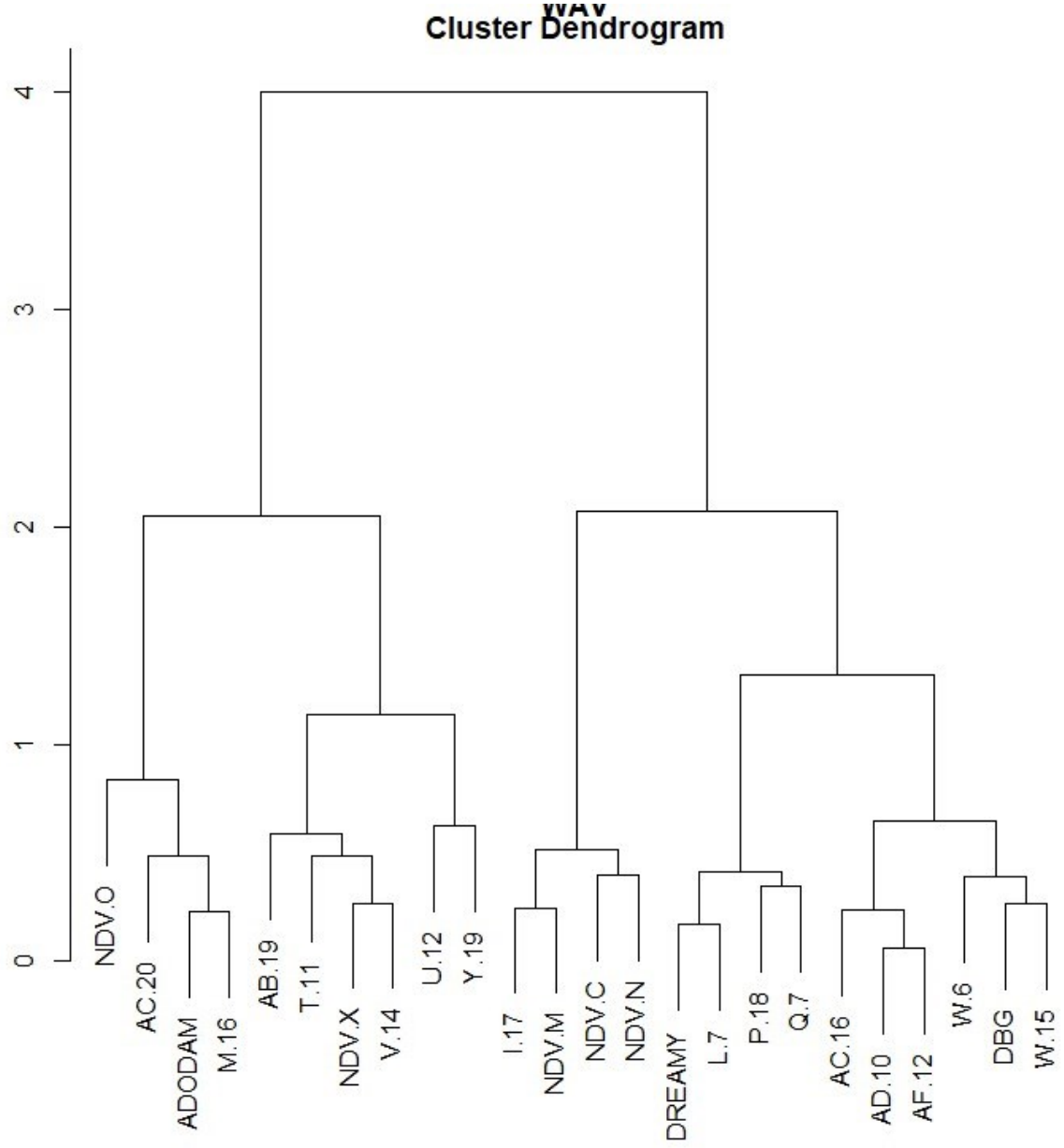

Figure 11: A dendrogram showing the optimal clusters generated by the CCF method and hierarchical clustering algorithm. The optimal number of clusters is three.

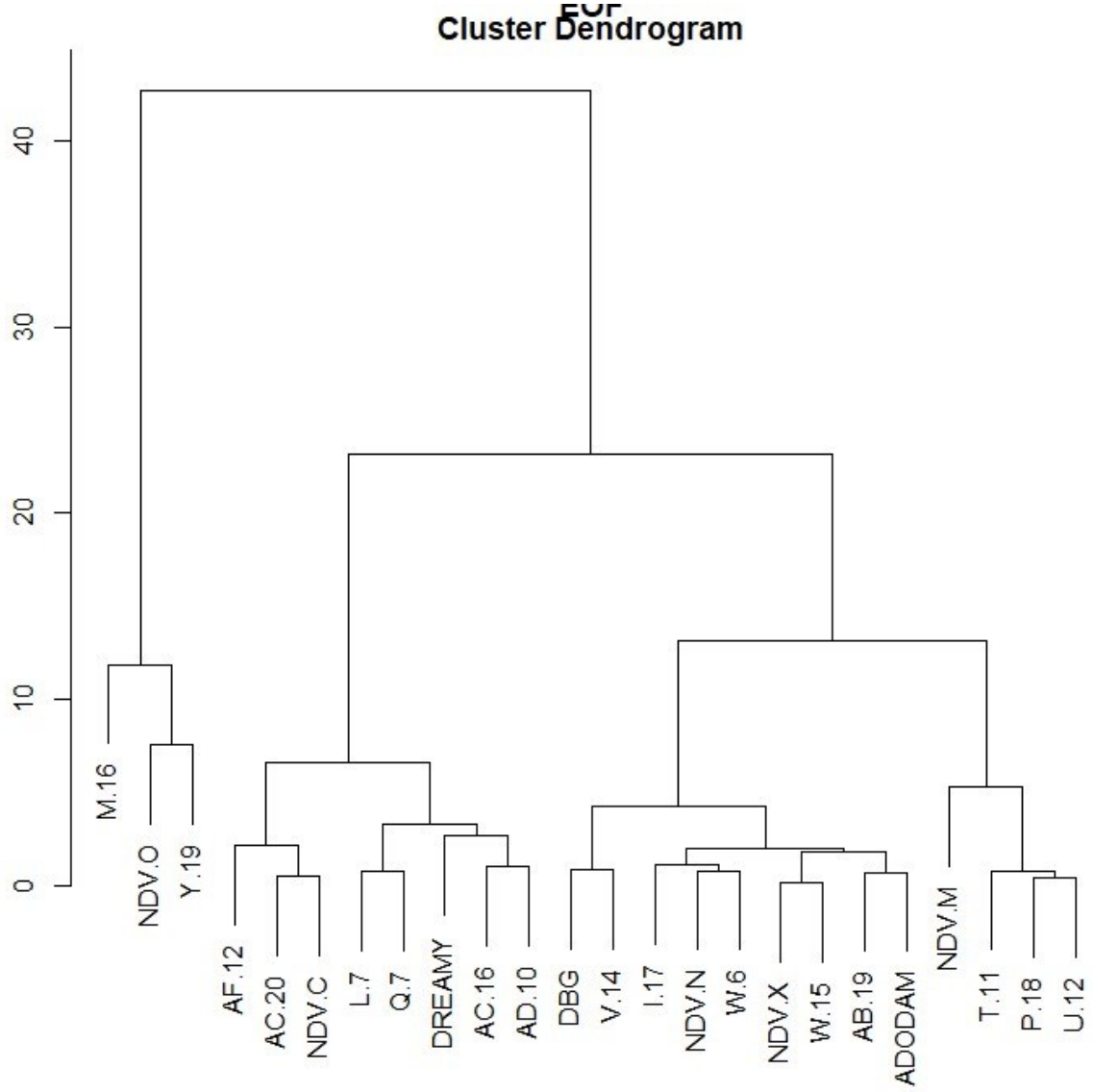

Figure 12: A dendrogram showing the optimal clusters generated by the CCF method and hierarchical clustering algorithm. The optimal number of clusters is one.

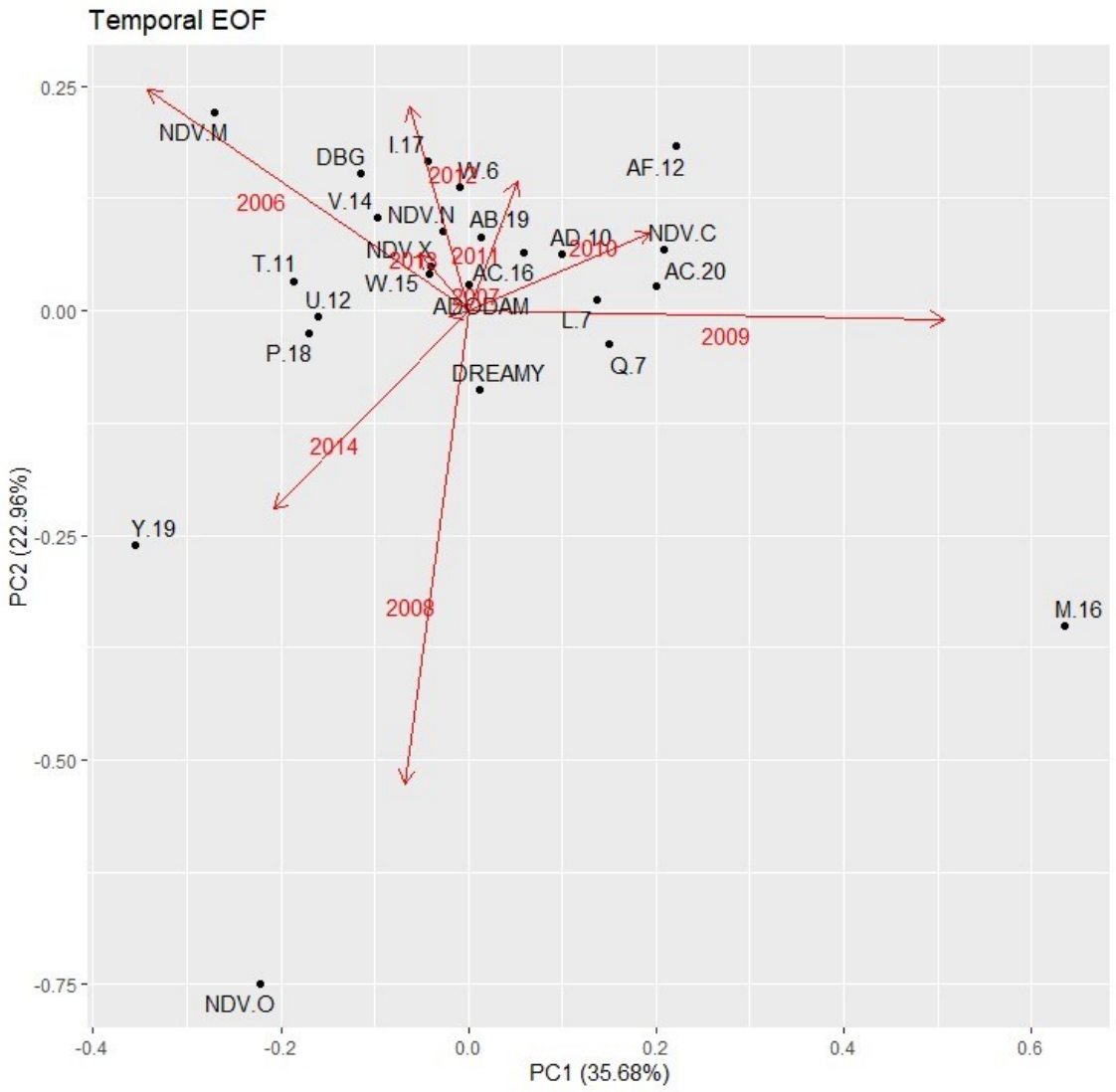

Figure 13: A principal components plot generated from the EOF analysis of the CAP-LTER pitfall data. The horizontal represents the value of the first principal component from the temporal EOF function while the vertical represents the value of the second principal component. These explain 35.68% and 22.96% of the variance in the abundance data respectively. Each site is plotted as a point according to these two values, with the site name labeled adjacent. The red arrows denote the eigenvectors of the covariance matrix of the dataset, each one therefore corresponding to one of the nine years over which the data was collected.

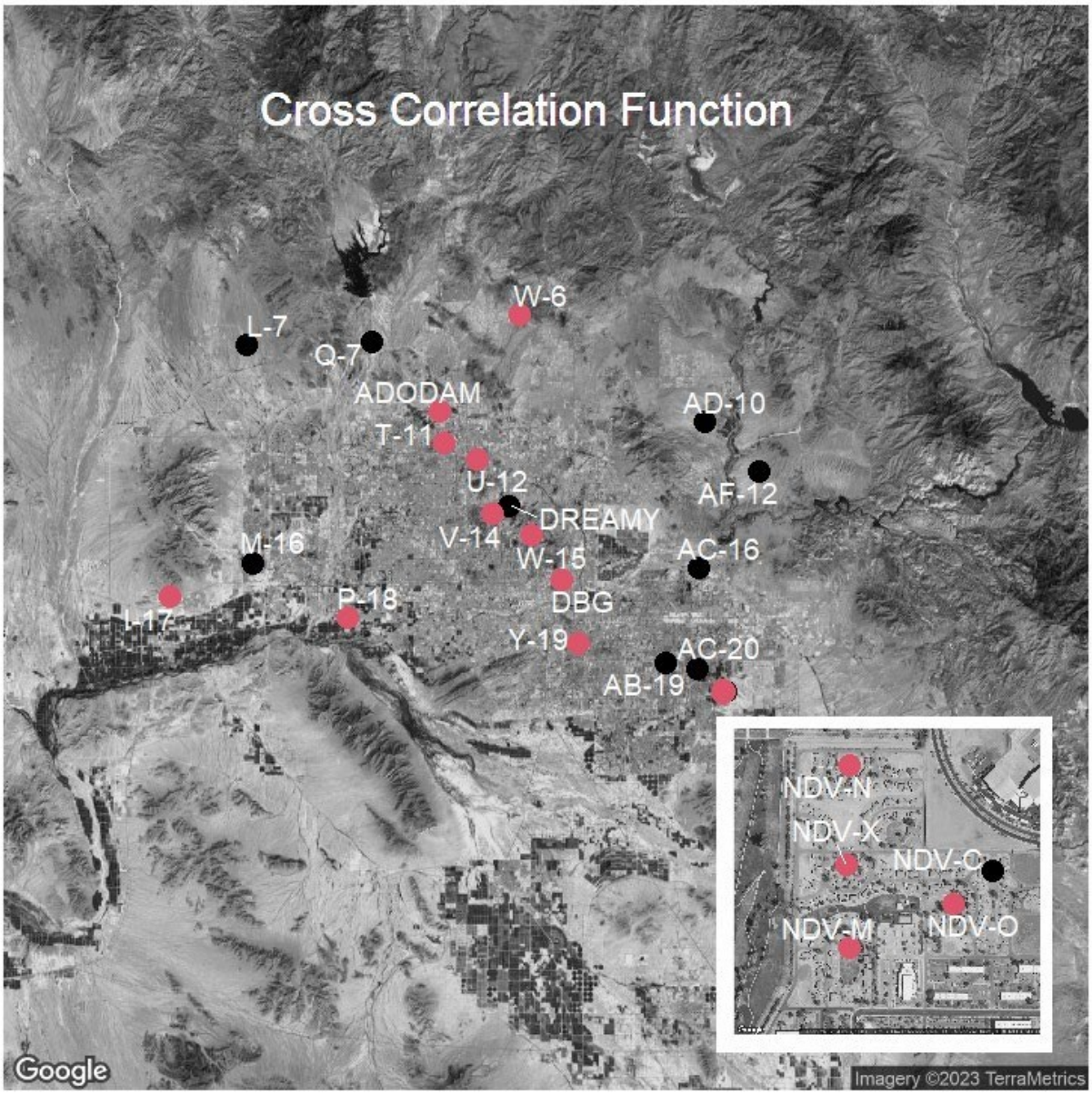

Figure 14: A satellite image of Phoenix, AZ with each of the 24 sites in the dataset overlaid. Sites are color coded by the optimal clusters determined using the cross-correlation function method. The smaller inset image is a higher magnification view of the group of five sites in the bottom right corner of the larger image. Satellite imagery was obtained from Google Maps.

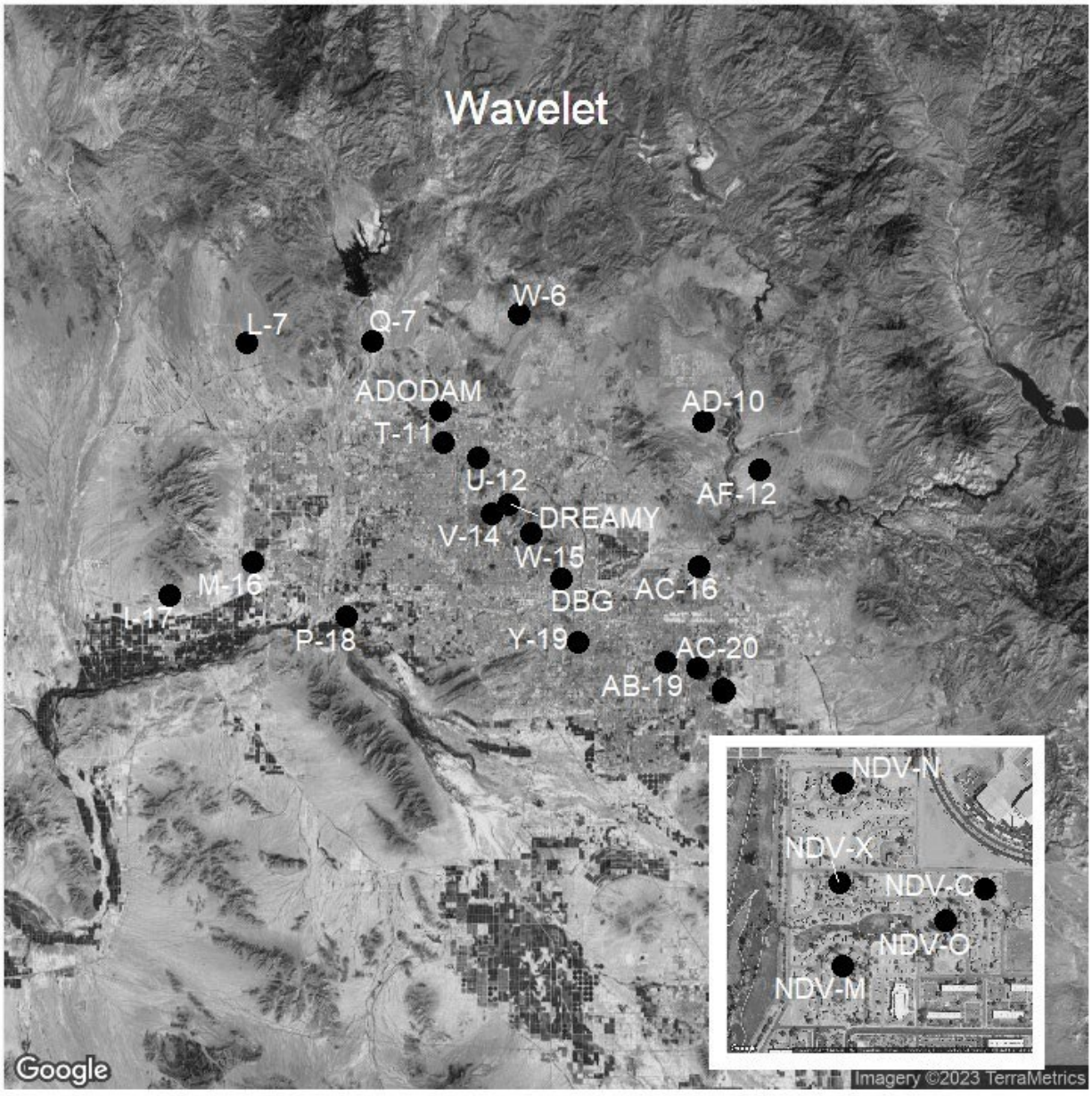

Figure 15: A satellite image of Phoenix, AZ with each of the 24 sites in the dataset overlaid. Sites are color coded by the optimal clusters determined using the wavelet method. The smaller inset image is a higher magnification view of the group of five sites in the bottom right corner of the larger image. Satellite imagery was obtained from Google Maps.

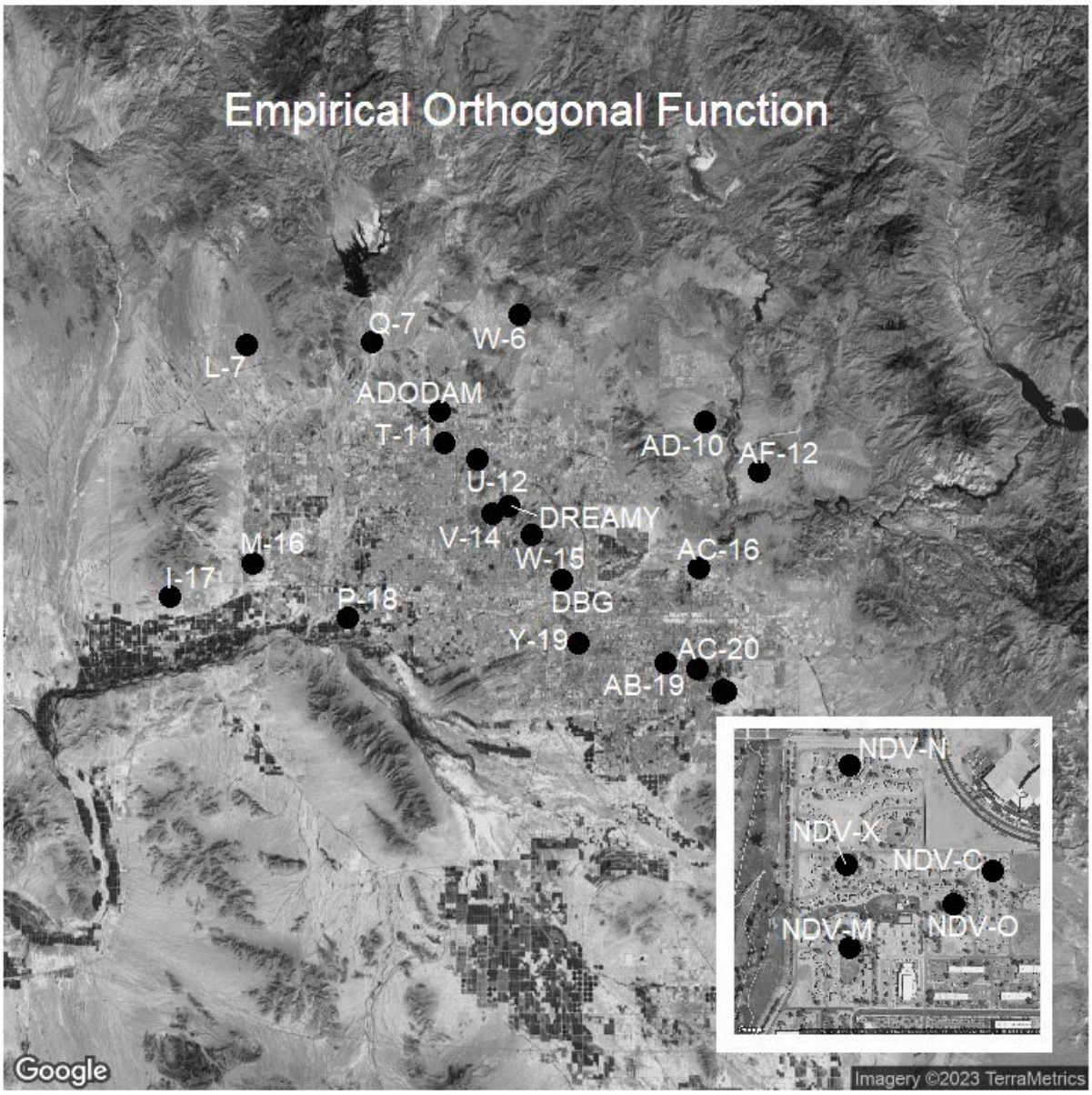

Figure 16: A satellite image of Phoenix, AZ with each of the 24 sites in the dataset overlaid. Sites are color coded by the optimal clusters determined using the empirical orthogonal function method. The smaller inset image is a higher magnification view of the group of five sites in the bottom right corner of the larger image. Satellite imagery was obtained from Google Maps.

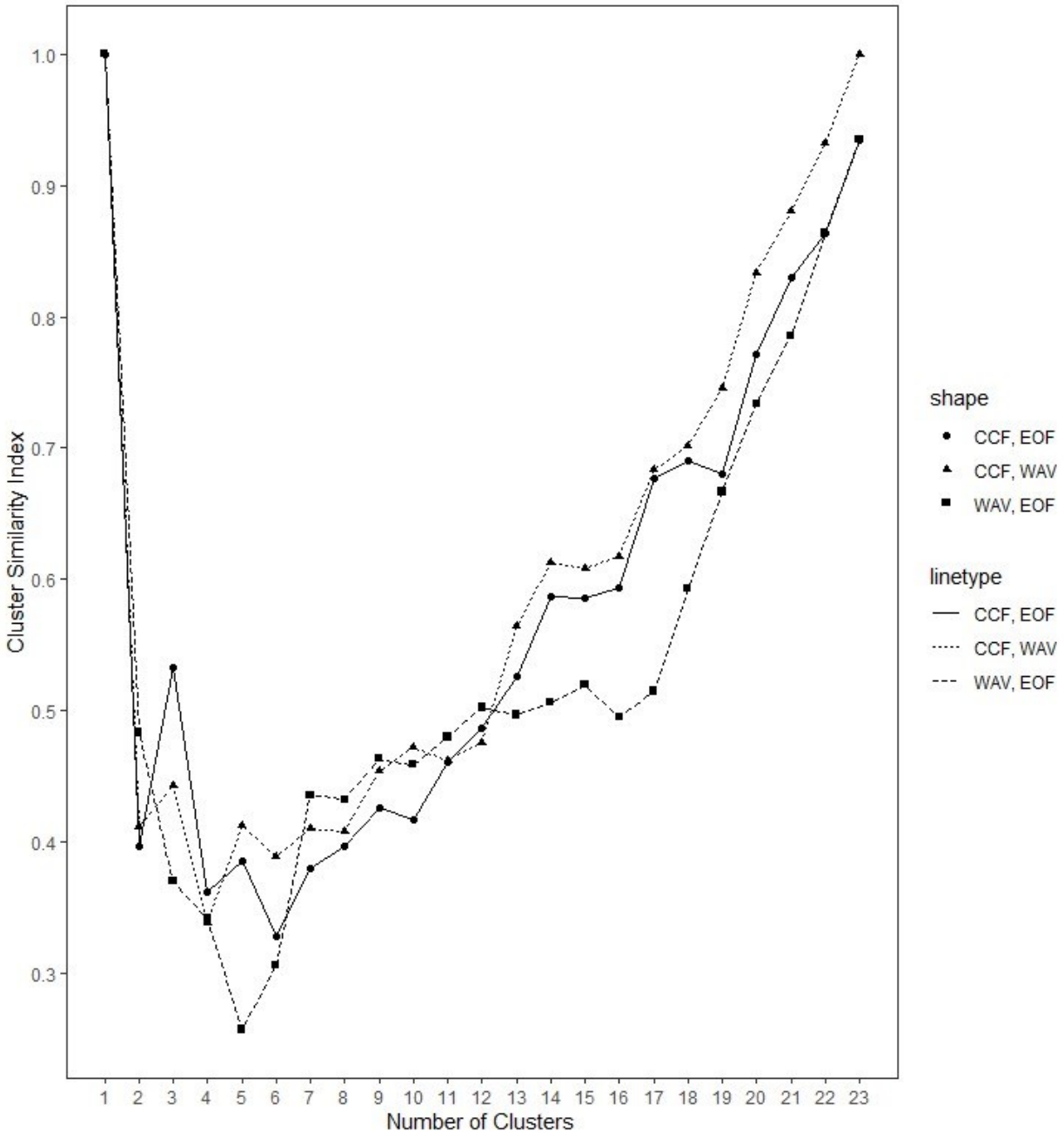

Figure 17: Plot showing the cluster similarity obtained through each of the three synchrony metrics against the predetermined number of clusters selected to group the Phoenix sites.

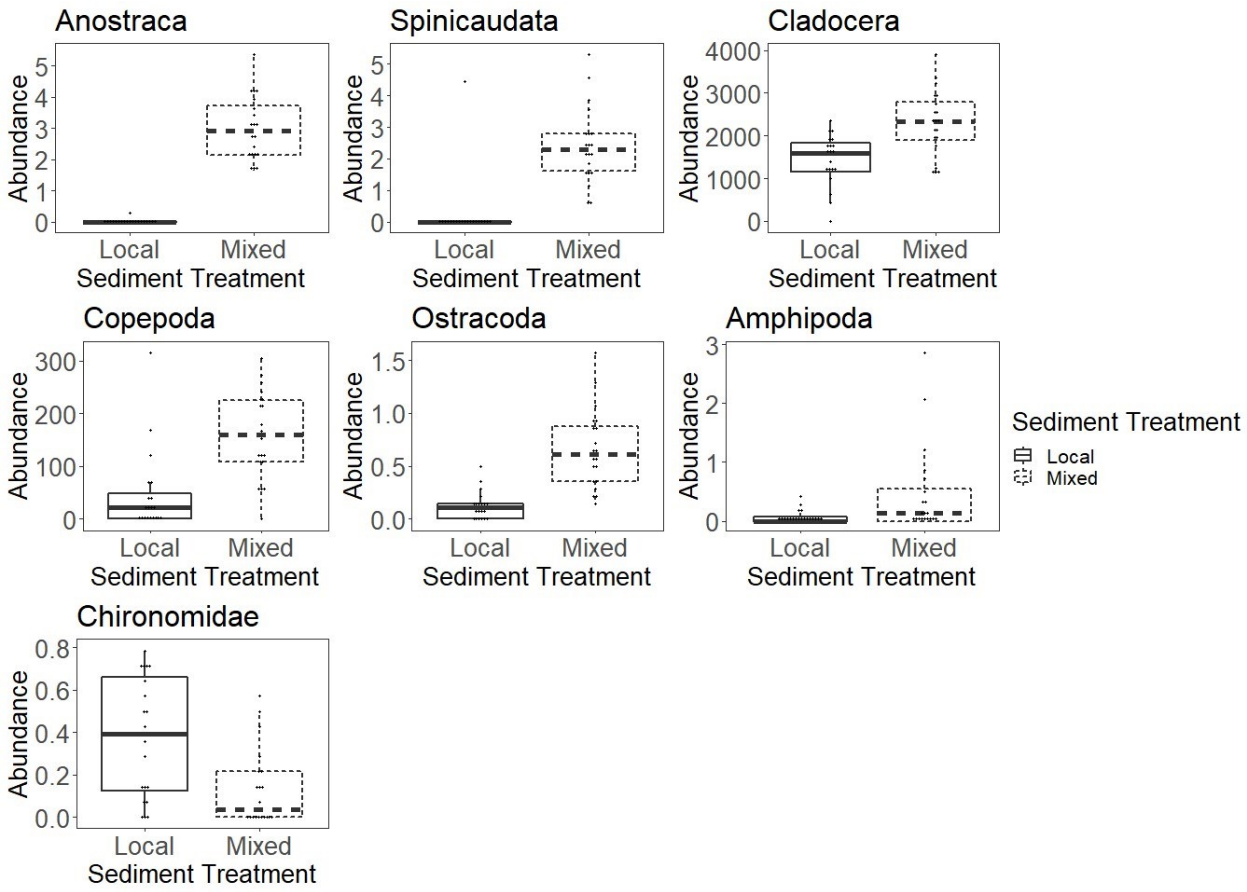

Figure 18: Box plots for the response variables which exhibited an effect due to sediment source from the MVGLM. Local sediment is denoted by solid lines while mixed sediment is denoted by dashed lines. Each plot represents a taxonomic group labeled above that plot.

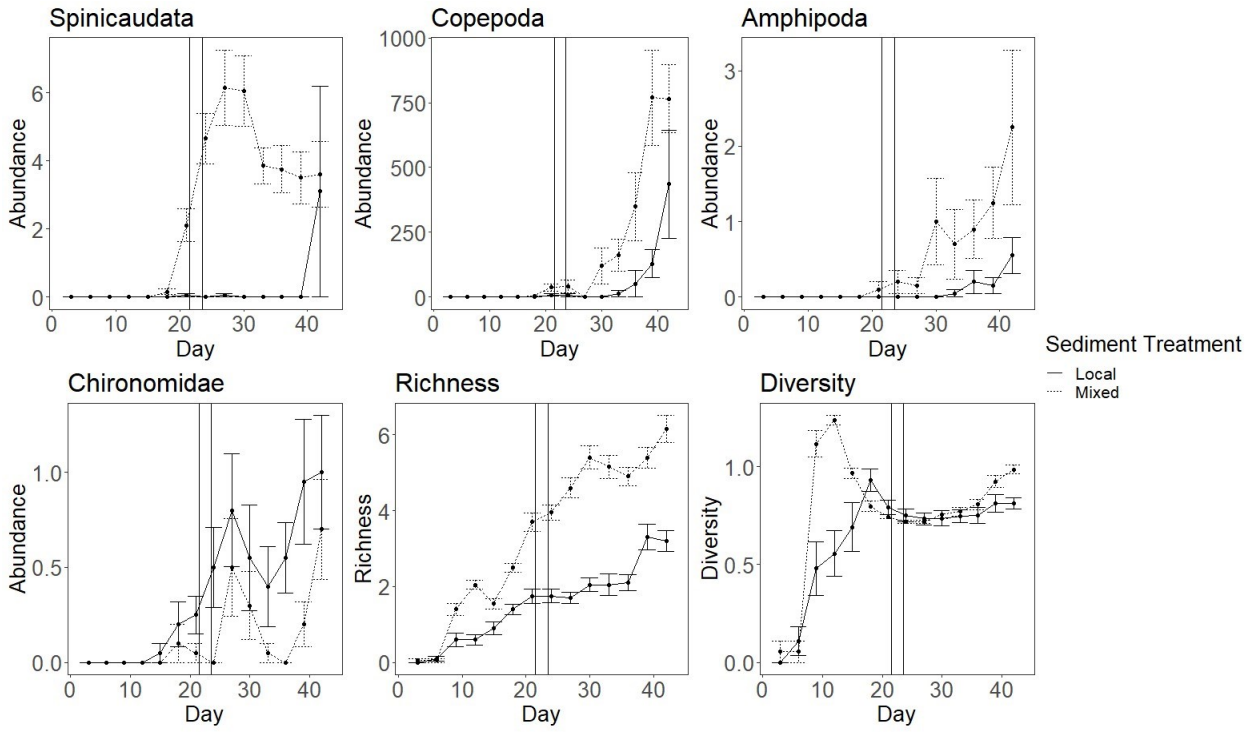

Figure 19: Line graphs for the response variables which exhibited an effect of a sediment*time interaction according to the repeated measures ANOVA. The sediment*time interaction implies that the response of the dependent variable to the sediment varies through time. Mesocosms with local sediment are denoted by solid lines while those with mixed sediment are denoted by dashed lines. Each plot represents a taxonomic group or variable labeled above that plot.

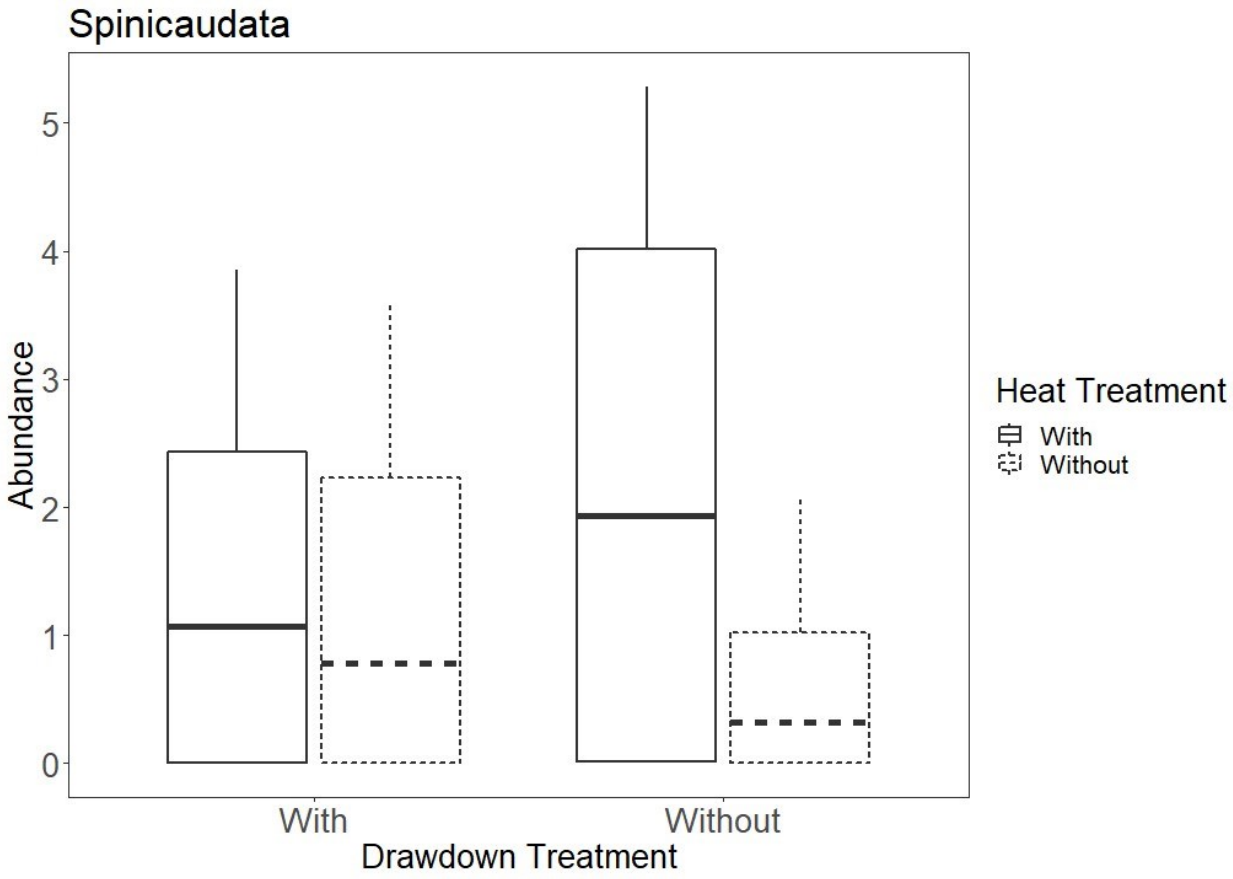

Figure 20: Box plot for the response variable, abundance of Spinicaudata, which exhibited an effect of a heat*drawdown interaction according to the repeated measures ANOVA. The sediment*heat interaction implies that the response of the dependent variable to the drawdown varies according to the heat treatment.

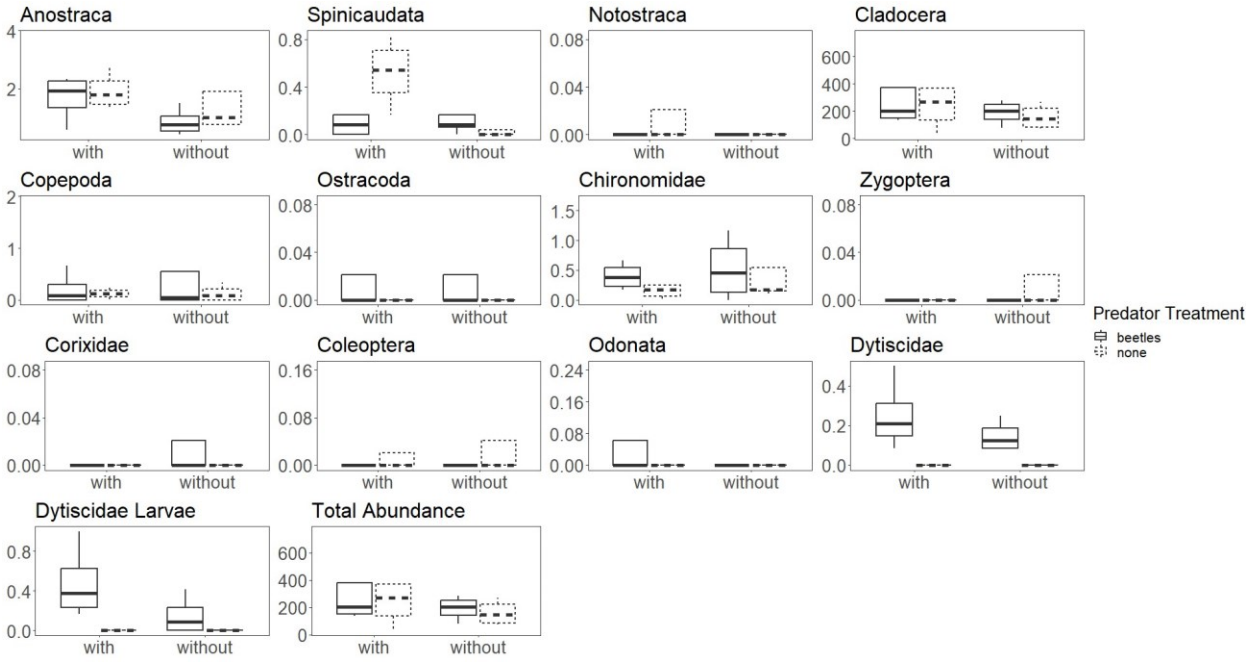

Figure 21: Abundance box plots for each taxa collected during the experiment separated by predator presence and sediment source. Solid lines are those where dysticids were present while dashed lines are those where dytiscids were absent. Sediment source is denoted by the x axis of each plot. Only mesocosms without additional heating were included in these plots.

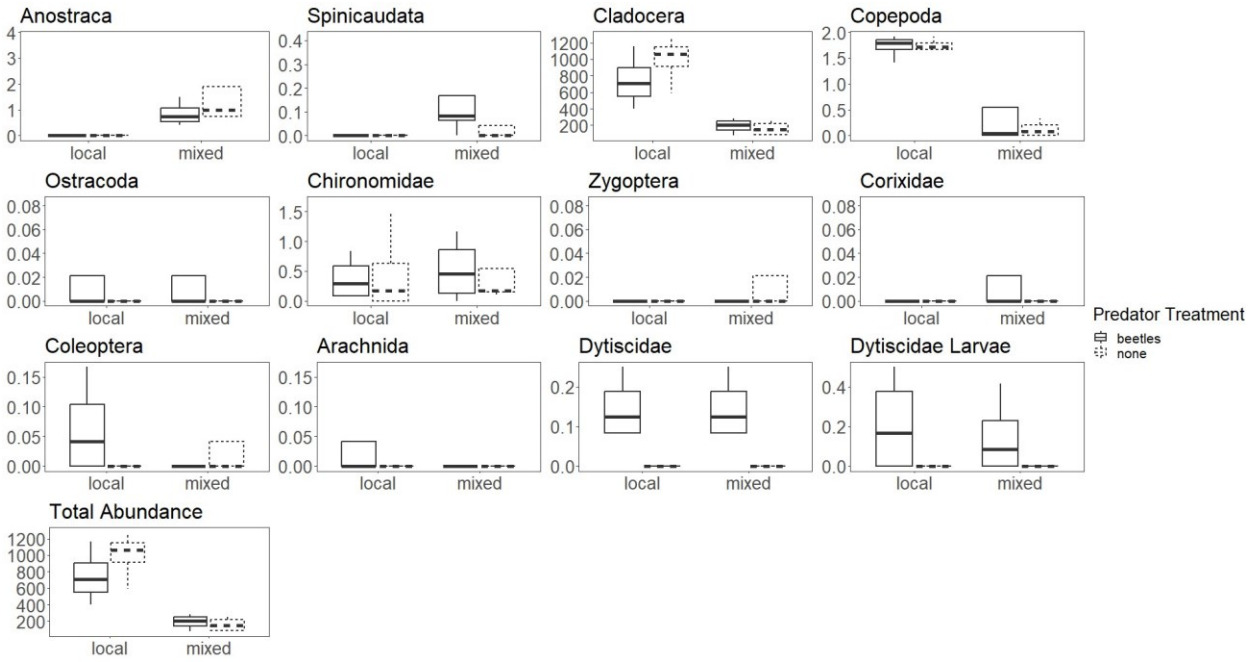

Figure 22: Abundance box plots for each taxa collected during the experiment separated by predator presence and warming. Solid lines are those where dysticids were present while dashed lines are those where dytiscids were absent. Warming is denoted by the x axis of each plot. Only mesocosms seeded with mixed sediment were included in these plots.

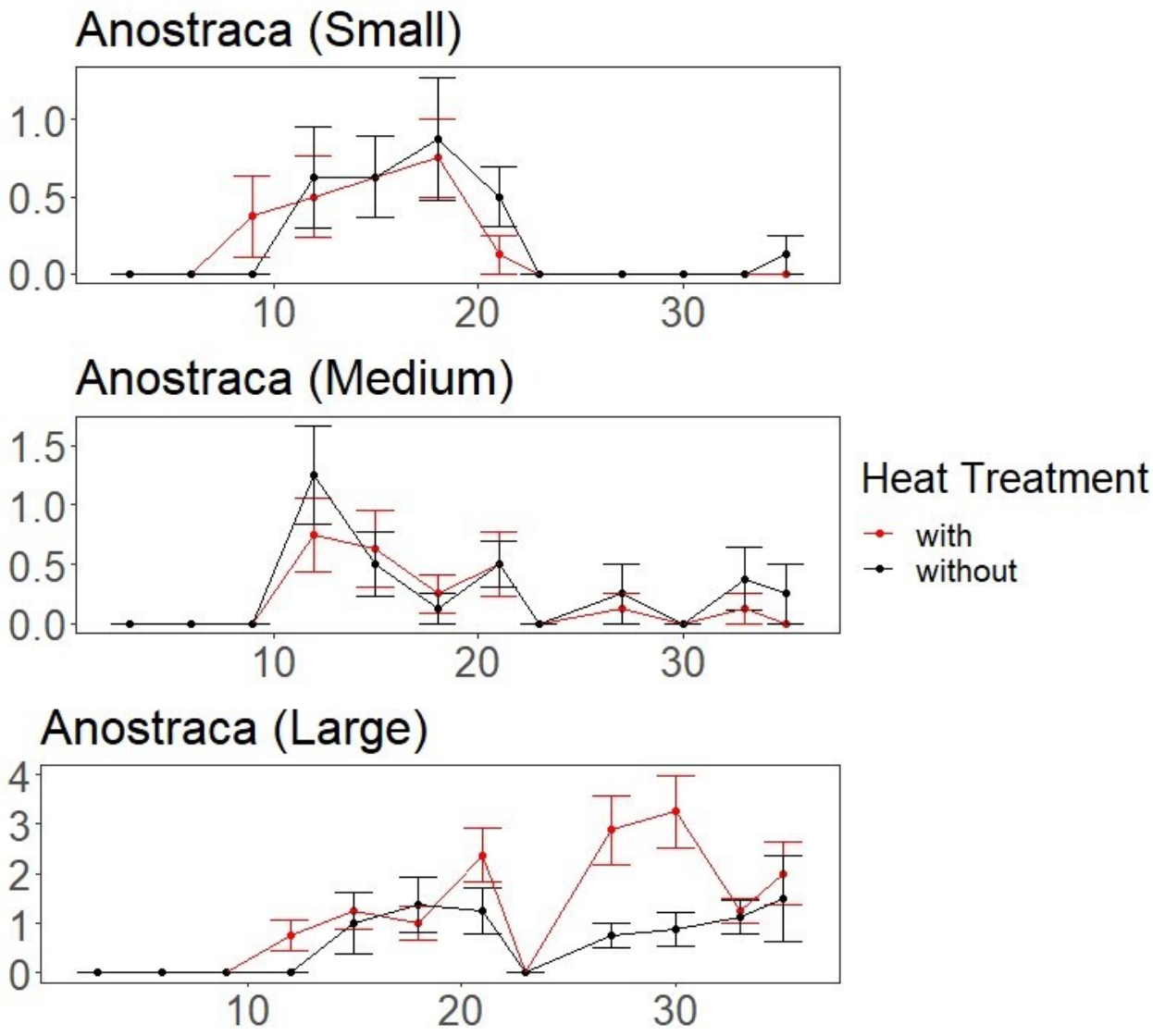

Figure 23: Abundance time series for each size class of fairy shrimp collected during the experiment and separated by predator presence and warming. Solid lines are those where

dysticids were present while dashed lines are those where dytiscids were absent. Warming is denoted by the x axis of each plot.

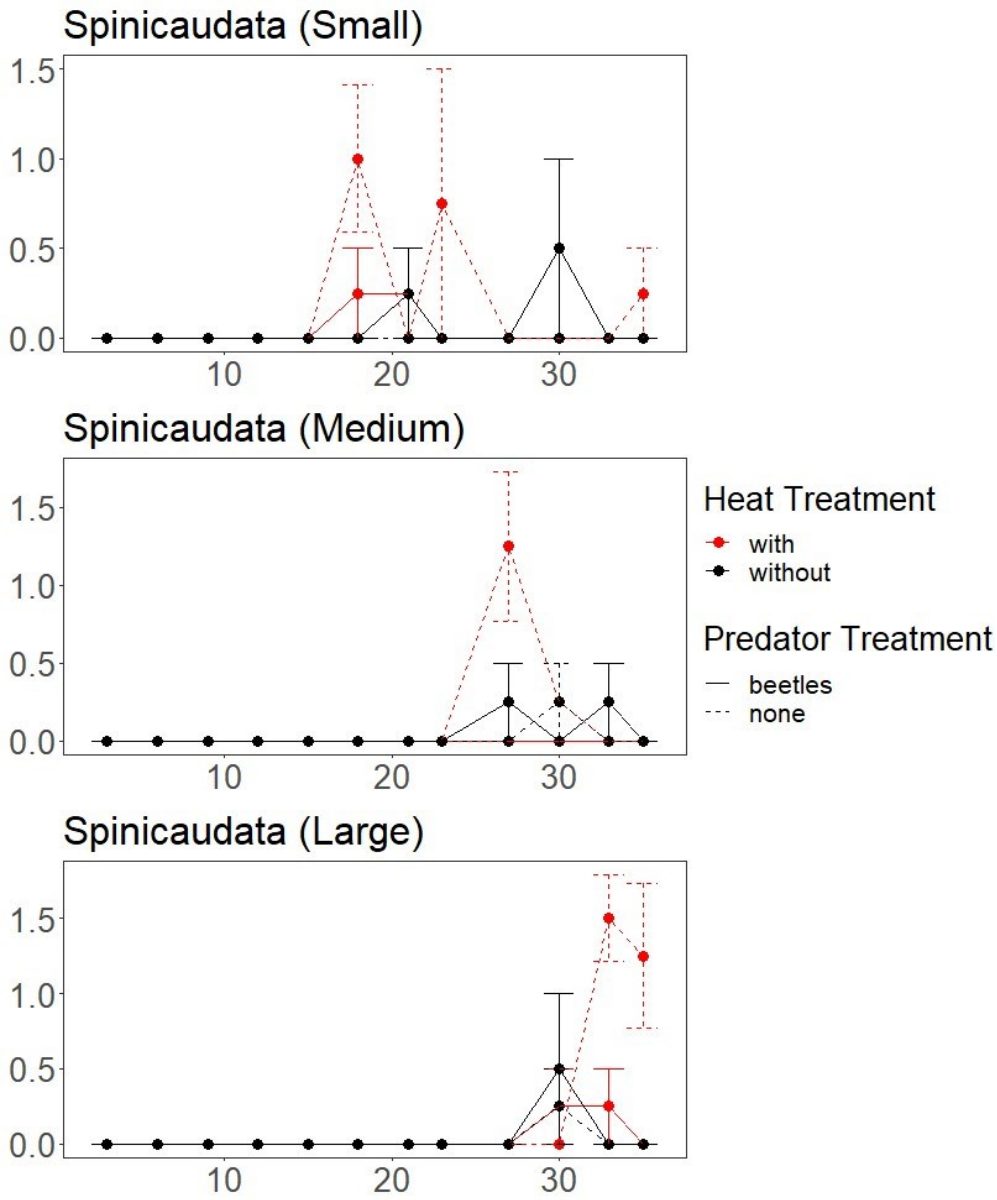

Figure 24: Abundance time series plots for each size class of clam shrimp collected during the experiment and separated by both predator presence and heat treatment. Red lines are those with additional warming while black lines are those without warming. Solid lines are those where dysticids were present while dashed lines are those where dytiscids were absent.

APPENDIX B. CHAPTER I SUPPLEMENTARY INFORMATION

Table S1: Summary of expected results for synchrony metric comparisons using simulated data. If the metric generates the expected number of clusters, listed below, then it is correctly operating at the particular set of parameters.

Test Parameter	Expected (Correct) Number of Clusters	Reasoning
Frequency	2	Frequency mode of treatment now differs from that of control; the 10 treatment time series have one frequency value, while the 10 control time series have a different frequency value
Phase Lag	2	Phase lag of treatment now differs from that of control; the 10 treatment time series have one phase lag value, the other 10 control time series have a different phase lag value
Magnitude	1	Any difference in magnitude between the treatment and control is still in phase and additive; all 20 time series should be part of the same cluster
Noise	1	Differences in noise between the treatment and control may inhibit the ability of the technique to detect clusters, but should not lead to different clusters on their own; all 20 time series are part of the same cluster

Table S2: Results summary table for the AIC test on the optimal clusters obtained by the crosscorrelation function method as explained by a linear combination of environmental covariates for each site

Variable	Estimate	Std. Error	t value	Pr(>|t|)	P<0.05
(Intercept)	-2.82E+01	8.55E+00	-3.3	0.001143	**
Mean.tmin.prev3d	1.85E+00	5.51E-01	3.355	0.000949	***
imp.sfc.2011	8.71E+01	5.59E+01	1.557	0.121012	
elevation.m	7.37E-	1.94E-	3.79	0.0001	***

	02	02	1	99	
disp.from.cent	1.26E+01	4.01E+00	3.139	0.001953	**
Mean.tmin.prev3d:imp.sfc.2011	-4.57E+00	3.36E+00	-1.36	0.1752	
Mean.tmin.prev3d:elevation.m	-4.55E-03	1.26E-03	-3.612	0.000385	***
imp.sfc.2011:elevation.m	-2.14E-01	1.41E-01	-1.521	0.1298	
Mean.tmin.prev3d:disp.from.cent	-7.25E-01	2.58E-01	-2.809	0.005467	**
imp.sfc.2011:disp.from.cent	-4.11E+01	3.11E+01	-1.32	0.1876	
elevation.m:disp.from.cent	-3.05E-02	8.82E-03	-3.455	0.000672	***
Mean.tmin.prev3d:imp.sfc.2011:elevation.m	1.14E-02	8.45E-03	1.343	0.1808	
Mean.tmin.prev3d:imp.sfc.2011:disp.from.cent	1.69E+00	1.87E+00	0.904	0.367153	
Mean.tmin.prev3d:elevation.m:disp.from.cent	1.76E-03	5.70E-04	3.081	0.002356	**
imp.sfc.2011:elevation.m:disp.from.cent	9.86E-02	7.82E-02	1.26	0.2091	
Mean.tmin.prev3d:imp.sfc.2011:elevation.m:disp.from.cent	-4.13E-03	4.71E-03	-0.876	0.382025	

Table S3: Results summary table for the AIC test on the two clusters obtained by the EOF method as explained by a linear combination of environmental covariates for each site

Variable	Estimate	Std. Error	t valu	Pr(>|t|)	P<0.05

			e		
(Intercept)	2.09E-01	4.58E-01	0.457	0.648017	
imp.sfc.2011	2.45E+00	3.41E+00	0.719	0.472956	
elevation.m	1.79E-03	1.10E-03	1.634	0.103883	
disp.from.cent	6.22E-01	2.37E-01	2.624	0.009358	**
Mean.ppt.prev3d	-6.42E-01	8.44E-01	-0.760	0.447978	
imp.sfc.2011:elevation.m	-5.66E-03	8.66E-03	-0.654	0.51418	
imp.sfc.2011:disp.from.cent	5.92E+00	2.12E+00	2.793	0.005723	**
elevation.m:disp.from.cent	-1.28E-03	5.39E-04	-2.378	0.018349	*
imp.sfc.2011:Mean.ppt.prev3d	3.35E+01	8.67E+00	3.86	0.000153	***
elevation.m:Mean.ppt.prev3d	1.48E-03	2.36E-03	0.629	0.529928	
disp.from.cent:Mean.ppt.prev3d	3.85E-01	4.05E-01	0.95	0.343285	
imp.sfc.2011:elevation.m:disp.from.cent	-1.53E-02	5.37E-03	-2.848	0.004864	**
imp.sfc.2011:elevation.m:Mean.ppt.prev3d	-8.35E-02	2.23E-02	-3.744	0.000237	***
imp.sfc.2011:disp.from.cent:Mean.ppt.prev3d	-1.80E+01	4.83E+00	-3.738	0.000242	***

elevation.m:disp.from.cent:Mean.ppt.prev3d	-7.87E-04	1.06E-03	-0.745	0.4573	
imp.sfc.2011:elevation.m:disp.from.cent:Mean.ppt.prev3d	4.45E-02	1.23E-02	3.618	0.000376	***

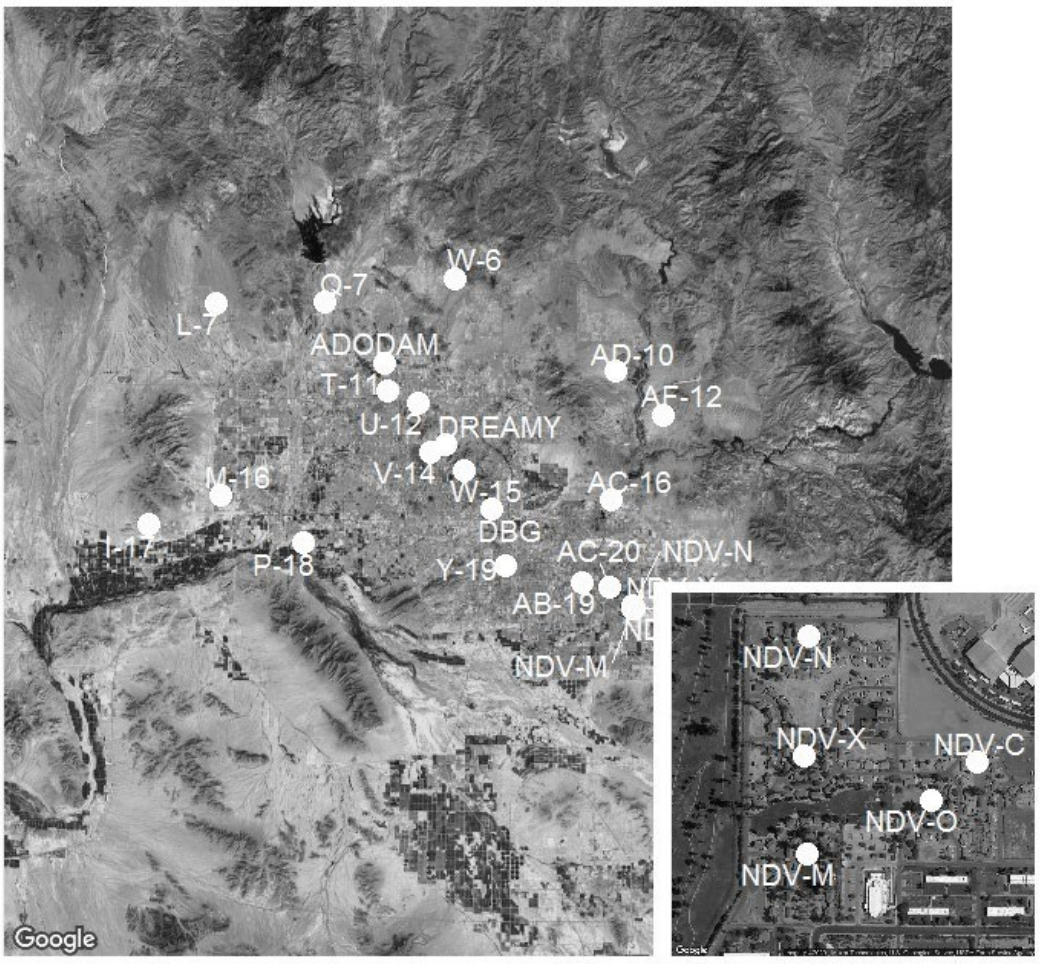

Figure S25: A satellite image of Phoenix, AZ with each of the 24 sites in the dataset overlaid. The smaller inset image is a higher magnification view of the group of five sites in the bottom right corner of the larger image. Satellite imagery was obtained from Google Maps.

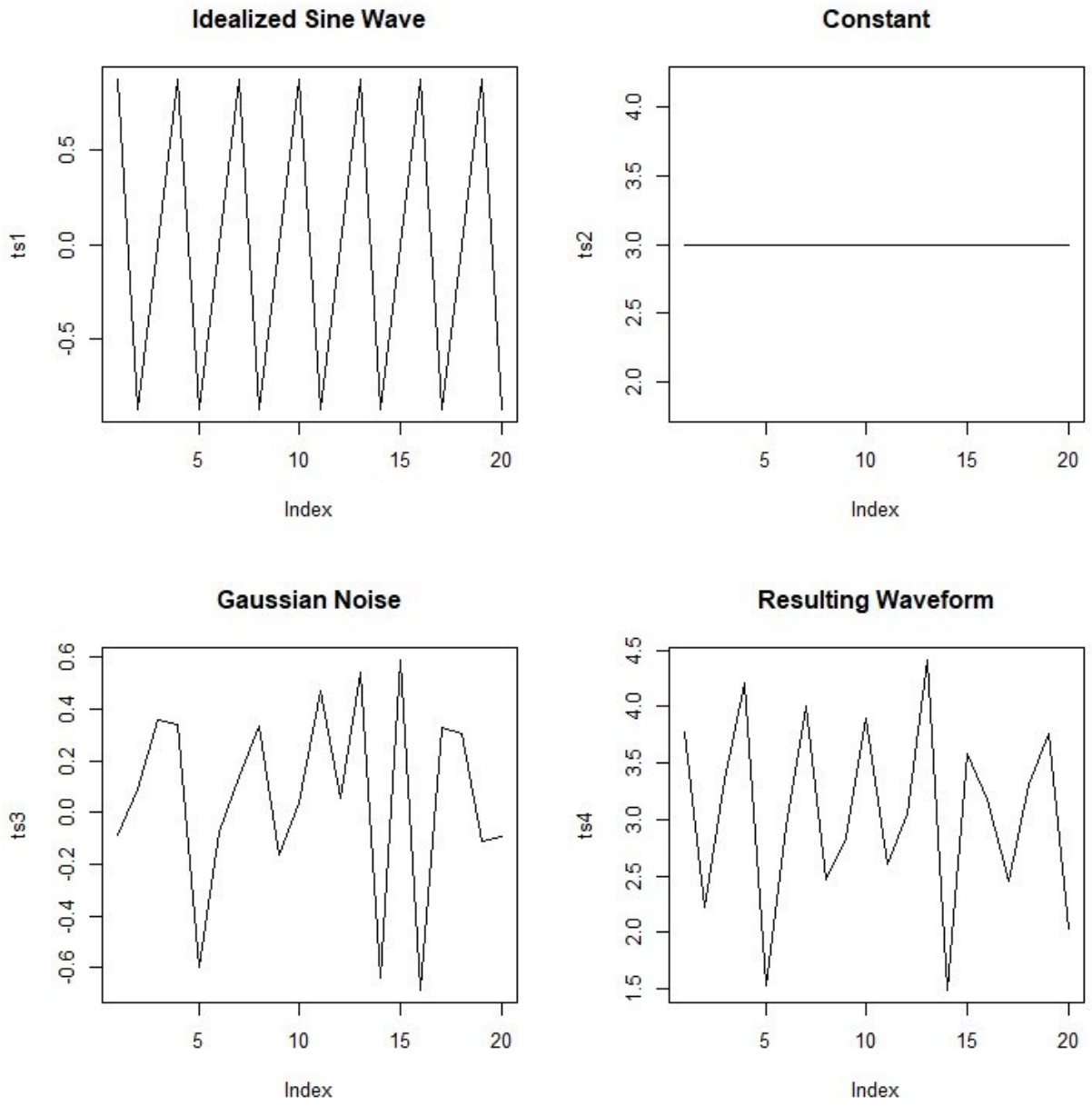

Figure S26: Example diagram showing the idealized sine wave, constant valued signal, Gaussian noise, and the resulting waveform representing time series data for a single site. The resulting waveform is the sum of the idealized sine wave, the constant, and the Gaussian noise.

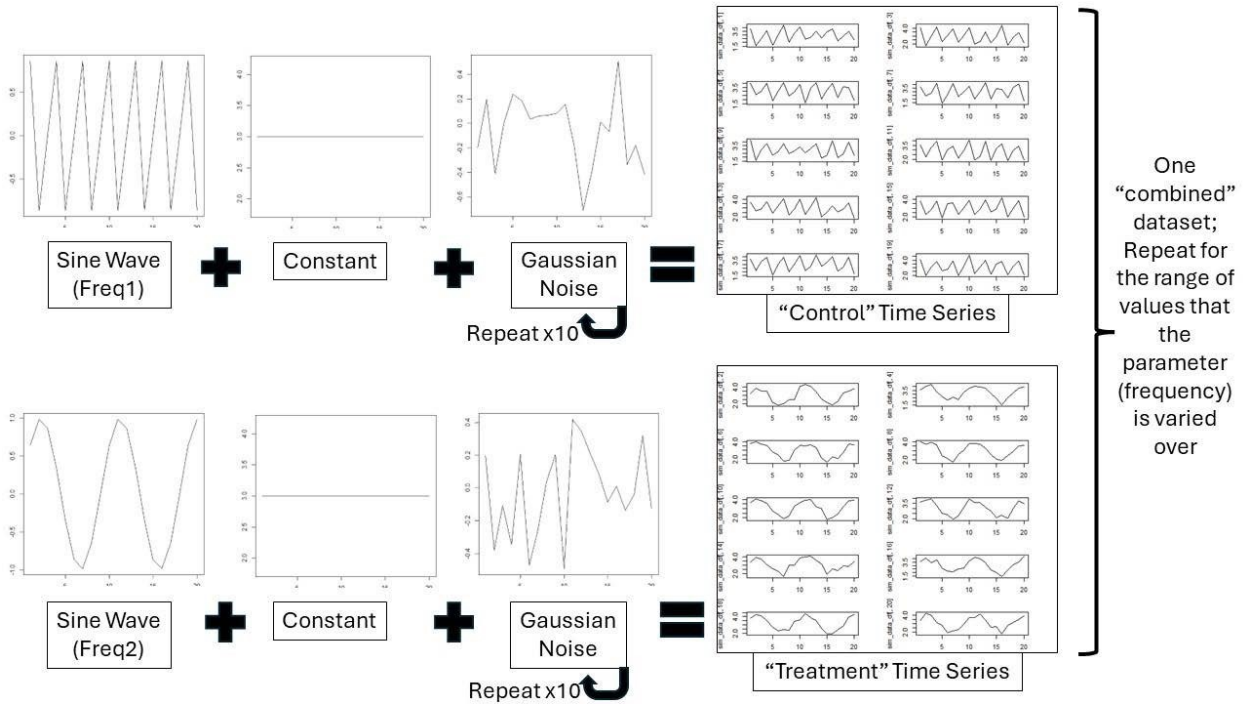

Figure S27: Example of the simulated dataset generation for two different values of frequency. The 20 waveforms to the right comprise the dataset for a single test using each synchrony metric. Note that the process pictured would be repeated for each value over the range that frequency is varied (from 1 to 9 in steps of 1).

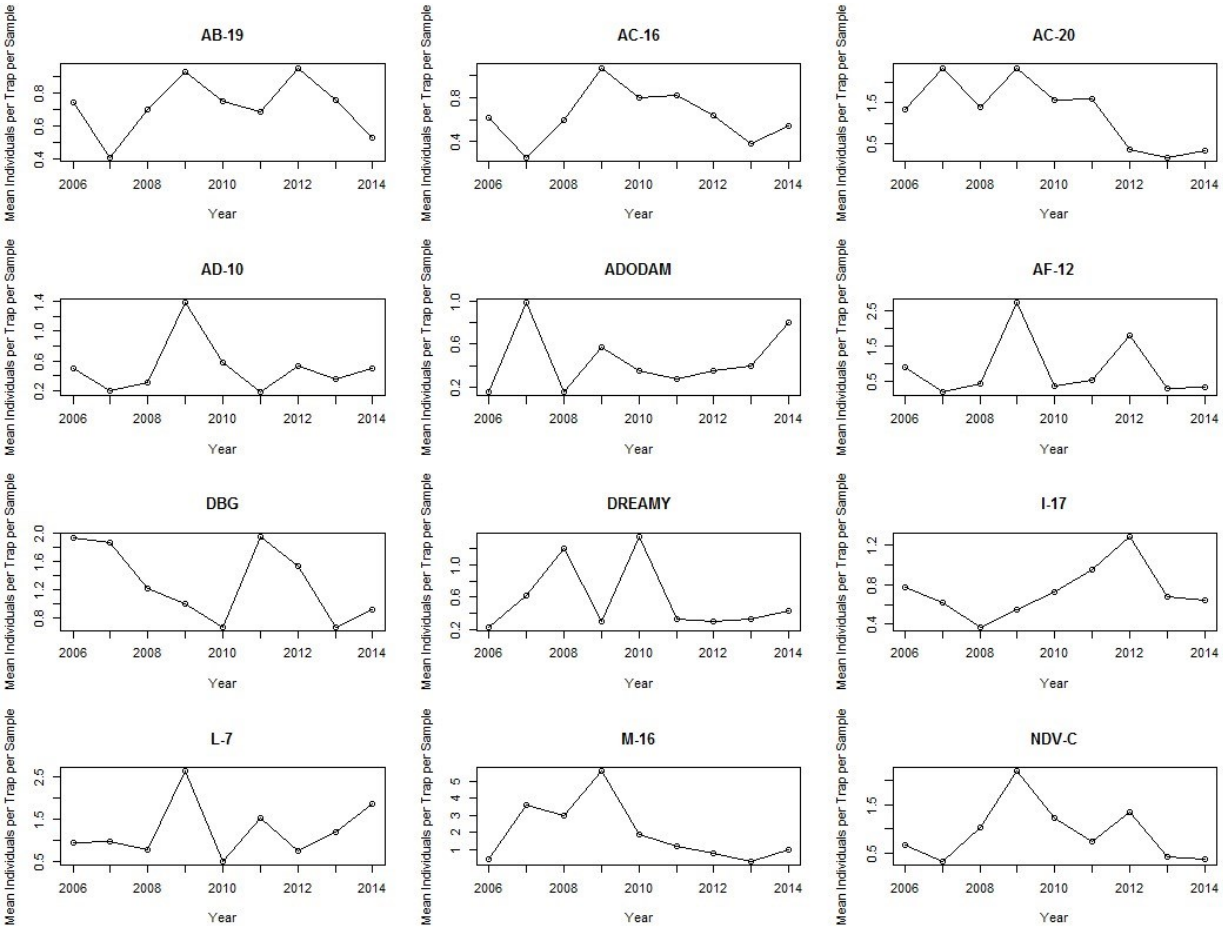

Figure S28: Time series plots showing the mean number of ground beetles per unit sampling effort as an annual average for the years 2006 through 2014. The time series are shown as they are before any normalization operations. These plots provide a way of visualizing the data prior to analysis. This panel contains the first 12 of the 24 total sites listed in alphabetical order by site name.

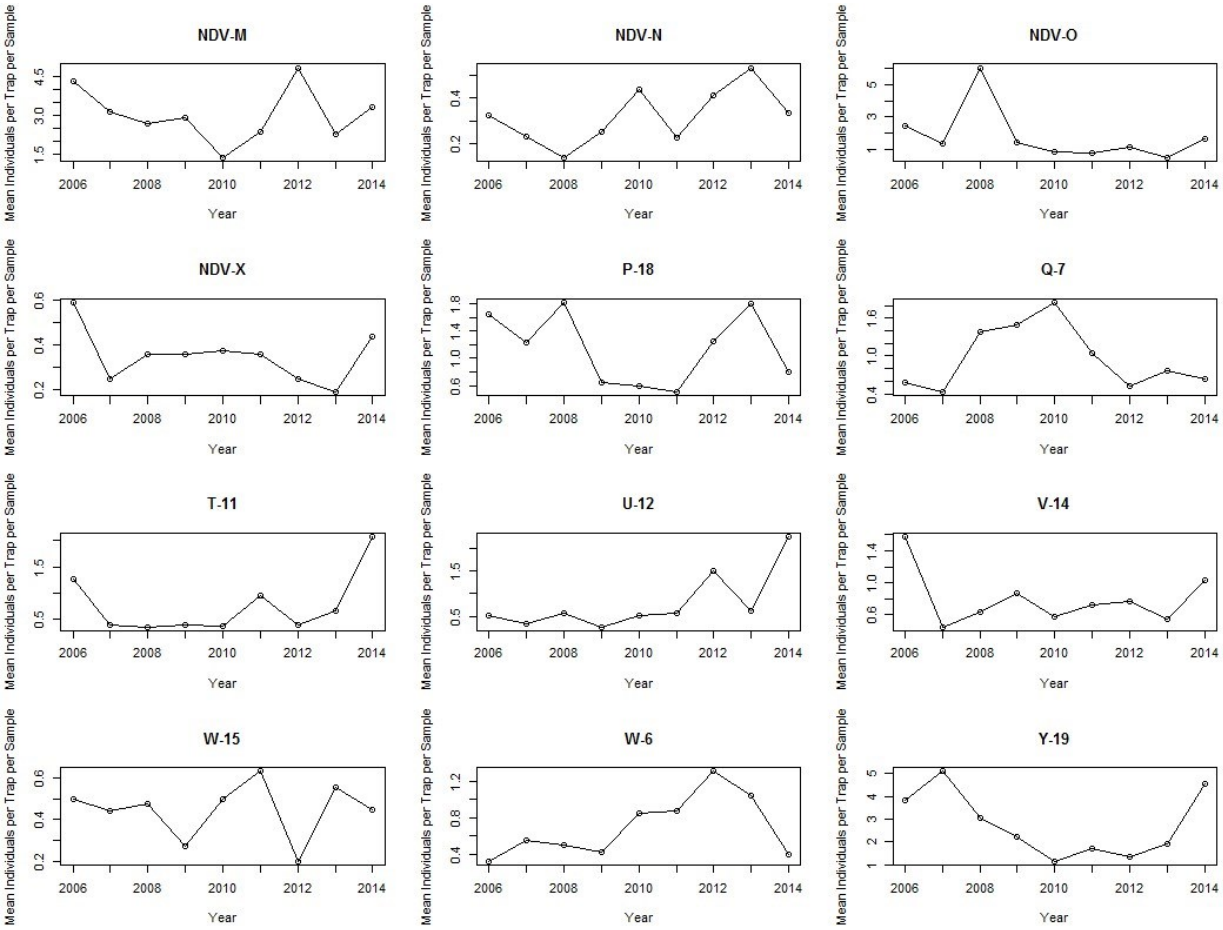

Figure S29: Time series plots showing the mean number of ground beetles per unit sampling effort as an annual average for the years 2006 through 2014. The time series are shown as they are before any normalization operations. These plots provide a way of visualizing the data prior to analysis. This panel contains the last 12 of the 24 total sites listed in alphabetical order by site name.

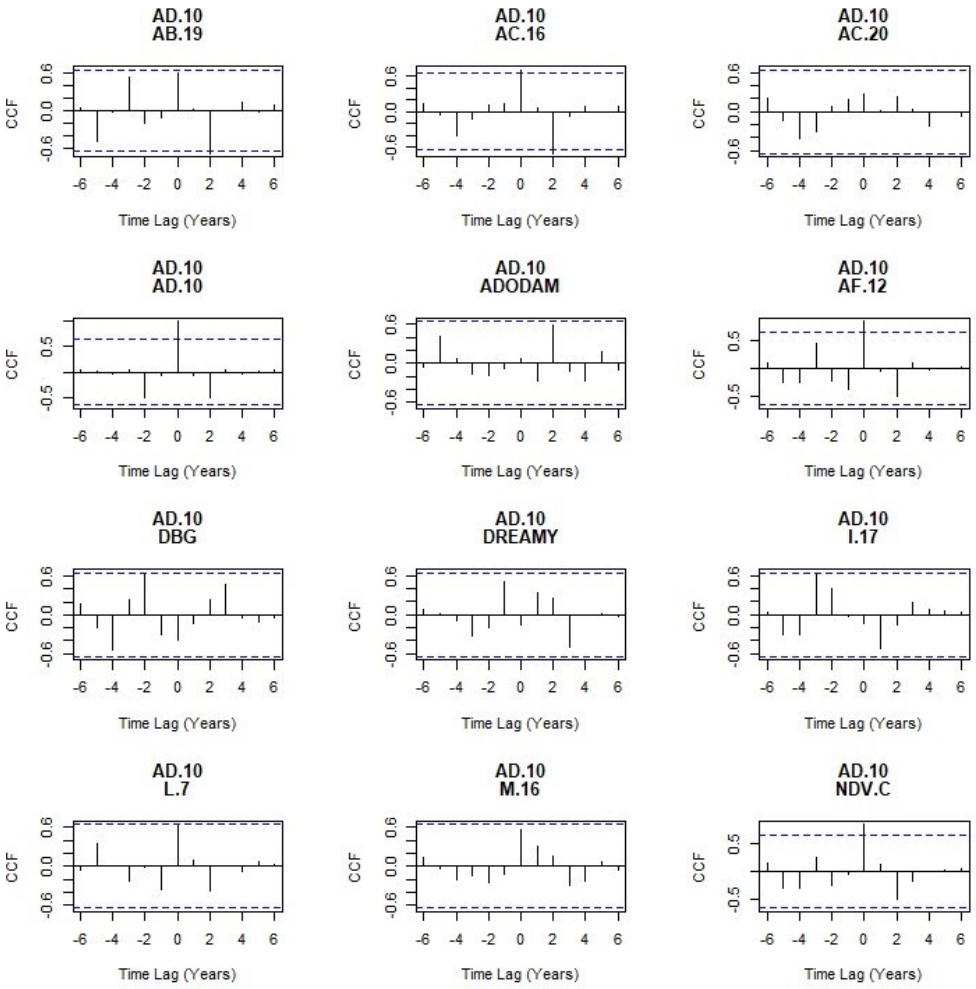

Figure S30: Plots showing the value of a cross-correlation function between the beetle abundance time series of the arbitrarily chosen site AD-10 and every other site. The value of the cross-correlation function takes values from -1, which denotes negative correlation, to 1, which denotes positive correlation. Values beyond the dotted lines are significant with a 95% confidence level. Time lags are represented on the horizontal, each integer corresponding to one year. The time lag is applied to the time series being compared to the reference site AB-19, with positive lags shifting that time series to the right and negative lags (also called leads) shifting that time series to the left. This panel contains the first 12 of the 24 total sites listed in alphabetical order by site name.

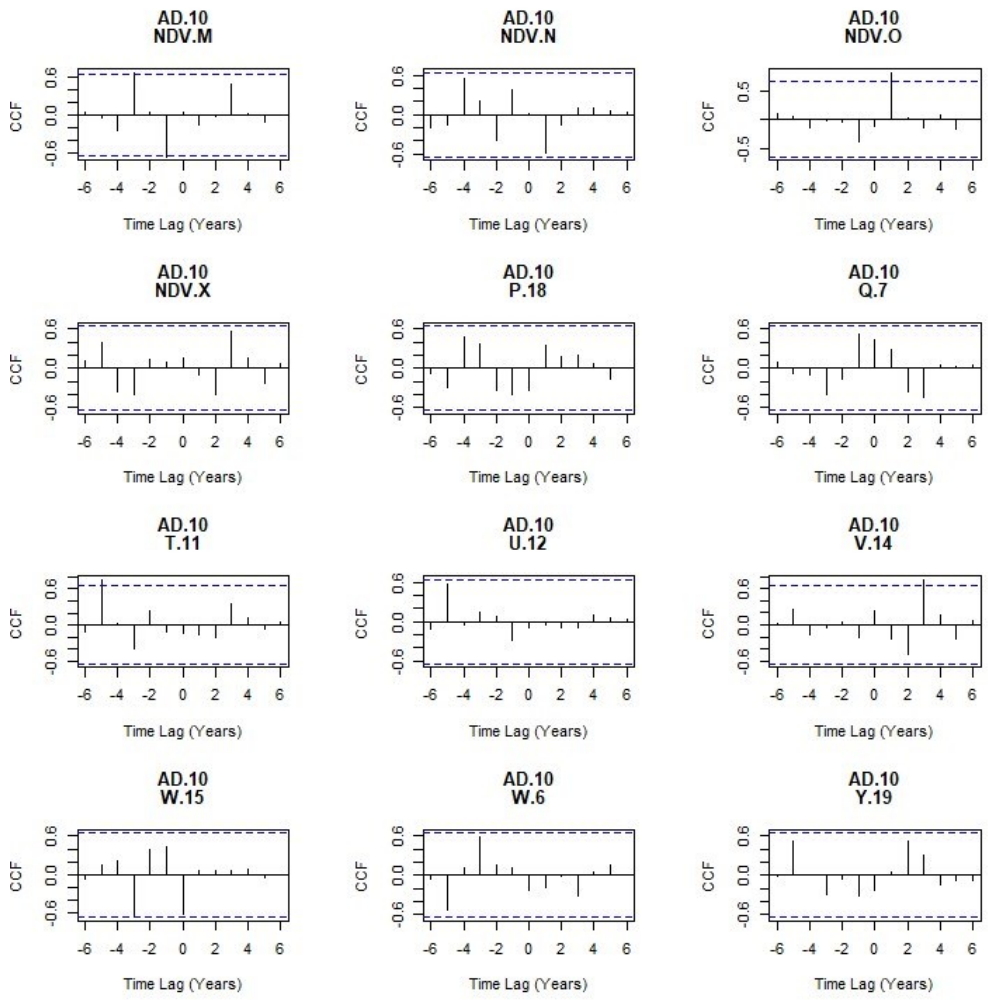

Figure S31: Plots showing the value of a cross-correlation function between the beetle abundance time series of the arbitrarily chosen site AD-10 and every other site. The value of the cross-correlation function takes values from -1, which denotes negative correlation, to 1, which denotes positive correlation. Values beyond the dotted lines are significant with a 95% confidence level. Time lags are represented on the horizontal, each integer corresponding to one year. The time lag is applied to the time series being compared to the reference site AB-19, with positive lags shifting that time series to the right and negative lags (also called leads) shifting that time series to the left. This panel contains the last 12 of the 24 total sites listed in alphabetical order by site name.

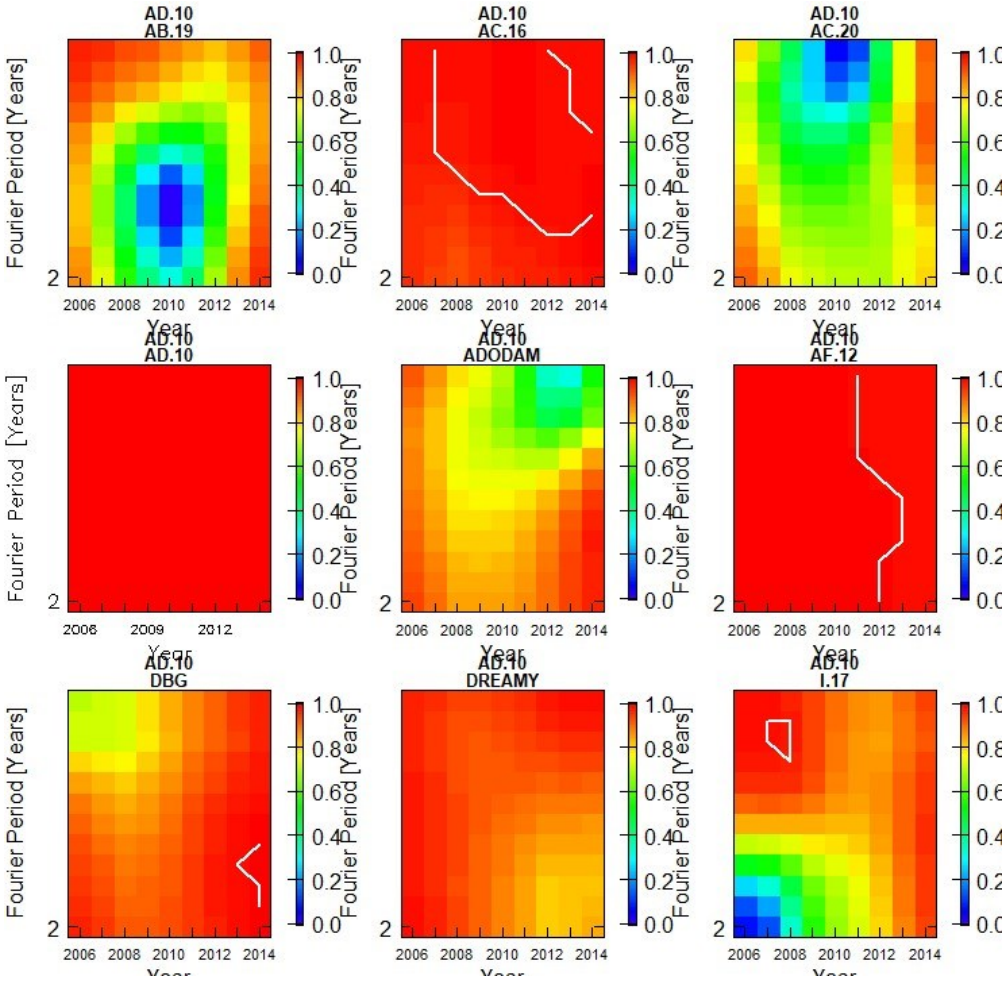

Figure S32: Wavelet scalograms showing the value of coherence between the beetle abundance time series of the arbitrarily chosen site AD-10 and every other site. The value of coherence is represented by the color gradient with values spanning 0 to 1. Regions bounded by the white contour are significant with a 95% confidence interval. Shaded regions outside of the cone of influence (COI) are subjected to edge effects. The vertical axis shows the Fourier period in years, which is the inverse of the Fourier frequency of both the time series and the wavelet. The horizontal axis denotes the years 2006 to 2014. This panel contains sites 1-9 listed in alphabetical order by site name.

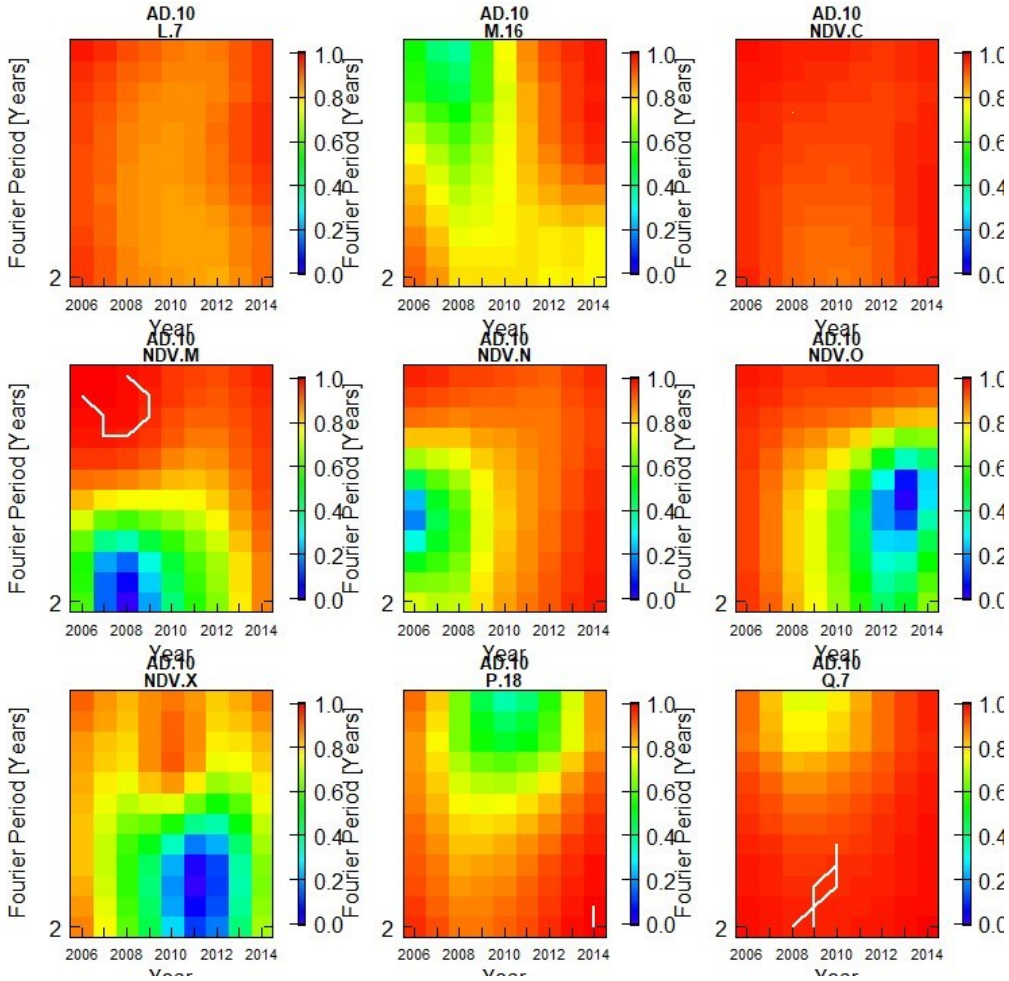

Figure S33: Wavelet scalograms showing the value of coherence between the beetle abundance time series of the arbitrarily chosen site AD-10 and every other site. The value of coherence is represented by the color gradient with values spanning 0 to 1. Regions bounded by the white contour are significant with a 95% confidence interval. Shaded regions outside of the cone of influence (COI) are subjected to edge effects. The vertical axis shows the Fourier period in years, which is the inverse of the Fourier frequency of both the time series and the wavelet. The horizontal axis denotes the years 2006 to 2014. This panel contains sites 10-18 listed in alphabetical order by site name.

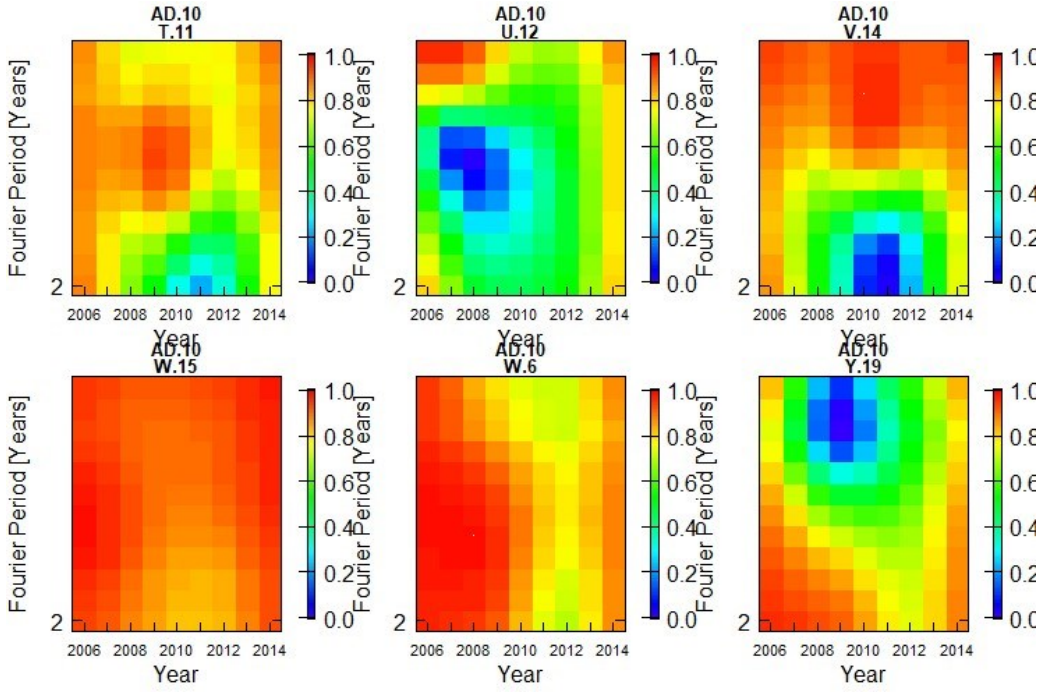

Figure S34: Wavelet scalograms showing the value of coherence between the beetle abundance time series of the arbitrarily chosen site AD-10 and every other site. The value of coherence is represented by the color gradient with values spanning 0 to 1. Regions bounded by the white contour are significant with a 95% confidence interval. Shaded regions outside of the cone of influence (COI) are subjected to edge effects. The vertical axis shows the Fourier period in years, which is the inverse of the Fourier frequency of both the time series and the wavelet. The horizontal axis denotes the years 2006 to 2014. This panel contains sites 19-24 listed in alphabetical order by site name.

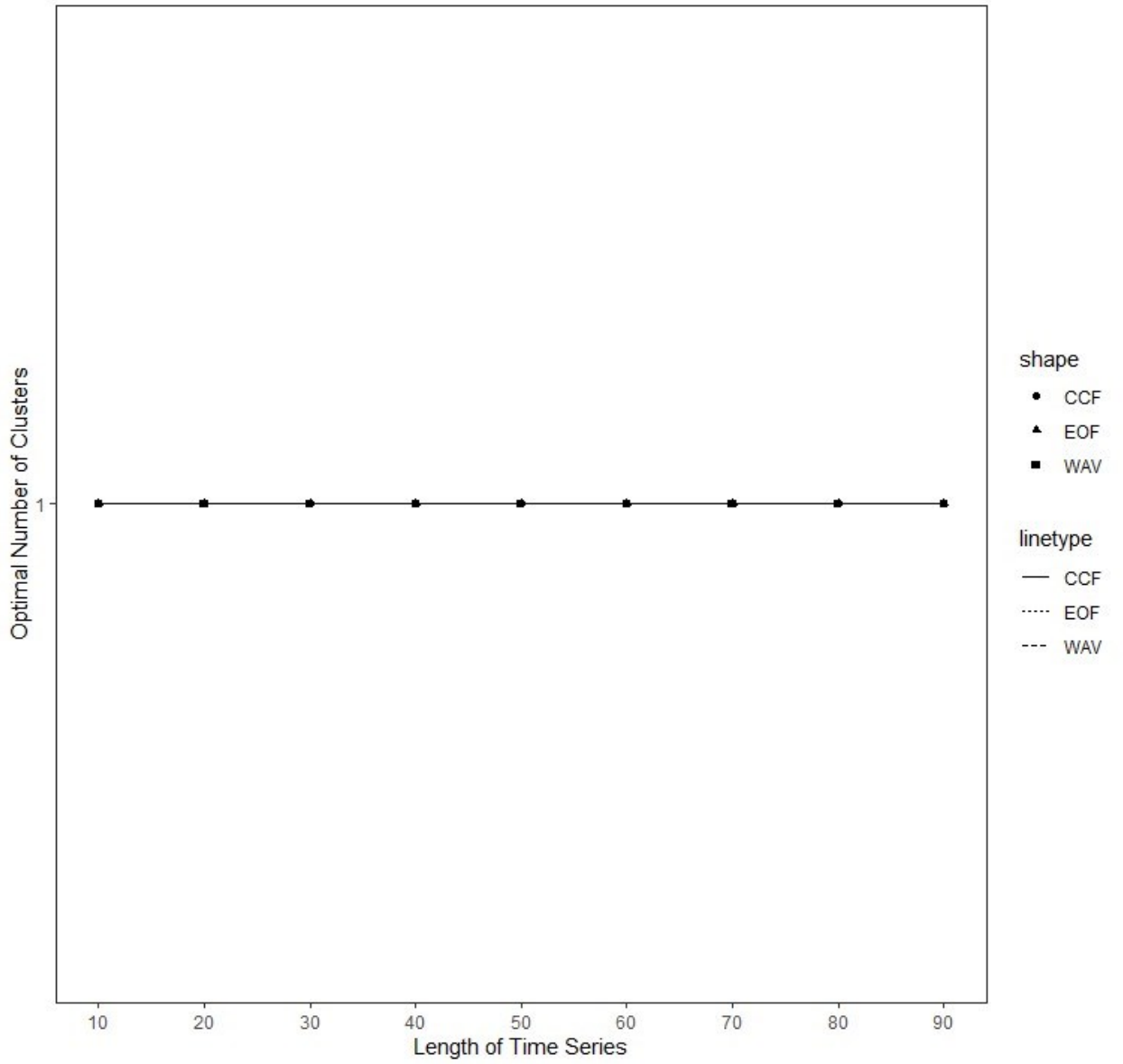

Figure S35: Plot showing the optimal number of clusters obtained through each of the three synchrony metrics against the length of the time series for the simulated data.

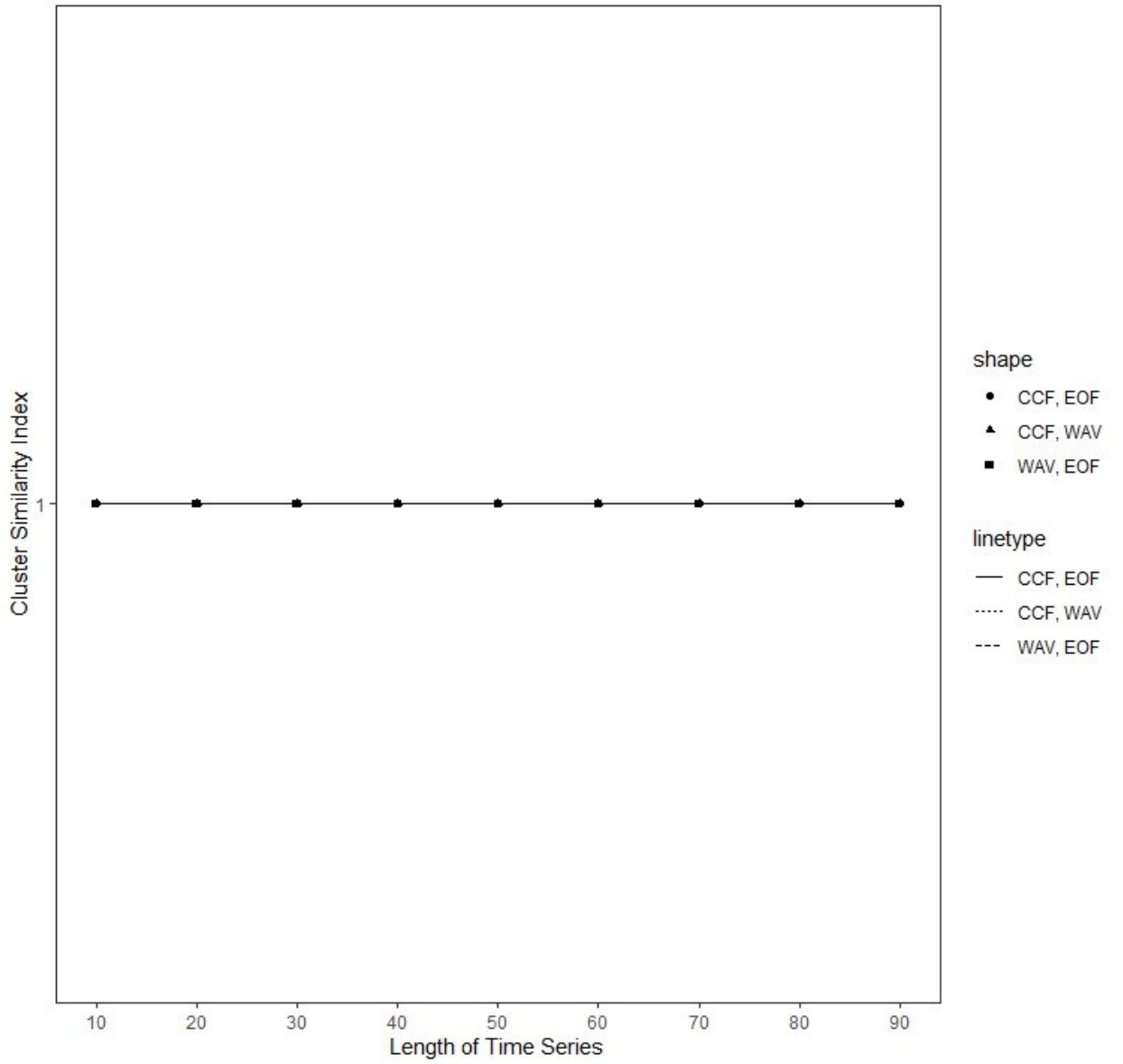

Figure S36: Plot showing the similarity of clusters obtained through each of the three synchrony metrics against the length of the time series for the simulated data.

APPENDIX C. CHAPTER II SUPPLEMENTARY INFORMATION

Table S4: Results summary table for the response of daily water temperature to the heating factor

Effect	DFn	DFd	F	p	P < 0.05
Heat	1	16	47.089	3.820e-06	***
Day	1	16	531.670	1.056e-13	***

Table S5: Significant multivariate analysis of deviance results for general effects of the three individual factors and each of those factors interacting with time

Effect	Residual DF	DF diff	Deviance	p	P < 0.05
Sediment	531	14	1264	0.001	***
Sediment*Day	531	13	253.7	0.001	***

Table S6: Univariate analysis of deviance results responding to the sediment

Effect	Deviance	p	P < 0.05
Anostraca	640.457	0.001	***
Spinicaudata	262.657	0.001	***
Cladocera	63.688	0.001	***
Copepoda	29.048	0.040	*
Ostracoda	93.398	0.001	***
Amphipoda	32.87	0.015	*
Chironomidae	33.329	0.014	*

Table S7: Univariate analysis of deviance results responding to sediment*time

Effect	Deviance	p	p < 0.05
Spinicaudata	84.026	0.001	***
Cladocera	32.164	0.015	*

Table S8: Univariate analysis of deviance results responding to the drawdown

Effect	Deviance	p	p < 0.05
Zygoptera	35.516	0.008	**

Table S9: Repeated measures ANOVA results for Spinicaudata

Effect	DFn	DFd	F	p	P < 0.05
Sediment*Day	1	32	11.124	0.002	**
Heat*Drawdown	1	32	4.302	0.046	*

Table S10: Repeated measures ANOVA results for Cladocera

Effect	DFn	DFd	F	p	P < 0.05
Sediment	1	32	5.192	0.030	*
Drawdown	1	32	17.099	2.393e-04	***
Day	1	32	235.577	2.600e-16	***

Table S11: Repeated measures ANOVA results for Copepoda

Effect	DFn	DFd	F	p	P < 0.05
Sediment*Day	1	32	14.378	6.262e-04	***

Table S12: Repeated measures ANOVA results for Chironomidae

Effect	DFn	DFd	F	p	P < 0.05
Sediment*Day	1	32	5.473	0.026	*

Table S13: Repeated measures ANOVA results for Coleoptera

Effect	DFn	DFd	F	p	P < 0.05
Day	1	32	6.704	0.014	*

Table S14: Repeated measures ANOVA results for Amphipoda

Effect	DFn	DFd	F	p	P < 0.05
Day	1	32	6.704	0.014	*

Table S15: Repeated measures ANOVA results for total abundance

Effect	DFn	DFd	F	p	P < 0.05
Sediment	1	32	4.467	0.042	*
Drawdown	1	32	21.508	5.680e-05	***
Day	1	32	266.283	4.544e-17	***

Table S16: Repeated measures ANOVA results for richness (Order)

Effect	DFn	DFd	F	p	P < 0.05

Sediment*Day 1		32	115.653	3.716e-12	***

Table S17: Repeated measures ANOVA results for Shannon diversity (Order)

Effect	DFn	DFd	F	p	P < 0.05
Sediment	1	32	5.746	0.022	*

Table S18: Repeated measures ANOVA results for sqrt(Anostraca)

Effect	DFn	DFd	F	p	P < 0.05
Heat*Drawdown*Sediment*Day 1		32	5.100	0.031	*

Table S19: Repeated measures ANOVA results for sqrt(Ostracoda)

Effect	DFn	DFd	F	p	P < 0.05
Sediment*Day 1		32	35.920	1.107e-06	***

Table S20: Repeated measures ANOVA results for sqrt(Zygoptera)

Effect	DFn	DFd	F	p	P < 0.05
Heat*Drawdown*Sediment*Day 1		32	4.215	0.048	*

Table S21: Results summary table for the ‘slope (before breakpoint)’ parameter in the breakpoint regression models

Effect	DFn	DFd	F	p	P < 0.05
Sediment	1	32	12.276	0.0014	**

Table S22: Clusters obtained using the CCF algorithm from Chapter I on total abundance

Mesocosm ID	Heat	Sediment	Drawdown	8 Clusters	4 Clusters	2 Clusters
1	Without	Mixed	Without	1	1	1
9	Without	Mixed	Without	1	1	1
22	With	Mixed	Without	1	1	1
26	With	Mixed	With	1	1	1
24	With	Mixed	With	1	1	1
34	Without	Mixed	With	1	1	1
39	With	Local	Without	1	1	1
2	With	Mixed	With	2	2	2

15	Without	Local	With	2	2	2
29	With	Local	Without	2	2	2
25	With	Local	With	2	2	2
40	Without	Local	Without	2	2	2
8	Without	Local	With	3	2	2
3	With	Local	Without	3	2	2
21	Without	Local	With	3	2	2
32	With	Local	With	3	2	2
4	With	Mixed	With	4	3	1
5	With	Local	Without	4	3	1
20	Without	Mixed	With	4	3	1
33	Without	Local	Without	4	3	1
38	With	Local	With	4	3	1
17	With	Local	With	5	4	2
23	Without	Local	With	5	4	2
6	Without	Local	With	5	4	2
10	Without	Local	Without	5	4	2
19	With	Local	Without	5	4	2
11	With	Mixed	Without	6	3	1
12	Without	Mixed	Without	6	3	1
16	Without	Mixed	Without	6	3	1
35	With	Mixed	Without	6	3	1
36	With	Mixed	Without	6	3	1
37	Without	Mixed	Without	6	3	1
7	With	Mixed	Without	6	3	1
13	Without	Mixed	With	7	3	1
14	Without	Local	Without	7	3	1
28	With	Local	With	7	3	1
18	Without	Mixed	With	8	1	1
27	With	Mixed	With	8	1	1
31	Without	Mixed	With	8	1	1
30	Without	Local	Without	8	1	1

Table S23: Clusters obtained using the CCF algorithm from Chapter I on richness (order)

Mesocosm ID	Heat	Sediment	Drawdown	8 Clusters	4 Clusters	2 Clusters
Without	1	1	1			
26	With	Mixed	With	1	1	1
2	With	Mixed	With	1	1	1
15	Without	Local	With	1	1	1
23	Without	Local	With	1	1	1
16	Without	Mixed	Without	1	1	1
35	With	Mixed	Without	1	1	1
18	Without	Mixed	With	1	1	1
24	With	Mixed	With	2	2	2
34	Without	Mixed	With	2	2	2
3	With	Local	Without	2	2	2
5	With	Local	Without	2	2	2
20	Without	Mixed	With	2	2	2

1
Without
Mixed

33	Without	Local	Without	2	2	2
6	Without	Local	With	2	2	2
14	Without	Local	Without	2	2	2
29	With	Local	Without	3	3	1
4	With	Mixed	With	3	3	1
17	With	Local	With	3	3	1
11	With	Mixed	Without	3	3	1
36	With	Mixed	Without	3	3	1
37	Without	Mixed	Without	3	3	1
39	With	Local	Without	4	4	2
7	With	Mixed	Without	4	4	2
9	Without	Mixed	Without	5	1	1
22	With	Mixed	Without	5	1	1
8	Without	Local	With	5	1	1
12	Without	Mixed	Without	5	1	1
13	Without	Mixed	With	5	1	1
27	With	Mixed	With	5	1	1
31	Without	Mixed	With	5	1	1
10	Without	Local	Without	6	4	2
19	With	Local	Without	6	4	2
21	Without	Local	With	7	4	2
32	With	Local	With	7	4	2
38	With	Local	With	7	4	2
28	With	Local	With	7	4	2
25	With	Local	With	8	4	2
40	Without	Local	Without	8	4	2
30	Without	Local	Without	8	4	2

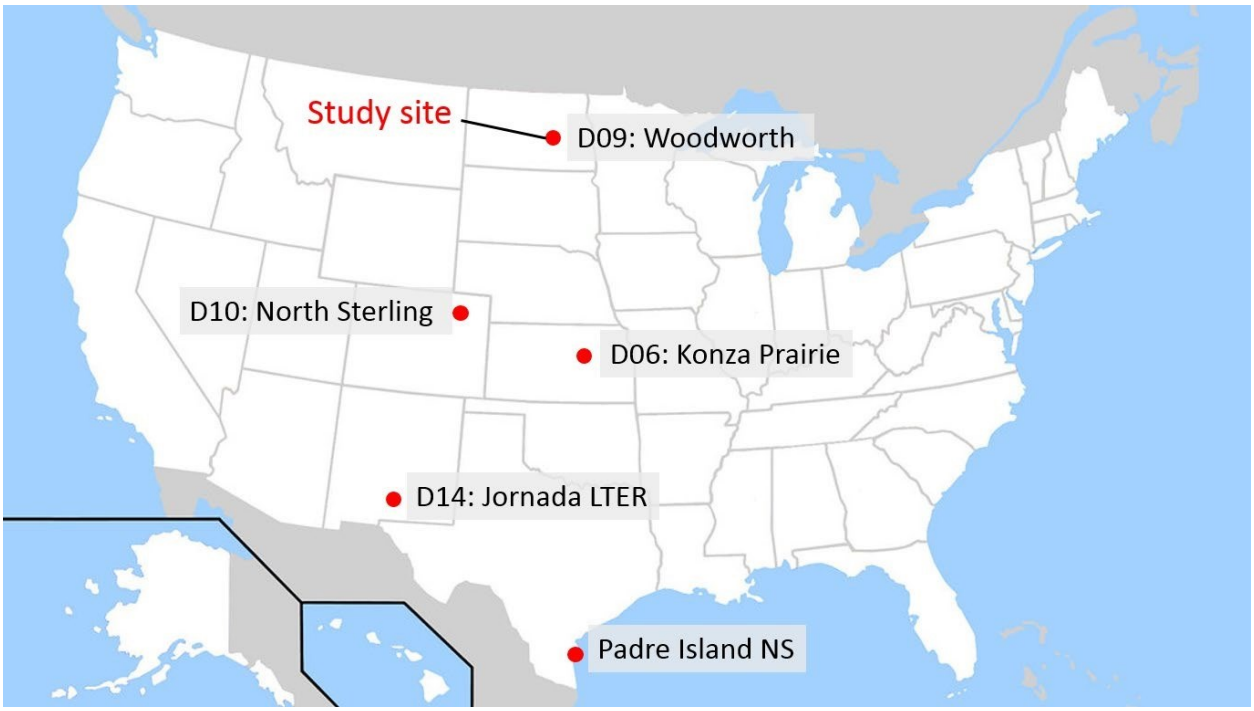

Figure S37: A map of the United States with the sediment locations marked. Half of the sediment collected near the Woodworth NEON site in North Dakota was retained on site and labeled 'local sediment' while the other half was homogenized with equal parts from each of the remaining four sites. This mixture was labeled 'mixed sediment'. The mesocosm experiment was conducted at the Woodworth site in North Dakota.

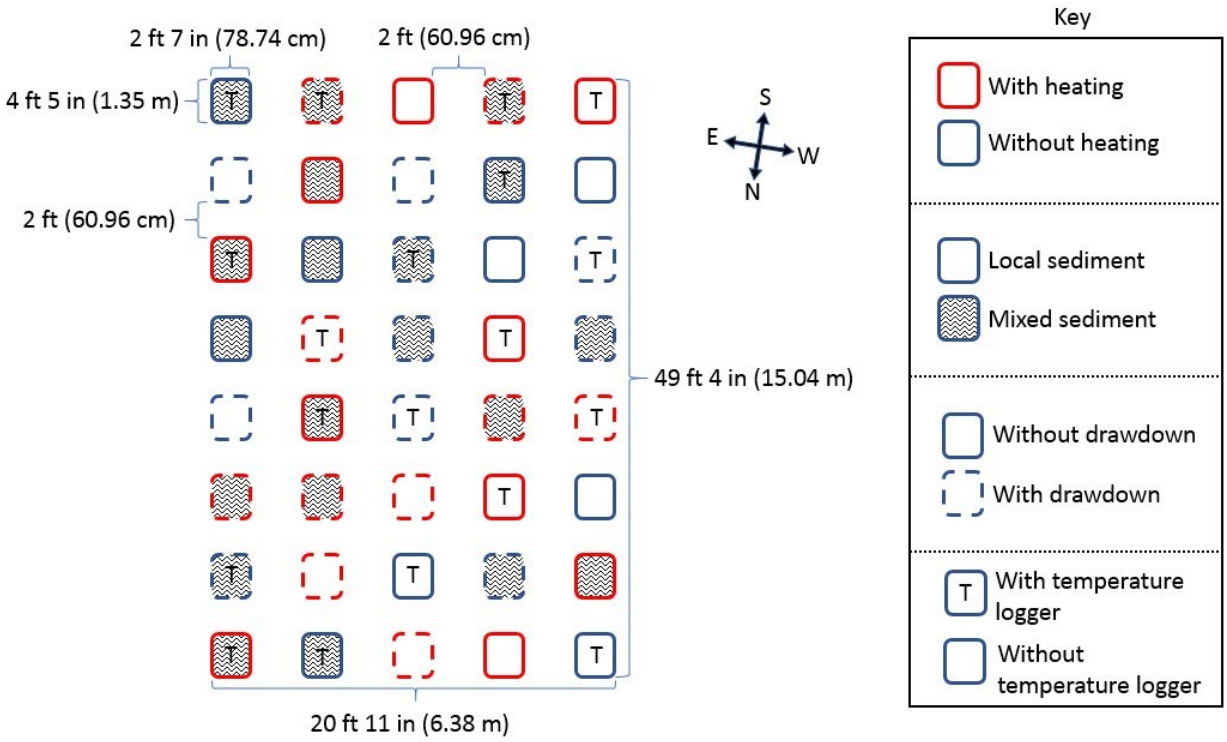

Figure S38: A diagram showing the arrangement of and the treatments applied to each mesocosm during the mesocosm study. The dimensions of an individual mesocosm, the spacing between mesocosms, and the area occupied by the entire array are noted. The compass denotes the orientation of the array along the cardinal directions. The key lists each factor: heating, sediment, and drawdown. For each mesocosm, the outline denotes the heat treatment, the fill shading denotes the sediment treatment, the line type of the outline denotes the drawdown treatment, and the 'T' in each shape denotes the mesocosms with temperature loggers included.

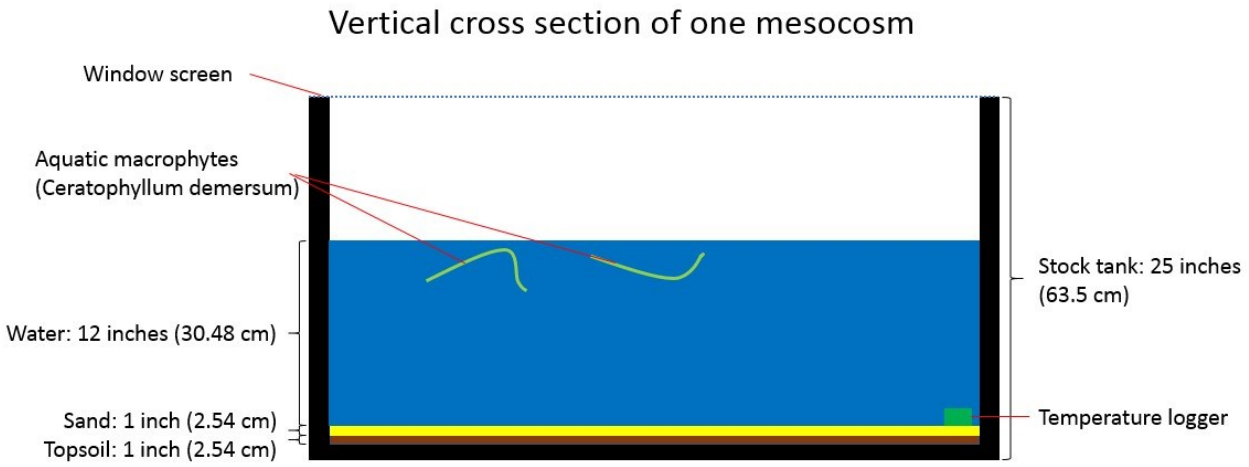

Figure S39: A vertical cross section of a single stock mesocosm as used during the mesocosm experiment. The substrate used was an inch-deep layer of sand atop an inch-deep layer of topsoil. If a temperature logger was present, it was placed atop the substrate. A depth of 30.5 cm (~12 inches) was maintained above the substrate, meaning the water depth as measured from the rigid bottom of the mesocosm was about 35.5 cm (~14 inches). Each mesocosm contained two stems of the macrophyte *Ceratophyllum demersum*, seen floating at the water's surface. A window screen was used to seal the top of the mesocosm.

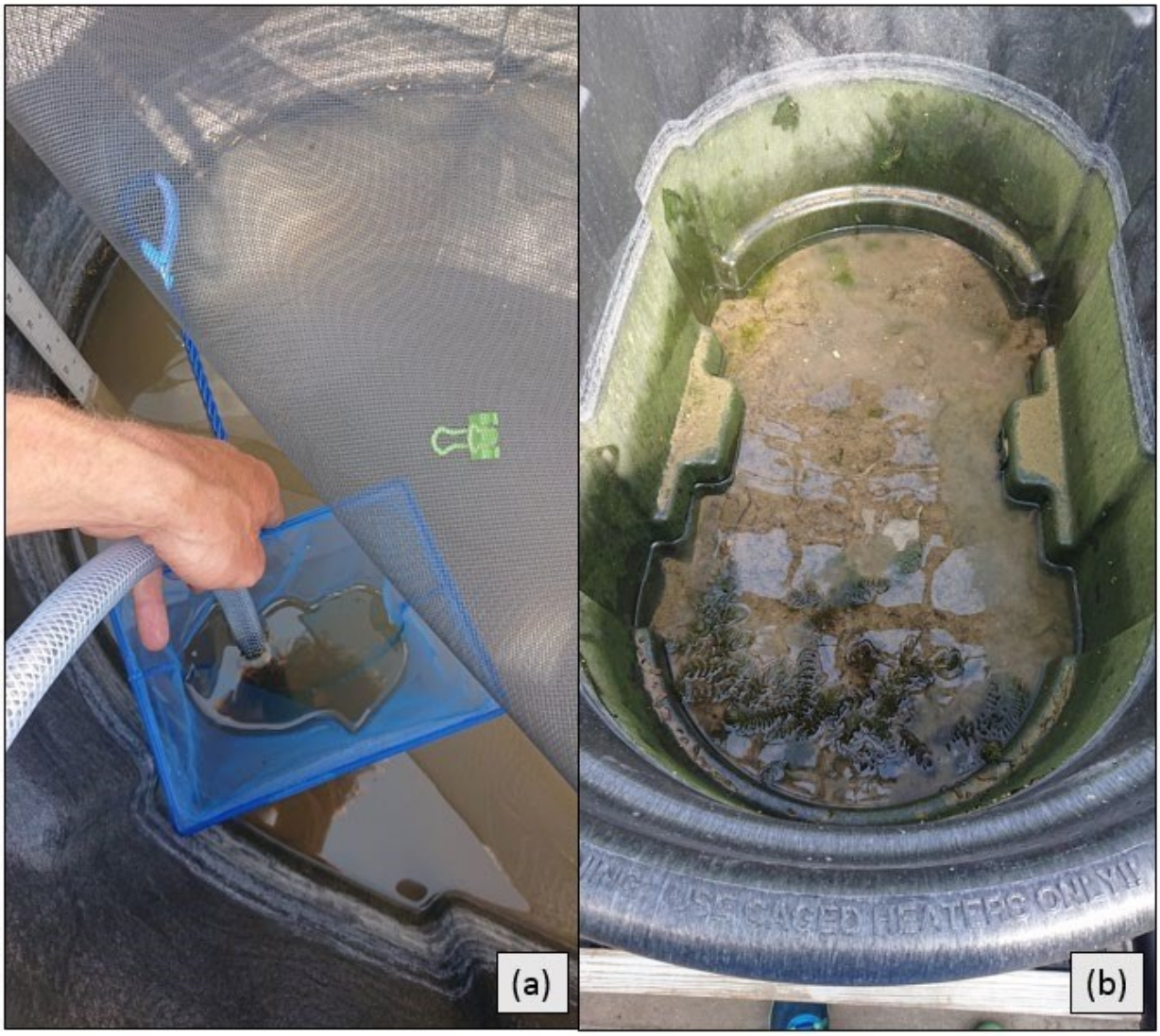

Figure S40: Pictures showing the process of draining the mesocosms during the drawdown. (a) The water is filtered through the net used for sampling and is drawn out using a transfer pump. (b) A mesocosm which has been drawn down to one inch of water remaining as specified in the drawdown treatment.

Figure S41: A picture showing the setup of the mesocosm study. 40 stock mesocosms were arranged in a five-by-eight array with randomization of the three factors being manipulated: heating, sediment source, and a drawdown. Passive heating was applied using the open top wooden framed greenhouses. The location of this experiment was at the Chase Lake Wetland Management District Headquarters in Woodworth, North Dakota (approximate GPS coordinates: +47.134253, -99.243489).

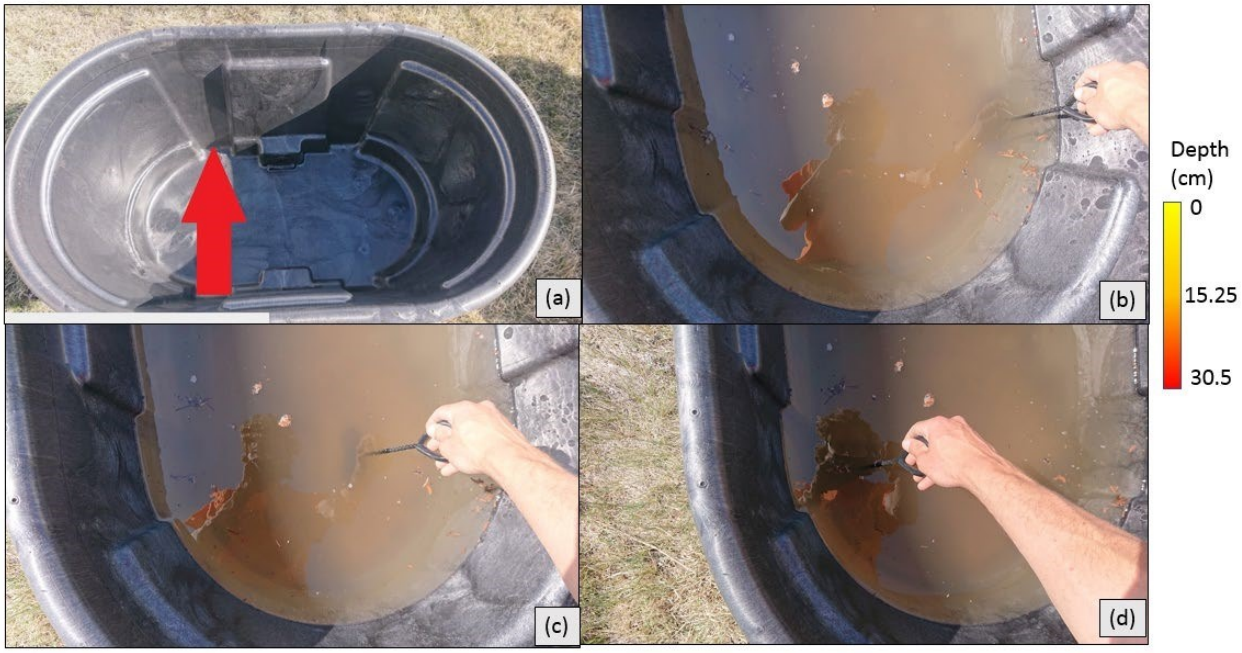

Figure S42: One of four methods used for the repeated community sampling by dip net. (a) The arrow shows the direction and depth of the sweep, in this case at the bottom of the water column. (b) The net is submerged vertically along the long wall until contacting the substrate. (b) It is then swept along the bottom while keeping contact with the substrate. (d) Upon reaching the opposite wall, it is swept upward vertically until breaching. This sweep is performed twice per sample.

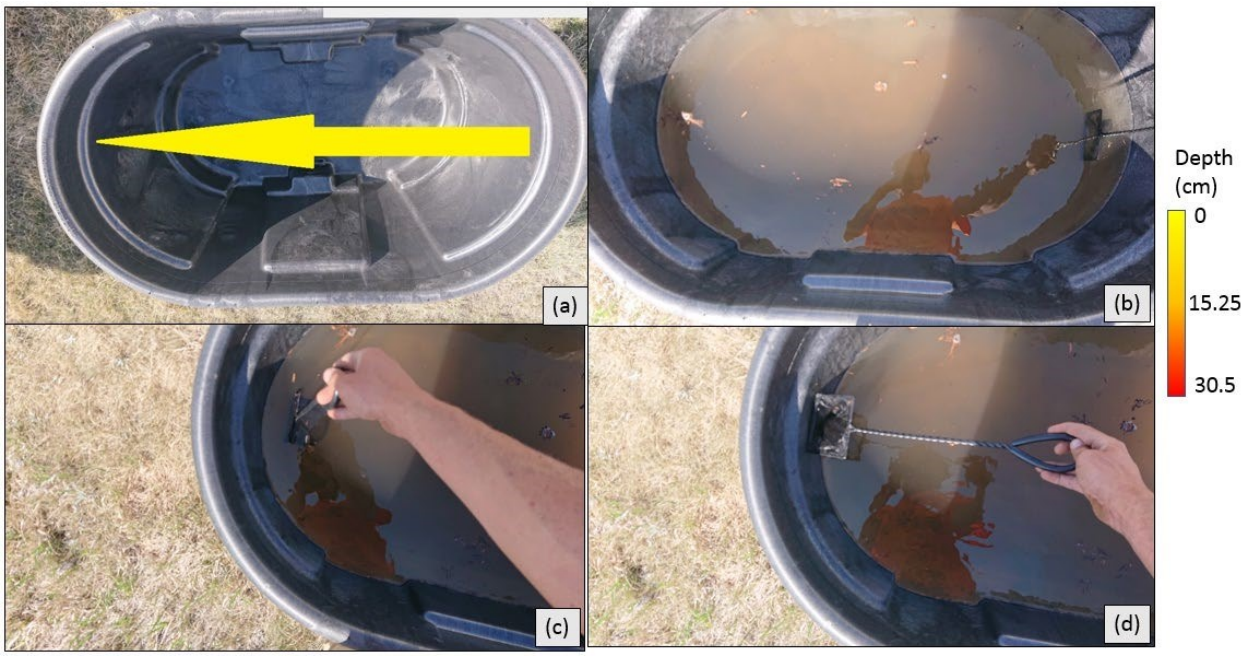

Figure S43: One of four methods used for the repeated community sampling by dip net. (a) The arrow shows the direction and depth of the sweep, in this case just below the surface of the water. (b) The net is submerged vertically along the short wall until the entire opening is submerged just below the water's surface. (c) It is then swept through the water until reaching the opposite wall. Upon reaching the opposite wall, it is swept upward vertically until breaching (d). This sweep is performed once per sample.

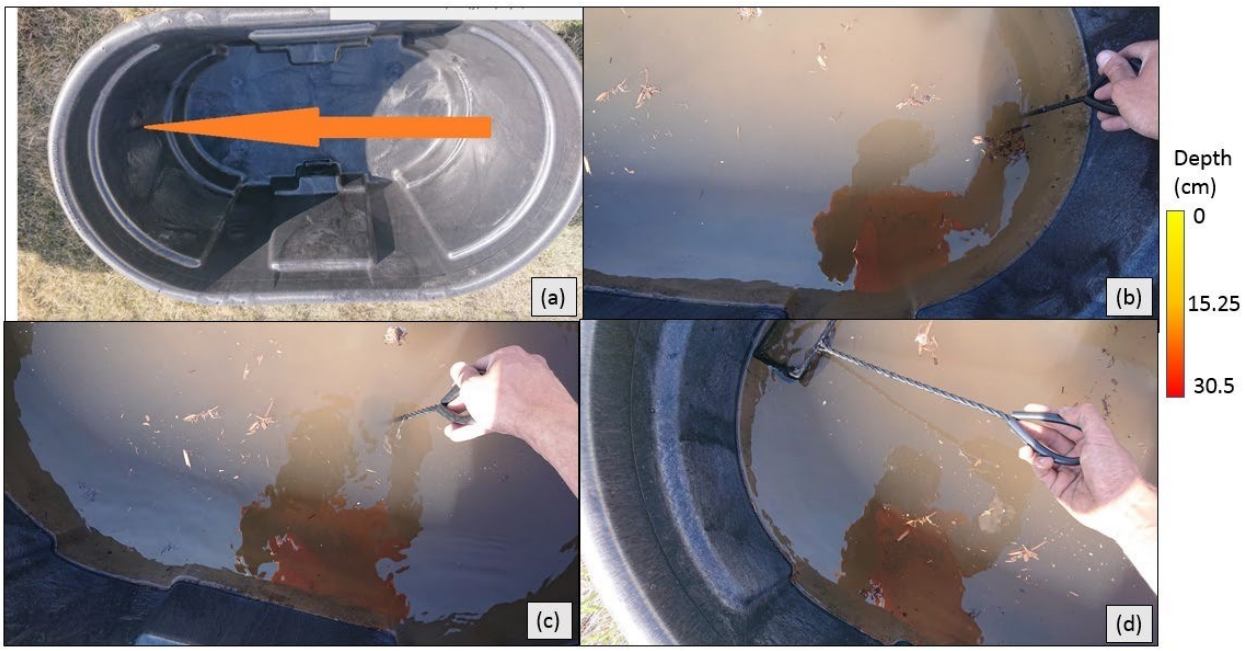

Figure S44: One of four methods used for the repeated community sampling by dip net. (a) The arrow shows the direction and depth of the sweep, in this case halfway down the water column. (b) The net is submerged vertically along the short wall until it is halfway down the water column. (c) It is then swept through the water until reaching the opposite wall. Upon reaching the opposite wall, it is swept upward vertically until breaching (d). This sweep is performed once per sample.

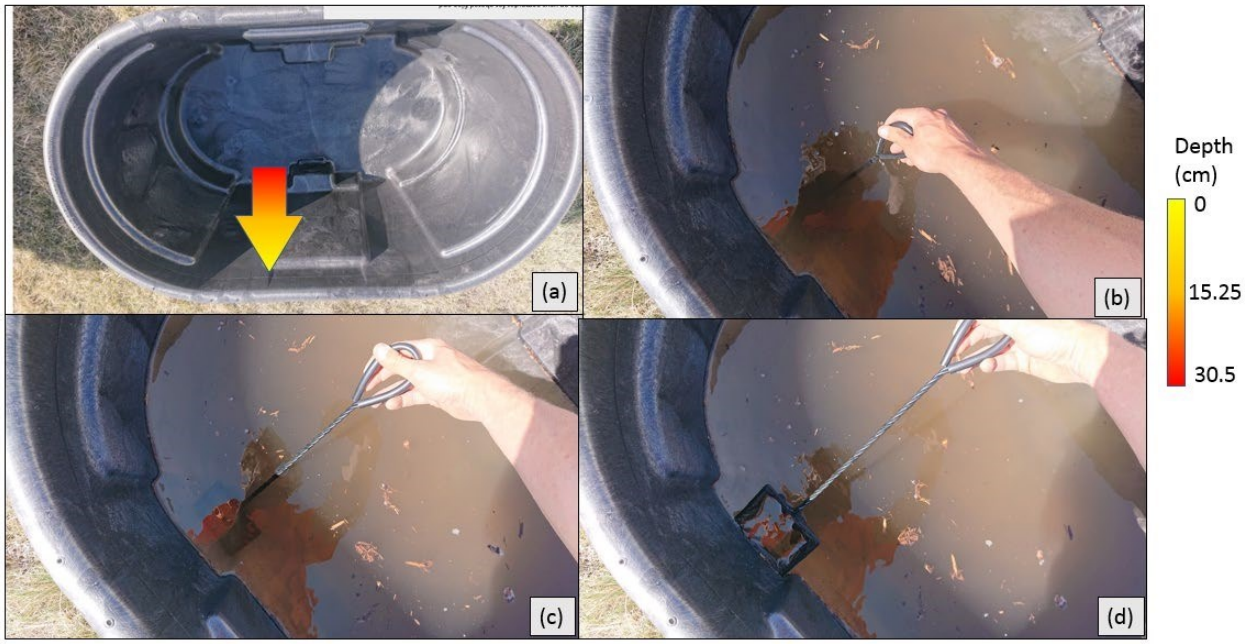

Figure S45: One of four methods used for the repeated community sampling by dip net. (a) The arrow shows the direction and depth of the sweep, in this case from the bottom to the top of the water column. (b) The net is submerged vertically along the short wall until contacting the substrate. (c) It is then rotated such that the bottom of the net is contacting the wall. (d) The next is swept upward while contacting the wall until breaching. This sweep is performed twice per sample.

Figure S46: (a) The white plastic dish bin into which the net sweeps are rinsed when collecting a community sample. (b) a smaller white enamel bowl containing a subsample of Cladocera collected from an original sample in the white dish bin above.

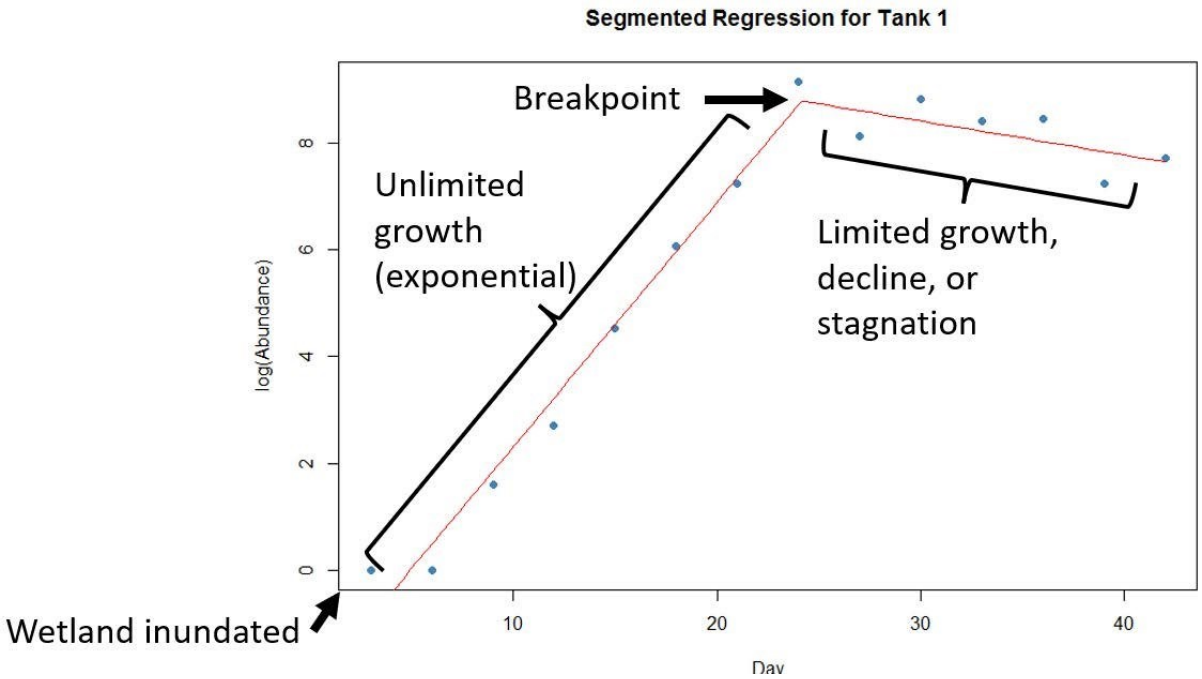

Figure S47: An example of the segmented regression analysis. The points plotted are the community-level abundances for each sample collected for one mesocosm mesocosm. An exponential curve was fitted to the data starting with the earlier samples. A natural breakpoint occurs when the newly assembling community switches from exponential growth to logistic growth due to some limiting factor. The breakpoint corresponds to a certain day which varies according to the treatment and between mesocosms with identical treatments. In the segmented regression analysis used, all mesocosms were averaged within a factor.

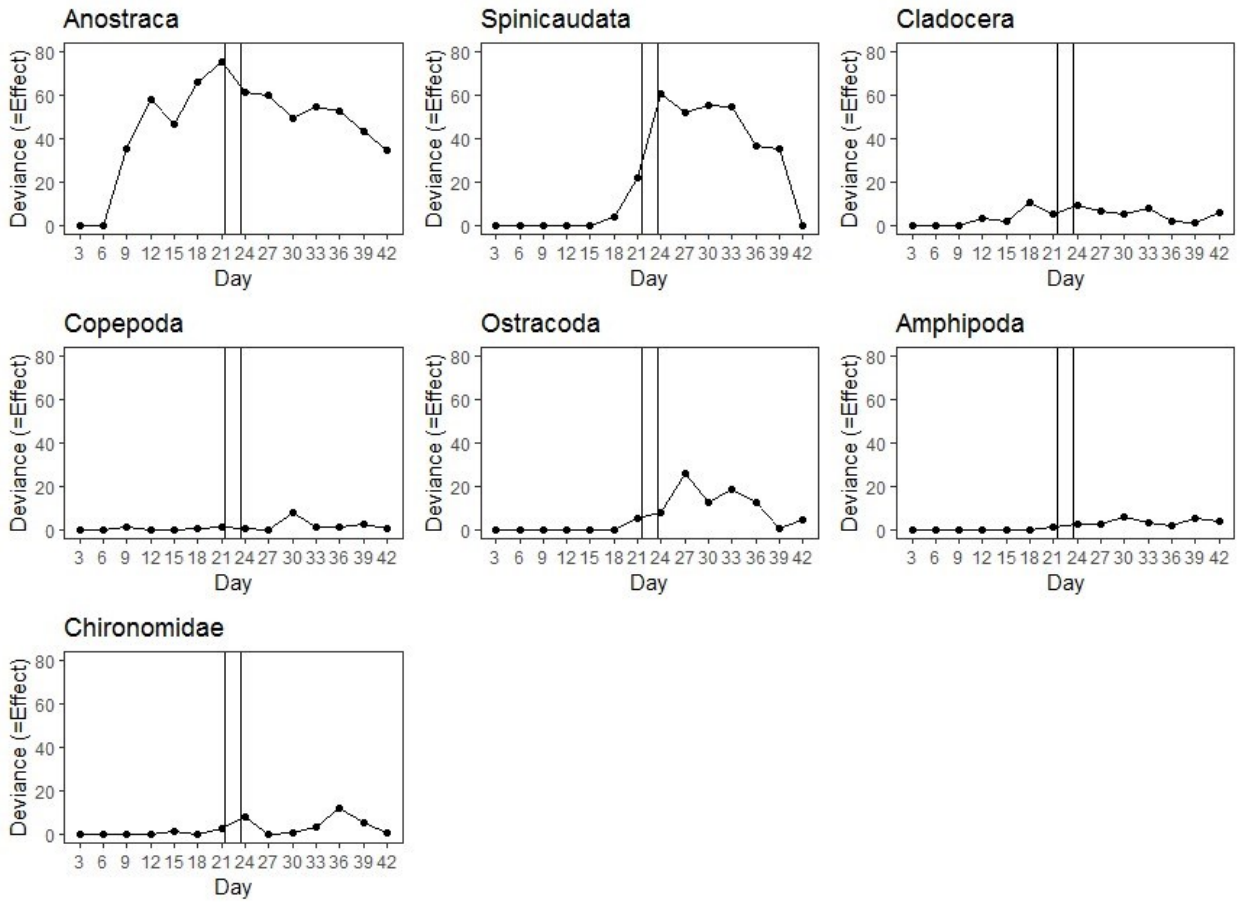

Figure S48: A time series of the general effect (deviance) of the sediment factor over the duration of the mesocosm experiment using the MVGLM. The effect of the treatment refers to differences in taxonomic abundances between the mesocosms seeded with mixed sediment and those seeded with local sediment. The vertical lines represent the start and end date of the drawdown, separating pre-drawdown time points to the left from post-drawdown time points to the right. Each taxon which showed a measurable effect in response to the sediment choice is shown as its own line graph.

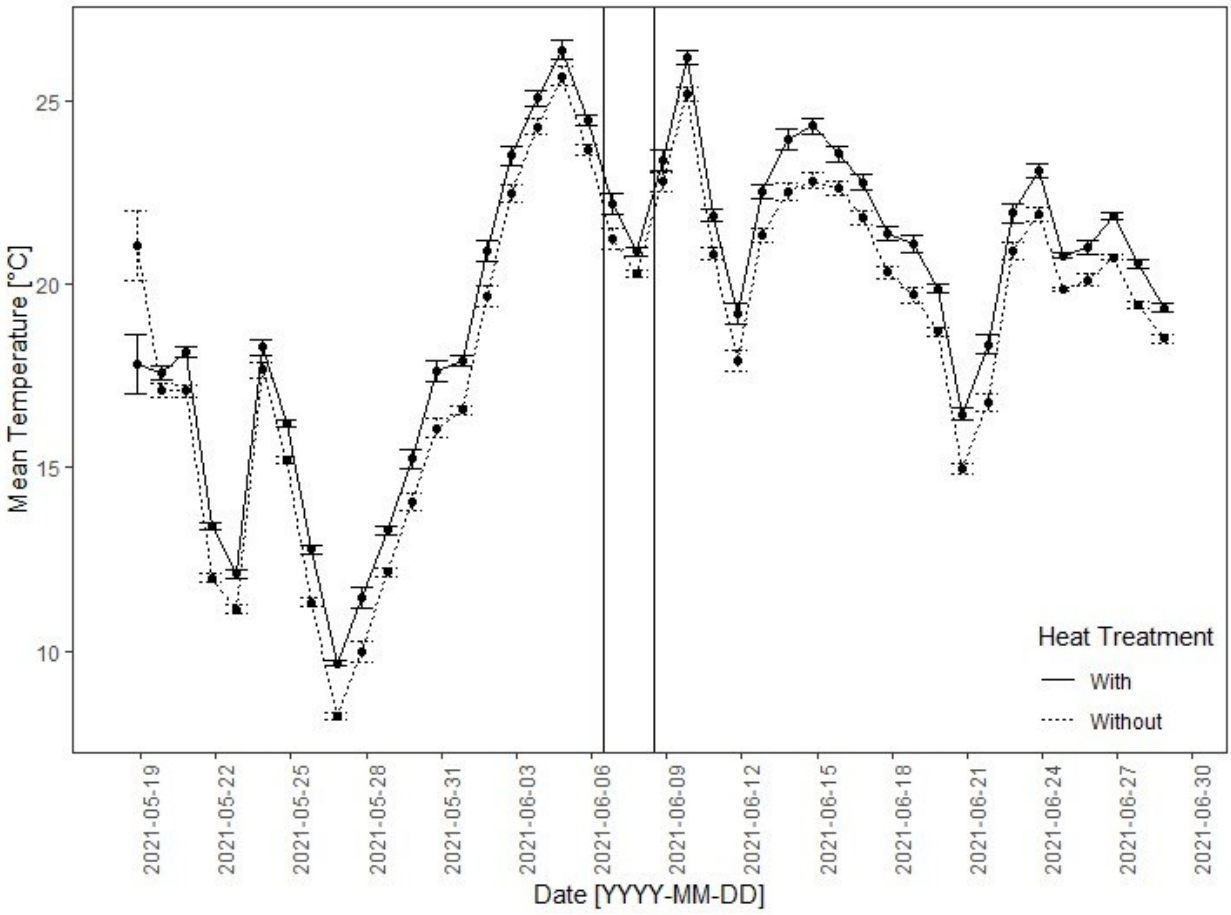

Figure S49: Time series graph of daily average water temperature by treatment over the duration of the mesocosm experiment. Mesocosms which were subjected to heating are denoted by solid lines while those without heating are denoted by dashed lines. The duration of the drawdown is the region bounded by the two solid vertical lines.

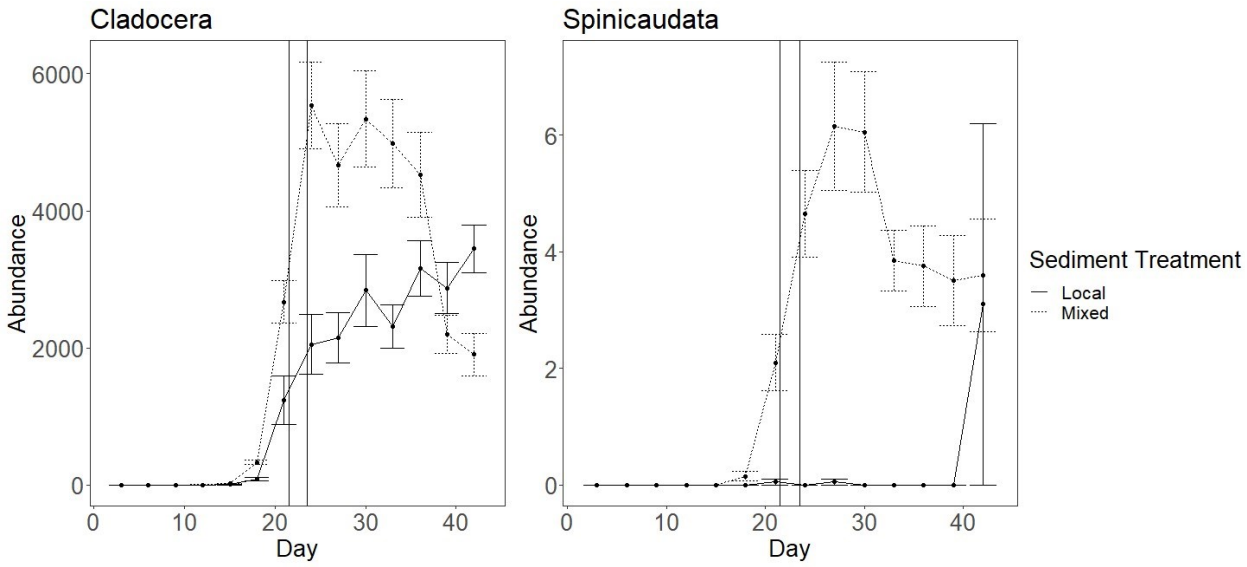

Figure S50: Line graphs of the abundances of the taxa, Cladocera and Spinicaudata, which showed a sediment*time interaction according to the MVGLM. Local sediment is denoted by solid lines while mixed sediment is denoted by dashed lines. The two solid vertical lines represent the bounds of the drawdown treatment.

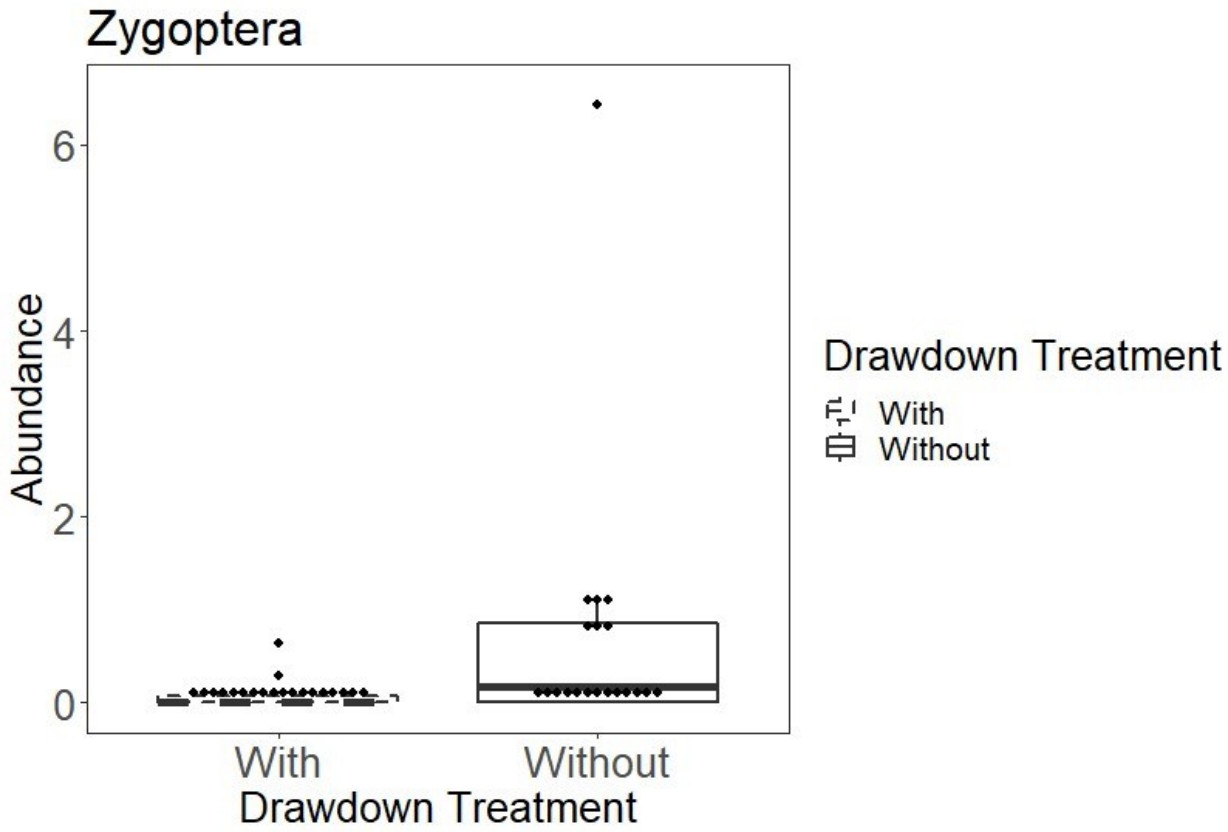

Figure S51: Bar graphs of the abundances of the Zygoptera which showed a response to the drawdown according to the MVGLM. Mesocosms subjected to a drawdown are denoted by dashed lines while those without a drawdown are denoted by solid lines.

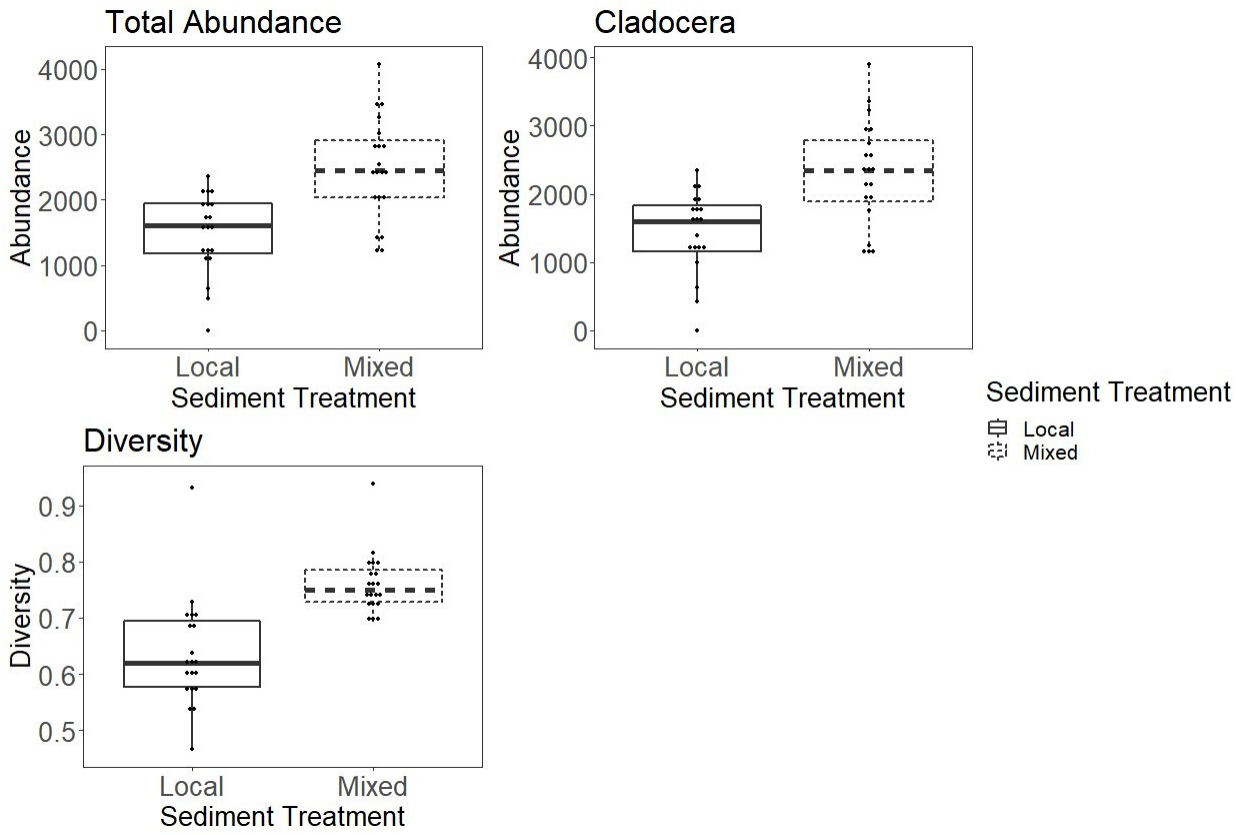

Figure S52: Box plots for the response variables which exhibited an effect of the sediment according to the repeated measures ANOVA. The sediment effect implies that the response of the dependent variable to the sediment is constant through time. Mesocosms with local sediment are denoted by solid lines while those with mixed sediment are denoted by dashed lines. Each plot represents a taxonomic group or variable labeled above that plot.

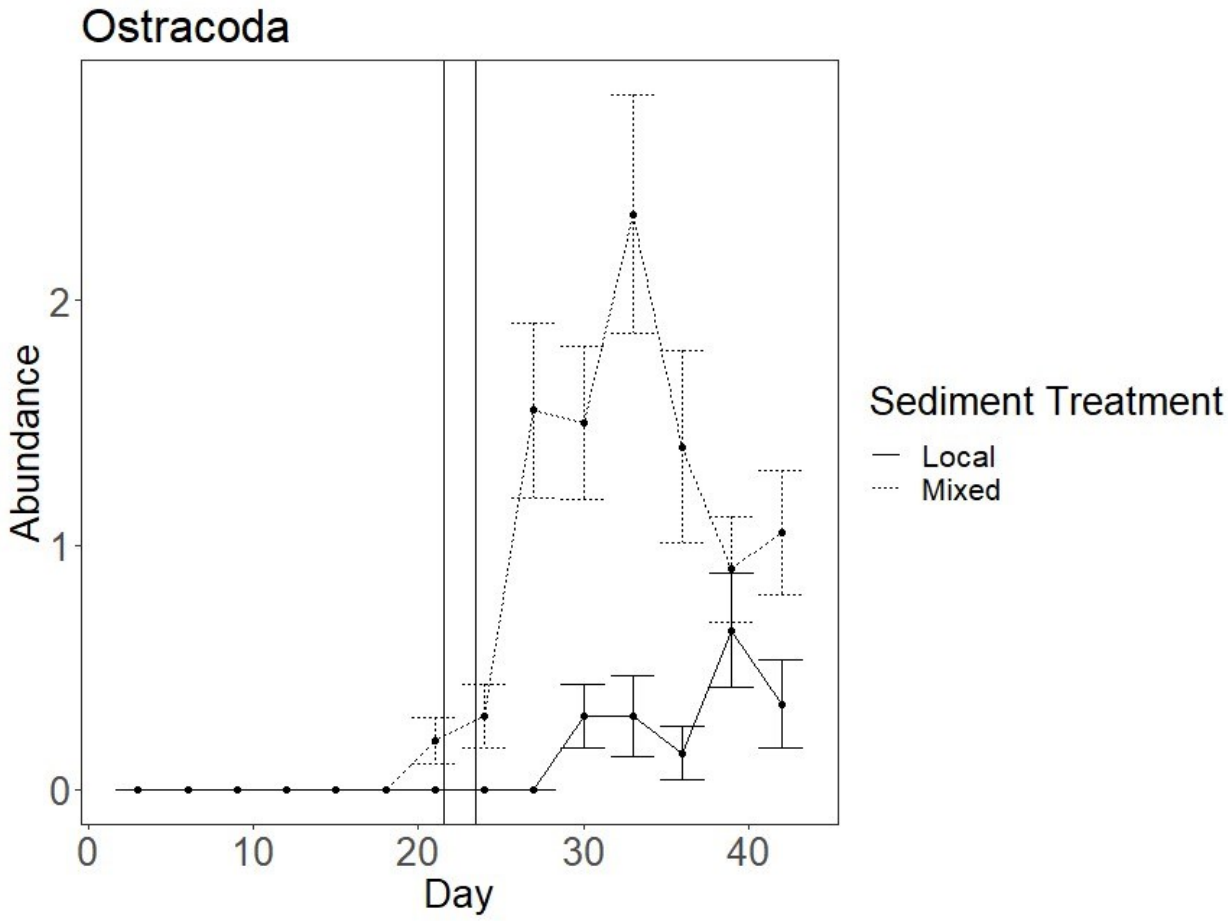

Figure S53: Line graphs for the response variable, square root transformed abundance of Ostracoda, which exhibited an effect of a sediment*time interaction according to the repeated measures ANOVA. The sediment*time interaction implies that the response of the dependent variable to the sediment varies through time. Mesocosms with local sediment are denoted by solid lines while those with mixed sediment are denoted by dashed lines. Each plot represents a taxonomic group or variable labeled above that plot.

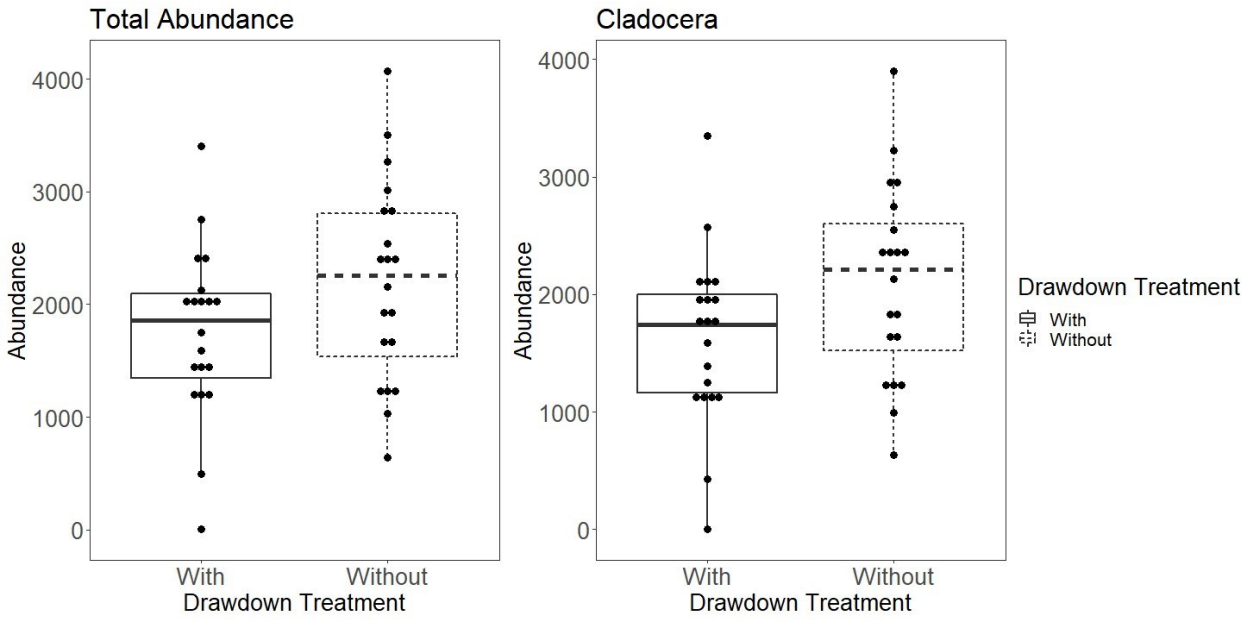

Figure S54: Box plots for the response variables which exhibited an effect due to the drawdown from the repeated measures ANOVA. Mesocosms given a drawdown are denoted by solid lines while those without a drawdown are denoted by dashed lines. Each plot represents a taxonomic group or variable labeled above that plot.

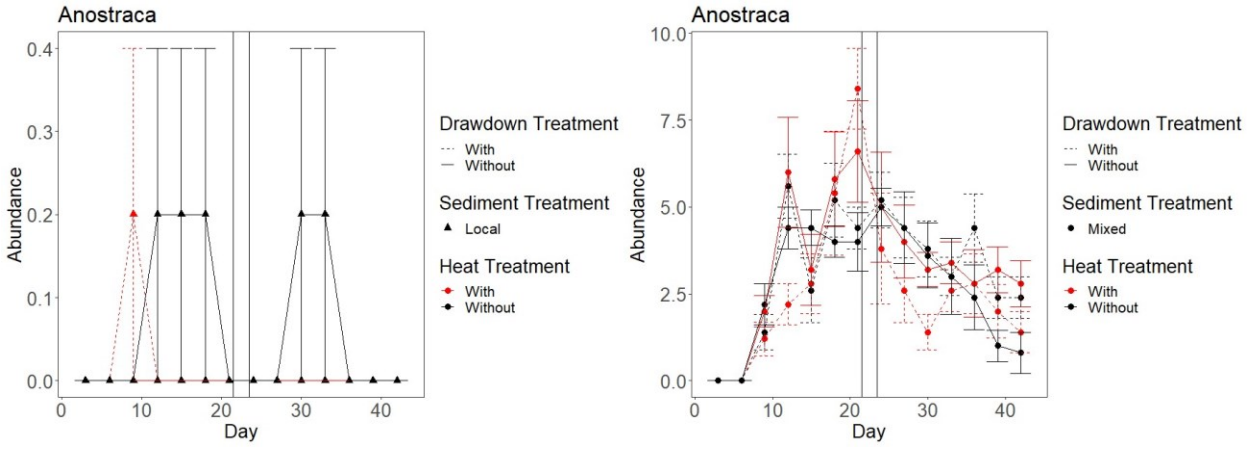

Figure S55: Line graphs for the response variable, square root transformed abundance of Anostraca, which exhibited an effect of a heat*drawdown*sediment*time interaction according to the repeated measures ANOVA. The heat*drawdown*sediment*time interaction implies that the response of the dependent variable to the drawdown varies according to the heat treatment in

a way that differs by the sediment source, and which has a time varying effect throughout the experiment, rather than a constant one.

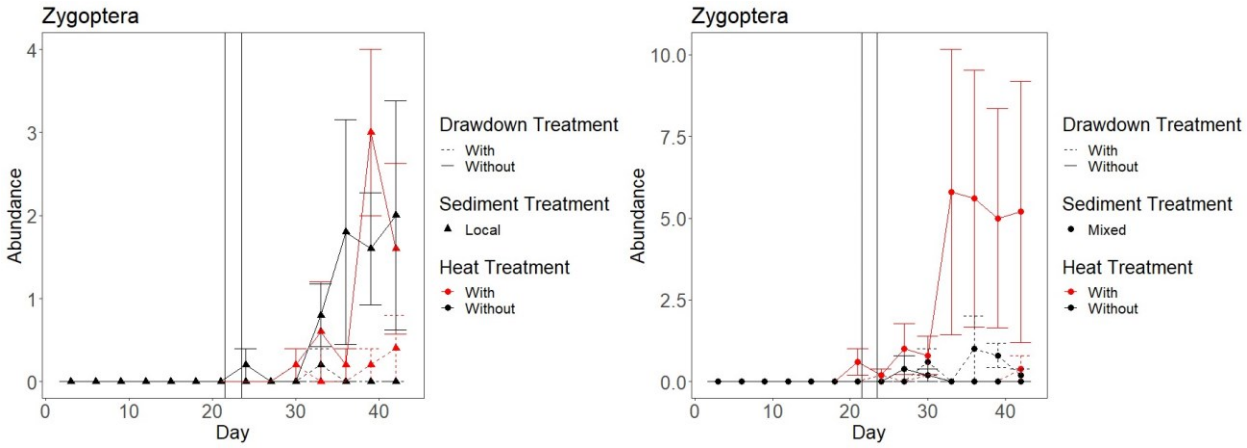

Figure S56: Line graphs for the response variable, square root transformed abundance of Zygoptera, which exhibited an effect of a heat*drawdown*sediment*time interaction according to the repeated measures ANOVA. The heat*drawdown*sediment*time interaction implies that the response of the dependent variable to the drawdown varies according to the heat treatment in a way that differs by the sediment source, and which has a time varying effect throughout the experiment, rather than a constant one.

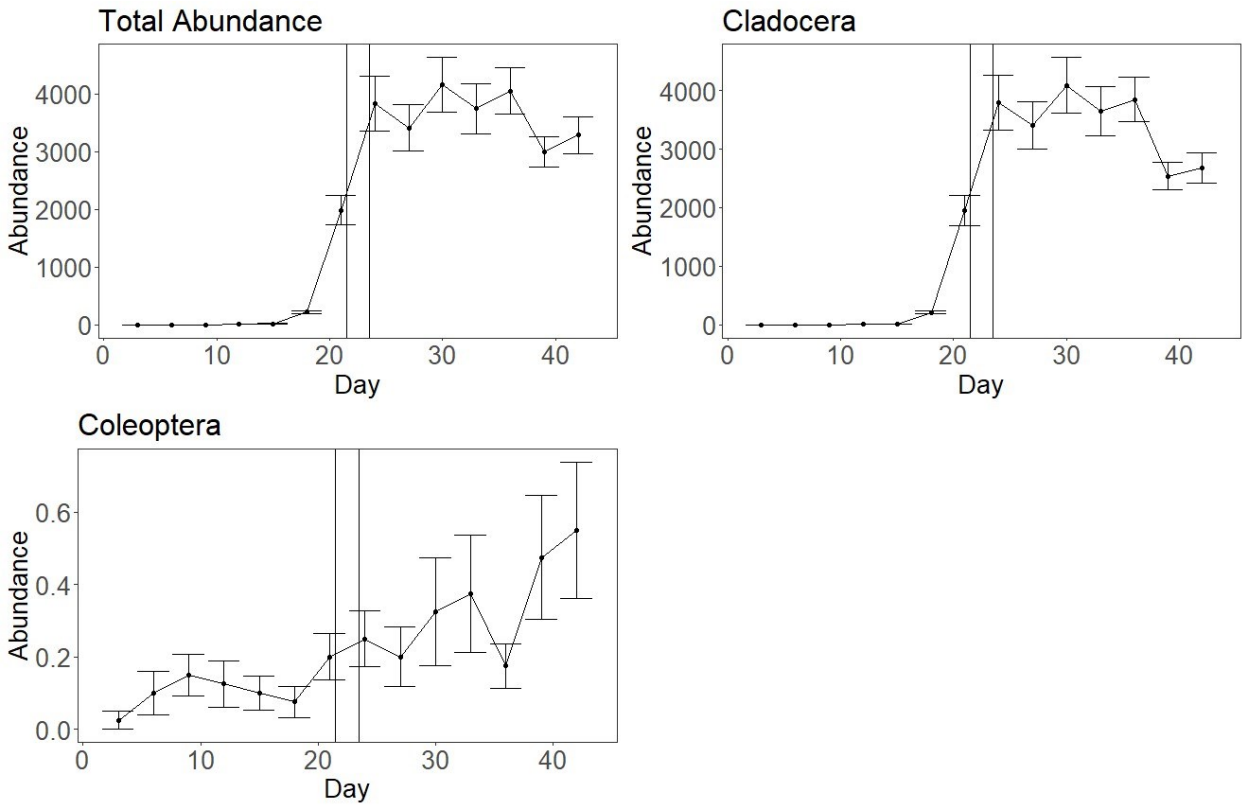

Figure S57: Line graphs for the response variables which exhibited an effect of time according to the repeated measures ANOVA. The time effect implies that the response of the dependent variable varies through time, but not necessarily in response to any of the three manipulated factors.

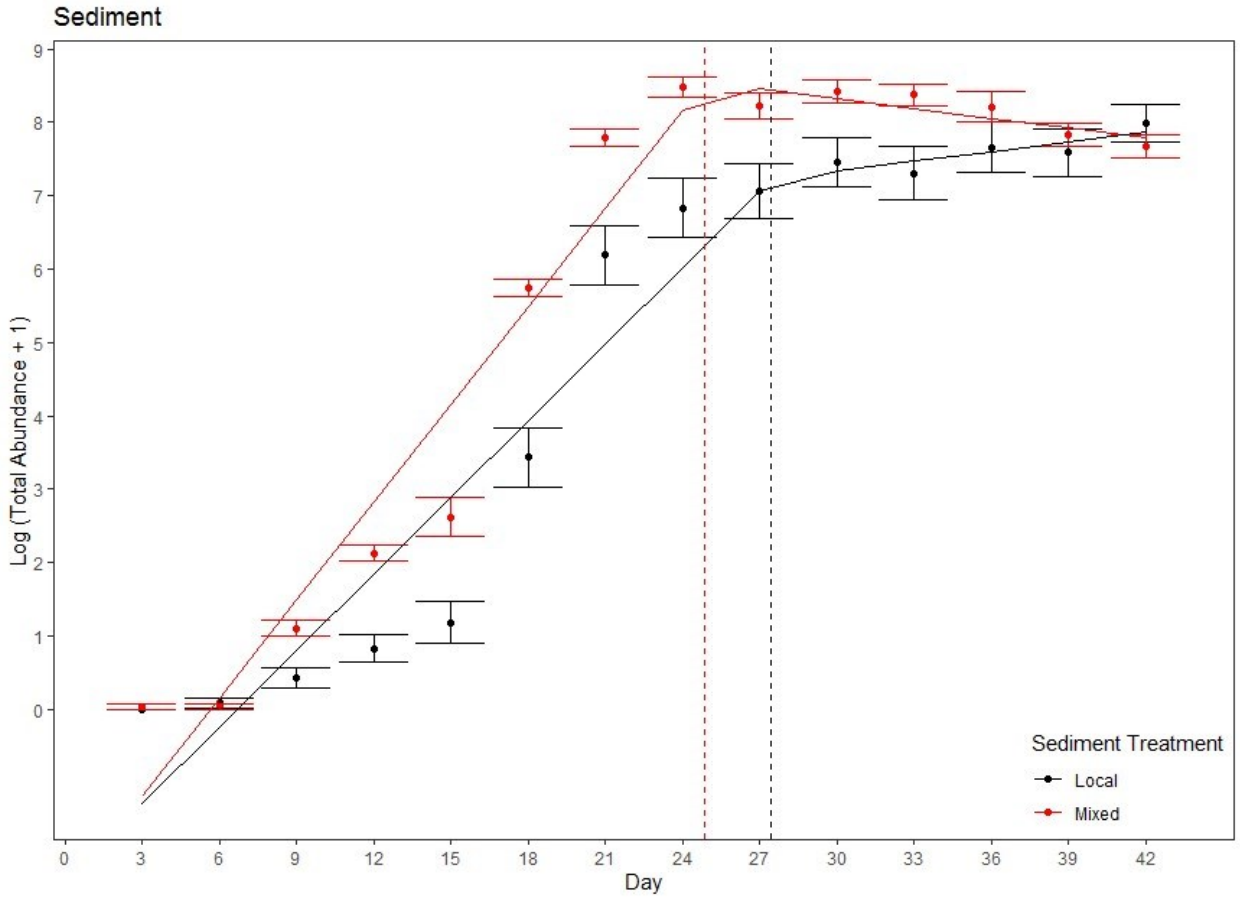

Figure S58: Breakpoint regression plots for the sediment treatment. The local sediment is shown in black and the mixed sediment is shown in red. An exponential function was fitted to the total abundances of all mesocosms within a treatment, with a total of 20 mesocosms in each. The breakpoints, represented by the vertical dashed lines, are the points at which the exponential function is no longer a good fit for the abundance curves. These breakpoints correspond to a single point in time. Each point is the mean of the 20 mesocosms within that treatment at that time and the error bars show the standard error at each time point.

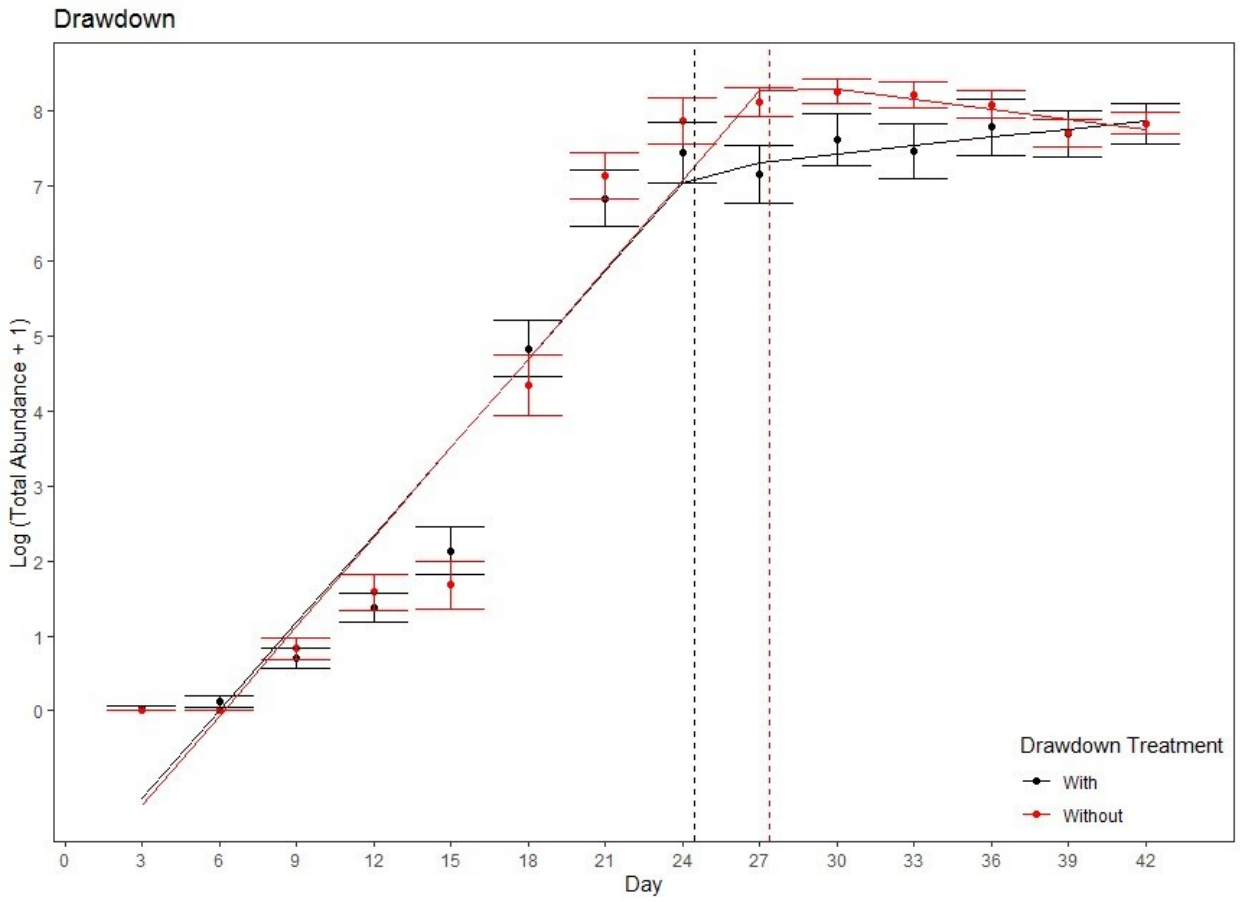

Figure S59: Breakpoint regression plots for the drawdown treatment. The mesocosms with a drawdown are shown in black and those without a drawdown are shown in red. An exponential function was fitted to the total abundances of all mesocosms within a treatment, with a total of 20 mesocosms in each. The breakpoints, represented by the vertical dashed lines, are the points at which the exponential function is no longer a good fit for the abundance curves. These breakpoints correspond to a single point in time. Each point is the mean of the 20 mesocosms within that treatment at that time and the error bars show the standard error.

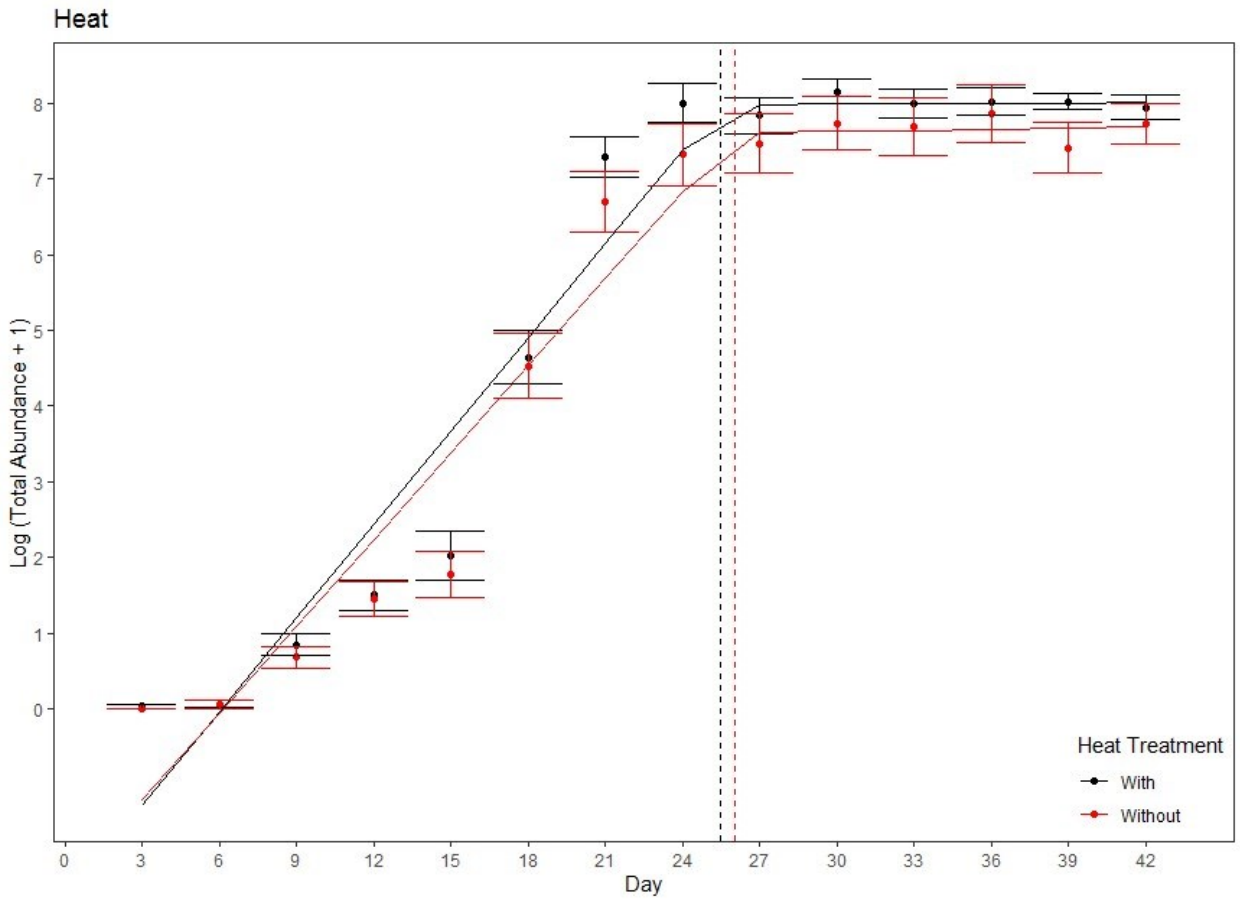

Figure S60: Breakpoint regression plots for the heat treatment. The mesocosms with heating are shown in black and those without heating are shown in red. An exponential function was fitted to the total abundances of all mesocosms within a treatment, with a total of 20 mesocosms in each. The breakpoints, represented by the vertical dashed lines, are the points at which the exponential function is no longer a good fit for the abundance curves. These breakpoints correspond to a single point in time. Each point is the mean of the 20 mesocosms within that treatment at that time and the error bars show the standard error.

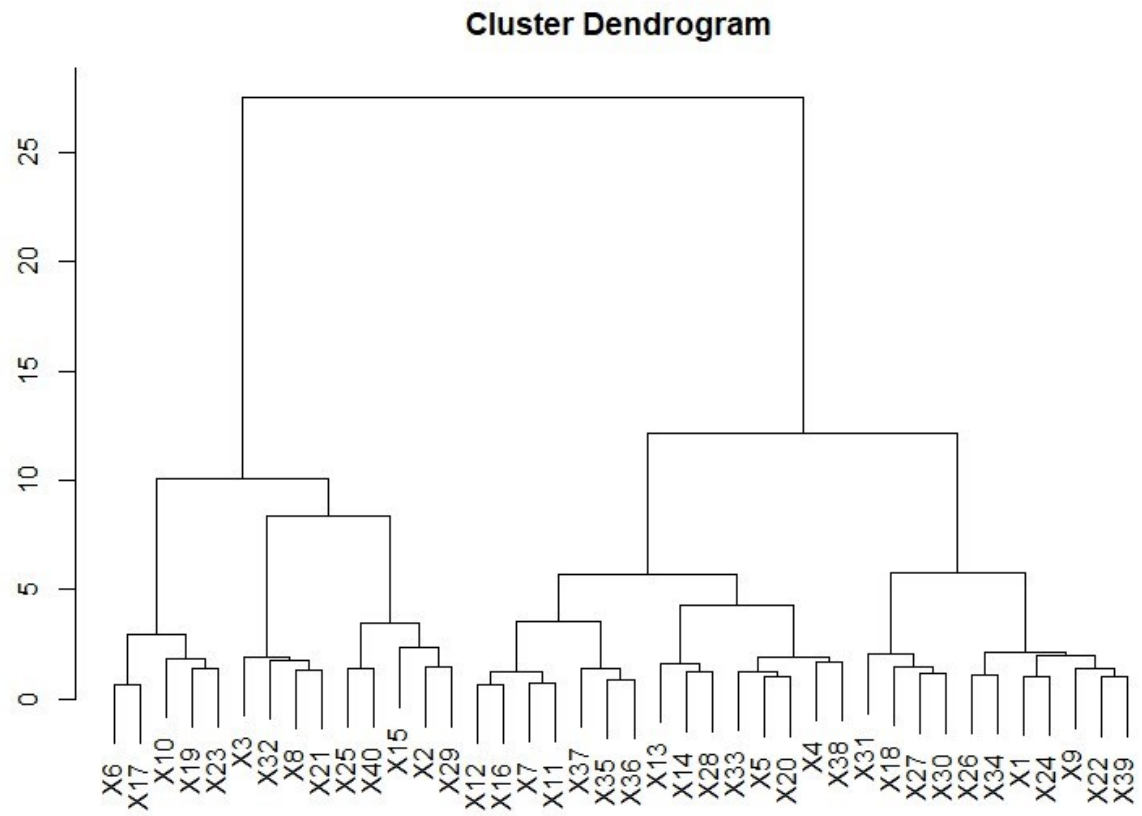

Figure S61: A dendrogram showing the clusters generated by the CCF method and hierarchical clustering algorithm from Chapter I. Clusters were generated using the time series of total abundance for each mesocosm. The mesocosms were grouped into 2-, 4-, and 8-cluster scenarios.

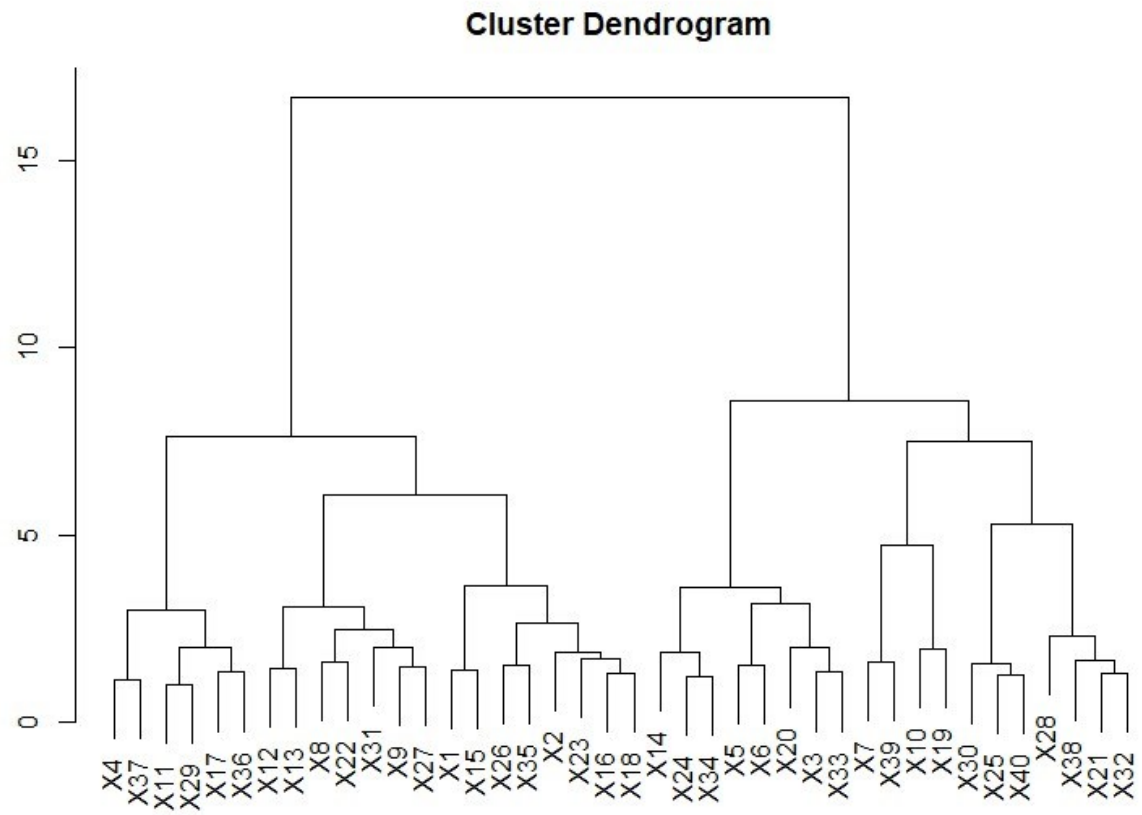

Figure S62: A dendrogram showing the clusters generated by the CCF method and hierarchical clustering algorithm from Chapter I. Clusters were generated using the time series of order-level richness for each mesocosm. The mesocosms were grouped into 2-, 4-, and 8-cluster scenarios.

APPENDIX D. CHAPTER III SUPPLEMENTARY INFORMATION

Table S24: Results summary table of the PERMANOVA using only mesocosms seeded with mixed sediment

Effect	Df	SumOfSqs	R2	F	Pr(>F)	P<0.05
day	1	14724346	0.3313	95.9871	0.001	***
pred_treat	1	173418	0.0039	1.1305	0.001	***
heat_treat	1	526285	0.01184	3.4308	0.001	***
day:pred_treat	1	211356	0.00476	1.3778	0.22	

day:heat_treat	1	531936	0.01197	3.4677	0.07	.
pred_treat:heat_treat	1	41663	0.00094	0.2716	0.001	***
day:pred_treat:heat_treat	1	9707	0.00022	0.0633	0.815	
Residual	184		0.63508			
Total	191	44444176	1			

Table S25: Results summary table of the PERMANOVA using only mesocosms without the heating treatment

Effect	Df	SumOfSqs	R2	F	Pr(>F)	P<0.05
day	1	93257232	0.28022	101.856	0.001	***
pred_treat	1	599772	0.0018	0.6551	0.001	***
sediment_treat	1	23289042	0.06998	25.4364	0.001	***
day:pred_treat	1	1199324	0.0036	1.3099	0.282	
day:sediment_treat	1	42890574	0.12888	46.8453	0.001	***
pred_treat:sediment_treat	1	973713	0.00293	1.0635	0.001	***
day:pred_treat:sediment_treat	1	2121002	0.00637	2.3166	0.154	
Residual	184	168466616	0.50621			
Total	191	332797274	1			

Table S26: Results summary table of the PERMANOVA for fairy shrimp size classes using only mesocosms with mixed sediment

Effect	Df	SumOfSqs	R2	F	Pr(>F)	P<0.05
day	1	70.03	0.13596	31.1013	0.001	***
pred_treat	1	5.52	0.01071	2.4497	0.001	***
heat_treat	1	16.06	0.03118	7.1316	0.001	***
day:pred_treat	1	1.13	0.0022	0.5031	0.56	
day:heat_treat	1	7.26	0.01409	3.224	0.029	*
pred_treat:heat_treat	1	0.77	0.00149	0.34	0.001	***
day:pred_treat:heat_treat	1	0.02	0.00004	0.0093	1	
Residual	184	414.29	0.80434			
Total	191	515.07	1			

Table S27: Results summary table of the PERMANOVA for clam shrimp size classes using only mesocosms with mixed sediment

Effect	Df	SumOfSqs	R2	F	Pr(>F)	P<0.05
day	1	2.782	0.04687	10.1075	0.001	***
pred_treat	1	0.51	0.0086	1.8541	0.001	***
heat_treat	1	0.823	0.01386	2.9893	0.001	***
day:pred_treat	1	0.861	0.01451	3.1291	0.035	*
day:heat_treat	1	1.183	0.01993	4.2975	0.014	*
pred_treat:heat_treat	1	1.198	0.02018	4.3515	0.001	***
day:pred_treat:heat_treat	1	1.354	0.02281	4.9184	0.001	***
Residual	184	50.652	0.85324			
Total	191	59.365	1			

Table S28: Results summary table of the repeated measures ANOVA for the effect of heating on water temperature over time

Effect	Effect	DFn	DFd	F	p	p<.05	ges
1	heat_treat	1	14	402.1491	1.04E-11	*	0.966358

Table S29: Results summary table of the post-hoc repeated measures ANOVA on clam shrimp abundance in mixed sediment mesocosms

Effect	df	dfd	MSE	F	ges	p.value	P<0.05
heat_treat	1,	12	0.41	5.13	0.051	0.043	*
pred_treat	1,	12	0.41	3.28	0.033	0.095	+
heat_treat:pred_treat	1,	12	0.41	8.67	0.084	0.012	*
day	11,	132	0.25	2.62	0.16	0.005	**
heat_treat:day	11,	132	0.25	2.33	0.145	0.012	*
pred_treat:day	11,	132	0.25	1.62	0.106	0.1	+
heat_treat:pred_treat:day	11,	132	0.25	1.64	0.107	0.094	+

Table S30: Results summary table of the post-hoc repeated measures ANOVA on richness (Order) in mixed sediment mesocosms

Effect	df	dfd	MSE	F	ges	p.value	P<0.05
heat_treat	1,	12	0.93	14.53	0.137	0.002	**
pred_treat	1,	12	0.93	4.07	0.043	0.067	+

heat_treat:pred_treat	1,	12	0.93	0.05	<.001	0.826	
day	5.72,	68.6	1.08	71.44	0.838	<.001	***
heat_treat:day	5.72,	68.6	1.08	0.79	0.054	0.574	
pred_treat:day	5.72,	68.6	1.08	0.59	0.041	0.729	
heat_treat:pred_treat:day	5.72,	68.6	1.08	1.76	0.113	0.123	

Table S31: Results summary table of the post-hoc repeated measures ANOVA on Shannon diversity (Order) in mixed sediment mesocosms

Effect	df	dfd	MSE	F	ges	p.value	P<0.05
heat_treat	1,	12	0.09	0.51	0.008	0.487	
pred_treat	1,	12	0.09	1.25	0.019	0.285	
heat_treat:pred_treat	1,	12	0.09	1.34	0.021	0.27	
day	11,	132	0.03	18.23	0.552	<.001	***
heat_treat:day	11,	132	0.03	3.93	0.21	<.001	***
pred_treat:day	11,	132	0.03	0.78	0.05	0.663	
heat_treat:pred_treat:day	11,	132	0.03	1.04	0.066	0.412	

Table S32: Results summary table of the post-hoc repeated measures ANOVA on copepod abundance in mesocosms without heating

Effect	df	dfd	MSE	F	ges	p.value	P<0.05
sediment_treat	1,	12	2.94	33.22	0.386	<.001	***
pred_treat	1,	12	2.94	0.51	0.01	0.488	
sediment_treat:pred_treat	1,	12	2.94	0.64	0.012	0.44	
day	11,	132	0.91	26.12	0.627	<.001	***
sediment_treat:day	11,	132	0.91	15.6	0.501	<.001	***
pred_treat:day	11,	132	0.91	3.92	0.202	<.001	***
sediment_treat:pred_treat:day	11,	132	0.91	2.03	0.116	0.03	*

Table S33: Results summary table of the post-hoc repeated measures ANOVA on non-dytiscid water beetle abundance in mesocosms without heating

Effect	df	dfd	MSE	F	ges	p.value	P<0.05
sediment_treat	1,	12	0.04	0.13	0.002	0.724	
pred_treat	1,	12	0.04	0.13	0.002	0.724	
sediment_treat:pred_treat	1,	12	0.04	3.26	0.039	0.096	+
day	11,	132	0.02	2.41	0.146	0.009	**
sediment_treat:day	11,	132	0.02	0.79	0.053	0.65	
pred_treat:day	11,	132	0.02	0.79	0.053	0.65	
sediment_treat:pred_treat:day	11,	132	0.02	2.41	0.146	0.009	**

Table S34: Results summary table of the post-hoc repeated measures ANOVA on fairy shrimp abundance in mesocosms without heating

Effect	df	dfd	MSE	F	ges	p.value	P<0.05
sediment_treat	1,	12	7.24	10.01	0.284	0.008	**
pred_treat	1,	12	7.24	1.04	0.04	0.328	
sediment_treat:pred_treat	1,	12	7.24	1.04	0.04	0.328	
day	11,	132	0.72	4.49	0.164	<.001	***
sediment_treat:day	11,	132	0.72	4.36	0.16	<.001	***
pred_treat:day	11,	132	0.72	0.88	0.037	0.565	
sediment_treat:pred_treat:day	11,	132	0.72	0.88	0.037	0.565	

Table S35: Results summary table of the post-hoc repeated measures ANOVA on cladoceran abundance in mesocosms without heating

Effect	df	dfd	MSE	F	ges	p.value	P<0.05
sediment_treat	1,	12	625616.48	37.23	0.302	<.001	***
pred_treat	1,	12	625616.48	0.96	0.011	0.347	
sediment_treat:pred_treat	1,	12	625616.48	1.56	0.018	0.236	
day	11,	132	350631.06	42.95	0.755	<.001	***
sediment_treat:day	11,	132	350631.06	20.46	0.595	<.001	***
pred_treat:day	11,	132	350631.06	1.01	0.067	0.444	

sediment_treat:pred_treat:day	11,	132	350631.06	1.48	0.096	0.146	

Table S36: Results summary table of the post-hoc repeated measures ANOVA on total abundance in mesocosms without heating

Effect	df	dfd	MSE	F	ges	p.value	P<0.05
sediment_treat	1,	12	626092.13	37.2	0.302	<.001	***
pred_treat	1,	12	626092.13	0.96	0.011	0.348	
sediment_treat:pred_treat	1,	12	626092.13	1.55	0.018	0.237	
day	2.18,	26.11	1775465.6	43.04	0.755	<.001	***
sediment_treat:day	2.18,	26.11	1775465.6	20.43	0.594	<.001	***
pred_treat:day	2.18,	26.11	1775465.6	1.01	0.067	0.385	
sediment_treat:pred_treat:day	2.18,	26.11	1775465.6	1.48	0.096	0.247	

Table S37: Results summary table of the post-hoc repeated measures ANOVA on richness (Order) in mesocosms without heating

Effect	df	dfd	MSE	F	ges	p.value	P<0.05
sediment_treat	1,	12	1.67	0.9	0.019	0.361	
pred_treat	1,	12	1.67	3	0.059	0.109	
sediment_treat:pred_treat	1,	12	1.67	0.15	0.003	0.703	
day	11,	132	0.45	78.67	0.831	<.001	***
sediment_treat:day	11,	132	0.45	2.35	0.128	0.011	*
pred_treat:day	11,	132	0.45	2.2	0.121	0.018	*
sediment_treat:pred_treat:day	11,	132	0.45	0.84	0.05	0.6	

Table S38: Results summary table of the post-hoc repeated measures ANOVA on Shannon diversity (Order) in mesocosms without heating

Effect	df	dfd	MSE	F	ges	p.value	P<0.05
sediment_treat	1,	12	0.05	16.23	0.221	0.002	**
pred_treat	1,	12	0.05	0.4	0.007	0.541	

sediment_treat:pred_treat	1,	12	0.05	0.34	0.006	0.573	
day	11,	132	0.02	17.78	0.539	<.001	***
sediment_treat:day	11,	132	0.02	10.29	0.404	<.001	***
pred_treat:day	11,	132	0.02	1.78	0.105	0.063	+
sediment_treat:pred_treat:day	11,	132	0.02	1.22	0.074	0.281	

Table S39: Results summary table of the post-hoc repeated measures ANOVA on fairy shrimp of the large size class in mixed sediment mesocosms

Effect	df	dfd	MSE	F	ges	p.value	P<0.05
heat_treat	1,	12	4.84	3.26	0.072	0.096	+
pred_treat	1,	12	4.84	1.03	0.024	0.329	
heat_treat:pred_treat	1,	12	4.84	0.13	0.003	0.724	
day	11,	132	1.1	9.82	0.369	<.001	***
heat_treat:day	11,	132	1.1	2.81	0.143	0.003	**
pred_treat:day	11,	132	1.1	0.77	0.044	0.673	
heat_treat:pred_treat:day	11,	132	1.1	0.72	0.041	0.722	

Table S40: Results summary table of the post-hoc repeated measures ANOVA on clam shrimp of the small size class in mixed sediment mesocosms

Effect	df	dfd	MSE	F	ges	p.value	P<0.05
heat_treat	1,	12	0.12	2.07	0.017	0.176	
pred_treat	1,	12	0.12	0.38	0.003	0.549	
heat_treat:pred_treat	1,	12	0.12	3.42	0.028	0.089	+
day	11,	132	0.1	1.63	0.109	0.096	+
heat_treat:day	11,	132	0.1	1.97	0.129	0.036	*
pred_treat:day	11,	132	0.1	1.48	0.1	0.145	
heat_treat:pred_treat:day	11,	132	0.1	0.92	0.064	0.525	

Table S41: Results summary table of the post-hoc repeated measures ANOVA on clam shrimp of the medium size class in mixed sediment mesocosms

Effect	df	dfd	MSE	F	ges	p.value	P<0.05

heat_treat	1,	12	0.05	1	0.008	0.337	
pred_treat	1,	12	0.05	2.78	0.022	0.121	
heat_treat:pred_treat	1,	12	0.05	5.44	0.042	0.038	*
day	11,	132	0.04	4.95	0.271	<.001	***
heat_treat:day	11,	132	0.04	2.35	0.15	0.011	*
pred_treat:day	11,	132	0.04	2.73	0.171	0.003	**
heat_treat:pred_treat:day	11,	132	0.04	4.76	0.264	<.001	***

Table S42: Results summary table of the post-hoc repeated measures ANOVA on clam shrimp of the large size class in mixed sediment mesocosms

Effect	df	dfd	MSE	F	ges	p.value	P<0.05
heat_treat	1,	12	0.08	6.52	0.055	0.025	*
pred_treat	1,	12	0.08	4.17	0.036	0.064	+
heat_treat:pred_treat	1,	12	0.08	6.52	0.055	0.025	*
day	11,	132	0.06	6.4	0.323	<.001	***
heat_treat:day	11,	132	0.06	6.5	0.326	<.001	***
pred_treat:day	11,	132	0.06	4.54	0.253	<.001	***
heat_treat:pred_treat:day	11,	132	0.06	3.89	0.224	<.001	***

Table S43: Results summary table of the linear regression of beetle surface counts versus temperature

Effect	Estimate	Std. Error	t value	Pr(>|t|)	P<0.05
(Intercept)	0.02121	0.85616	0.025	0.980396	
temperature	0.15599	0.04051	3.850	0.000575	***

Table S44: Results summary table of the ANOVA for concentration of green algae

Effect	Df	Sum Sq	Mean Sq	F value	Pr(>F)	P<0.05
pred_treat	1	10166	10166	0.465	0.50463	
heat_treat	1	231086	231086	10.563	0.00471	**
sediment_treat	1	1040	1040	0.048	0.83001	
tank_pair	1	159312	159312	7.282	0.01522	*
pred_treat:heat_treat	1	9	9	0	0.98416	
pred_treat:sediment_treat	1	2	2	0	0.99167	

Residuals	17	371904	21877			

Table S45: Results summary table of the ANOVA for chromophoric dissolved organic matter (CDOM; also called yellow substance)

Effect	Df	Sum Sq	Mean Sq	F value	Pr(>F)	P<0.05
pred_treat	1	1.42	1.424	0.628	0.4392	
heat_treat	1	0.22	0.221	0.097	0.7587	
sediment_treat	1	18.38	18.379	8.099	0.0112	*
tank_pair	1	3.1	3.103	1.367	0.2584	
pred_treat:heat_treat	1	4.38	4.383	1.931	0.1826	
pred_treat:sediment_treat	1	0.1	0.096	0.043	0.8391	
Residuals	17	38.58	2.269			

Table S46: Results summary table of the ANOVA for total algal concentration

Effect	Df	Sum Sq	Mean Sq	F value	Pr(>F)	P<0.05
pred_treat	1	13167	13167	0.493	0.49211	
heat_treat	1	250506	250506	9.379	0.00705	**
sediment_treat	1	3599	3599	0.135	0.71808	
tank_pair	1	189130	189130	7.081	0.01646	*
pred_treat:heat_treat	1	311	311	0.012	0.91527	
pred_treat:sediment_treat	1	997	997	0.037	0.84911	
Residuals	17	454061	26709			

Table S47: Results summary table of the ANOVA for percent transmission of the water sample

Effect	Df	Sum Sq	Mean Sq	F value	Pr(>F)	P<0.05
pred_treat	1	129.4	129.4	0.944	0.3448	
heat_treat	1	1453.8	1453.8	10.612	0.00464	**
sediment_treat	1	34.1	34.1	0.249	0.62402	
tank_pair	1	593.3	593.3	4.331	0.05286	.
pred_treat:heat_treat	1	65	65	0.474	0.50038	

pred_treat:sediment_treat	1	35.2	35.2	0.257	0.61866
Residuals	17	2329	137		

Table S48: Results summary table of the repeated measures ANOVA for dytiscid larvae abundance in mixed sediment mesocosms

Effect	df	dfd	MSE	F	ges	p.value	P<0.05
heat_treat	1,	12	0.54	2.48	0.039	0.141	
pred_treat	1,	12	0.54	8.71	0.124	0.012	*
heat_treat:pred_treat	1,	12	0.54	2.48	0.039	0.141	
day	11,	132	0.2	2.12	0.124	0.023	*
heat_treat:day	11,	132	0.2	0.81	0.051	0.63	
pred_treat:day	11,	132	0.2	2.12	0.124	0.023	*
heat_treat:pred_treat:day	11,	132	0.2	0.81	0.051	0.63	

Table S49: Results summary table of the repeated measures ANOVA for medium sized dytiscid larvae in mixed sediment mesocosms

Effect	df	dfd	MSE	F	ges	p.value	P<0.05
heat_treat day	1,	14	0.06	5.6	0.034	0.033	*
heat_treat:day	11,	154	0.06	1.48	0.088	0.144	
	11,	154	0.06	1.48	0.088	0.144	

Table S50: Clusters obtained using the CCF algorithm from Chapter I on total abundance for the conditions of H1 (examining heating and predators)

Mesocosm			Mesocosm	4	2
ID	Predator	Heat	Pair	Clusters	Clusters
25	none	with	5	1	1
28	none	without	6	1	1
30	none	with	7	1	1
31	none	without	8	1	1
32	beetles	without	8	1	1
34	none	without	9	1	1
37	none	with	11	1	1
40	beetles	without	12	1	1
26	beetles	with	5	2	2
27	beetles	without	6	2	2
29	beetles	with	7	2	2

33	beetles	without	9	2	2
36	none	with	10	2	2
35	beetles	with	10	3	1
39	none	without	12	3	1
38	beetles	with	11	4	2

Table S51: Clusters obtained using the CCF algorithm from Chapter I on richness (order) for the conditions of H1 (examining heating and predators)

Mesocosm ID	Predator	Heat	Mesocosm Pair	4 Clusters	2 Clusters
25	none	with	5	1	1
26	beetles	with	5	1	1
29	beetles	with	7	1	1
30	none	with	7	1	1
33	beetles	without	9	1	1
27	beetles	without	6	2	1
28	none	without	6	2	1
31	none	without	8	2	1
32	beetles	without	8	2	1
34	none	without	9	2	1
36	none	with	10	2	1
39	none	without	12	2	1
40	beetles	without	12	2	1
35	beetles	with	10	3	2
38	beetles	with	11	3	2
37	none	with	11	4	2

Table S52: Clusters obtained using the CCF algorithm from Chapter I on total abundance for the conditions of H2 (examining sediment source and predators)

Mesocosm ID	Predator	Sediment	Pair		Mesocosm 4 Clusters	Predator	Sediment	2 Clusters
1	none	local	1	1	1 10	none	local	2
	1	1 22	beetles		local	2	1	1
16	none	local	3	2	1 21	beetles		
	local	1	2	1				
24	beetles	local	4	2	1			
32	beetles	mixed	8	2	1 34	none		
	mixed	9	2	1 40	beetles	mixed	12	
	2	1 20	none	local	4	3	1	
28	none	mixed	6	3	1			
31	none	mixed	8	3	1 39	none	mixed	12
	3	1 23	beetles		local	3	4	2
27	beetles	mixed	6	4	2			
33	beetles	mixed	9	4	2			

Table S53: Clusters obtained using the CCF algorithm from Chapter I on richness (order) for the conditions of H2 (examining sediment source and predators)

Mesocosm ID	Predator	Sediment	Pair	Clusters	Mesocosm ID	Predator	Sediment	Pair	Clusters
1	none	local	1	1	10	none	local	2	1
20	none	local	4	1	1				
16	none	local	3	2	23	beetles	local	3	2
21	beetles	local	1	3	2				
22	beetles	local	2	3	2				
24	beetles	local	4	3	2				
33	beetles	mixed	9	3	2				
27	beetles	mixed	6	4	28	none	mixed	6	4
1									
31	none	mixed	8	4	32	beetles	mixed	8	4
1	34	none	mixed	9	4	1	39	none	mixed
12	4	1							
40	beetles	mixed	12	4	1				

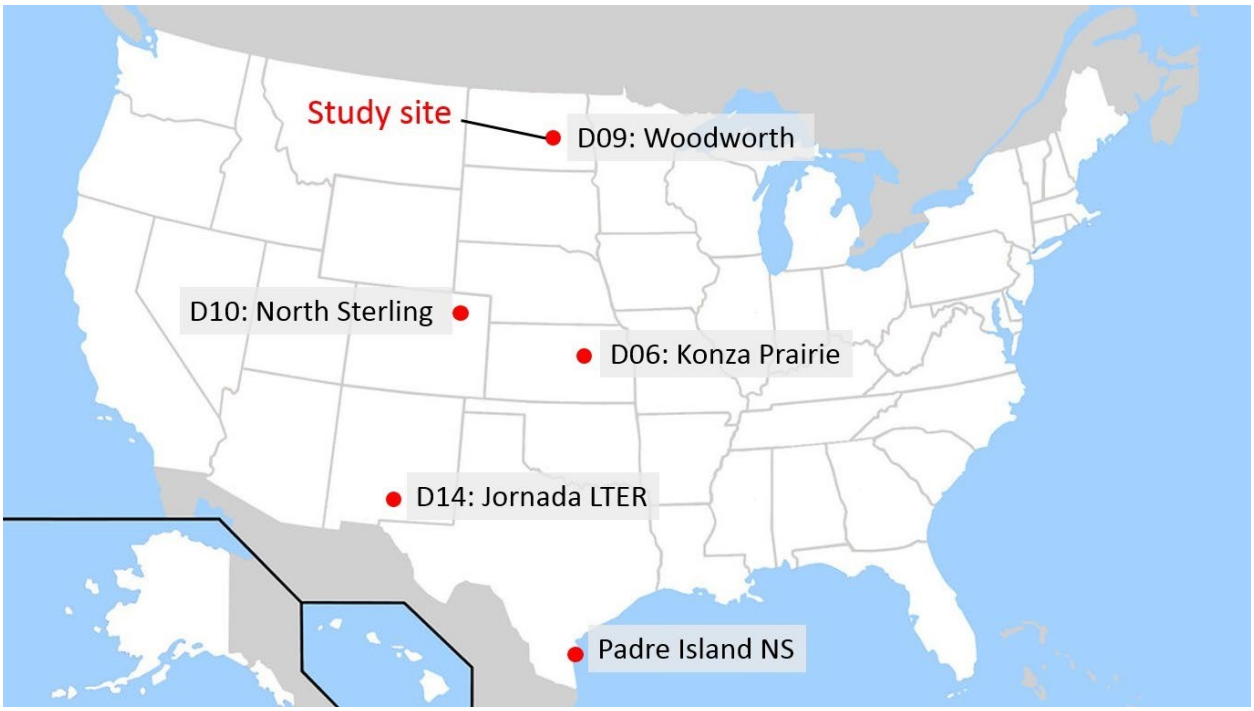

Figure S63: A map of the United States with the sediment locations marked. Half of the sediment collected near the Woodworth NEON site in North Dakota was retained on site and labeled 'local sediment' while the other half was homogenized with equal parts from each of the remaining four sites. This mixture was labeled 'mixed sediment'. The mesocosm experiment was conducted at the Woodworth site in North Dakota.

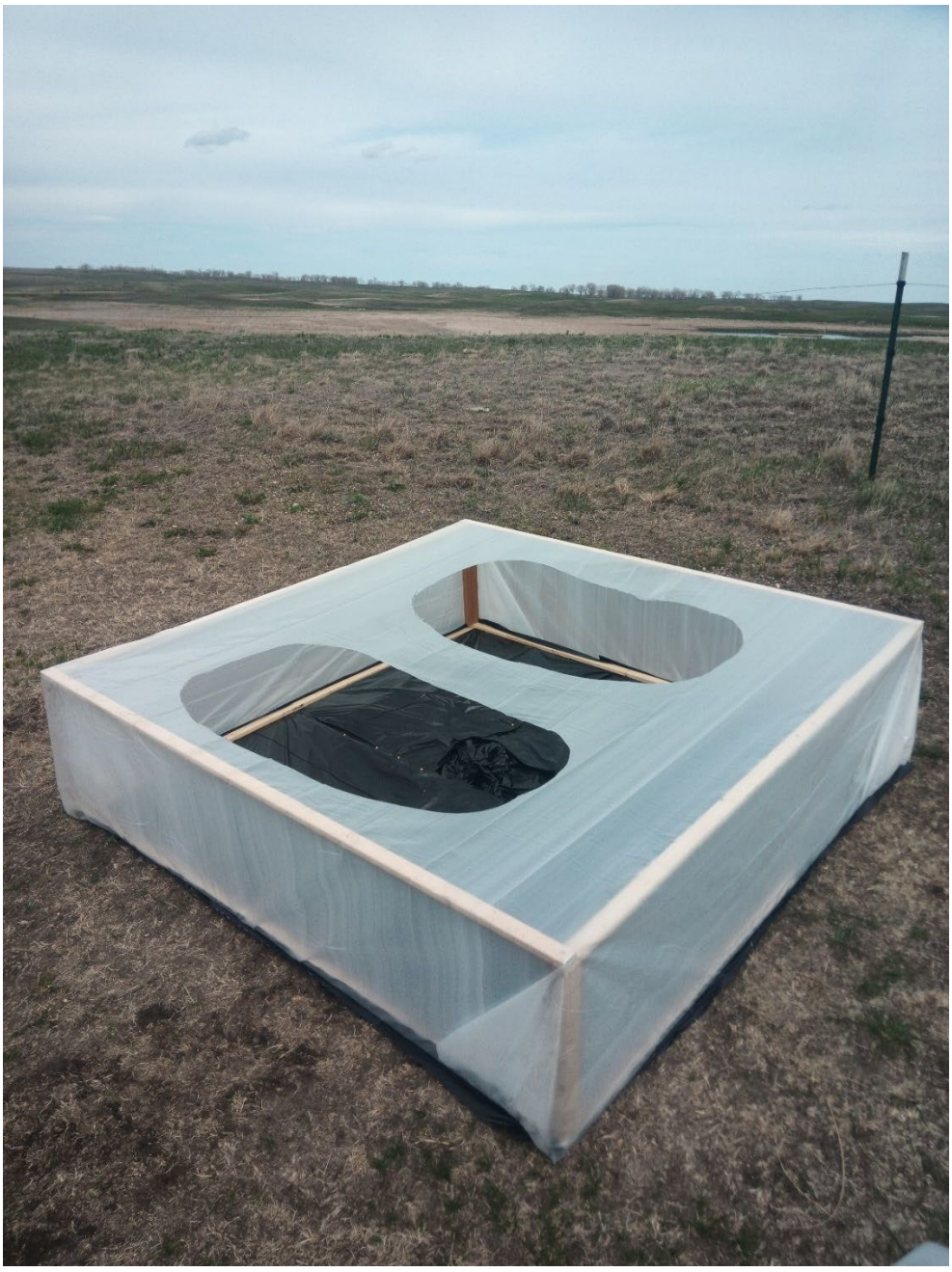

Figure S64: One constructed open-top greenhouse used to warm a pair of mesocosms. The frame consists of pressure treated lumber, the side and top walls are translucent 6 mil polyethylene sheeting, and the floor is a double layer of 6 mil contractor garbage bags.

Figure S65: Each mesocosm within a greenhouse was placed upon two pieces of lumber to minimize heat loss via ground contact.

Figure S66: A bird's-eye view of one mesocosm. The sand upon topsoil substrate is visible through the 30.5 cm deep water. A window screen was placed over top of each mesocosm and held on by binder clips.

Figure S67: Physical arrangement of the array of mesocosms showing the pairs of mesocosms. The eight pairs in the foreground are those seeded with mixed sediment. Behind these is a second array of mesocosms for a separate experiment. Along the outer edges of that array are four additional mesocosms with local sediment. Each of those mesocosms is paired with the adjacent mesocosm in that array. These eight mesocosms, in total, make up the local sediment seeded mesocosms used in the current study.

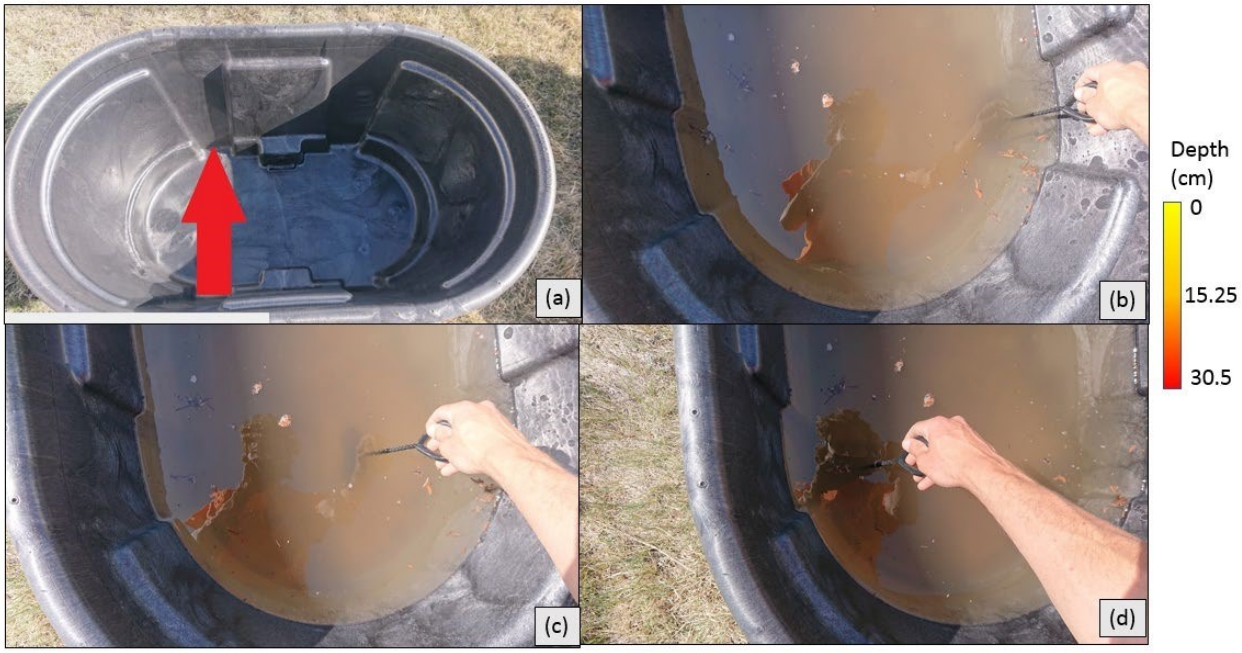

Figure S68: One of four methods used for the repeated community sampling by dip net. (a) The arrow shows the direction and depth of the sweep, in this case at the bottom of the water column. (b) The net is submerged vertically along the long wall until contacting the substrate. (b) It is then swept along the bottom while keeping contact with the substrate. (d) Upon reaching the opposite wall, it is swept upward vertically until breaching. This sweep is performed twice per sample.

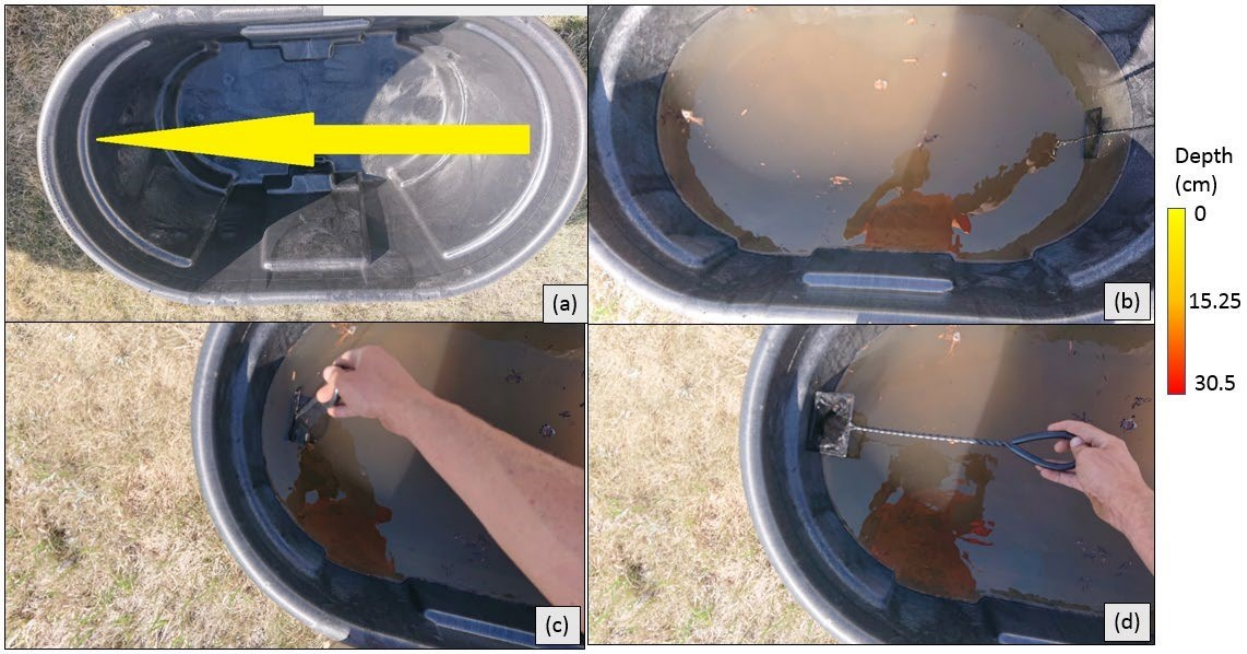

Figure S69: One of four methods used for the repeated community sampling by dip net. (a) The arrow shows the direction and depth of the sweep, in this case just below the surface of the water. (b) The net is submerged vertically along the short wall until the entire opening is submerged just below the water's surface. (c) It is then swept through the water until reaching the opposite wall. Upon reaching the opposite wall, it is swept upward vertically until breaching (d). This sweep is performed once per sample.

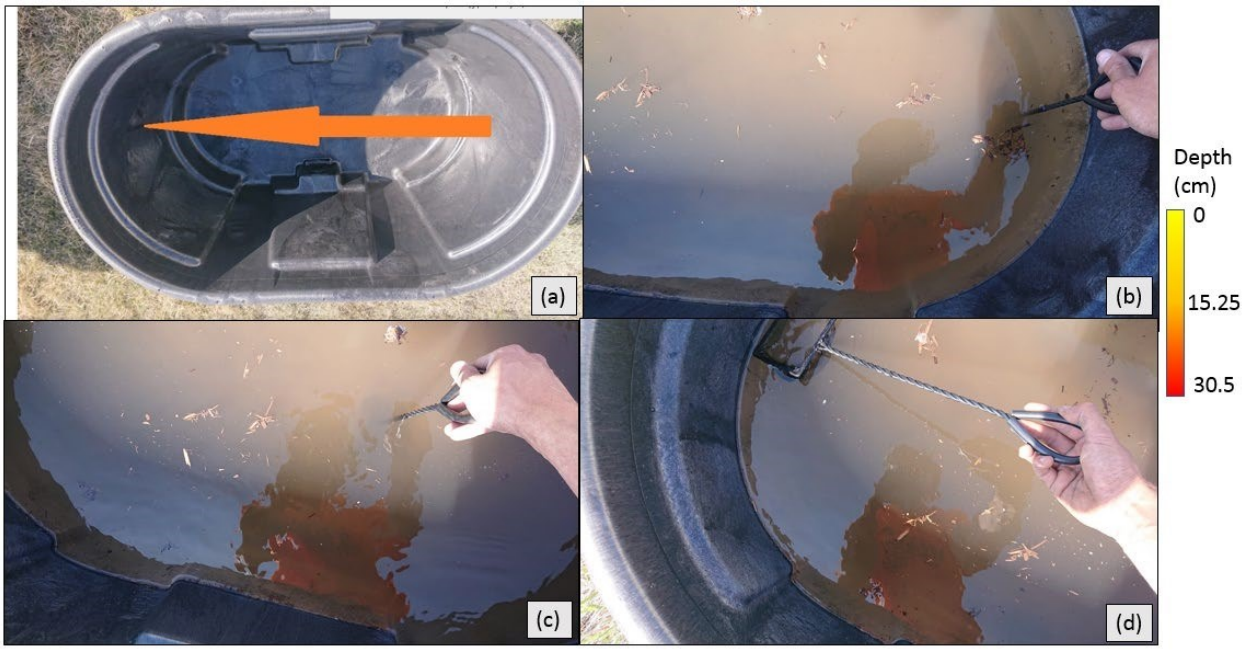

Figure S70: One of four methods used for the repeated community sampling by dip net. (a) The arrow shows the direction and depth of the sweep, in this case halfway down the water column. (b) The net is submerged vertically along the short wall until it is halfway down the water column. (c) It is then swept through the water until reaching the opposite wall. Upon reaching the opposite wall, it is swept upward vertically until breaching (d). This sweep is performed once per sample.

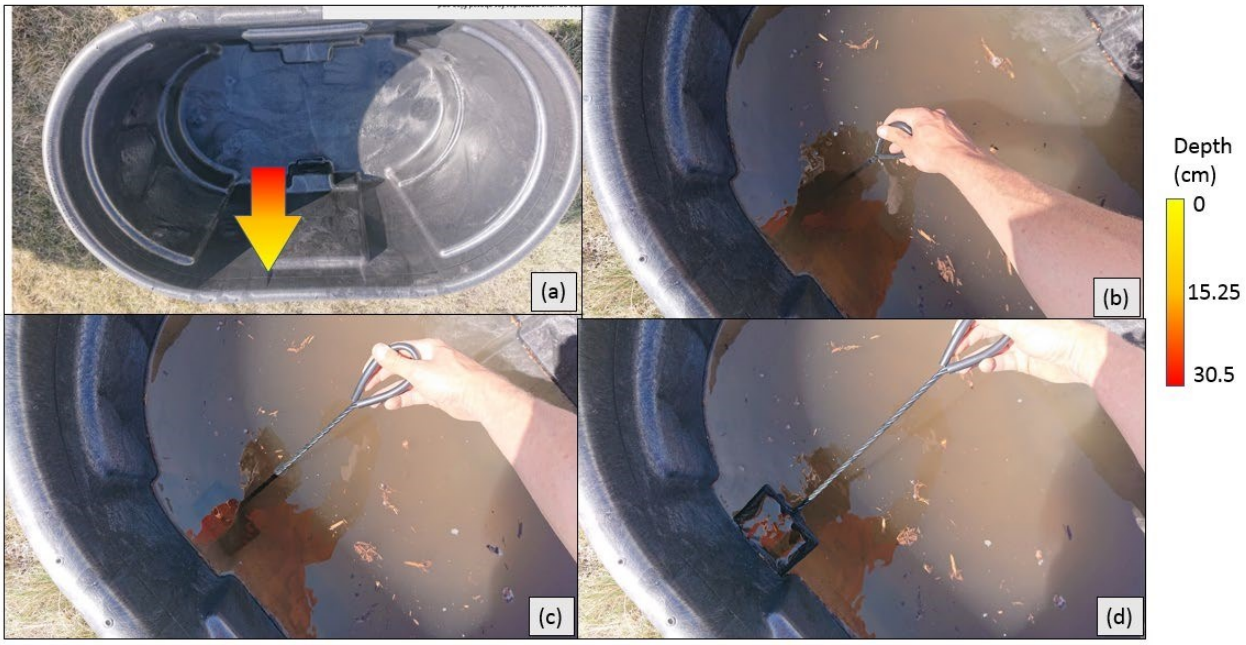

Figure S71: One of four methods used for the repeated community sampling by dip net. (a) The arrow shows the direction and depth of the sweep, in this case from the bottom to the top of the water column. (b) The net is submerged vertically along the short wall until contacting the substrate. (c) It is then rotated such that the bottom of the net is contacting the wall. (d) The next is swept upward while contacting the wall until breaching. This sweep is performed twice per sample.

Figure S72: (a) The white plastic dish bin into which the net sweeps are rinsed when collecting a community sample. (b) a smaller white enamel bowl containing a subsample of Cladocera collected from an original sample in the white dish bin above.

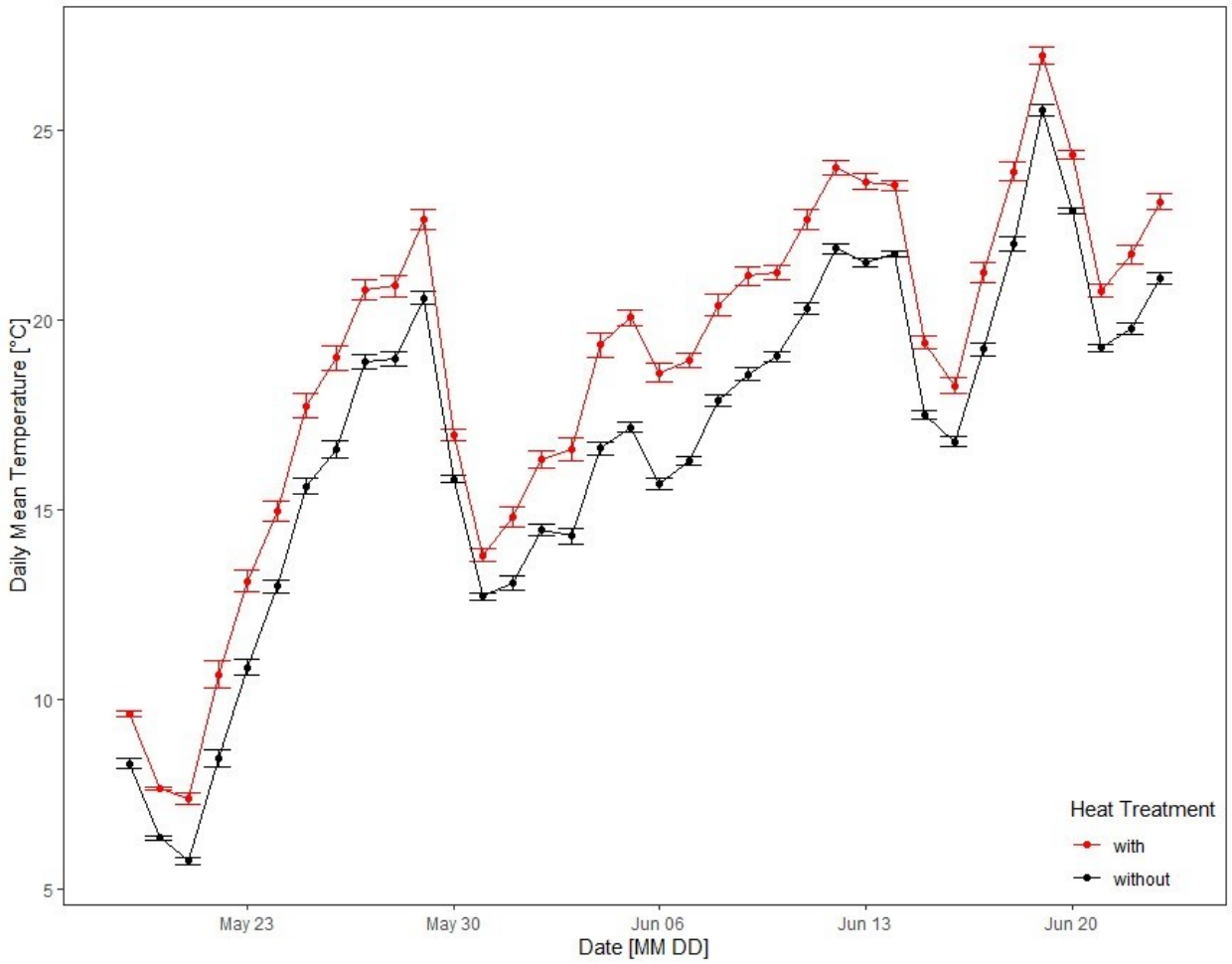

Figure S73: Time series of daily mean water temperature in the mesocosms with (red) and without (black) additional heating via the greenhouses. The range of dates encompass the entirety of this study.

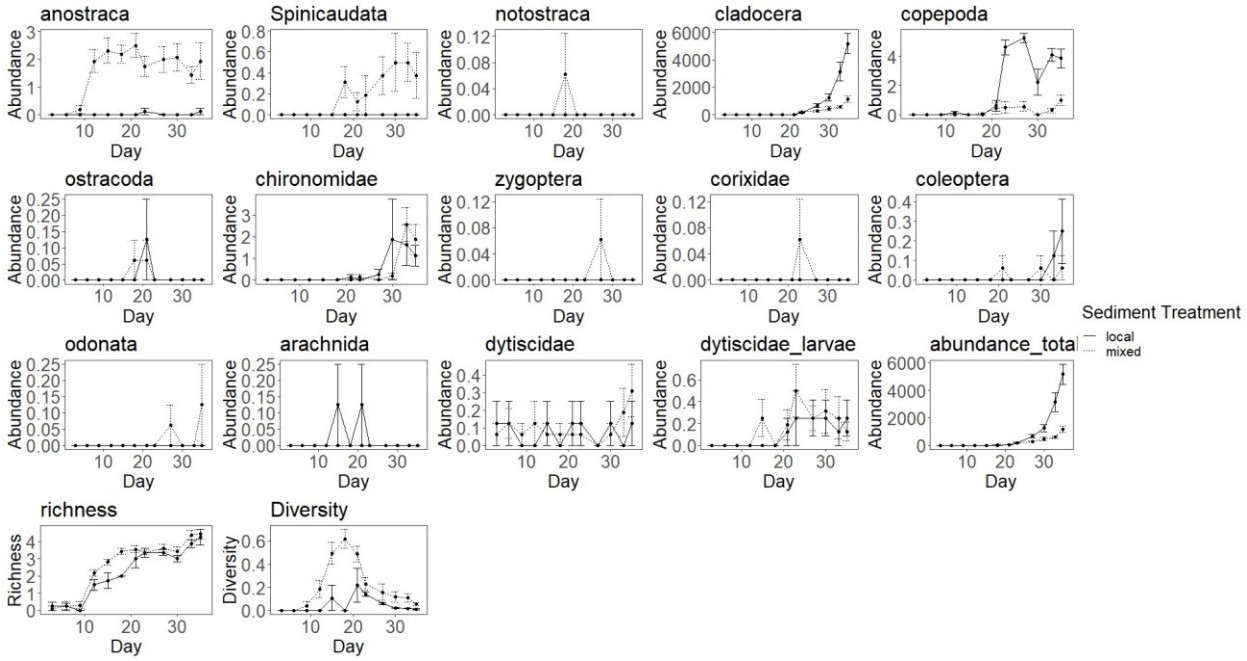

Figure S74: Abundance time series for each taxa collected during the experiment separated by sediment source with ND-only (local) sediment shown in solid lines and the five state mixture of sediment (mixed) shown in dashed lines.

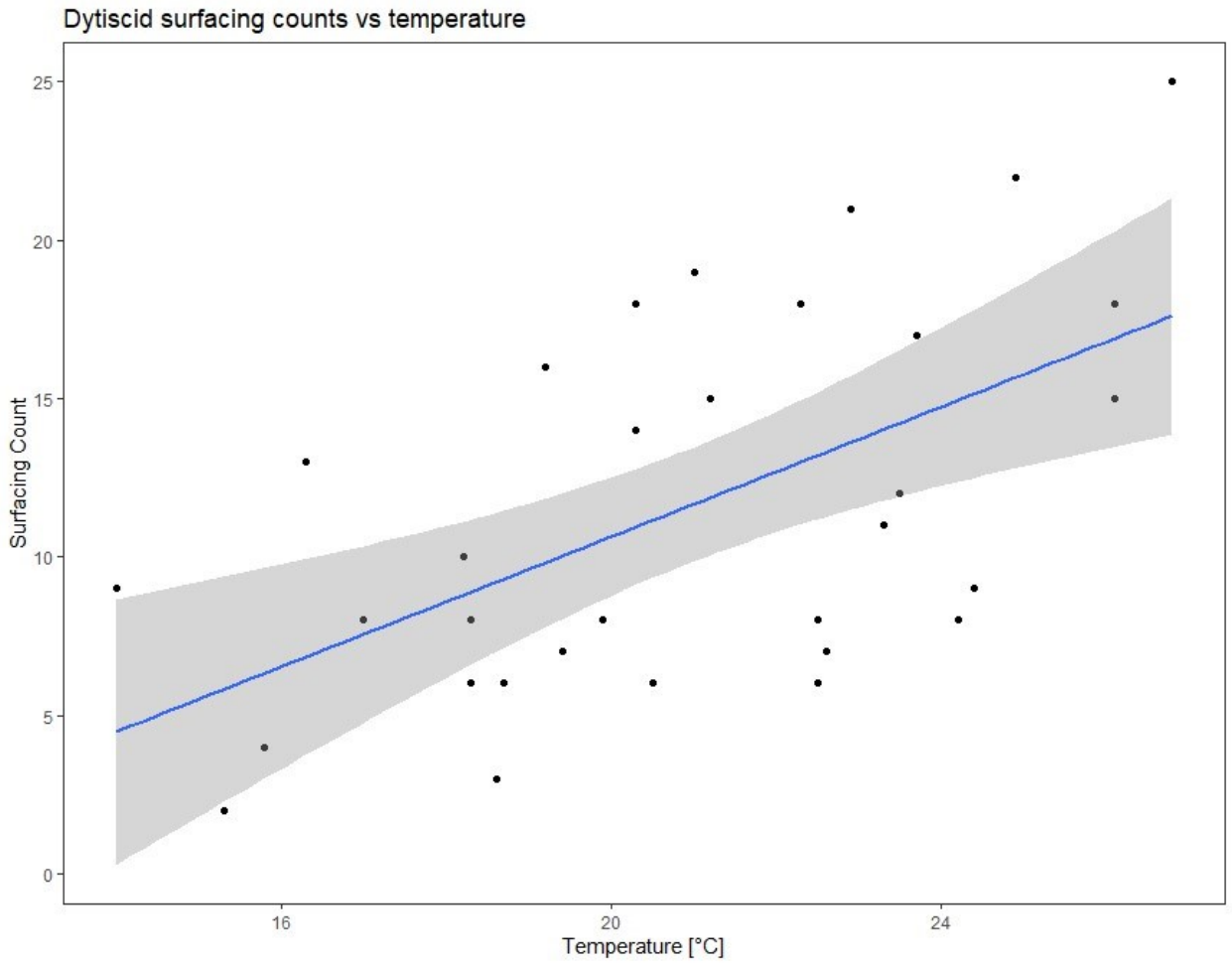

Figure S75: Linear regression of the number of dytiscid surfacing events counted during 15minute observation windows and water temperature.

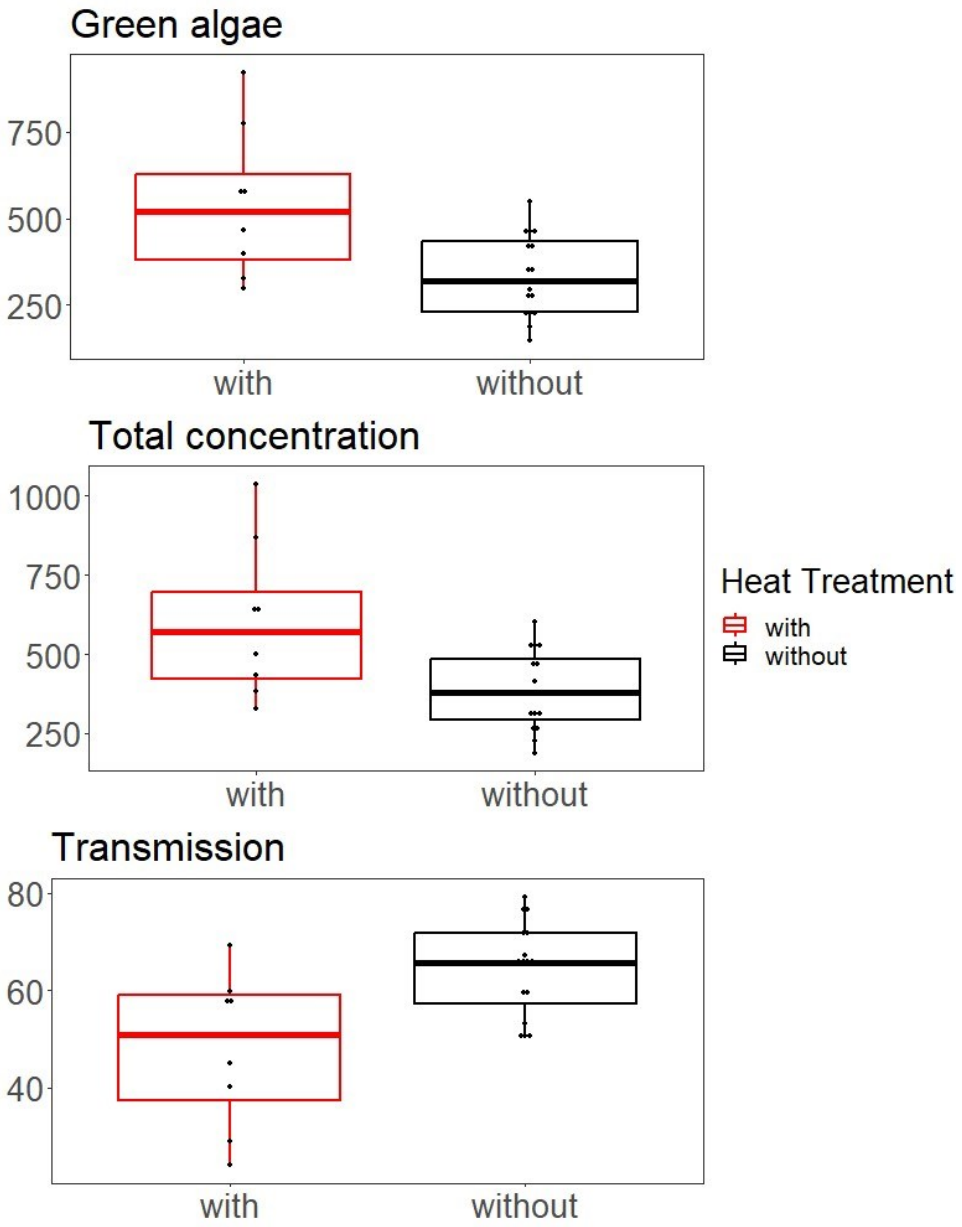

Figure S76: Box plots for each fluoroprobe measurement separated by heat treatment. The measured values include concentration of green algae and all algae and percent optical transmission. Red lines are those where additional warming was present while black lines are those without warming. Warming is also denoted by the x axis of each plot.

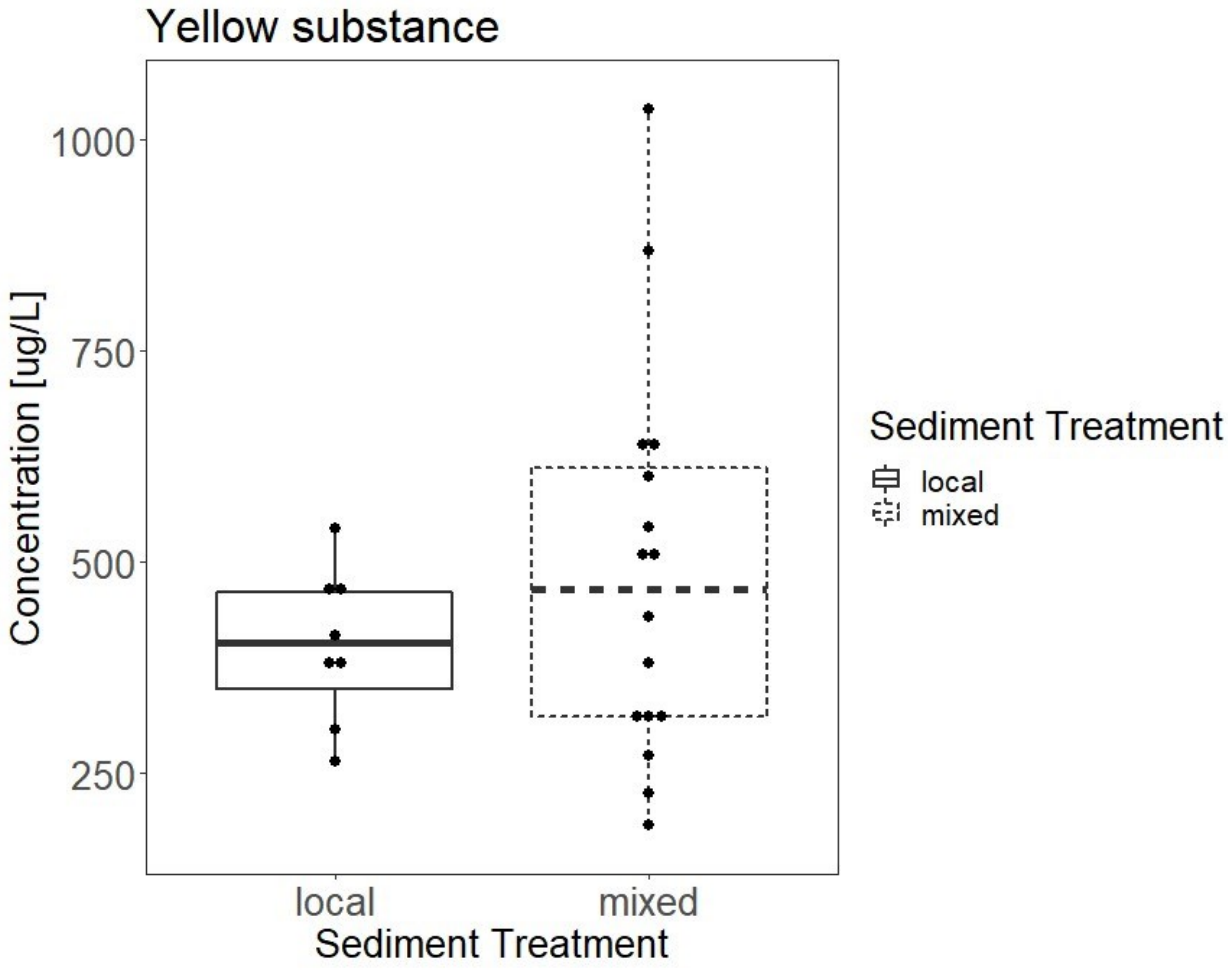

Figure S77: Box plots for the fluoroprobe measurement chromophoric dissolved organic matter (CDOM), also known as yellow substance, separated by sediment treatment. solid lines are those mesocosms seeded with local sediment while dashed lines are those seeded with mixed sediment.

Sediment treatment is also denoted by the x axis.

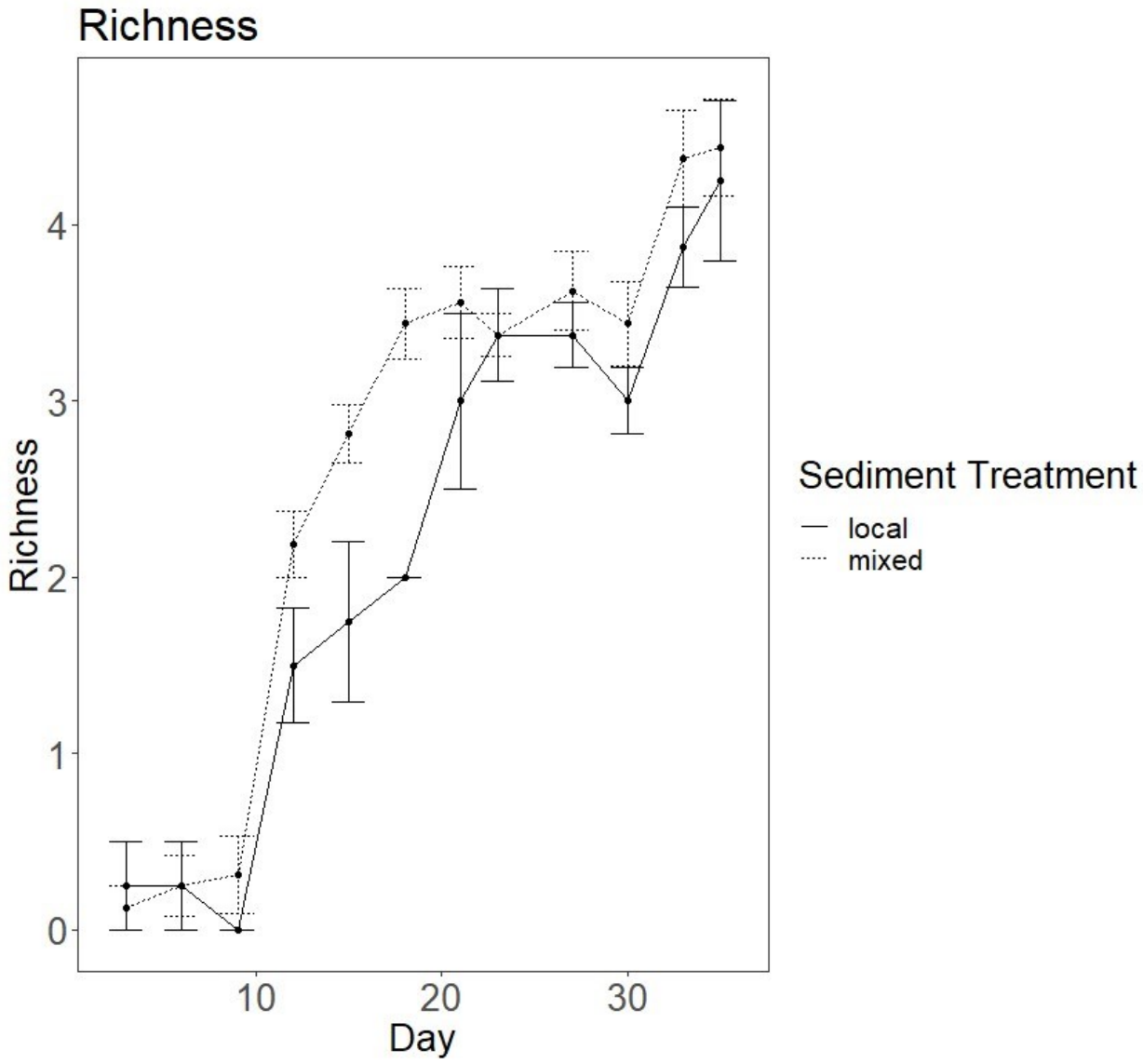

Figure S78: Time series of richness (Order) for each sediment source. Mesocosms seeded using local sediment are denoted by the solid line while those seeded with mixed sediment are denoted by the dashed line.

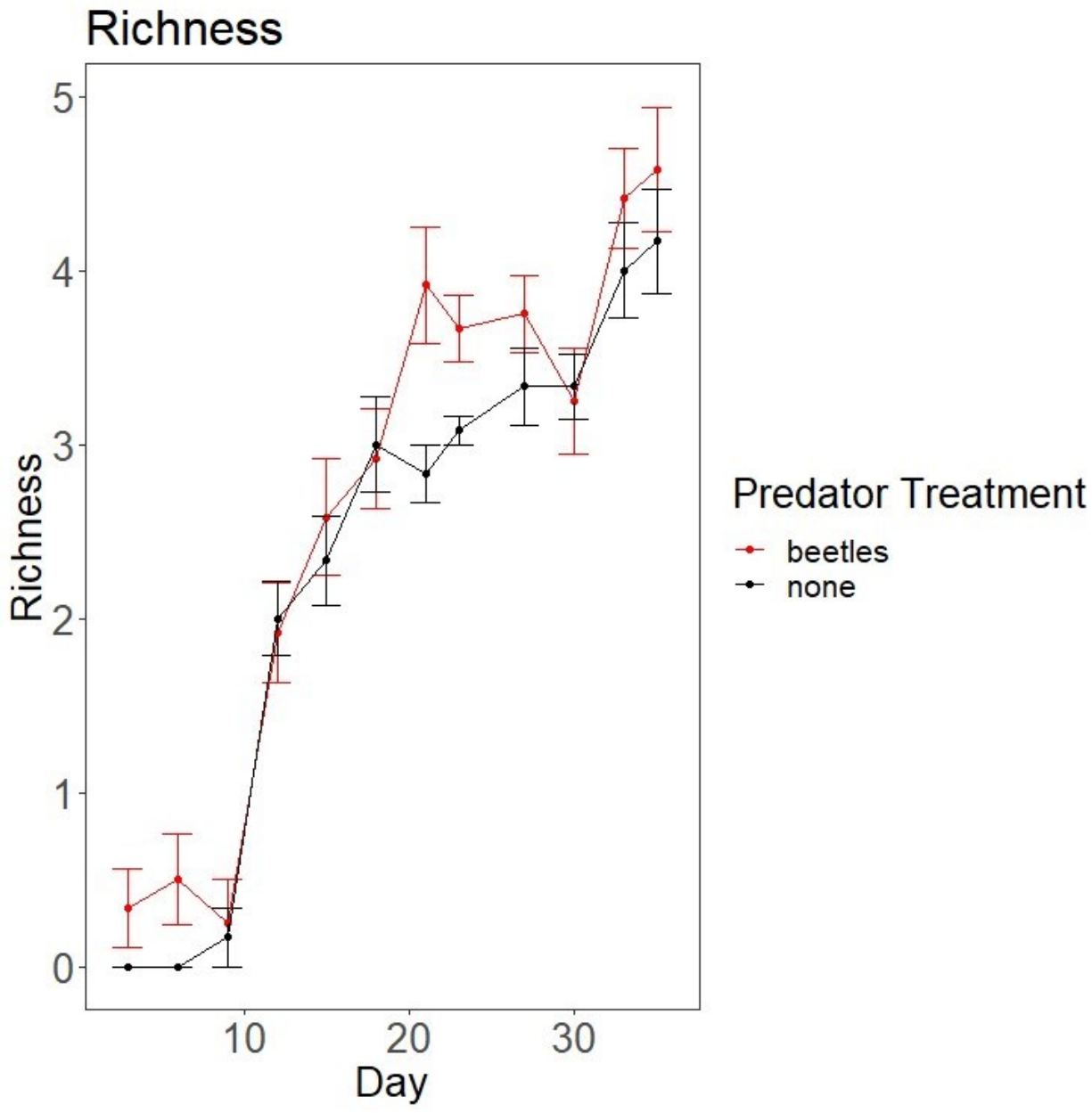

Figure S79: Time series of richness (Order) against predator treatment. Mesocosms containing dytiscids are denoted by the red line while those without dytiscids are denoted by the black line.

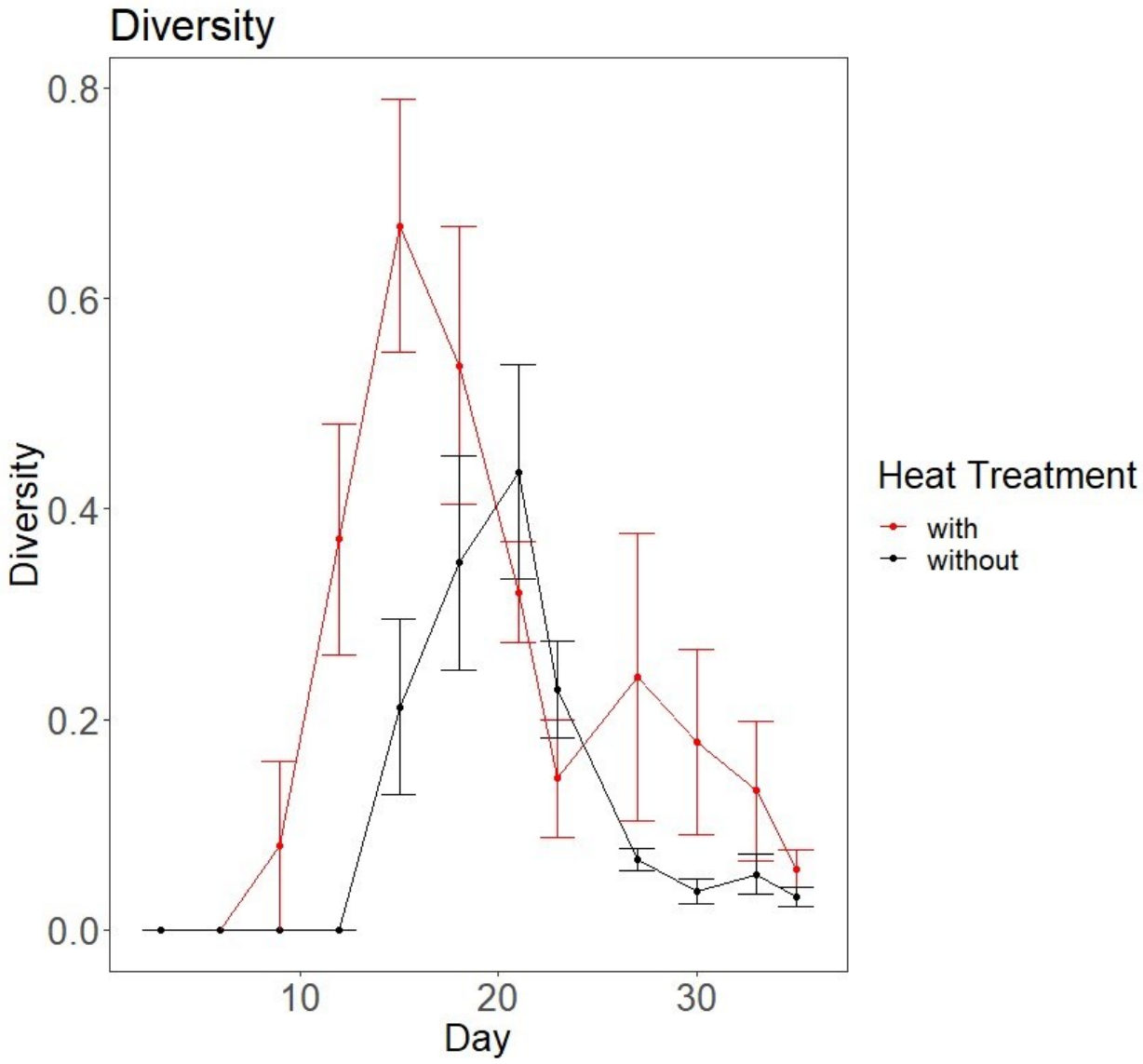

Figure S80: Time series of Shannon diversity (Order) against heat treatment. Mesocosms with heating are denoted by the red line while those without heating are denoted by the black line.

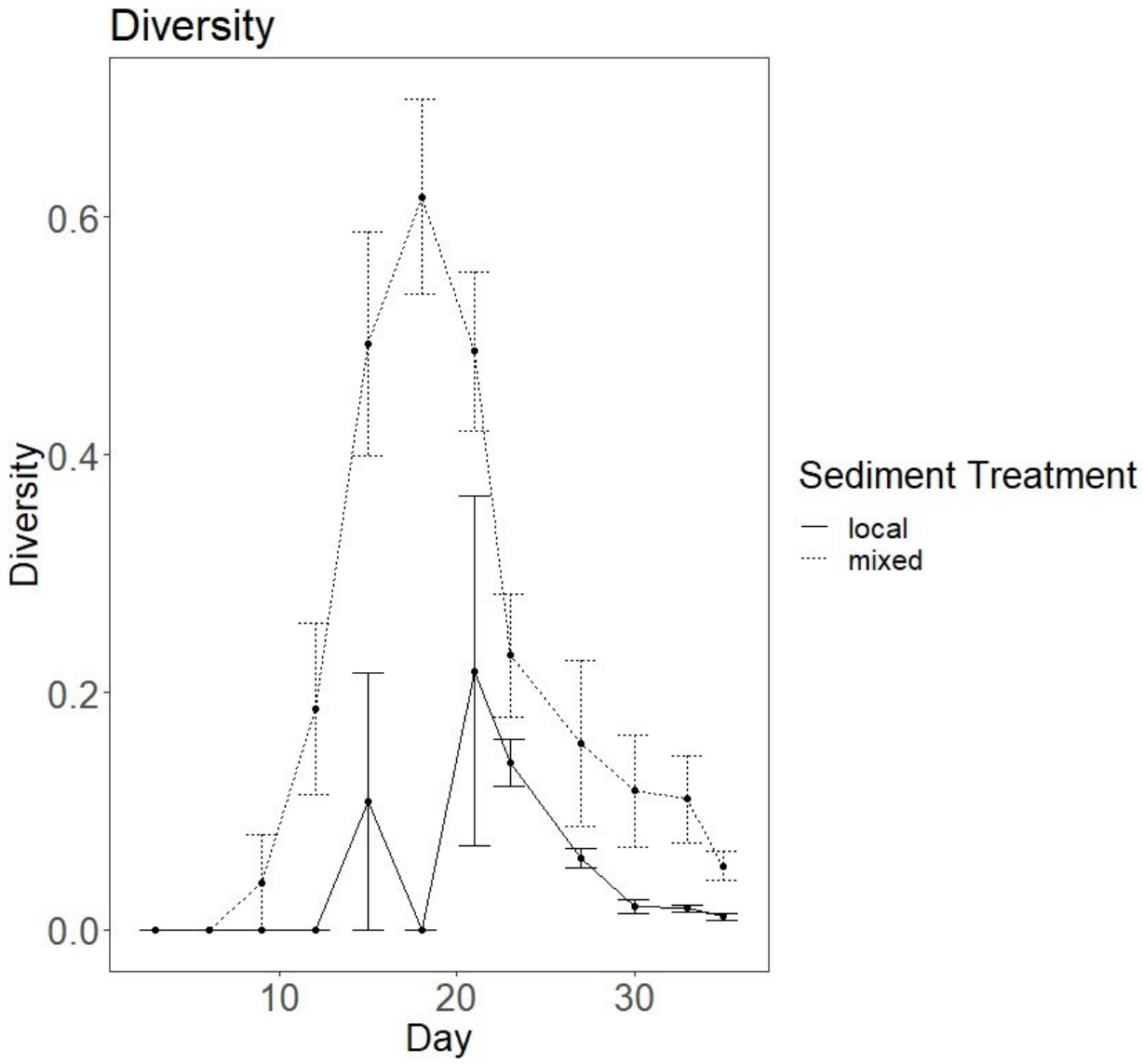

Figure S81: Time series of Shannon diversity (Order) for each sediment source. Mesocosms seeded using local sediment are denoted by the solid line while those seeded with mixed sediment are denoted by the dashed line.

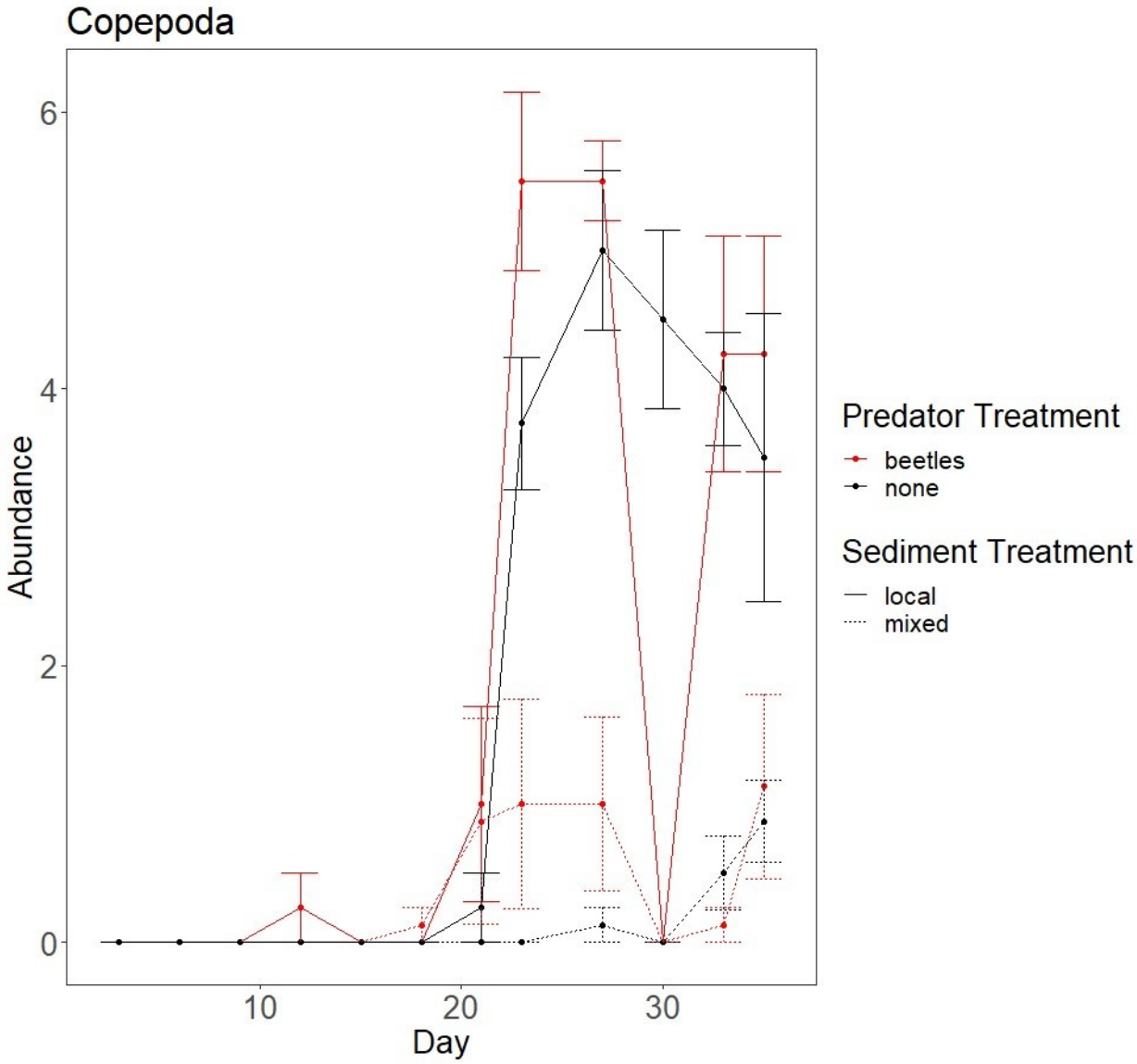

Figure S82: Time series plot of the abundance of copepods over time in the mesocosms without experimental heating, separated by sediment and predator treatments. Solid lines represent mesocosms with local sediment while dashed lines are those with mixed sediment. Red lines represent mesocosms with dytiscid predators while black lines are those without predators.

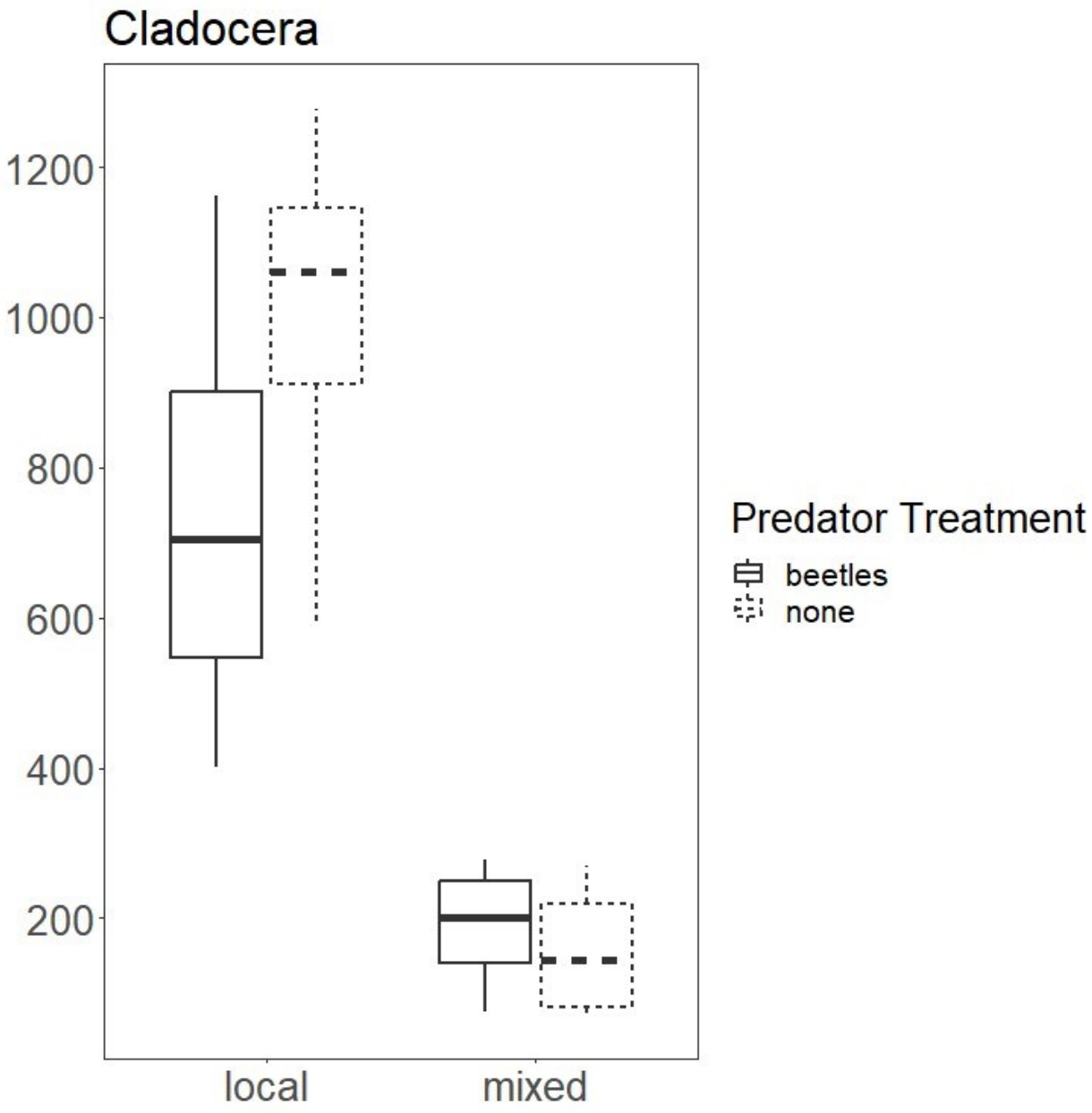

Figure S83: Box plots of the abundance of cladocera in the mesocosms without experimental heating, separated by sediment and predator treatments. Solid lines represent mesocosms with predator additions while dashed lines are those without predators. Sediment treatment is denoted by the x axis.

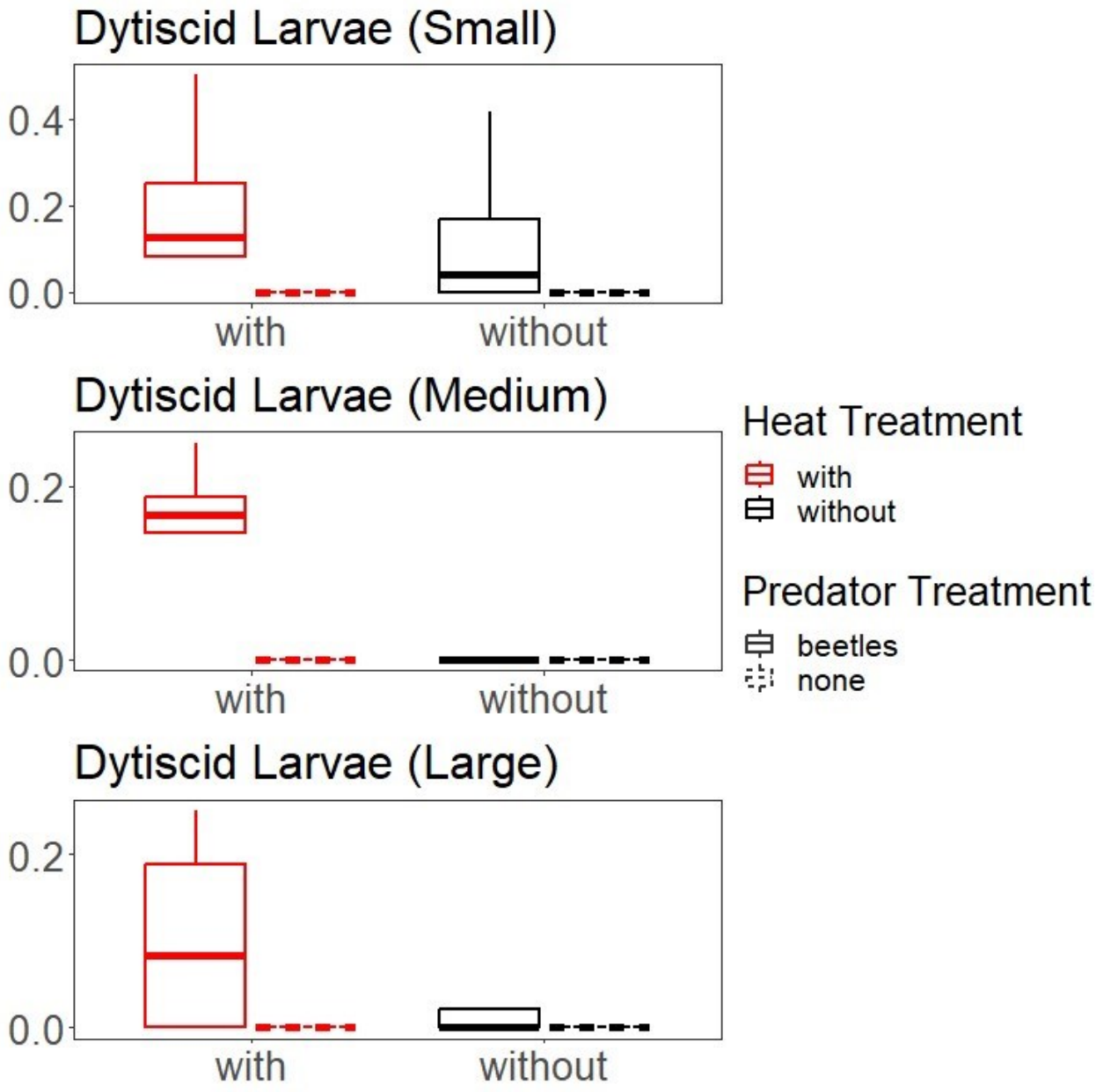

Figure S84: Box plots of the abundance of each size class of dytiscid larvae in the mesocosms seeded with mixed sediment, separated by heat and predator treatments. Solid lines represent mesocosms with predator additions while dashed lines are those without predators. The heat treatment is denoted by the x axis and coloring, where red lines represent mesocosms with heating and black lines represent mesocosms without heating.

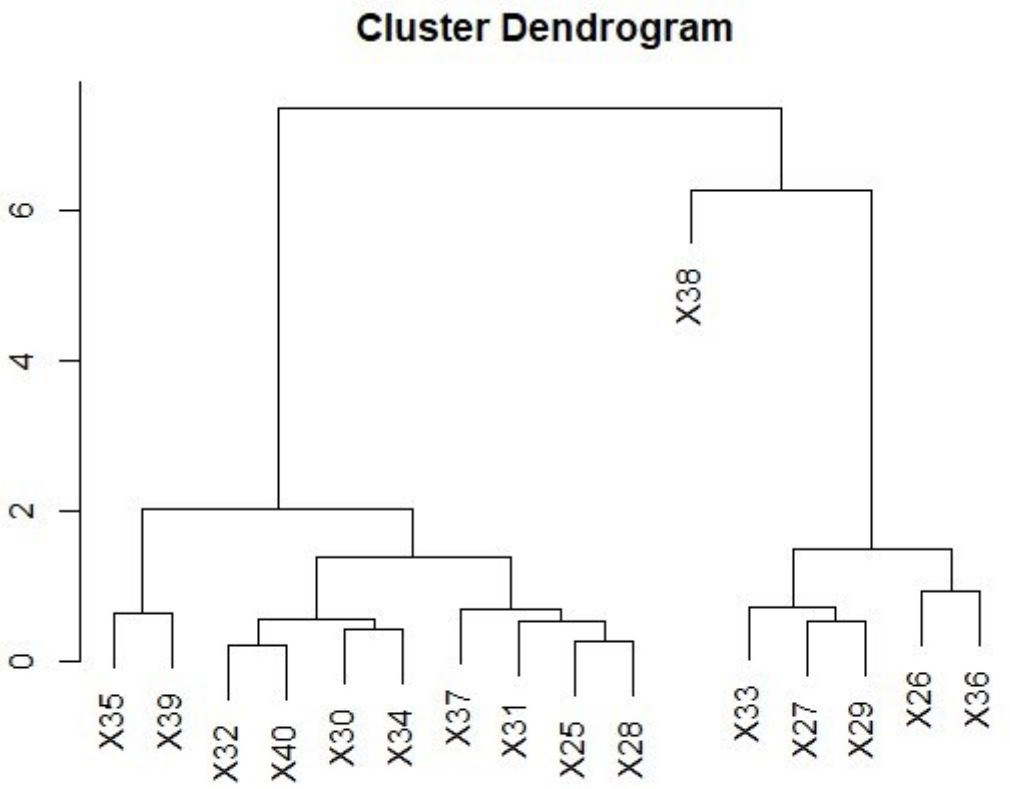

Figure S85: A dendrogram showing the clusters generated by the CCF method and hierarchical clustering algorithm from Chapter I. Clusters were generated using the time series of total abundance for each mesocosm. The mesocosms included are those used to address hypothesis H1, examining heating and predators.

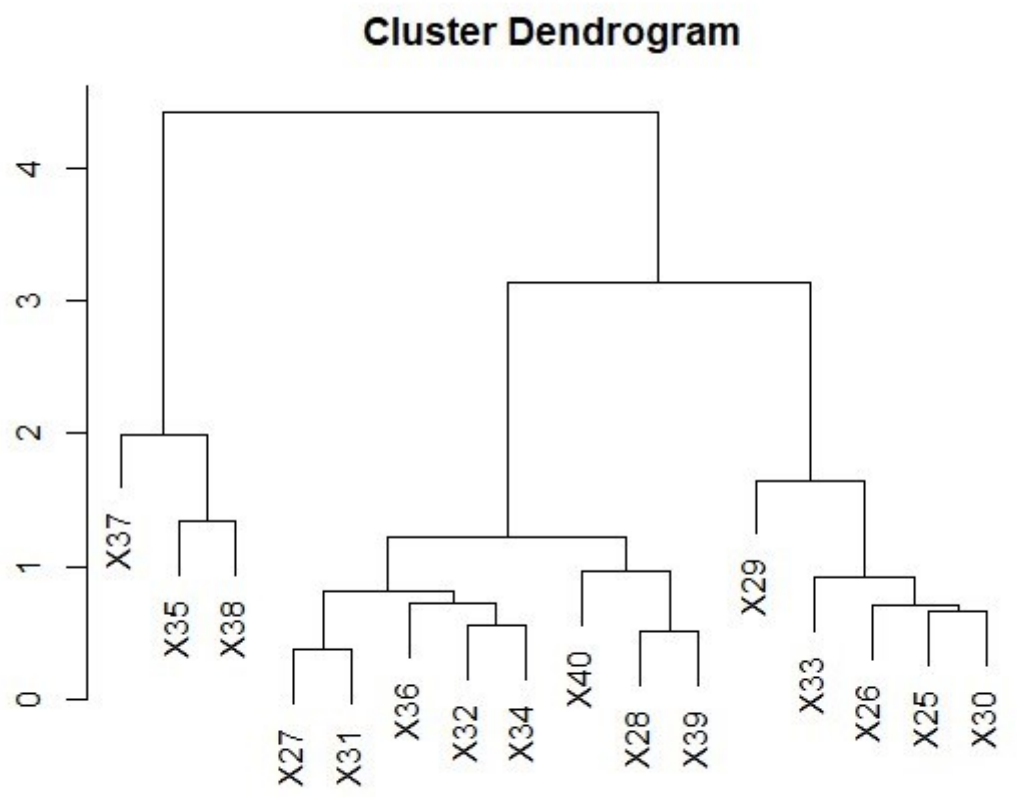

Figure S86: A dendrogram showing the clusters generated by the CCF method and hierarchical clustering algorithm from Chapter I. Clusters were generated using the time series of order-level richness for each mesocosm. The mesocosms included are those used to address hypothesis H1, examining heating and predators.

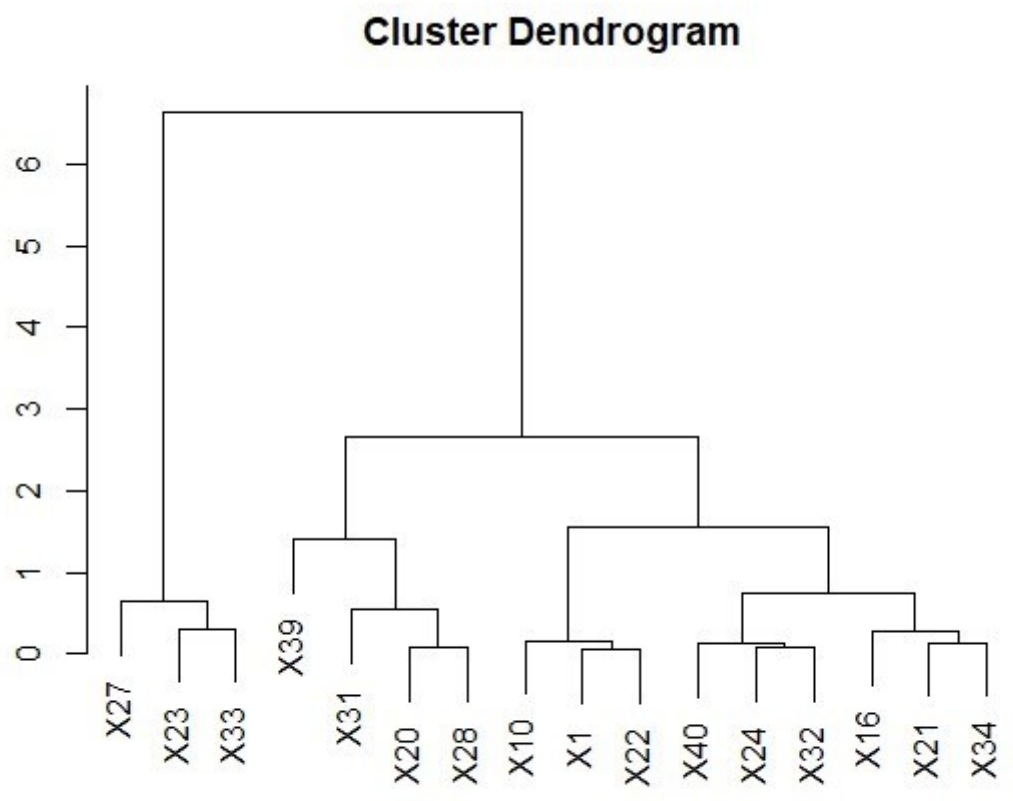

Figure S87: A dendrogram showing the clusters generated by the CCF method and hierarchical clustering algorithm from Chapter I. Clusters were generated using the time series of total abundance for each mesocosm. The mesocosms included are those used to address hypothesis H2, examining sediment source and predators.

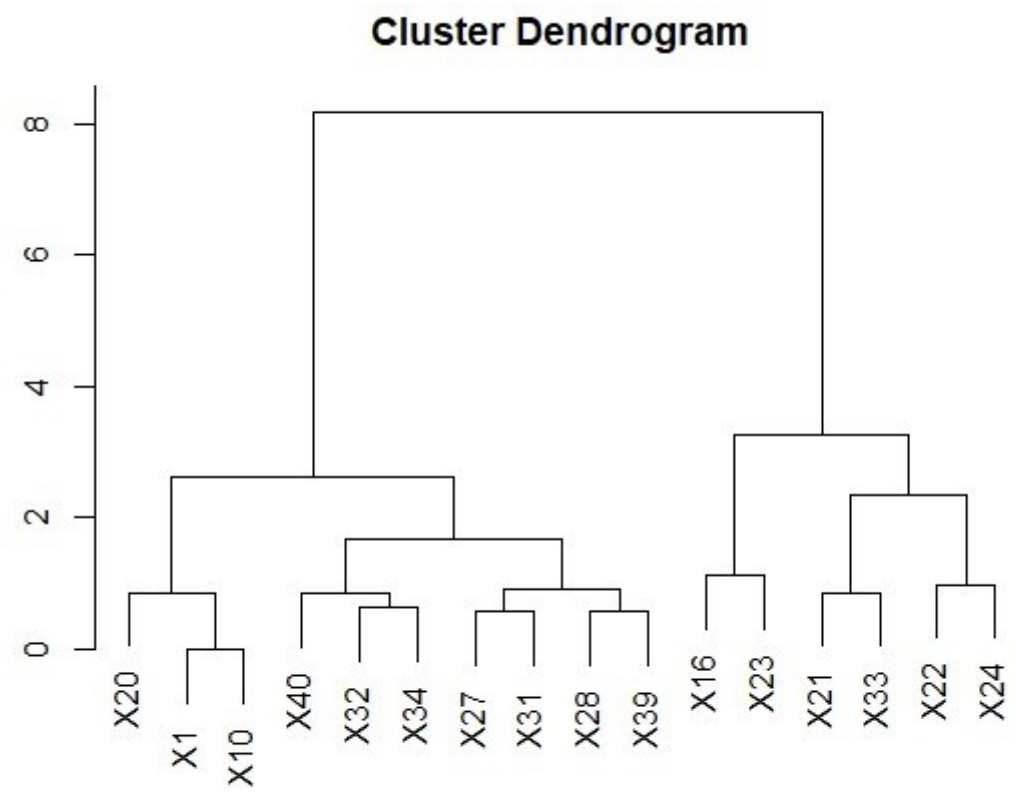

Figure S88: A dendrogram showing the clusters generated by the CCF method and hierarchical clustering algorithm from Chapter I. Clusters were generated using the time series of order-level richness for each mesocosm. The mesocosms included are those used to address hypothesis H2, examining sediment source and predators.